Neural evidence underlying phasic and tonic states of breathlessness and COVID-19



Lin Qiu

Nuffield Department of Clinical Neurosciences
University of Oxford

This dissertation is submitted for the degree of
Doctor of Philosophy

St Peter's College

Michaelmas 2024

I would like to dedicate this thesis to my loving parents, whose unwavering support has guided me through every challenge and decision, no matter how unconventional.

Declaration

I hereby declare that, except where specific references are made to the work of others, the contents of this dissertation are entirely my own and have not been submitted, either in whole or in part, for consideration for any other degree or qualification at this or any other university. This dissertation represents my individual effort, and contains no work that has been done in collaboration with others, unless explicitly noted in the text or Acknowledgements.

I have used ChatGPT-4 for the following purposes: debugging my Python and MATLAB scripts, and for assisting with text refinement, including grammar correction and enhancing the formality of the language. No other generative use of ChatGPT-4 was employed in the creation of this dissertation.

Parts of the data collected for this dissertation have been published in the following article:

Rua, C., Raman, B., Rodgers, C. T., Newcombe, V. F. J., Manktelow, A., Chatfield, D. A., Sawcer, S. J., Outtrim, J. G., Lupson, V. C., Stamatakis, E. A., et al. (2024). *Quantitative susceptibility mapping at 7 T in COVID-19: brainstem effects and outcome associations.* *Brain*, 147(12), 4121–4130. Oxford University Press UK. (Co-author)

Research based on Chapters 2, 3, 4, and 5 is in preparation for publication.

Lin Qiu
Michaelmas 2024

Acknowledgements

I want to first thank my supervisor, Kyle Pattinson, for his guidance and unwavering support throughout my research and life. I will miss the time when we brainstorm my thesis while walking in the muddy Warneford meadow during the pandemic. I also thank my secondary supervisor, Martyn Ezra, particularly for helping me decode the historical dataset like an archaeologist, digging through layers of directories and saving broken files.

Within the WIN community, I want to give a special thanks to – Miriam Klein-Flugge, Hossein Rafipoor, Saad Jbabdi, Ludovica Griffanti, Marieke Martens, and Thomas Nichols – for patiently putting up with my constant "harassment" by the numerous emails and office drop-ins with my analysis questions. I'm also grateful to the MRI radiographers, David, Jon, and Michael, who endured nearly two years of scanning sessions with me in masks, and to the participants who braved COVID to take part in my study and share your experience in long COVID. These studies would not have been possible without their contribution.

I'm immensely grateful to Ben Seymour for welcoming me into his Pain lab and to his amazing team for all the fizzy sessions, Asian snacks, and loud brainstormings. This have changed my last two years massively. Also, massive thanks Rachel Crockett for proofing reading my thesis - it made all the differences.

Thanks to my writing buddies, Shu Wei and Kangning Zhang, for our summer sessions at the good old Bod - although magically my writing hands always ended up holding a glass of cocktail. And thanks to the lovely Jingyi Zhao, Verena Hinze, Rongqin Yu, Sarah Schreiber, Danielle Hewitt, and Qi Feng, whom I'm lucky to call friends. I can always walk away feeling pumped and amazing about myself again after spending time with them.

Finally, I couldn't have made it without my most amazing parents, who flew all the way from China to help care for my dog and treated me to a luxury of hot meals every day, featuring the most delicious Chongqing food. And, of course, to my Goldador, Louis, who never fails to remind me to keep the tail wagging and take walks to top up my vitamin D!

Abstract

Breathlessness involves complex interactions between physiological and psychological processes, particularly neural mechanisms in the amygdala and allostatic-interoceptive networks. This thesis explores phasic(adaptive) and tonic(maladaptive) breathlessness in healthy individuals and post-COVID patients using 7T functional MRI to offer mechanistic insights.

Phasic breathlessness was studied in healthy participants using a respiratory threat task. Activation and connectivity analyses showed that the basolateral amygdala (BLA) deactivated during both resistive breathing and its anticipation, with limited evidence of deactivation in the central and anterior amygdala. Increased BLA connectivity with the mediodorsal thalamus during respiratory resistance correlated with anxiety levels, linking amygdala-thalamic circuits to the emotional experience of breathlessness. At rest, intrinsic BLA connectivity patterns—heightened coupling with the temporal pole and reduced coupling with the precuneus—were linked to breathlessness intensity, emphasizing their role in interpreting respiratory signals. Tonic breathlessness was studied in COVID patients 334 ± 213 days post-infection, who exhibited breathlessness despite limited evidence of pulmonary dysfunction, using resting-state fMRI. Functional decoupling between the dorsal periaqueductal gray (dPAG) and posterior insula (PoI1), indicative of impaired visceral signal integration, and increased connectivity between the BLA and dorsal anterior cingulate cortex (dACC), suggestive of exaggerated anticipatory responses, were linked to breathlessness symptom. These findings support a dual-component model characterized by increased coupling in viscero-motor structures and decreased coupling in primary interoceptive regions. The dPAG-PoI1 decoupling may reflect a pre-existing neural characteristic, worsened by severe ventilation use, while the BLA-dACC coupling is associated with anxiety levels and infection severity. A multivariate analysis was conducted to identify disruptions in whole-brain connectomes associated with post-COVID symptoms, underscoring the complex nature of post-COVID experiences and the potential to delineate distinct neurophysiological phenotypes.

This work involves the theoretical and mechanistic development of an understanding of the neural mechanisms underlying phasic and tonic breathlessness, offering new avenues for understanding and managing this experience.

Table of contents

List of figures **xvii**

List of tables **xxi**

1 Introduction **1**

1.1 Abstract 2
1.2 Introduction to the clinical condition of breathlessness 2
1.3 The affective processes and breathing 5
1.3.1 Anxiety affecting breathing perception 5
1.3.2 Breathing regulation affecting affective state 6
1.3.3 Summary of the two lines of affection-breathing research 7
1.4 Theoretical framework 8
1.4.1 Breathlessness under the "Bayesian brain" framework 8
1.4.2 Active Inference as a more appropriate theory for respiration 10
1.4.3 Reconceptualising reflex breathing, phasic and tonic breathlessness 14
1.4.4 The allostatic–interoceptive (allo-intero) network 19
1.5 Amygdala in breathing regulation and perception 21
1.5.1 Position and structure of the amygdala 21
1.5.2 Amygdala during spontaneous breathing 24
1.5.3 Amygdala upon direct stimulation 24
1.5.4 Amygdala lesion and respiration 25
1.5.5 Amygdala during breathlessness 25
1.5.6 Pavlovian fear conditioning, breathlessness, and the amygdala . . . 27
1.5.7 Opioids suppress amygdala during anticipation of breathlessness . . 28
1.6 Functional brain evidence for long COVID 29
1.7 Summary of literature review and research roadmap 33
1.8 Thesis outline 34

2 Conditioned respiratory threat in amygdala **35**
2.1 Abstract . . . 35
2.2 Introduction . . . 36
2.2.1 Hypotheses . . . 37
2.3 Methods . . . 38
2.3.1 Materials . . . 38
2.3.2 Analysis . . . 39
2.4 Result . . . 46
2.4.1 Functional activity of the amygdala during task . . . 47
2.4.2 Functional task connectivity of the BLA seed . . . 54
2.4.3 Functional resting-state connectivity of the BLA seed . . . 56
2.5 Discussion . . . 58
2.5.1 BLA in the perceptual and freeze response to respiratory threats . . . 59
2.5.2 "Belief update" - task BLA-thalamus connectivity during resistance 60
2.5.3 Interpreting “deactivation” of BLA and its FC during task . . . 63
2.5.4 Lack of evidence for CMA’s role in breathlessness . . . 66
2.5.5 "Attention deployment" - resting-state BLA-precuneus connectivity 68
2.5.6 ‘Trait anxiety’ - resting-state BLA-temporal pole connectivity . . . 68
2.5.7 Limitations . . . 69
2.6 Conclusion . . . 70

3 Methods and pre-processing of post-COVID brain imaging data **73**
3.1 Background . . . 73
3.2 MRI scanning sequence . . . 74
3.3 Image preprocessing . . . 74
3.3.1 Anatomical data preprocessing . . . 74
3.3.2 Resting-stage functional data preprocessing . . . 74
3.4 ROIs selection . . . 76
3.4.1 ACC and insula . . . 76
3.4.2 Subcortical regions . . . 77
3.4.3 Other cortical regions . . . 78
3.4.4 Quality control of ROIs . . . 79
3.5 Group-level ICA . . . 84
3.5.1 Group ICA parcellation . . . 84
3.5.2 Subject time series for each ICA component . . . 85
3.5.3 Dimension reduction for BM . . . 85
3.6 Conclusion . . . 85

4 Characteristic of the behavioural outcomes of the post-COVID sample 87
4.1 Abstract . . . 87
4.2 Introduction . . . 88
4.3 Methods . . . 89
4.3.1 Participants . . . 89
4.3.2 Materials . . . 90
4.3.3 Analysis . . . 97
4.4 Results . . . 98
4.4.1 Basic demographic information . . . 98
4.4.2 Post-COVID outcomes . . . 103
4.4.3 Domain-based dimension reduction . . . 115
4.5 Discussion . . . 118
4.5.1 Summary . . . 118
4.5.2 Contextualising the current sample within the post-COVID population 119
4.5.3 Patient heterogeneity . . . 120
4.5.4 Stratification of post-COVID patients using non-imaging data . . . 121
4.5.5 The control group . . . 122
4.5.6 Dimension reduction . . . 123
4.6 Conclusion . . . 124

5 Node-based allostatic-interoceptive network and breathlessness post-COVID 125
5.1 Abstract . . . 125
5.2 Introduction . . . 126
5.2.1 Breathlessness in long-COVID . . . 126
5.2.2 The "anxiety hypothesis" for breathlessness . . . 127
5.2.3 Explain breathlessness using Active Inference . . . 128
5.2.4 Why resting-state . . . 129
5.2.5 Hypotheses . . . 130
5.3 Methods . . . 131
5.3.1 Subjects . . . 131
5.3.2 Questionnaires . . . 132
5.3.3 Clinical Measures . . . 132
5.3.4 Analysis . . . 133
5.4 Results . . . 135
5.4.1 Behavioural data . . . 135
5.4.2 Interoceptive networks and D-12 . . . 141
5.4.3 Interoceptive networks and BCS . . . 144

5.4.4 Role of piriform cortex . . . 154
5.5 Discussion . . . 154
5.5.1 Main findings . . . 154
5.5.2 Hypothesis 1 . . . 155
5.5.3 Hypothesis 2 . . . 155
5.5.4 Hypothesis 3 . . . 157
5.5.5 Hypothesis 4 . . . 158
5.5.6 Hypothesis 5, 6, 7 . . . 159
5.5.7 Limitations . . . 160
5.6 Conclusion . . . 160

6 Large brain networks underlying post-COVID symptom clusters 163
6.1 Abstract . . . 163
6.2 Introduction . . . 164
6.2.1 Multiple intrinsic brain networks underlying breathlessness . . . 164
6.2.2 Functional brain evidence post-COVID . . . 165
6.2.3 Research approach and objectives . . . 165
6.3 Methods . . . 166
6.3.1 Participants . . . 166
6.3.2 Analysis . . . 166
6.4 Results . . . 169
6.4.1 Summary of SMs before CCA . . . 169
6.4.2 Summary of BMs before CCA . . . 170
6.4.3 CCA results . . . 173
6.5 Discussion . . . 186
6.6 Conclusion . . . 189

7 Discussion 191
7.1 Summary of results . . . 191
7.2 Breathlessness as an affective disorder? . . . 193
7.3 Breathlessness as a functional neurological disorder? . . . 197
7.4 Distinguishing tonic and phasic breathlessness . . . 198
7.5 Reflecting on negative results . . . 199
7.6 Methodological considerations . . . 201
7.7 Final conclusion . . . 203

References 205

Appendix A Cognitron task **235**

Appendix B Breathlessness task **239**

B.1 Aversive Delay-conditioning breathlessness task 239

B.2 Breathing system 239

List of figures

1.1 Simplified illustration of Active Inference and model update during respiration 12
1.2 Hierarchical message passing and prediction error elimination in predictive coding of 'reflex breathing' . . . 15
1.3 Hierarchical message passing and prediction error elimination in predictive coding during "phasic breathlessness" . . . 17
1.4 Hierarchical message passing and prediction error elimination in predictive coding during "tonic breathlessness" . . . 19
1.5 Illustration of amygdala subnuclei . . . 23

2.1 Design matrix of subject-level GLM within FEAT . . . 41
2.2 Design matrix of task group-level GLM within FEAT . . . 43
2.3 Design matrix of subject-level resting-state GLM within FEAT . . . 46
2.4 Amygdala task response illustration . . . 49
2.5 Amygdala segmented into 9 sub-regions using Freesurfer - example of one subject . . . 52
2.6 Illustration of amygdala segmentation using Freesurfer's atlas in MNI space 52
2.7 BLA-thalamus FC during resistance and relationship to anxiety . . . 55
2.8 Mean rs-fMRI FC to the de-active seed located at the BLA . . . 57
2.9 Regions where rs-fMRI FC to the BLA seed scaled with intensity rating scores 58
2.10 Whole brain activation during conditioned breathlessness task . . . 61

3.1 Illustration of the PAG seeds . . . 78
3.2 Seed choice of insula regions based on atlas and coordinate-derived spheres 81
3.3 Improvement of tSNR after FIX+PNM pre-processing . . . 83

4.1 Cognitron tasks . . . 95
4.2 Heatmaps of all raw question/task items . . . 104
4.3 Heatmaps of all subscales . . . 106

4.4 Correlations between demographic and clinical characteristics and COVID-19 outcomes . . . 108
4.5 Boxplot of domain means by group . . . 109
4.6 Scatter plot of Neighborhood Component Analysis . . . 111
4.7 K-Means Clustering and distribution among clinical groups . . . 113
4.8 Scatterplort of K-Means Clusters and loadings . . . 114
4.9 Domain-based PCA:Cumulative Explained Variance for 11 domains . . . 115

5.1 Boxplot of spirometry data . . . 136
5.2 Correlations of demographic and clinical information with D-12, BCS and GAD-7 . . . 138
5.3 Heatmap of D-12 regression coefficients for all edges . . . 143
5.4 Heatmap of BCS regression coefficients for all edges . . . 145
5.5 Scatterplot and 5-fold cross-validation test for regressing dPAG-PoI1 FC on BCS . . . 147
5.6 Scatterplot of dPAG-PoI1 regression on BCS adjusted for anxiety or severity 148
5.7 Effect of ventilator use during the acute phase on the regression of dPAG-PoI1 on BCS . . . 149
5.8 Scatterplot and 5-fold cross-validation test for regressing BLA-dACC FC on BCS . . . 151
5.9 Scatterplot of BLA-dACC regression on BCS adjusted for anxiety or severity 152
5.10 Effect of ventilator use during the acute phase on the regression of BLA-dACC on BCS . . . 153

6.1 Clustered heatmap of 11 SMs . . . 170
6.2 Connectomes of Group ICA100 nodes on group average . . . 172
6.3 Clustergram of Group ICA100 nodes . . . 173
6.4 Heatmap of top 3 modes' weights and correlations to SM features . . . 175
6.5 Mode 1 Connectomes illustration . . . 177
6.6 Scatter plot of BM and SM weights for Mode 1 . . . 178
6.7 Mode 2 Connectomes illustration . . . 180
6.8 Scatter plot of BM and SM weights for Mode 2 . . . 181
6.9 Mode 3 Connectomes illustration . . . 183
6.10 Scatter Plot of BM and SM Weights for Mode 3 . . . 184
6.11 Scatter Plot of BM and SM Weights for all 3 modes with breathlessness scores 185

7.1 Schematic illustration of possibly neural disruptions in post-COVID tonic breathlessness . . . 195

B.1 Breathing system used for administering hypercapnic challenges. 240

List of tables

2.1 Summary of conditioned breathlessness task maxima within the amygdala . 48
2.2 Summary of mask sizes after amygdala segmentation 51
2.3 Summary of one sample t-test for 9 amygdala sub-regions 53

3.1 Information about ROIs identification 79
3.2 Volume and voxel number for each ROI 82
3.3 Percentage increase in tSNR for each ROI 84

4.1 Summary of subscales, their explanations, and corresponding domains for most items. 96
4.2 Summary of main demographic and clinical characteristics 100
4.3 Occupation, Income, and Education by Group 102
4.4 Principal components and variance explained for each Domain 116
4.5 Top 4 tasks of the principal components of objective cognitive impairment . 118

5.1 Demographic Information of Participants 132
5.2 Information about ROIs identification 133
5.3 Correlation between Post-COVID outcome and Clinical/Demographic Variables 141
5.4 Top ten edges with the highest coefficients where D-12 was regressed . . . 142
5.5 Top ten edges with the highest coefficients where BCS was regressed 146

6.1 Canonical Correlation Analysis (CCA) results 174

Chapter 1

Introduction

Preface

This thesis represents work conducted during my DPhil studies, a period shaped by the unprecedented challenges of the SARS-CoV-2 (COVID-19) pandemic. With most laboratory research suspended except for COVID-related studies in 2020 and 2021, I adapted my original proposal, shifting from behavioural experiments to a 7-tesla (7T) functional Magnetic Resonance Imaging (fMRI) study investigating resting-state brain mechanisms underlying post-COVID symptoms. During the lockdown, I took on recruitment and data collection responsibilities of the COVID study, while re-analysed a historical task fMRI dataset with a particular focus on the amygdala, a project intended to develop comprehensive MRI analysis skills alongside completing the MRI graduate course.

The following chapters are composed over two topics. The first (Chapter 2) investigates the functional and connectivity characteristics of the amygdala's subnuclei in the expression phase of conditioned breathlessness among healthy individuals. The second subsumed the focus to encompass the entire allostatic-interoceptive respiration network (Chapters 3, 4, 5) and large intrinsic networks (Chapter 6) during rest in post-COVID patients. This shift reflects both the adaptive nature of my research in response to the pandemic and the opportunity to explore complementary aspects of emotion, breathlessness, and brain networks. Importantly, the research questions and discussions are informed by a novel theorisation of reflex breathing, phasic breathlessness, and tonic breathlessness, grounded in active inference theories and the 'Bayesian brain' hypothesis.

Together, these sections bridged the theoretical (active inference of breathing regulation and perception) and mechanistic (specific brain regions) aspects of respiration perception, and added to the literature of understanding of higher-order affective circuitry's role in respiration perception.

1.1 Abstract

This chapter addresses the complex phenomenon of breathlessness, providing an overview of the empirical evidence and theoretical foundations underpinning its neural mechanisms. It introduces a conceptual framework based on Active Inference [125, 311, 310], highlighting the 'action-perception' cycle within the respiratory system and its mechanistic and biological foundation of Embodied Predictive Interoception Coding (EPIC) model. This framework serves as a cohesive theoretical basis for understanding reflex breathing, phasic and tonic breathlessness.

The chapter also includes literature reviews on two primary research areas: (1) current findings from animal and human studies regarding the role of amygdala subnuclei in respiratory regulation and perception; and (2) evidence of functional brain network alterations underlying neurophysiological symptoms in post-COVID patients.

Building on this foundation, the chapter proposes a research roadmap that investigates the roles of the amygdala, the intrinsic allostatic–interoceptive (allo-intero) network, and large-scale intrinsic networks, drawing on brain imaging data from healthy individuals and post-COVID patients. It hypothesises that specific nuclei within the amygdala, along with the top-down regulatory (visceromotor) and bottom-up perceptual (interoceptive) pathways of the allo-intero network, are critical in shaping the perception of breathlessness, and that these insights may extend to other interoceptive experiences reflected in whole brain large networks, such as the neurophysiological symptoms post-COVID.

By enhancing our understanding of the neural mechanisms underlying breathlessness, this thesis seeks to provide deeper insights into the fundamental processes that shape this complex and debilitating experience.

1.2 Introduction to the clinical condition of breathlessness

Respiration stands out among physiological processes due to its unique reliance on a broad neural network in the brain, rather than being governed solely by reflex arcs or pacemaker cells, as seen in the heart. This reliance on complex neural mechanisms can become metabolically expensive, particularly when gas-exchange cannot be regulated at the level of simple reflex arcs. The very evolution of the respiratory system into a sophisticated neural architecture that enables flexibility and context-sensitive regulation also introduces significant challenges in addressing its dysfunctions.

Breathlessness is a highly debilitating yet understudied experience, observed trans-diagnostically in conditions such as asthma, chronic obstructive pulmonary disease (COPD),

congestive heart failure, terminal cancer, and panic disorders [153, 183, 368]. It is also a hallmark symptom of acute COVID-19 and persists post-discharge in nearly half of affected patients [155, 227]. Furthermore, breathlessness is a strong predictor of poor quality of life [43], a more reliable indicator of adverse prognosis in cardiorespiratory illnesses than objective physiological markers (e.g., forced expiratory volume in one second [FEV1] in COPD) [258, 3, 87], and predicts all-cause mortality in the general population in a severity-dependent manner [118, 129].

In the context of long COVID, respiratory dysfunctions are among the most commonly reported symptoms. These symptoms, often described as 'shortness of breath', dyspnea, or breathlessness—whether or not accompanied by oxygen dependence or fibrotic lung damage—are estimated to affect 20% to 50% of patients at 60 to 100 days of follow-up [136, 47, 55, 156], and reported in more than half of post-ICU discharged patients at a 90 days follow-up[134]. Persisting breathlessness after more than a year is not uncommon [308, 303]. Of note, evidence for structural or functional pulmonary impairments at the lung in these cases remain preliminary. Many patients suffering from post-COVID breathlessness showed normal or near-normal results in conventional pulmonary function tests [245, 388]. Despite its prevalence and the profound debilitating consequences it has on physical activity, quality of life, and psychological well-being [227, 155], its underlying mechanism remains poorly understood.

The discordance between subjective perceptions of breathlessness and objective measures of pulmonary obstruction [175, 22, 345] is not unique to long COVID. This phenomenon, 'breathlessness with an unclear cause or that appears disproportionate to underlying causes[182]', is particularly pronounced in asthma and COPD patients described as "difficult-to-treat," who exhibit limited responsiveness to conventional pharmacological interventions and may benefit from psychophysiological rehabilitation strategies such as "breathing retraining" [159]. Moreover, breathlessness is reported in up to 16% of healthy individuals without any apparent dyspnoea-inducing conditions, as evidenced by a "low-risk" subgroup analysis from a 15-country population study [149]. In fact, "medically unexplained symptoms," including breathlessness, are prevalent in primary care settings, accounting for an estimated 15% to 35% of cases [277]. Collectively, this complex phenomenon has been variously termed in the literature, including "complex dyspnoea" [182, 181], "dysfunctional breathlessness" [330], "intractable or refractory breathlessness" [37], and "medically unexplained breathlessness" [159] in different context. For a comprehensive overview, Hull and Haines [182] provide an in-depth examination of recent developments and challenges in research and clinical practice in their 2022 monograph, *Complex Breathlessness*, published by the European Respiratory Society.

Recent research has emphasised the multidimensional nature of breathlessness, encompassing physiological, cognitive, contextual, and affective dimensions [169, 212]. The subjective experience of breathlessness is shaped by factors such as anxiety, attention, interoception, and beliefs about breathing-related cues, often operating independently of measurable pulmonary function [114, 357, 166, 229]. Notably, these factors do not merely additively contribute to the ultimate subjective experience of breathlessness but interact in complex ways. Recently, the "Bayesian brain" hypothesis [64, 128, 225] has gained significant traction in explaining breathlessness perception, often described as an "inferential leap" in respiratory research [357, 112]. According to this hypothesis, higher-order constructs such as anxiety modify prior expectations or incoming sensory information, influencing perception and increasing susceptibility to symptom misinterpretation. This theoretical framework will be explained in detail in Section 1.4.

This thesis specifically focuses on the affective dimension of breathlessness, particularly anxiety. However, the implications extend beyond affect alone, as processes such as attentional, cognitive, and contextual information share similar neural cortico-limbic pathways. These shared pathways may also contribute to the manifestation of other psychophysiological symptom expressions, such as fatigue, depression, cognitive disruptions, as observed in populations with long COVID.

Issues of definition Finally, it is essential to acknowledge the lack of a definitive standard for distinguishing between "maladaptive" or over-perception of breathlessness and adaptive breathlessness, particularly in clinical populations with varying degrees of pulmonary obstruction. Of note, "under-perception" of breathlessness, where the increased effort in breathing and associated affective arousal are not adequately recognised, is not uncommon. This under-report can lead to serious consequences, such as delays in seeking medical attention, increased risk of undertreatment, and potentially avoidable mortality [25].

It is unclear whether individuals reporting higher breathlessness symptoms, currently labelled as exhibiting maladaptive breathlessness, represent a normal response that only appears more severe when compared to a reference group of "under-perceivers". To address this ambiguity, this introductory chapter includes a theoretical section that proposes a person-centred definition of maladaptive breathlessness from an information-processing perspective, utilising the Active Inference framework (Section 1.4). This framework offers a theoretical foundation for understanding gas-exchange inference by integrating respiratory regulation with perceptual processes. Prior to introducing this framework, the affective component of breathlessness will be examined.

1.3 The affective processes and breathing

There are two lines of research examining the relationship between respiration and affective processes in higher-order cortical, limbic, and paralimbic regions. The first line of research investigates why breathlessness is perceived as more debilitating in certain individuals, as discussed in the context of breathlessness symptom burden [85, 35] in clinical populations. This perspective treats the experience of breathlessness as a modality of perception, akin to pain. It inherently focuses on the evaluative aspect of perception and is often conceptualised and operationalised as an overall self-reflection on respiratory efficacy over a period of time.

The second line of research explores how the act of respiration recruits affect-related higher-order circuitries during each inspiration-expiration loop [19]. In this context, respiration is treated as an action, with breathlessness conceptualised as a functional phenomenon. This perspective emphasises the emergence of emotions, such as anxiety or fear, as a consequence of interoception (e.g., CO_2-O_2 exchange and blood pH levels) [69], rather than as a cause. This interpretation aligns with the constructed emotion theory, as recently proposed by Barrett and colleagues [26].

These two avenues, one focusing on the influence of anxiety on respiratory perception and the other on the impact of respiratory regulation on affective processes, highlight complementary perspectives on the interplay between respiration and higher-order functions. The following sections will review evidence from both perspectives.

1.3.1 Anxiety affecting breathing perception

The role of affective processes in respiratory perception, breathlessness, particularly, has been extensively supported by prior cohort research, empirical studies and interventional research[178, 72, 52, 319, 21, 327, 165, 188, 240, 85, 35]. In cross-sectional samples, variables such as trait anxiety, anxiety sensitivity, dyspnoea-specific anxiety, suffocation fear, air hunger, and perceptions of inescapability [319, 21, 327, 165] have been shown to correlate with the burden of breathlessness symptoms, independent of objective disease markers.

In experimental settings, these affective dimensions were suggested to influence the extent to which individuals perceive respiratory difficulties during loaded breathing tasks [188] and exhibit varying degrees of predictive power to the over-perception of breathlessness [240]. In addition, the causal relationship between anxiety and breathlessness has been recognised as bidirectional and may represent a "dyspnea-anxiety-dyspnea cycle" [257, 21], which echo with the second line of affection-respiration research that will be elaborated later.

With regard to interventional studies, research by Abdallah and colleagues [2] demonstrated that, in both patients with chronic breathlessness treated with morphine and healthy

individuals administered remifentanil, slight declines in mood, characterised by increased anxiety or depression, were associated with reduced efficacy of opioid treatment for breathlessness relief. This finding suggests a potential causal relationship, wherein worsening symptoms of depression or anxiety diminish the therapeutic benefits of opioids in managing breathlessness. Pulmonary rehabilitation, a well-established intervention for chronic obstructive pulmonary disease (COPD) [237], provides additional evidence regarding the affective dimensions of breathlessness. While this intervention reliably enhances patients' self-reported well-being. It does so without improving lung function [48]. These improvements are thought to be mediated by reductions in negative emotional states, as observed in related studies [363].

Collectively, these findings suggest that breathlessness in some individuals may arise less from direct physiological dysfunction and more from the way individuals process and respond to breathing-related sensations.

1.3.2 Breathing regulation affecting affective state

The involvement of higher-order processes, or the brain, in spontaneous breathing has been a subject of inquiry since ancient Greek times, when a "respiratory control centre" was searched for [119]. In later periods, scientists identified the brainstem as the primary site responsible for respiratory rhythmicity[7]. Subsequently, the discovery of the preBötzinger Complex (preBötC) within the brainstem as a respiratory "pacemaker" in animals further advanced our understanding of breathing regulation[322, 19].

Advancements in research methods, such as neuroimaging and electrophysiological techniques, have revealed the involvement of higher-order cortical regions in respiration. The first line of evidence comes from direct stimulation studies, which demonstrate that stimulation of the motor cortex elicits diaphragmatic contractions[135]. Of interest, stimulation of limbic and insular regions, including the amygdala, hippocampus, and insula, also influences respiratory rate[130, 164, 193, 10]. These suggest both sensorimotor pathways and affective cortico-limbic circuitry are involved in the regulation of breathing [102].

Additional evidence arises from electrophysiological recordings, such as electroencephalography (EEG). Voluntary breathing was found to activate regions including the motor cortex, premotor cortex, and supplementary motor cortex[133, 360]. Furthermore, rhythmic oscillations of breathing cycles have been consistently linked to the well-documented theta rhythm (6 to 10 Hz) observed in the brain. During wakefulness, the hippocampus exhibits neuronal activity oscillating at the theta frequency, a phenomenon observed across multiple species, including humans[46, 53]. The theta rhythm is closely associated with cognitive

functions such as memory and decision-making, and it is suggested to support multimodal signal integration in neurons[62, 192].

Human studies further underscore the role of natural breathing patterns in synchronising neural oscillations. Zelano and colleagues[380] demonstrated that nasal breathing synchronises neural activity across regions such as the hippocampus and amygdala, which are known to be critical for emotional processing. Notably, this synchronisation diminishes during mouth breathing, suggesting the importance of olfaction input in respiration's modulatory role in the whole brain function.

This line of research collectively suggests that a broader brain network, particularly regions involved in cognitive and affective processing, is intricately coordinated within each respiratory cycle. These regions operate between the pacemaker in the brainstem and the execution of muscle contraction directed by the motor cortex. The complex interactions within this "black box"—linking the brainstem and motor cortex—may underpin the bidirectional relationship between respiration and affective processes, forming the central focus of this thesis.

1.3.3 Summary of the two lines of affection-breathing research

The two lines of research diverge due to differences in conceptual focus, methodologies, and theoretical underpinnings. Path 1 conceptualises respiration as a passive sensory experience influenced by affect, whereas Path 2 regards respiration as an active physiological process that may give rise to affect. This fundamental disconnect hinders their integration, as each operates within a distinct paradigm. Bridging this gap would require reconciling subjective perceptual research with objective neuroscientific approaches. Of note, research on breathlessness [169, 212, 175, 22, 345, 182] often aligns with the conceptual framework of Line 1. However, this perspective risks adopting a reductionist approach by treating respiration merely as a modality of perception, thereby neglecting the dynamic interplay within the action-perception loop.

This reductionist perspective, as noted in Line 1, is further exemplified by the 'dyspnoea–anxiety–dyspnoea cycle', which treats the affective and interoceptive networks as independent constructs, each acting as both cause and effect of the other. However, assuming an independence between the affective and interoceptive systems is problematic, given their substantial overlap in neural substrates, particularly within the limbic regions. The interplay between interoceptive processes and emotion is well-documented, with respiratory sensations potentially representing a primitive form of affect [19]. This aligns with contemporary theories of emotion, such as Barrett's Theory of Constructed Emotion [26], which posits that emotions are not innate, pre-programmed responses to specific stimuli, but are instead

constructed in the moment by the brain, drawing upon sensory input (e.g. cardiorespiratory signals), prior experiences, and conceptual knowledge.

The tendency in Line 1 to treat affective processes as external influences on perception reflects a limited understanding of interoception and brain–body integration. Furthermore, this perspective risks perpetuating stigma by framing individuals with "maladaptive" breathlessness as simply "overreacting" or misinterpreting their sensations. In the following section, I propose a unified theoretical framework to reconcile these two lines of research, conceptualising emotion, such as respiration-associated anxiety, through the lens of the action–perception loop.

1.4 Theoretical framework

Having introduced the clinical phenomenon of breathlessness that is discordant with airway obstruction, it is important to acknowledge that the definition of "maladaptive breathlessness" remains elusive and context-dependent, varying according to the reference population. Additionally, I have reviewed evidence on two lines of research on how affective processes relate to the perception of respiration (Line 1) and its regulation (Line 2). The theoretical framework provided here aims to crystallise these issues and establish a foundation for the empirical chapters that follow in this thesis.

1.4.1 Breathlessness under the "Bayesian brain" framework

The traditional understanding of perception is grounded in a “stimulus-response” framework, which assumes that organisms, such as the human brain and body, passively await external signals and respond subsequently. Building on Helmholtz’s concept of unconscious inference [172] and its reformulation through the “Bayesian brain” hypothesis [90], the past two decades have shifted this perspective towards understanding the brain as a statistical inference organ [125, 126, 64, 336]. According to this view, the brain actively constructs explanations for incoming stimuli by forming and testing hypotheses against sensory inputs.

This predictive coding process involves updating prior information (top-down predictions) about the most likely causes of sensations using sensory stimuli (bottom-up evidence). From this interaction, "Bayesian surprise" is generated and subsequently utilised to refine the generative model for future predictions. The generative model serves as a proxy for the hidden states of the actual world that the organism inhabits. This theoretical framework offers a probabilistic approach to updating beliefs (posterior distributions) based on prior expectations and sensory prediction errors.

Recent research on breathlessness has employed a Bayesian brain or predictive coding theoretical framework [357, 112]. Breathlessness that is perceived discordantly with pulmonary function is thought to reflect an over-reliance on the brain's priors in shaping respiratory perception [229]. Negative emotional states or catastrophising tendencies are suggested to act as modulatory factors, exacerbating this bias by increasing the precision (or confidence) of these priors. It is also postulated that this top-down influence can become particularly pronounced due to the nature of weak and ambiguous visceral sensory signals. For example, during states of anxiety, faint respiratory sensations that might ordinarily be dismissed can become amplified, leading to the perception of breathlessness [229]. However, this perspective remains preliminary and may oversimplify the complexities of breathlessness for several reasons.

First, the hypothesis lacks mechanistic evidence identifying the specific brain regions or neural pathways that support it. Second, it conceptualises affective states—such as anxiety, fear, or negative affectivity—as external modulators of breathlessness perception, rather than as integral components of the allostatic and interoceptive loop. This limitation parallels the issue raised in Path 1 of affective-respiratory research, as discussed in Section 1.3.1. Given the substantial overlap between the interoceptive (and allostatic) network and brain regions involved in affective processing—particularly within the limbic system—this distinction is overly simplistic.

Third, the framework treats breathlessness as a static perceptual phenomenon, akin to vision or hearing. Unlike classical examples of Bayesian inference in vision—such as visual illusions where perceptual inference updates beliefs (e.g., interpreting an ambiguous image as either a rabbit or a duck due to bias of the prior)—the perception of respiration is inherently dynamic. It undergoes continuous updates with each respiratory cycle. Importantly, respiration's primary function is not merely to update beliefs or form perceptual representations but to maintain homeostasis. For example, an updated belief such as, "there is a high level of CO_2 in my blood," cannot suffice in isolation. Instead, respiration actively regulates physiological parameters, ensuring they remain within the narrow range required for survival.

This interplay between perception and action forms a causal loop, where each serves as both a cause and an effect of the other. Consequently, it is insufficient to discuss respiratory perception without simultaneously addressing its regulatory component. Future research must consider this dynamic and integrative perspective to advance our understanding of breathlessness.

1.4.2 Active Inference as a more appropriate theory for respiration

Active Inference [125] extends the Bayesian brain hypothesis and predictive coding frameworks by incorporating action into the minimisation of prediction errors. This theory posits that organisms do not merely passively update their beliefs but actively engage in behaviours that align sensory inputs with internal predictions. Perception and action are thus conceived as complementary processes, both aimed at minimising surprise[1] [310, 309].

In this thesis, I will refer to these two types of inference as "perceptual inference" and "active inference"[2]. "Perceptual inference" achieves this by updating beliefs in a Bayesian fashion, thereby aligning internal models with sensory input. Conversely, "active inference" operates by changing the sampling of the sensory evidence, through actions, to match existing beliefs and goals. These inferential processes may operate over slower timescales, where "perceptual inference respond to habituation and "active inference" corresponds to learning. Together, they enable a gradual adaptation of beliefs and behaviours to reduce long-term surprise.

The inclusion of the action component is especially vital in understanding the interoceptive and allostatic domains, respiration included. In these domains, beliefs or priors are not merely beliefs to be freely updated; rather, they are constrained by the organism's homeostatic imperatives. Active Inference offers a more suitable theoretical model for understanding respiration. It captures the dynamic interplay between perception and action inherent in gas exchange, while also suggesting a unified neural architecture for both respiratory perception and control.

In the following subsections, I apply the Active Inference framework to examine how respiratory inference maintains and updates its internal "model of world" in relation to gas exchange. Furthermore, I re-conceptualise the distinctions between reflexive breathing, breathlessness, and its maladaptive forms.

Model updates during dynamic respiratory regulation and perception

Two key definitions

> 'Every good regulator of a system must be a model of that system' ([65], p. 89).

[1] Or, equivalently, free energy [125]

[2] In cybernetic terms, following Seth [309], the process here described as "active inference" is termed epistemic active inference, while "perceptual inference" is referred to as instrumental active inference. More precisely, this pertains to leveraging predictive models to exert control over sensory variables. However, for clarity and to avoid unnecessary jargon, the simplified terms "active inference" and "perceptual inference" are used throughout this thesis.

To examine how homeostasis and allostasis in gas exchange (respiration) are governed within the active inference framework, it is essential first to clarify two key definitions: (1) the boundary between the internal system and the external "world", and (2) the hidden "world" and its generative model.

First, I define the central nervous system (CNS) as the internal system from which inferences are made, while the rest of the body and the entire external environment constitute the external "world" [11]. This boundary[3] is drawn arbitrarily; it could be positioned differently, such as between the combined body and brain and the external environment, or between the brainstem and the remainder of the brain, body, and environment. Each delimitation offers a distinct perspective on the process. The choice of placing the boundary at this point is to constrain the discussion of maladaptive breathlessness to the CNS, not environmental or peripheral disruptions.

Second, the collective parameters and knowledge of the external world (e.g., the efficiency of exchanging of CO_2 for O_2 at the alveolar level or the oxygen demand during weightlifting) represent the "world" for gas exchange, which is hidden from the organism (in this case, the CNS). The organism aggregates evidence of the "world" through respiratory activity, which develops and sustains the generative model of gas exchange in the "world" it inhabits. The generative model held by the CNS is, therefore, an approximation of the true model of the "world".

The following section reconceptualises respiration regulation and perception within the framework of Active Inference, under these two aforementioned definitions. In this model, the viable ranges of parameters (such as chemoreceptor signals corresponding to pH levels, CO_2 concentrations, etc.) are established as priors, which are then tested against interoceptive, proprioceptive, and somatosensory observations, within each gas-exchange cycle. As illustrated in the schematic in Figure 1.1, this process demonstrates how signals are integrated during breathing and how the model is updated in response to any disturbances.

[3] Markov blanket [125]

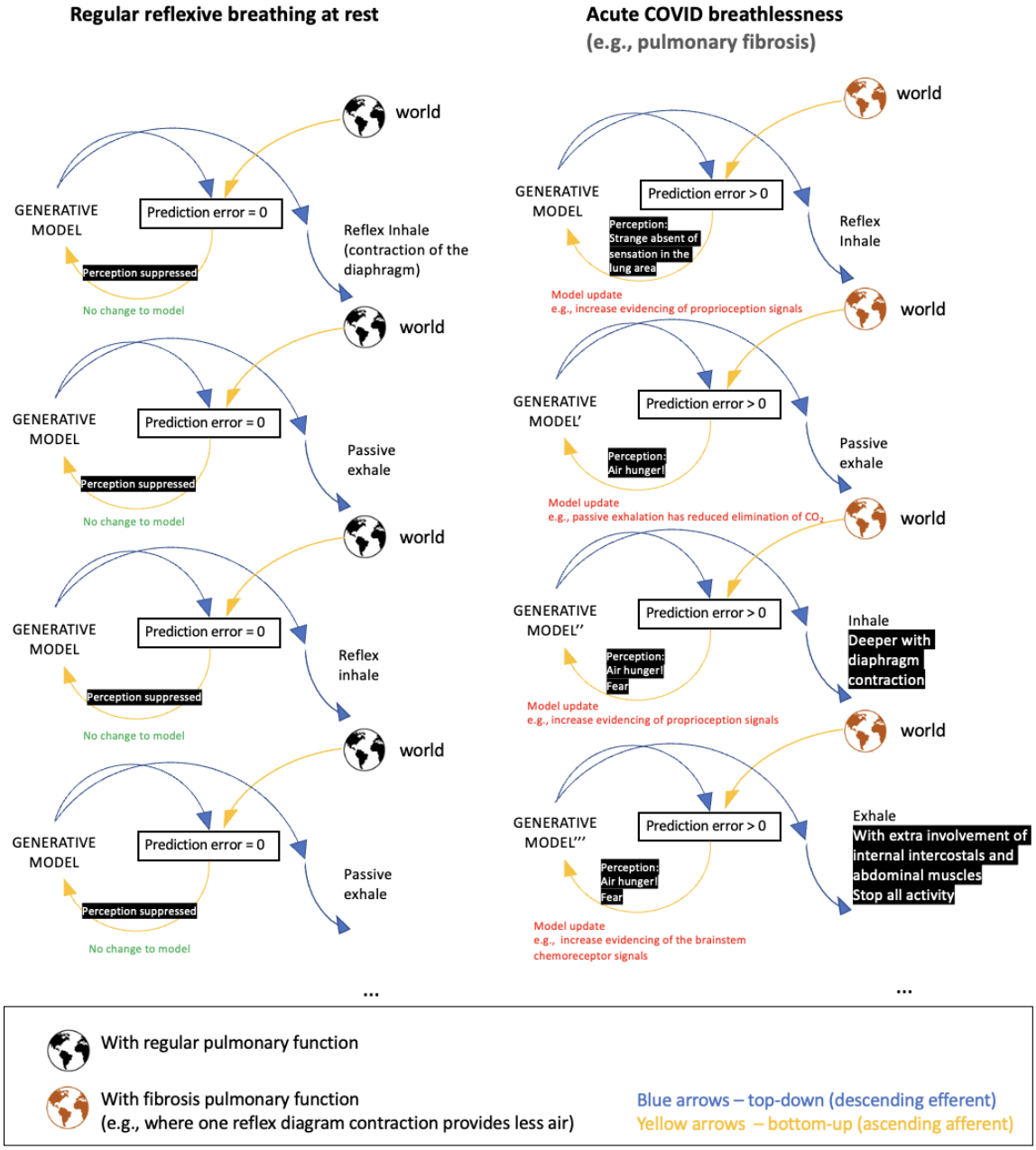


Fig. 1.1 Simplified illustration of active inference and model update during respiration, in both regular reflexive breathing (left) and in a state of breathlessness (right) in response to changes in the external 'world,' exemplified by the onset of acute COVID-19 infection. Blue arrows represent top-down prediction and action signals, while yellow arrows denote bottom-up sensory signals, including visceral, proprioceptive, and exteroceptive afferents. During natural breathing at rest (left panel), respiration is governed entirely by reflex arcs, with no prediction error arising between the action (inhalation or exhalation) and the sensory feedback from the external "world" (i.e. a world of a healthy human lung living on earth). Consequently, there is no requirement for Bayesian model updating. However, when natural gas exchange is disrupted (right panel), such as by fibrosis during acute COVID-19 infection, the same reflexive actions no longer elicit corresponding sensory inputs. This discrepancy generates a prediction error, prompting updates to the Bayesian model and adjustment of the inhale-exhale actions. Perception of breathlessness emerges - which may signal a 'danger state,' indicating that physiological adaptation alone is insufficient. Conscious intervention may then become necessary, such as ceasing activity, opening a window, or seeking medical attention.

As shown in the left panel of Figure 1.1, during simple reflexive breathing, each inhalation and exhalation generates sensory outcomes that almost precisely match the predictions made by the brain's generative model. As there is no prediction error, the model of the gas-exchange "world" remains stable (symbolised by the default black "earth" icon in the figure), and the cognitive and emotional perception of respiration is suppressed (not noticeable or salient).

As shown in the right panel of Figure 1.1, disturbances to the "world", such as engaging in an unfamiliar sport or experiencing acute COVID-19 accompanied by pulmonary fibrosis (restricted lung function), disrupt this equilibrium. In such scenarios, the external "world", symbolised by the red "earth" icon in the figure, is new and initially hidden from the organism. Prediction errors arise. For instance, an inhalation following the usual reflex arc would fail to generate the expected sensory feedback due to lung restriction during acute COVID infection. Similarly, a default passive exhalation may fail to eliminate elevated levels of CO_2, such as during weightlifting for novices, where increased metabolic activity leads to greater CO_2 production. During this stage, there might be cognitive realisation of discomfort, such as a "weird" chest sensation or feeling of air hunger.

To mitigate prediction errors, actions may be employed to restore congruence between predictions and sensory outcomes. For instance, more effortful expiration may enhance CO_2 elimination; deliberate deeper and diaphragmatic inhalation could be used to increase O_2 intake in one inhalation. Alternatively, instead of, or in addition to, engaging in compensatory actions, individuals may update their prior beliefs regarding respiratory efficiency to a certain extent, effectively "bearing with" reduced levels of O_2 intake or CO_2 elimination. Such passive adaptation may correspond to a pathological state characterised by diminished responsiveness and a restricted behavioural repertoire—a "disease mode" of reduced action. I argue that this may correspond to clinical manifestations such as chronic fatigue and depression [27].

By resolving prediction errors in each gas-exchange cycle, the generative model is iteratively updated to more accurately reflect the hidden states of the external world (represented as the red "earth"). I argue that the ability, and the policies available, to update the generative model in accordance with the new model of the "world" may vary across individuals. This forms the basis for the distinction I propose between adaptive phasic breathlessness and maladaptive tonic breathlessness in the next Section. Furthermore, I suggest that the ultimate aim of this process is to establish a new set of respiratory motor commands that operate reflexively again, without the need for cognitive or emotional involvement. In the example illustrated in Figure 1.1, these updates remain incomplete after two respiratory cycles and may require additional time to fully adapt to the altered gas-exchange dynamics—or may necessitate external ventilatory support. This reasoning underpins the hypothesis of a hierar-

chical architecture within the CNS, in which prediction errors are resolved and propagated across multiple levels, also elaborated in the next Section.

1.4.3 Reconceptualising reflex breathing, phasic and tonic breathlessness

This section addresses the issue of blurred definitions concerning respiratory function and perception, as discussed in Section 1.2. I propose a reconceptualisation of three distinct states—regular (reflexive) breathing, adaptive (phasic) breathlessness, and maladaptive (tonic) breathlessness—through the lens of Active Inference. My hypothesis posits that the critical differences between these states lie in the hierarchical level within the human nervous system at which prediction errors are resolved.

Reflex Breathing

Firstly, we consider the optimal "healthy" state to be one in which spontaneous breathing occurs effortlessly, whether at rest or during task engagement. This represents the simplest regulatory loop, governed by arc reflexes. As illustrated in the left panel of Figure 1.1 and Figure 1.2 shown below.

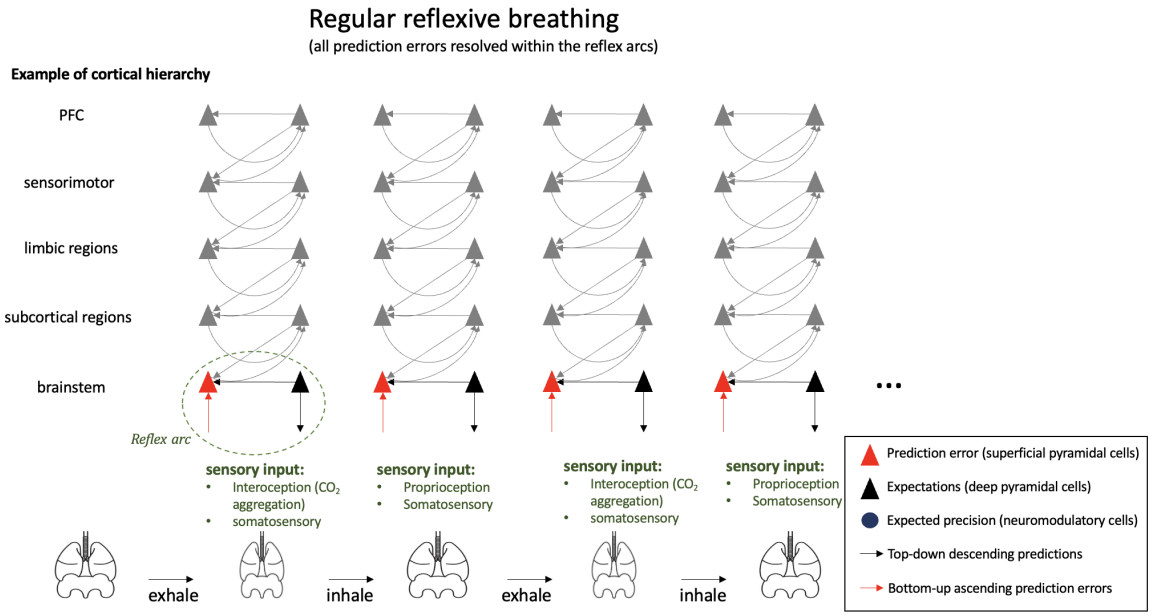


Fig. 1.2 This schematic illustrates the alternating dynamics of inspiration and expiration, each occurring within a simplified cortical hierarchy, characterised by ascending prediction errors and descending predictions. The minimisation of prediction error relies on recurrent neuronal interactions across various levels of the cortical hierarchy. In the case of effortless, regular reflexive breathing, prediction error is resolved within a single inhalation/exhalation cycle, without propagating to higher-order cortical regions. It is hypothesised that superficial pyramidal cells (red triangles) compare expectations at each hierarchical level with top-down predictions from deep pyramidal cells (black triangles) at higher levels, as reviewed in [28]. Neuromodulatory gating or gain control (represented in dark blue), potentially involving projections from the ventral tegmental area (VTA) and substantia nigra (STN), indicates the weight assigned to prediction error based on expected precision. This figure is adapted from Seth and Friston [311].

In reflexive breathing, prediction errors are minimised within each reflex arc at the lowest level of the cortical hierarchy—the brainstem. No prediction errors propagate to higher levels of the hierarchy, resulting in the attenuation of any conscious perception of respiration. Unless specifically prompted, an individual would not be aware of the ongoing process of gas exchange.

Adaptive phasic breathlessness

Secondly, we consider an adaptive, phasic breathlessness state in which effective regulatory strategies are recruited when regular reflexive breathing fails to eliminate prediction errors. This state represents an adaptive learning phase, wherein prediction error minimisation strategies work toward the global objective of correctly updating the generative model—namely,

reducing the discrepancy between the internal model of gas exchange and the hidden states of the new "world". This discrepancy shall be reduced incrementally, either approaching zero or stabilising at a non-zero minimum constrained by biological limitations (e.g., leading to death if unresolved). For example, during weightlifting, active exhalation constitutes an adaptive strategy, whereas hyper-inhalation may be maladaptive, as the primary physiological challenge lies in elevated CO_2 production rather than oxygen limitation.

We further hypothesise that within this phasic breathlessness state, the locus of prediction error resolution gradually shifts from higher-order cortical regions back to lower-level neural structures, effectively re-establishing reflex arcs and relieving the metabolically costly engagement of higher-order cortices. A novice may experience breathlessness more intensely—both cognitively and affectively—while an experienced athlete may be able to unconsciously recruit appropriate exhalation patterns to compensate for increased CO_2 production, rendering the response largely reflexive.

As illustrated in Figure 1.3, when first encountering a new "world" of gas exchange, prediction errors pass beyond the reflex arc in the brainstem and propagate across the cortical hierarchy[4], including subcortical structures (e.g., the periaqueductal grey [PAG]), limbic regions (e.g., the amygdala, anterior cingulate cortex [ACC], and insula), and the sensorimotor and prefrontal cognitive cortices. These unsuppressed prediction errors result in heightened awareness or alarm, signalling the salience of the situation, just like the novice weightlifters or some acute COVID patients. Crucially, they serve to motivate volitional regulation (e.g., deepening the inspiration, suppressing fear responses, or recruit abdominal and intercostal muscle for expiration) and decision-making (e.g., using a ventilator), with the goal of returning gas-exchange activity to the metabolically minimal reflexive style. This process involves a subsequent update of the generative model for the new "world", or a decision to revert to the old "world" (e.g., by ceasing exercise).

Updating the generative model for gas exchange is, in essence, a learning process, which may occur on different timescales. For example, a novice swimmer may take a year to learn to regulate breathing effortlessly and reflexively (with one quick inhalation followed by a prolonged, smooth expiration underwater) during long-distance swimming. Conversely, a person may only require several cycles of breathing to be able to breath effortlessly when wearing a mask.

Notably, I propose that feelings such as the fear of suffocation may commonly arise but are not necessary. For instance, an experienced swimmer may respond differently to the same level of deviation from anticipated sensory consequences (e.g., an accumulation

[4]This is an oversimplification of the hierarchy for respiratory interoceptive processes. The exact regions and their relationships are shown for illustration purposes.

of CO_2) compared to a novice swimmer. A novice may be more prone to an emotional response, potentially leading to the decision to cease the activity. This response is not necessarily maladaptive, as novice swimmers have yet to master volitional regulation of breathing in this context. In contrast, an experienced swimmer may intentionally suppress the amygdala response, achieving relatively autonomous breathing after several cycles of volitional breathing with intentional motor control (e.g., exhalation facilitated by active contraction of abdominal and intercostal muscles). This suppression may be mediated by neuromodulatory cells that reduce the precision of prediction errors. Such a process is depicted in Figure 1.3, where the round dark blue cells with a negative sign appear after the first inhalation and second exhalation.

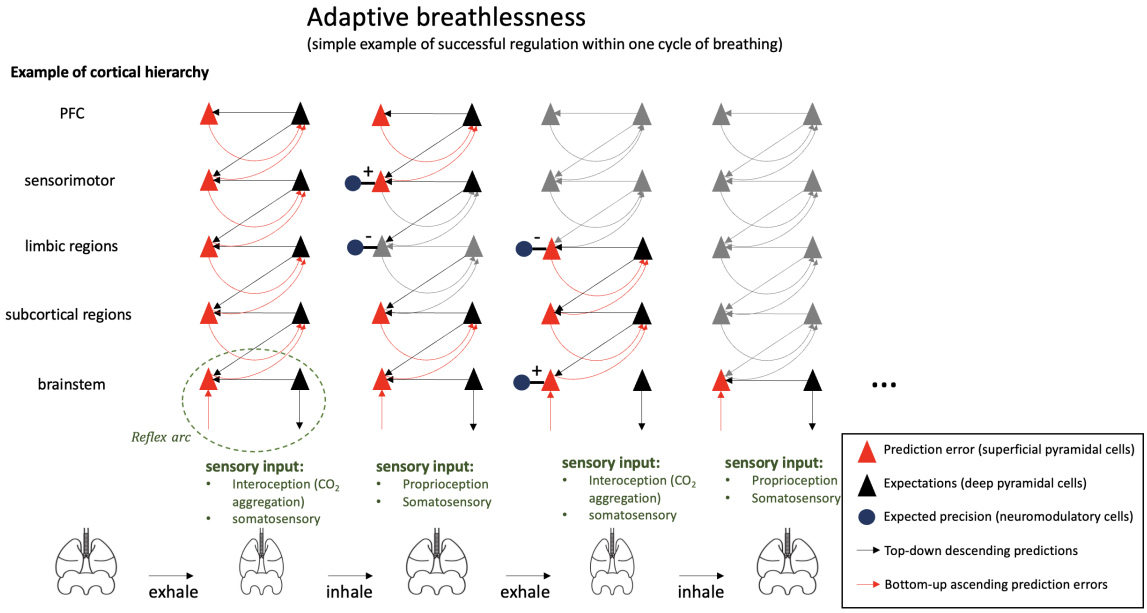


Fig. 1.3 Hierarchical message passing and prediction error elimination in predictive coding during "phasic breathlessness". This schematic illustrates the alternating dynamics of inspiration and expiration, each occurring within a simplified cortical hierarchy, characterised by ascending prediction errors and descending predictions. The minimisation of prediction error relies on recurrent neuronal interactions across various levels of the cortical hierarchy. In the case of breathlessness, prediction errors cannot be resolves within a reflex arc and propagate upwards to the higher-order cortical regions. It returned to reflexive breathless after cycles of volitional respiration. It is hypothesised that superficial pyramidal cells (red triangles) compare expectations at each hierarchical level with top-down predictions from deep pyramidal cells (black triangles) at higher levels, as reviewed in [28]. Neuromodulatory gating or gain control (represented in dark blue), potentially involving projections from VTA and STN, indicates the weight assigned to prediction error based on expected precision. This figure is adapted from Seth and Friston [311].

Maladaptive tonic breathlessness

The aforementioned state of breathlessness may become maladaptive when regulatory/perceptual strategies either fail to support, or counteract, the updating of the generative model in the appropriate direction. For instance, if a novice incorrectly relies on hyperventilation (or have unrealistic fear about suffocation) in response to increased CO_2 production during weightlifting, this strategy is unlikely to effectively eliminate prediction errors, restore reflexive breathing, or lead to meaningful updating of the generative model. A continued inability to update the model despite persistent (albeit misguided) effort may result in sustained recruitment of higher-order processes, thereby giving rise to secondary affective, cognitive, and meta-cognitive changes. Crucially, this may underlie the phenomenon of discordant breathlessness observed in conditions such as long COVID, asthma, or COPD—where patients exhibit a healthy lung profile, yet even minor deviations from regular reflexive breathing elicit prediction errors that cannot be resolved.

As illustrated in Figure 1.4, persistent propagation of prediction errors across multiple levels of cortical hierarchy occurs after each respiratory action (e.g., inhalation or exhalation), signalling that the regulatory actions are insufficient to resolve the discrepancy. This state manifests as an over-reliance on volitional breathing, which may or may not be accompanied by emotional responses such as fear or anxiety.

In this case, suppressing prediction errors solely at the affective fear response (if possible), without adequate improvement at other regulatory levels, would be insufficient and harmful to resolve the issue, potentially leading to under-reporting of the symptom.

This maladaptive(tonic) state may result from disruptions at various levels and locations within the neural processes governing gas exchange. For example, impaired modulation of prediction error precision at the brainstem level may prevent the transition to reflexive breathing, as seen in chronic hyperventilation syndrome, where rapid, shallow breathing exacerbates CO_2 imbalance and perpetuates breathlessness. Additionally, cortical overactivation may involve the persistent engagement of regions such as the amygdala and anterior cingulate cortex. This is exemplified in panic-induced breathlessness, which can be conceptualised as a form of ‘respiratory hallucination’, where heightened top-down anticipation of minor prediction errors obstructs the return to reflexive control. These mechanisms highlight the complexity of maladaptive breathlessness within neural networks, necessitating interventions to recalibrate interoceptive precision, restore reflexive breathing, and mitigate emotional interference.

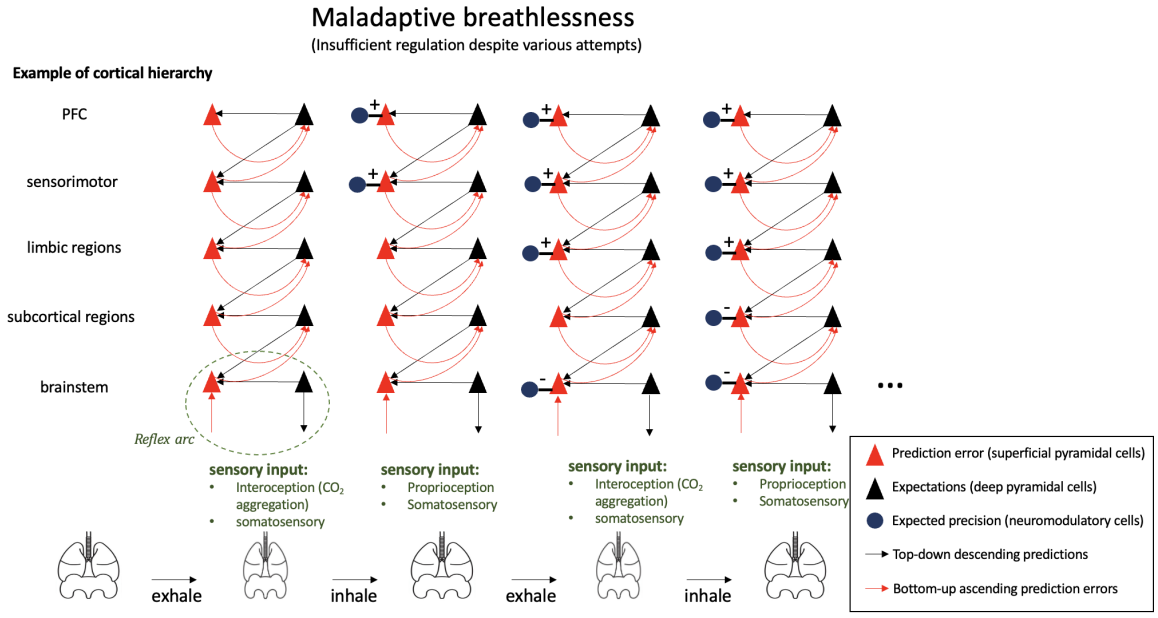


Fig. 1.4 Hierarchical message passing and prediction error elimination in predictive coding during "tonic breathlessness'. This schematic illustrates the alternating dynamics of inspiration and expiration, each occurring within a simplified cortical hierarchy, characterised by ascending prediction errors and descending predictions. The minimisation of prediction error relies on recurrent neuronal interactions across various levels of the cortical hierarchy. In the case of maladaptive breathlessness, prediction errors cannot be resolves within a reflex arc and propagate upwards to the higher-order cortical regions, in prolonged cycles of respiratory regulation. It is hypothesised that superficial pyramidal cells (red triangles) compare expectations at each hierarchical level with top-down predictions from deep pyramidal cells (black triangles) at higher levels, as reviewed in [28]. Neuromodulatory gating or gain control (represented in dark blue), potentially involving projections from VTA and STN, indicates the weight assigned to prediction error based on expected precision. This figure is adapted from Seth and Friston [311].

1.4.4 The allostatic–interoceptive (allo-intero) network

Recent advances [310, 27, 311, 304, 151] have synthesised the concepts of Active Inference and allostasis[5] into a unified framework, known as the Embodied Predictive Interoception Coding (EPIC) model [27, 199, 384] to provide mechanistic foundations underlying human allostasis and interoception.

This model suggests that the more differentiated regions of the insula (granular and dysgranular), receiving afferent signals from the brainstem, serve as the primary interoceptive

[5]Allostasis refers to the process by which the body maintains stability through physiological or behavioural changes, adapting to internal and external stressors to preserve homeostasis.

sensory cortex. In contrast, the less differentiated (agranular) anterior cingulate cortex (ACC), projecting efferent predictive signals to the insula, functions as the visceromotor cortex [199].

Specifically, bottom-up ascending visceral signals carried by the vagus nerve and small-diameter C and Aδ fibres are proposed to be mediated by the "primary interoceptive cortex", which encompasses the more differentiated regions of the insula, specifically the dysgranular dorsomedial insula and the granular dorsal posterior insula [67]. These regions contain superficial pyramidal cells, hypothesised to compute prediction errors in active inference, represented as red triangles in Figures 1.2, 1.3, and 1.4. The dorsal regions of the mid-to-posterior insula are therefore of particular interest for understanding how interoceptive respiratory signals—or signals from other modalities of the body's internal milieu—are initially processed.

Top-down descending anticipatory signals are proposed to be mediated by deep pyramidal cells in the agranular regions of the ACC, including the subgenual ACC (sgACC), pregenual ACC (pACC), and dorsal ACC (dACC, also referred to as the anterior midcingulate cortex; aMCC), as well as the agranular medial portion of the ventral anterior insula cortex (mvaIns), potentially with input from the dorsal amygdala [252]. The agranular lateral portion of the ventral anterior insula cortex (lvaIns), part of the orbitofrontal area, is hypothesised to process sensory integration [263]. These deep pyramidal cells are also represented as black triangles in Figures 1.2, 1.3, and 1.4.

These top-down prediction signals are thought to flow from these medial visceromotor regions down the cortical hierarchy to regions with greater laminar development (in the opposite direction to the bottom-up interoceptive pathways described above), ultimately reaching the hypothalamus, PAG, and other brainstem nuclei responsible for regulating the body's internal milieu.

EPIC model for respiration

A major critique of the Bayesian brain hypothesis or Active Inference theories [125, 269] lies in their predominantly theoretical nature[63, 64] [6] and lack of mechanistic explanations in the biological brain. The EPIC model offers a promising foundation to address these limitations by providing mechanistic insights into how respiratory regulation and perception, conceptualised as gas-exchange information within the framework of hierarchical active inferencing, are implemented in the brain. These are grounded by evidence from the tract-tracing evidence [27] and cell lamination information from the monkey models[23, 249, 241](albeit preliminary).

[6] Its claimed 'unified' nature, and the issue of taking a realist view of current neuroscience field.

Respiratory afferents encompass interoceptive, proprioceptive, and exteroceptive signals [75]. Interoceptively, the act of breathing generates a strong afferent influx from bronchopulmonary mechanoreceptors, transmitted via the vagus nerve to the Nucleus of the Solitary Tract (NTS) in the brainstem. These signals are integrated in the medullary and pontine respiratory centres for rhythm generation and control (relexive breathing), with further modulation occurring in higher-order structures, potentially within regions of the allo-intero network described by the EPIC model [75]. Other interoceptive signals may include inputs from central chemoreceptors located in the medulla oblongata.[7] Proprioceptive feedback arises from the rib cage, diaphragm, tracheal muscles, and upper airways, while exteroceptive inputs, such as environmental temperature, odours, or the sensation of wearing a facial mask (e.g., during the COVID-19 pandemic), also contribute to respiratory afferent signalling [5, 229].

These diverse sensory modalities may be integrated within specific brain regions, such as the orbitofrontal cortex(OFC), and participate in the hierarchical active inference underpinning respiratory regulation and perception. Whether the regions implicated in the EPIC model are directly involved in respiratory regulation, or how alterations in nodes or connectivity between interoceptive and visceromotor pathways contribute to maladaptive breathlessness, remains an open question.

1.5 Amygdala in breathing regulation and perception

1.5.1 Position and structure of the amygdala

The term "amygdala" was introduced by the anatomist Burdach in the early 19th century to describe an almond-shaped cell mass located in the anterior portion of the temporal lobe. Modern usage of "the amygdala" or "the amygdaloid complex" refers to this almond-shaped cell mass, known as the basolateral nuclei, along with its adjacent superficial centromedial nucleus and the bed nucleus of the stria terminalis (BNST). Situated deep within the temporal cortex bilaterally, the amygdala occupies a volume of only 1.24–1.63 cm^3 [39]. Although often treated as a single structure in human neuroscience research, the amygdala comprises at least 13 distinct nuclei that are richly interconnected and extensively linked to other regions of the brain, as demonstrated by animal and human histology studies [298, 214, 215]. The sub-segmentation and precise boundaries of the amygdala remain a topic of ongoing debate.

[7] Note that peripheral chemoreceptors, stretch receptors, baroreceptors, irritant receptors, and juxtapulmonary capillary receptors are located outside the CNS and are therefore not signals of of interest here, as the active inference framework in this context defines the internal system as the entire CNS. These signals are considered external to the system and part of the model of "world".

This paper adopts an evolutionary-based segmentation approach, drawing on the comparative analysis of vertebrate species by Johnston (1923) [191], which emphasises the distinction between phylogenetically older (primitive) and newer (cognitive) groups of nuclei.

The 'evolutionarily primitive division' ([214] p. 869) refers to the superficial, cortico-medial region (CMA), which comprises the cortical, medial, and central (CeA) nuclei, as well as, in some instances, the bed nucleus of the stria terminalis (BNST). These nuclei project to autonomic networks in the brainstem and are notably associated with the olfactory system. This group of nuclei is responsible for maintaining autonomic control in animals as ancient as amphibians. Over the course of evolution, from basal insectivores to primates, a reduction in the olfactory regions has been observed [307, 335].

With regard to respiration, animal studies have demonstrated that the CeA projects to the PAG [293] as well as the ventrolateral region of the solitary tract nucleus (NTS), an area within the medullary respiratory region [163]. Additionally, both the CeA and the BNST project to the parabrachial nucleus in the pons, which is considered part of the respiratory circuitry.

The 'evolutionarily newer (cognitive) division' ([214] p. 869) refers to the deep, basolateral region (BLA), which includes the lateral, basal, and accessory basal nuclei, as shown in the right panel of Figure 1.5. The size of the deep nuclei shows significant growth over the course of evolution towards primates [335], as illustrated in the left panel of Figure 1.5. Notably, the human brain possesses a disproportionately larger lateral region compared to non-human primates of similar size, receiving extensive input from the neocortex [24, 307].

These nuclei exhibit rich reciprocal projections to and from the temporal, prefrontal, and orbitofrontal association cortices, which are involved in higher-order cognitive processes. The lateral amygdala, for example, is often described as the gatekeeper or sensory interface of the amygdala. It receives inputs from the visual, auditory, olfactory, and taste systems [214] and plays a central role in establishing conditioned responses (e.g., breathlessness) to environmental cues.

I did not identify studies specifically addressing the involvement of the deep nuclei in respiration or their projections to, or from, the evolutionarily primitive division of the amygdala in integrated respiratory control.

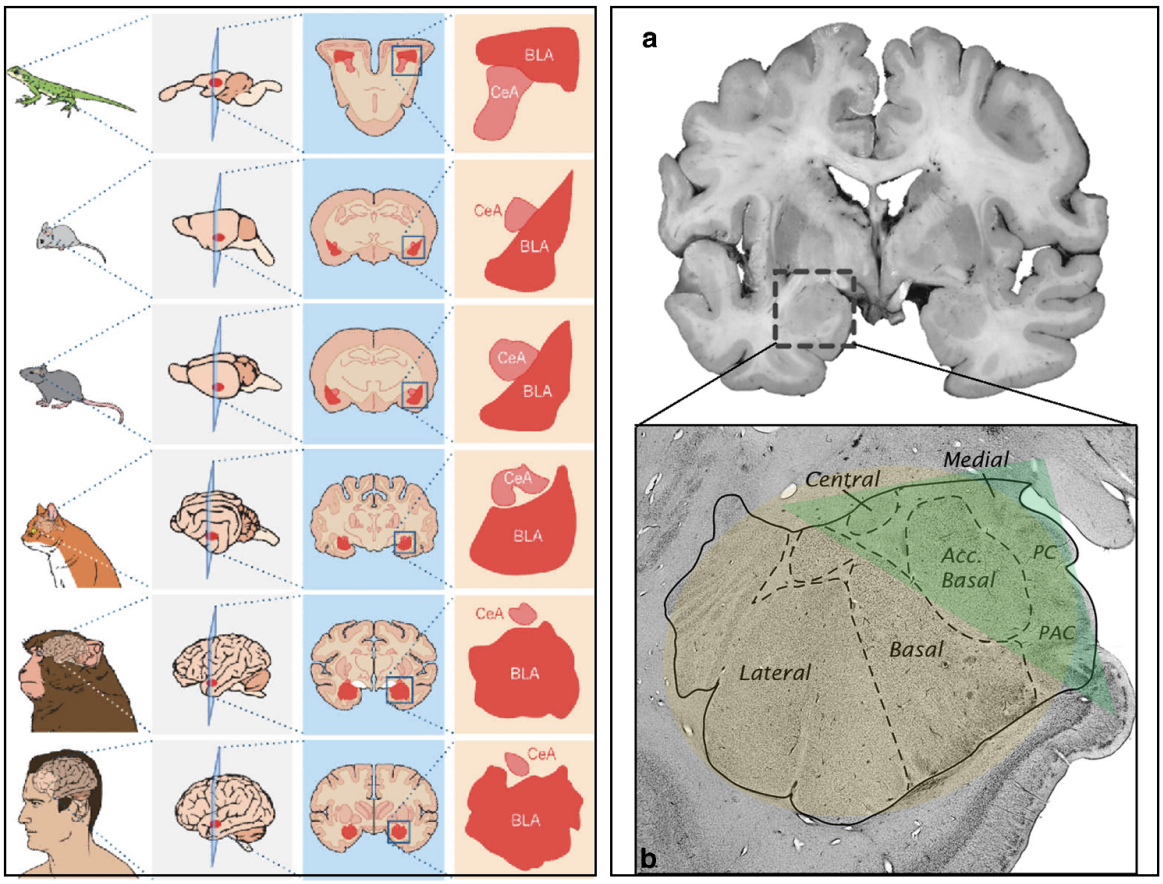


Fig. 1.5 Illustration of the amygdala subnuclei. The left panel (A) depicts coronal sections of the amygdala from the brains of a lizard, mouse, rat, cat, monkey, and human, illustrating the evolutionary expansion of the basolateral region of the amygdala. This figure is adapted from [187]. The right panel presents a Nissl-stained segmentation of the post-mortem human amygdala. The evolutionarily newer, deep areas (lateral, basal, and accessory basal nuclei) are highlighted in yellow, while the evolutionarily primitive, superficial areas (central and medial nuclei) are highlighted in green. Regions labelled PC (Periamygdaloid Cortex) and PAC (Paralaminar Amygdala Cortex) are not discussed in the current context. This figure is adapted and modified from [307].

In summary, the amygdala nuclei contribute to both visceral and higher-order processes in the human brain and may serve as a critical site for integrating autonomic behaviours (including involuntary and voluntary respiratory patterns) with the perception of physiological needs (e.g., anxiety related to breathing or the urge for gas exchange). A detailed review of the potential involvement of the different amygdala divisions in respiratory regulation and perception follows.

1.5.2 Amygdala during spontaneous breathing

The CeA has been identified as particularly important during spontaneous breathing in both animal and human studies [385, 389, 18, 163, 380, 259]. In animals, direct recordings from implanted electrodes have demonstrated that a significant proportion of CeA neurons discharge in phase with the respiratory pattern [385, 389]. This activity appears to be state-dependent, influenced by sleep-wake cycles, and is potentially mediated by the CeA's extensive reciprocal connections with the parabrachial pons, which play a key role in respiratory phase switching [131, 385, 163].

Additionally, research indicates that this effect is dependent on nasal breathing in both animals [122] and humans, as demonstrated by Zelano and colleagues [380, 259] using intracranial EEG data from epilepsy patients. These findings highlight the importance of the olfactory network in respiration-limbic oscillations. It is not surprising as the phylogenetically primitive CeA receives projects from the olfactory system [214]. The ability to detect and respond to odours has likely been instrumental in survival and reproductive success throughout vertebrate evolution. The pleasantness of odours has also been shown to influence human respiratory patterns: pleasant odours increase tidal volume (VT) and decrease respiratory frequency (fR) even before participants become consciously aware of the smell [234]. This may be attributed to the unique organisation of the olfactory pathway, where olfactory sensory neurons project directly to the olfactory bulb, bypassing the thalamus, and subsequently project to limbic and paralimbic regions, including the cortical nucleus of the amygdala, the olfactory tubercle, the lateral entorhinal cortex, and the anterior olfactory nucleus [154, 284]. The significance of this primitive olfactory-amygdala circuitry in human respiratory control and perception, as well as its interactions with other respiratory-related brain regions, such as the PAG, remains to be fully elucidated.

1.5.3 Amygdala upon direct stimulation

Animal studies showed that direct stimulation to the sub-nucleus (possibly within the CMA region) of amygdala introduce apnoea in cats [163], rabbits [18], monkeys [15, 290]. The respiratory arrest effect was extended to human [193, 66] and has recently been replicated[291, 210, 88] with higher precision in the amygdala loci, in small patient samples of N = 8, 3, 2. Attempts have been made to pinpoint the focal site in the amygdala that reliably produces apnoea (i.e. the 'Amygdala Inhibition of Respiration' site, or the 'AIR' site, coined by Rhone and colleagues [291]), which, although limited by small sample sizes and the inclusion of a non-adult group, may pave the way for new therapeutic avenues. After the test, participants reported not being consciously aware of this effect[88], or experiencing

a feeling of 'losing distinction between herself and an external object and having a fear of losing herself' ([179, 234] p. 1013).

However, the effect was not consistent. Stimulation of the amygdala in rabbits increases respiratory rate and other movements that are observed in response to threat [18, 163]. It may be a result of differential site of the stimulation within the central nucleus, or due to the exact frequency electric stimulation was applied. Nevertheless, mixed results in response to stimulation upon amygdala suggest a more complex mechanism through which the amygdala influence the respiratory control.

1.5.4 Amygdala lesion and respiration

Lesions of the temporal region containing the amygdala in non-human primates have been shown to result in deficits in recognising fearful facial expressions [6], reduced social dominance [294], diminished aggression [201], and alterations in autonomic functions, including respiration, heart rate, and skin conductance [216, 177]. Lesions in the CeA attenuate autonomic responses to stressors, though respiratory alterations were often not the key outcome measure [299].

Moreover, the distinct regions to which the CeA projects influence specific aspects of conditioned fear responses. For instance, lesions induced by either electrolytic or ibotenic acid injections in the lateral hypothalamic area selectively disrupt autonomic responses, as evidenced by changes in arterial pressure. In contrast, lesions in the caudal midbrain central grey region uniquely impair behavioural responses, such as the freezing behaviour, in animal models [216].

In rare human cases, bilateral damage to the amygdala has been associated with impaired processing of emotional facial expressions, particularly those depicting fear [233]. Patients with epileptic spikes localised to the left amygdala, which is functionally similar to lesions in the left amygdala, exhibit reduced anxiety and altered respiratory patterns during the anticipation of fear. Davenport and colleagues [74] further reported that amygdala lesions impair both somatosensory and affective perception of respiratory loads, indicating the possible role of the amygdala in integrating affective and physiological responses.

Together, previous research suggests that lesions of the amygdala, particularly its central nucleus, affect respiration in the context of fear, as part of the autonomic responses.

1.5.5 Amygdala during breathlessness

The aforementioned evidence linking the amygdala to respiration is primarily confined to autonomic control (the action, not the perception) and predominantly associated with the

phylogenetically primitive nuclei of the amygdala, such as the central nucleus. Evidence regarding the role of the amygdala in respiratory discomfort, such as breathlessness, and its relationship to higher-order cognitive and affective processes—particularly networks centring on the phylogenetically newer cognitive division of the amygdala—remains relatively limited.

Although a 'cortico-limbic' circuitry, including the amygdala, ACC, supplementary motor area (SMA), dorsolateral prefrontal cortex(dlPFC), thalamus, and cerebellar vermisis, is gaining recognition for its role in respiratory perception (see review by Evans and colleagues [102]), direct evidence concerning the specific role of the newer cognitive division of the amygdala in respiratory discomfort and its integration with higher-order cognitive and affective processes remains sparse.

Evidence of the whole amygdala activity during breathlessness has been investigated using tasks that induce inspiratory resistance, including breath-holding, resistive loads applied via a restrictive breathing mouthpiece, or breathing through a mixture of CO_2 and air, typically in an MRI scanner [272, 103, 34, 362]. Although not the primary region of interest in many studies, evidence suggests that the amygdala exhibits elevated deactivation during the anticipation of breathlessness threat [114, 113, 339, 340]. However, findings regarding its involvement during the experience of breathlessness itself remain inconsistent. For instance, Corfield and colleagues [66] reported no amygdala activity in their study, potentially due to the small sample size (N = 5) or the treatment of the amygdala as a single structure, which may have masked differential activity across its subregions.

Evidence on how the amygdala communicates with other brain regions during breathlessness is scarce. Faull and Pattinson [114] identified FC between the ventral lateral PAG and the amygdala during resting state, as well as FC between the left amygdala, lateral PAG, and anterior hippocampus during breathlessness. These FC strengths were shown to scale with self-reported anxiety scores in a conditioned breathlessness task. However, research on brain activity during breathlessness has primarily focused on the cerebral cortex, including the medial prefrontal cortex, OFC, dlPFC, and the ACC. The role of respiratory-relevant subcortical regions, such as the amygdala, remains largely unexplored [273].

Nevertheless, the precise role of the phylogenetically newer cognitive and affective subdivisions of the amygdala in human respiratory perception and control remains unclear. This may be partly due to the fact that detailed sub-segmentation of the amygdala has only recently become available in human neuroimaging. Moreover, the mechanisms by which the amygdala integrates interoceptive and exteroceptive signals with autonomic regulation remain poorly understood.

1.5.6 Pavlovian fear conditioning, breathlessness, and the amygdala

Pavlovian fear conditioning paradigms have been widely employed to investigate maladaptive breathlessness [267, 113]. These models utilise either exteroceptive cues (e.g., visual stimuli) or interoceptive cues (e.g., mild breathlessness induction) as the conditioned stimulus (CS), and experimentally induced dyspnoea as the unconditioned stimulus (US), eliciting conditioned responses (CR).

A series of studies by van den Bergh and colleagues demonstrated that, following just a few pairings of a respiratory threat (US) with a specific CS, presentation of the CS alone was sufficient to elicit respiratory symptoms and behaviours—such as hyperventilation—and fear of suffocation in the absence of any actual respiratory threat, in both healthy individuals and psychosomatic patients [276, 355, 268]. The US typically involved CO_2-enriched air inhalation, inspiratory resistive loads, or complete respiratory occlusions (e.g., [4, 356, 267]). The CS varied according to the study aim, ranging from innocuous odours (e.g., in models of multiple chemical sensitivity [84, 354–356, 353]), to emotional imagery (e.g., in fear conditioning models of panic or psychosomatic disorders [77, 334]), and to interoceptive breathlessness sensations (e.g., in interoceptive fear learning in panic disorder [31, 4, 267, 266, 268]).

Similar conditioned responses have been observed in individuals with asthma. For example, one study found that participants with mild asthma reported increased respiratory symptoms (e.g., chest tightness, congestion, and discomfort) and fatigue following inhalation of a harmless saline solution, without any changes in physiological parameters or dyspnoea, on the day following a histamine inhalation challenge [276].

This phenomenon, termed symptom learning or the nocebo effect [29], appears to be more pronounced in individuals with high trait negative affectivity and neuroticism [276, 352]. Additionally, individuals with allergic rhinitis have shown greater generalisation of learned symptoms to novel triggers [189]. These psychological traits have been proposed as underlying factors in the over-expression of respiratory symptoms observed in both psychogenic and physiological conditions, including panic disorder, respiratory diseases, and medically unexplained symptoms involving breathlessness [352, 354, 355, 189].

Learned respiratory symptoms can persist for several days. Symptom extinction appears to depend on the intensity of the US: extinction was achievable with mild stimuli (e.g., 5.5% CO_2-enriched air [334]), but was impaired with stronger stimuli (e.g., 20% CO_2-enriched air [242]), even in healthy participants. One study found that higher resting heart rate variability—a marker of prefrontal inhibitory control—was associated with more effective extinction learning in an interoceptive respiratory fear paradigm [266]. However, research on

extinction learning in asthma patients, or more broadly on individual variability in updating prior expectations using bottom-up safety signals, remains limited.

CS–US associations represent one form of top-down influence on respiratory perception, operating at relatively lower levels of the perceptual hierarchy. Importantly, conscious awareness of these associations is neither necessary [268] nor sufficient (e.g., when the CS is a non-aversive odour [356]) for the conditioned effects to occur. Higher-level cognitions—such as explicit beliefs about respiratory contexts—also modulate learning. For instance, simply reading news articles on air pollution has been shown to enhance associative learning effects [371]. In another study, individuals with asthma who were told that rescue medication would be unavailable during a rebreathing challenge reported greater respiratory unpleasantness—particularly those with high symptom fear—than participants with perceived access to medication [188]. Notably, these top-down cognitive influences often involve emotional arousal. However, whether explicit beliefs can influence breathing perception independently of emotional changes remains unclear. Direct evidence is lacking on how perception evolves when confronted with disconfirmatory sensory information (e.g., safety signals), particularly in clinical populations, such as those recovered from COVID-19.

The amygdala plays a central role in fear conditioning [278], particularly in Pavlovian paradigms where a neutral CS, when paired with a US—such as a painful stimulus or a resistive breathlessness sensation—elicits conditioned fear responses, including freezing and associated physiological changes. Rodent studies have identified the lateral amygdala—a component of the evolutionarily newer amygdaloid complex—as a key site for fear memory formation. Specifically, long-term potentiation (LTP) occurs in the lateral amygdala during CS–US pairings, facilitating the encoding and storage of fear memories [359, 108]. Once the association is established, presentation of the CS alone activates these potentiated synapses, propagating signals to downstream "output" regions—predominantly within the phylogenetically older divisions of the amygdala—to drive behavioural and physiological responses, including respiratory manifestations of fear [214]. This suggests the involvement of distinct amygdaloid nuclei in both the learning and expression of respiratory-related fear. To date, however, no study has explicitly examined the role of the amygdala—or its subdivisions—in Pavlovian conditioning models of breathlessness.

1.5.7 Opioids suppress amygdala during anticipation of breathlessness

Low-dose of opioids have been used to treat chronic breathlessness [95]. Opioids are known to significantly influence associative learning and memory formation related to aversive experiences [300, 106, 238], likely through their action on the abundant opioid receptors located in the amygdala and hippocampus [271]. Hayen and colleagues [170] has shown that

the activity of amygdala during the anticipatory stage of breathlessness can by suppressed by opioids (low-dose remifentanil), and that opioids use reduced breathlessness unpleasantness but not intensity. Opioids seem to dissociate (and depress) the emotional aspect of the respiratory experience by acting on amygdala while maintaining the conditioned ventilatory responses. It is unlikely the whole amygdala act unitedly - It remains a question which columns of the amygdala can be depressed by opioids and to what extend this may lead to development of inventions (e.g. sites for electric stimulation or psychotherapies targeting this circuitry).

1.6 Functional brain evidence for long COVID

COVID-19, caused by the SARS-CoV-2 virus, is primarily recognised as an acute respiratory syndrome. However, increasing evidence reveals that its effects extend beyond the respiratory system to impact both the central nervous system (CNS) and the peripheral nervous system (PNS), resulting in a spectrum of neurological manifestations and complications following acute infection [254, 344]. These symptoms can persist beyond the acute phase of the illness, giving rise to "long COVID", a post-viral syndrome where patients experience lingering symptoms, including neuro-related issues, even after testing negative for SARS-CoV-2 [296].

The neurological effects of COVID-19 range from mild symptoms, such as fatigue, cognitive decline, anxiety, depression, and post-traumatic stress disorder (PTSD), ageusia (loss of taste), and anosmia (loss of smell), to severe conditions, such as acute brain damage following respiratory failure, stroke, and metabolic dysfunction [286, 132, 30, 275, 213, 228]. Critically ill patients often present with altered consciousness, delirium, and other psychiatric disorders during hospitalisation, which may persist long after discharge[213, 228]. Studies report that up to 80% of severe cases exhibit neurological symptoms, and radiological as well as post-mortem analyses have demonstrated significant brain pathology associated with the virus [92, 248].

Brain imaging studies have identified various abnormalities, including parenchymal brain damage, subcortical micro- and macro-bleeds, cortico-subcortical swelling, and non-specific deep white matter changes[92, 54]. However, these findings often focus on structural changes without clarifying the specific brain regions involved or their functional implications. Also, it remains unclear whether these neurological signs are due to direct viral invasion via the olfactory pathways, entry through the brainstem's medullary cardiorespiratory centre, or secondary effects such as virus-induced neuroinflammation [44].

Rs-fMRI offers a valuable approach to investigating functional brain changes in post-COVID conditions. Rs-fMRI is a non-invasive technique that measures blood-oxygen-

level-dependent (BOLD) signals in the brain during rest. BOLD signals reflect changes in blood flow, oxygenation, and volume, which are indirect indicators of neuronal activity and metabolic demand in specific brain regions. The degree to which different brain regions co-activate is commonly used to infer intrinsic functional connectivity (FC) between these regions. Rs-fMRI FC measures have been employed as biomarkers of neural function for psychological conditions and have demonstrated a remarkable 60%–80% accuracy in predicting treatment responsiveness for conditions such as generalised anxiety disorder (GAD), major depressive disorder (MDD), and obsessive-compulsive disorder (OCD) [200, 289, 343, 381]. Despite its promise, evidence on post-COVID functional brain networks is limited. To date, studies have primarily explored three symptom categories:(1) cognitive impairment [86, 265, 351, 364, 347]; (2) depression and post-traumatic stress disorder (PTSD) [30, 132, 347]; and (3) olfactory dysfunction [98, 251, 369, 382].

Rs-fMRI for Post-COVID cognitive impairment

Cognitive decline has been identified as one of the most prevalent neurological symptoms following COVID-19 [86] and and has been most extensively studied using rs-fMRI. A broad range of cognitive domains, including attention, memory, executive function, and vigilance, have been significantly affected in both severe hospitalised cases and mild to moderate non-hospitalised cases [387, 86, 265, 301, 351, 364]. Cognitive assessment in these studies has predominantly relied on task-based evaluations or screening tools such as the Montreal Cognitive Assessment (MoCA) [255], the Stroop Test, and the Digit Span Test. While one study examined the acute phase of infection [301], the majority have focused on long-term sequelae, evaluating cognitive impairments from several months to a year post-infection.

Rs-fMRI FC alterations associated with cognitive deficits have been observed across several large-scale brain networks, including the default mode network (DMN), dorsal attention network (DAN), salience network (SN), sensorimotor network (SMN), and ventral attention network (VAN) [265, 351, 364]. Within the SN and DAN, regions such as the bilateral insular cortex, ACC, and precentral gyrus have exhibited hyperconnectivity, which correlates with cognitive impairments [265, 364, 301].

In contrast, hypoconnectivity has been reported in DMN regions, including the left and right parahippocampal gyrus and OFC, which have been linked to deficits in learning, recall, and memory [86]. Additional hypoconnectivity has been observed in the bilateral occipital cortex, posterior cingulate gyrus, middle temporal gyrus, and right cerebellum, with some regions showing widespread alterations across multiple clusters [301, 265].

These findings underscore the intricate relationship between post-COVID-19 cognitive impairments and alterations in large-scale brain networks. Nevertheless, further investigations are required to elucidate these associations and their broader implications.

Rs-fMRI for Post-COVID depression and PTSD

Post-COVID patients frequently exhibit psychological symptoms such as depression and PTSD. These manifestations are hypothesised to arise either from the direct effects of the viral infection or as secondary consequences of the traumatic experiences endured during the acute phase, particularly among hospitalised individuals[30, 132].

Disrupted connectivity patterns linked to PTSD have been identified in the dlPFC, inferior parietal sulcus, and cerebellum, with these alterations attributed to inflammatory reactions[30]. Notably, negative correlations in networks such as the DMN and positive correlations in the SMN and SN were observed. Similarly, Fu and colleagues [132] reported alterations in dynamic functional network connectivity (dFNC) states involving the DMN, SMN, visual network, and cognitive-control networks. Specific connections between the SMN and visual network were found to be more prevalent in COVID-19 survivors, with these disruptions correlating with PTSD symptom severity.

Furthermore, decreased FC between the language network (LN) and frontoparietal networks (FPN), as well as reduced connectivity within the DMN, was associated with elevated systemic immune-inflammation indices[30]. These disruptions potentially contribute to psychological conditions such as depression and PTSD[30]. Increased FC in regions such as the posterior cingulate cortex (PCC) and ACC has also been linked to PTSD and depression[30]. Conversely, reductions in FC between the caudate and temporal cortex, as well as between the thalamus and inferior parietal lobe, were correlated with elevated levels of C-reactive protein (CRP)[132].

Despite these advancements, significant limitations persist. The relatively small sample sizes (42 to 44 patients), the short interval from acute infection (<6 months), and the heterogeneity of symptoms and pre-existing conditions in the studied populations complicate data interpretation. Longitudinal studies with larger cohorts are essential to comprehensively elucidate the trajectory and mechanisms underlying these neuropsychiatric effects. Nevertheless, these findings highlight the critical need for mental health interventions in long COVID patients, with a specific emphasis on addressing depression and PTSD.

Rs-fMRI for Post-COVID olfactory disorders

Alterations in the olfactory-related cortex following COVID-19 infection have received robust evidence through neuroimaging studies. Douaud and colleagues demonstrated significant longitudinal structural changes in the olfactory system, using the largest sample from the UK Biobank (UKB) [89]. These changes include regions with neural connectivity to and from the olfactory bulb, such as the piriform cortex (primary olfactory cortex) and other limbic and memory-associated areas, including the parahippocampal, OFC, and entorhinal cortices. FC studies have often employed a priori defined seeds, such as the anterior piriform cortex [98], or a priori defined regions of interest within the olfactory network. Regions within the olfactory system and the DMN, particularly the dorsal anterior cingulate cortex (dACC), insula [369], OFC, and thalamus [251], have been identified to show alterations after COVID.

In addition, alterations in the olfactory network, which are associated with hyposmia and anosmia, are hypothesised to serve as the neural basis for the widely reported cognitive disruptions following COVID-19 [369, 251]. The affected regions of the primary and secondary olfactory cortex overlap with areas commonly linked to memory and executive control, including the dACC, OFC, visual association cortex, and cerebellum (within the FPN, SN and DAN) [369]. These alterations have been proposed as potential compensatory mechanisms of the olfactory system alteration. Additionally, task-based fMRI studies using trigeminosensory tests in individuals with post-COVID olfactory loss identified absent activity in the OFC [186, 378]. However, the evidence supporting this link remains preliminary [251, 369].

Muccioli and colleagues [251] reported reduced global modularity and increased thalamic connectivity in a relatively small sample (N=23 patients). These findings were associated with hyposmia severity and impairments in visuospatial memory and executive functions, though no significant differences were observed when compared to a control group. The extent to which olfactory-centred neural alterations contribute to other cognitive or psychophysiological symptoms post-COVID remains uncertain.

Overall, these findings suggest that COVID-19-related disruptions in the integrity and connectivity of the olfactory network are pronounced. However, it remains unclear whether these disruptions extend beyond sensory deficits. An additional limitation of existing studies is their focus on short intervals post-infection, typically ranging from a few days to less than two months. This leaves a significant knowledge gap regarding the long-term impacts, particularly in the context of long COVID, which is characterised by persistent symptoms beyond three months. Further research is needed to investigate potential long-term manifestations.

1.7 Summary of literature review and research roadmap

This section provides an overview of breathlessness and its maladaptive tonic variants, both from clinical and theoretical perspectives, through the lens of Active Inference and hierarchical predictive coding. It also discusses a range of topics supporting the research aims of this thesis. A summary of the key points and current gaps in the literature is presented below.

1. Despite the substantial body of evidence linking respiratory perception with affective processes, the neural mechanisms underlying this relationship remain unclear. The amygdala, a critical structure involved in fear and the fight-or-flight response, has been extensively studied for its role in respiratory regulation and perception. However, the specific subregions of the amygdala that respond to respiratory threats and their connection to the subjective experience of breathlessness have not yet been explored.

2. Theoretical developments in understanding the brain as an inferencing organ suggest that it 1) makes predictions by exerting actions to generate sensory evidence that aligns with homeostatic set points, and 2) engages in perception as a process of hypothesis testing, or as the inverse of a generative model of the "world" it inhabits. This framework has motivated the integration of respiration control and perception into a unified model. Researchers have proposed that certain brain regions contribute to allostasis and interoceptive regulation, collectively referred to as the EPIC model. However, there is a lack of mechanistic evidence, particularly in the context of respiratory research, to demonstrate how these brain regions contribute to interoceptive perception—specifically, the perception of respiratory regulation.

3. Post-COVID, numerous neurophysiological symptoms continue to debilitate patients, potentially as a result of alterations or predispositions within brain networks. The relationship between changes in functional brain networks and the manifestation of various post-COVID physio-neurological symptoms remains poorly understood. No research has adopted a multivariate approach to integrate the wide range of neurological symptoms expressed in post-COVID patients, potentially uncovering distinct neurophysiological phenotypes based on functional connectomes.

4. A significant proportion of post-COVID patients continue to experience breathlessness months after recovering from the acute infection. However, no study has investigated whether functional neural network alterations underlie post-COVID breathlessness.

1.8 Thesis outline

This thesis comprises two primary research foci.

The first research focus (Chapter 2) builds upon established work in conditioned breathlessness to investigate the functional and connectivity characteristics of the amygdala—the core region implicated in fear responses—during acute, phasic breathlessness. This analysis was conducted using a historical dataset of 40 healthy participants who completed an aversive delay-conditioning breathlessness paradigm while undergoing scanning in a 7T MRI scanner.

The second research focus (Chapters 3, 4, 5, and 6) aimed to characterise the cortical and subcortical functional networks—both predefined regions of interest and large-scale whole-brain networks—underlying maladaptive breathlessness. It further tested whether these functional connectivity markers constitute domain-general features associated with a broad spectrum of neurophysiological experiences following COVID-19. This work leveraged a unique sample of 53 post-COVID individuals, scanned using ultra-high field 7T MRI at 334 ± 213 days post-infection. These participants exhibited varying degrees of maladaptive breathlessness, and the analysis integrated a rich set of behavioural and clinical data collected by myself and collaborators during the COVID-19 pandemic.

In the final chapter (Chapter 7), I synthesise the findings from these two lines of inquiry, highlighting their contributions to the understanding of maladaptive breathlessness, the neurobiological mechanisms underpinning long COVID, and their implications for the interoceptive–allostatic framework with a specific emphasis on respiratory control.

Chapter 2

Conditioned respiratory threat in amygdala

2.1 Abstract

Breathlessness often exhibits a mismatch between objective pulmonary function and subjective experience, frequently linked to psychological factors like anxiety. However, the neural mechanisms driving this phenomenon remain poorly understood. The amygdala, a key region for emotional processing and integration of respiratory signals, has not been thoroughly explored in this context.

This study aimed to investigate activation and functional connectivity (FC) patterns within amygdala nuclei during the anticipation and perception of inspiratory resistance, as well as at rest, to explain individual variability in breathlessness perception. I performed a secondary analysis of data from 40 healthy volunteers who underwent ultra-high-field (7 Tesla) functional magnetic resonance imaging (fMRI) during an aversive delay-conditioned respiratory resistance task and at rest. Analyses included voxel-wise clustering within a whole-amygdala mask or segmentation of nine amygdala subnuclei to identify task-relevant regions, followed by investigations regarding FC between a BLA-seed and the rest of the brain, in relation to self-reported anxiety and intensity.

A large cluster in the basolateral amygdala (BLA) showed reduced activity during both anticipation and perception of breathlessness. Subnuclei analysis, though underpowered, suggested reduced activity of central and anterior nuclei of amygdala during resistance. During resistance, BLA connectivity with the mediodorsal thalamus (MD) increased and scaled subthresholdly with anxiety. At rest, breathlessness intensity—but not anxiety—was

associated with increased BLA-temporal pole connectivity and decreased BLA-precuneus connectivity.

These findings highlight the role of BLA-centred FC in modulating breathlessness perception. Intrinsic BLA-temporal pole and BLA-precuneus FC at rest, along with BLA-MD connectivity during resistance, may explain individual differences in respiratory perception. This connectivity profile may contribute to misinterpretation of respiratory signals in clinical populations, although the CMA's role remains unclear.

2.2 Introduction

Breathlessness is a highly debilitating experience and has been closely linked to existential fear [368]. While elevated fear—and its accompanying behavioural and physiological responses—can be adaptive when confronting actual threats, such responses are typically phasic and context-appropriate. Breathlessness may become maladaptive when safety signals are misinterpreted as threats, leading to the over-perception of respiratory distress. This maladaptive form of breathlessness, often chronic and tonic in nature, is observed across a range of diagnostic categories. It affects patients with chronic airway disease, long COVID, congestive heart failure, terminal cancer, and panic disorder, many of whom report significant respiratory symptoms despite objectively normal pulmonary function, as measured by pathophysiological indices such as forced expiratory volume in one second (FEV1) [258, 3, 87, 174, 345]. The over-perception of breathlessness has been shown to correlate positively with anxiety, fear of suffocation, and trait negative affectivity across multiple clinical populations [341, 22, 276, 352], suggesting a substantial psychological component.

The amygdala plays a central role in affective processing, fear learning, and regulation of autonomic functions [214]. The amygdala contains various nuclei, which maintain reciprocal connections with both cortical and subcortical regions of the brain [214]. The phylogenetically primitive centromedial complex (CMA) of the amygdala projects to the brainstem and is believed to be involved in autonomic regulation and the fight-or-flight response. In contrast, the more recently evolved basolateral complex (BLA) is rich in connections to higher-order areas of the neocortex and has been shown to play a key role in learning exteroceptive cues during conditioning, as well as in the Salience Network [215]. For a detailed review, please refer to Chapter 1.

Conceptually, the CMA and BLA may subserve distinct functions in the context of confronting previously learned threats. The CMA is thought to support active coping by recruiting subcortical defensive responses and initiating physiological changes across the brain and body [217]. In contrast, the BLA is likely involved in the passive perception of bodily

states—particularly respiration—through engagement with higher-order association cortices. Within the Active Inference framework [125, 311, 310, 27], introduced in Section 1.4 of Chapter 1, processes involving the CMA may correspond to "active inference", while those engaging the BLA align with "perceptual inference". The latter is possibly particularly implicated in the conscious emotional and cognitive appraisal of respiratory efficiency.

A natural methodological choice for investigating amygdala functional activity and connectivity (FC) in response to respiratory challenges—and how these contribute to subjective perception—is task-based fMRI employing a breathlessness paradigm. However, due to the amygdala's deep anatomical location, small size, and susceptibility to signal drop-out and distortion, as discussed in Chapter 1, no previous studies have comprehensively examined the distinct roles of its subdivisions in the context of breathlessness.

This is a secondary analysis of a dataset previously collected by our group using 7-Tesla (7T) ultra-high-field functional magnetic resonance imaging (fMRI) and published in Faull and colleagues[114]. The dataset involves healthy individuals performing a conditioned breathlessness task in the scanner. The improved resolution of 7T can better differentiate amygdala subnuclei or areas involvement in the task. Based on this dataset, our group has substantiated the role of suprapontine areas, especially the periaqueductal gray (PAG, also known as the central gray), in the anticipation and experience of breathlessness threats (resistive loading). Specifically, the ventrolateral PAG (vlPAG) activates during anticipation of resistive loading, corresponding to the passive response to inescapable stress, while the lateral PAG (lPAG) activates during the perception of resistive loading [113] [114], corresponding to active response to threat. The amygdala as a whole was found to deactivate during both the anticipation and perception of breathlessness compared to baseline [114]. However, the specific contributions of the amygdala sub-divisions to this observed deactivation, and their roles within broader brain networks during breathlessness, as well as their relationships to the subjective perception of breathlessness remain unclear.

2.2.1 Hypotheses

The primary aim of this chapter is twofold: (1) to deepen our understanding of the amygdala's role in the expression of conditioned breathlessness; and (2) to investigate the neural correlates underlying individual differences in respiratory perception. This exploration is crucial for elucidating the adaptive phasic responses to genuine respiratory threats. Such insights provide a foundation for examining maladaptive, tonic forms of breathlessness, in which individuals report substantial respiratory distress despite the absence of pulmonary dysfunction, as discussed in Chapter 1.

I hypothesised that the spatially and temporally distinct involvement of the PAG columns, as demonstrated in previous research [114], would also be reflected within the amygdala during the expression of a conditioned breathlessness task. Specifically, I anticipated that activity centred in the BLA—which facilitates perceptual inference and is connected with higher-order affective and cognitive cortices—along with its intrinsic resting-state connectivity and task-evoked interactions with broader brain networks, would be selectively associated with the anticipation phase and predictive of subjective ratings of "anxiety". By contrast, activity and FC centred in the CMA—which supports active inference and is connected with motor-execution pathways projecting to the brainstem—was expected to be specifically engaged during the resistance phase and to predict subjective ratings of "intensity".

2.3 Methods

To identify which subnuclei or regions of the amygdala are involved in the anticipation and experience of breathlessness, two analytical approaches were employed in this study. The first approach involved voxel-wise single-subject and group analyses to identify clusters within the amygdala that responded to respiratory threats. The second, complementary, region-of-interest (ROI)-based approach involved parcellating each subject's amygdala in their native anatomical space into nine subnuclei/areas, followed by a separate investigation of their activity patterns. Statistical tests were then conducted based on ROI contrasts of blood-oxygen-level-dependent (BOLD) signal values, specifically the contrast of parameter estimate (COPE). The FC analysis used the seed derived from peak de-activation of the first method.

2.3.1 Materials

This study was based on a previously published dataset [114]. Forty healthy volunteers (mean age: 26 ± 7 years; 20 females) participated in a standardised protocol comprising a training session on an "Aversive Delay-Conditioning Paradigm", followed by a 7 Tesla MRI scanning session within 24 hours. During the scanning session, participants completed the same task inside the scanner, during which task-based functional, resting-state functional, and structural MRI data were acquired.

The "Aversive Delay-Conditioning Paradigm" trained participants to associate simple visual shapes with an aversive inspiratory resistive load stimulus, simulating respiratory stressors akin to those experienced by patients with chronic airway disease. Participants learned to associate distinct visual cues (a star or a square) with two breathing conditions:

(1) certain inspiratory resistance (always paired with resistance), and (2) no resistance (never paired with resistance). The conditioning (acquisition phase) was conducted 12–24 hours prior to the MRI scan (expression phase). During scanning, each condition was presented 14 times in a semi-randomised order. After each trial, participants rated their perceived breathing difficulty ("intensity") and anxiety using a visual analogue scale (VAS).

In the original study design, participants were further categorised into two groups—endurance athletes and matched sedentary controls—based on their physical activity levels[1]. As "exercise" was not a variable of interest in the present analysis, it was treated primarily as a confounding factor.

Full details of the tasks and the breathing system used are available in Faull and colleagues [114, 113]. The fMRI sequence, elaborated details of the task, and the breathing system is also presented in the Appendix B.

MRI scanning sequence

The 7-Tesla (7T) Siemens MAGNETOM scanner with 70 mT/m gradient strength and a 32 channel Rx with single channel birdcage Tx head coil (Nova Medical) were used.

The T2*-weighted, gradient echo Echo-planar imaging (EPI) was collected for the whole brain functional fMRI during both task and rest. During the task, the scan lasted for 27 mins 30 s, with a repetition time (TR) of 3s (550 time points), echo time (TE) of 24ms, flip angle 90°, isotropic resolution of 2 mm, 63 slices, GRAPPA factor of 3, echo spacing of 0.57 ms, and with a descending slice acquisition order. During the resting-state acquisition (eyes open), a matching scan sequence was undertaken, which takes 9 mins 30s (190 volumes).

The T1-weighted (T1w) MPRAGE anatomical images were collected with 0.7mm isotropic voxels, TE of 2.96ms, TR of 2200ms, bandwidth of 240 Hz/pixel, inversion times at 1050ms, flip angles 7°, for anatomical localisation and registration.

Fieldmap scans of the B_0 field were acquired with TEs of 4.08 ms and 5.1 ms, TR of 620 ms, flip angle of 39°, isotropic resolution of 2 mm, 7°, to aid distortion-correction.

2.3.2 Analysis

fMRI analysis was carried out using the Oxford Centre for Functional Magnetic Resonance Imaging of the Brain Software Library (FMRIB, Oxford, UK; FSL version 6; http://www.fmrib.ox.ac.uk/fsl/).

[1] Exercise exposure score = number of hours of exercise per week × intensity (1 = easy, 2 = moderate, 3 = intense)

Functional voxel-wise subject and group analysis

fMRI data processing was performed using FEAT (FMRI Expert Analysis Tool), version 6.0, part of FSL (FMRIBs Software Library; www.fmrib.ox.ac.uk/fsl). The same pre-processing steps and parameters as described in the previously published [114] study were applied. These included motion correction, brain extraction, spatial smoothing, high-pass filtering, B_0 field unwarping, and data denoising using a combination of independent component analysis (ICA) and retrospective image correction (RETROICOR). The first level analysis incorporated a general linear model (GLM) as demonstrated in Figure 2.1. The cleaned BOLD signals were regressed with breathlessness periods, anticipation of breathlessness, unloaded breathing, with additional regressors of $PETCO_2$ (partial pressure of end-tidal carbon dioxide), finger opposition, relief from breathlessness, periods of rating using the button box, demeaned ratings of intensity between trials, and a period of no loading following the final anticipation period, to control for confounding factors. The activation time-course was modelled using an optimal basis set of three waveforms (FLOBS: FMRIB's Linear Optimal Basis Sets, default FLOBS supplied in FSL [375], instead of the standard gamma waveform. This method is more resilient to changes in the haemodynamic response function (HRF), which may be due to slice-timing delays, individual differences in HRF, or HRF differences between different brainstem and cortex [114] [83] [161]. Time-series statistics was performed using FILM (FMRIB's Improved Linear Model), with local autocorrelation correction [376].

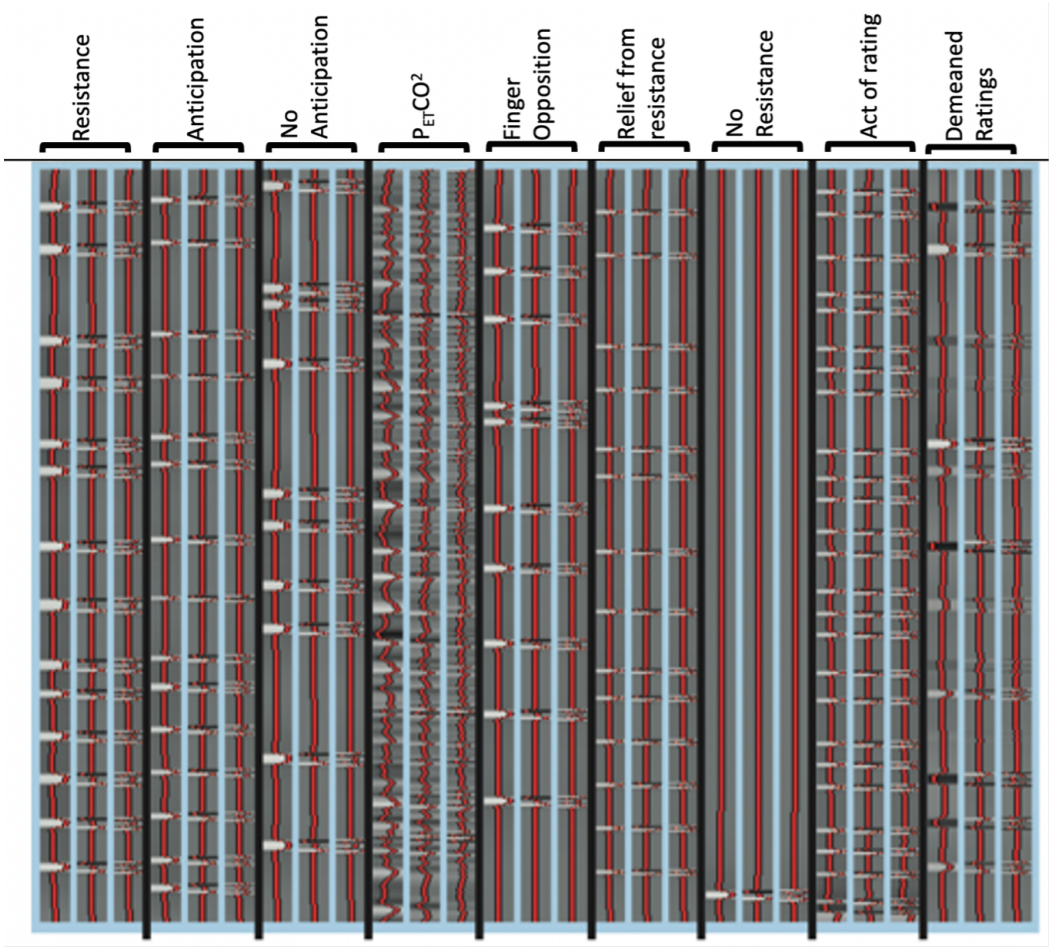


Fig. 2.1 Design matrix of subject-level GLM within FEAT Three EVs were created from the FLOBS function for each regressor. The single-subject GLM in the current analysis was replicated using the same EV settings as the previous publication, with details in Faull (2015, p. 57 [109]): "The 'resistance' onset and duration were calculated from the recorded inspiratory pressure physiological traces, while the anticipation durations were calculated from the onset of the stimulus to the beginning of the resistance. For the 'no resistance' trials, where the resistance was not applied, the anticipation duration was calculated from the onset of the stimulus to the maximum anticipation duration for each subject. The remainder of the presentation of the uncertain anticipation cue was modelled in a separate regressor ('no resistance'). The 'PET CO_2' trace was included to de-correlate the CO_2-induced BOLD changes from the respiratory stimuli throughout the functional scan, and was formed by linearly interpolating between the expired CO_2 peaks. Anticipation of no resistance ('no anticipation') and 'finger opposition' onset and duration represented the presentation of the corresponding stimuli on the screen, and 'relief from resistance' was modelled as the rest periods immediately following each resistance application, prior to ratings (4 s duration). The 'act of rating' regressor was included to remove noise from the physical act of pressing the button box, and spanned each of the rating periods. Finally, 'demeaned ratings' matched the 'resistance' regressor for timings, and the intensity of the regressor was the demeaned intensity value assigned to each of the inspiratory resistance blocks. Contrasts consisted of mean values of the first EV of each set of three regressors."

At the group level, for the analysis of BOLD activity within the amygdala, an a priori region of interest was defined, using a mask created from the Harvard Oxford cortical and subcortical structural atlases (Harvard-Oxford atlas) on a 1mm MNI152 standard brain, thresholded to include voxels with at least 50% probability of being in the amygdala. I adopted the thresholding value from published neuroscience analyses that utilised the amygdala as a region of interest, using the Harvard-Oxford atlas [185, 197]. Demeaned breathlessness intensity and anxiety scores were included as covariates to examine how BOLD activity scaled with these self-reported behavioural measures. Group differences of no interest(athletes[2] vs. sedentary control) and subject-specific residual motion (DVARS) [3] values were also included as regressors (see Figure 2.2 for details). Permutation testing with Threshold-Free Cluster Enhancement (TFCE) [324] and a (FWE-corrected) cluster significance threshold of $p < 0.05$ was employed. The contrasts of interest were:

- *Anticipation of resistance vs. no anticipation of resistance* [4]
- *Resistance vs. baseline*

[2]The original study design of the dataset[112, 111] aimed to explore the differences between athletes who regularly participated in endurance sport and sedentary controls, both of whom were healthy. However, all healthy participants were grouped together in this study as the effect of exercise was not central to the research goal. In fact, the exercise variable was not found to be significant in any of the subsequent analyses, as shown in following result section.

[3]DVARS (D referring to the temporal derivative of time courses and VARS denoting the root mean square (RMS) variance across voxels) is a measure that quantifies the rate of change of the BOLD signal throughout the brain at each frame of fMRI data, enabling the identification of motion artifacts and the characterization of data quality [281].

[4]The anticipation period is defined as the time between the presentation of the visual stimulus and the onset of inspiratory resistance.

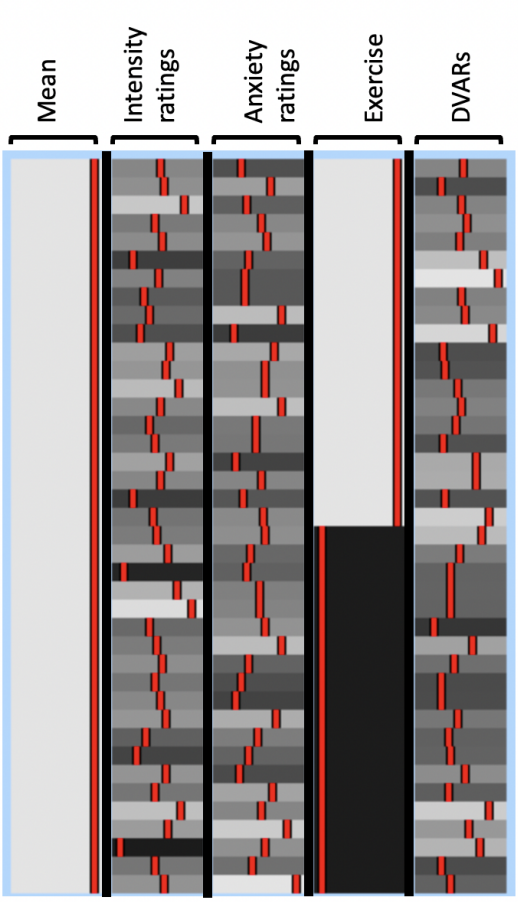


Fig. 2.2 Design matrix of task group-level GLM within FEAT (and 'randomise'). Each EV represents lower-level contrast. For each lower level contrast, positive and negative contrasts were calculated for the group mean ('mean'), plus covariates of the average resistive loading intensity ('average intensity'; calculated from lower level intensity ratings for each subject) and anxiety of upcoming resistance ('anticipation anxiety'). Lastly, an 'exercise' group comparison regressor was included to investigate differences between athletes and sedentary subjects, as a confound.

Supplementary ROI-based analysis

Freesurfer pre-processing and segmentation Pre-processing of the 7T MRI anatomical images was carried out using the Freesurfer pipeline, following the instructions outlined in https://surfer.nmr.mgh.harvard.edu/fswiki/HiResRecon and https://neurobren.com/freesurfer-masks/. Specifically, bias field correction was initially performed in SPM with the following parameters: Bias regularisation (very light: 0.0001), Bias FWHM = 60mm cutoff, and Sampling distance = 2. The "recon-all" procedure was then applied to the raw T1-weighted anatomical images, followed by the execution of the "segmentHA_T1.sh" [302]

command for segmentation of the amygala. The segmentation was subsequently transformed from Freesurfer space to native anatomical space using the command `mri_label2vol`. Each subject was assigned 9 sub-regions for the amygdala in each hemisphere, in volumetric anatomical space, ready for use in FSL (details in Table 2.2). For subsequent analysis, the left and right amygdala sub-region masks were merged and warped into the echo-planar imaging(EPI) functional space. The registration was also re-performed in FSL using the anatomical images pre-processed by the Freesurfer pipeline.

Given that the exact task timeline varied across subjects, statistical tests at the mean timeseries level could not be conducted. Instead, the voxel mean of the contrast of parameter estimate (COPE) values was extracted. These values were obtained from the first-level single-subject FEAT analysis as shown in Figure 2.1: COPE1 represents the resistive period against baseline; COPE10 represents the period anticipating a pending resistive loading, minus the period with no anticipation of loading. Additionally, for exploratory purposes, COPE2 represents the anticipation period against baseline. In total, 3 COPE values for each of the 9 bilateral amygdala sub-region masks were generated for each subject.

Statistics Statistical tests were performed on the voxel-mean COPE values for each task-related contrast in each mask. To assess whether there was activation during the different contrasts, one-sample t-tests were conducted under the null hypothesis that the mean equals 0. To investigate the relationship between sub-region activity across contrasts (3 COPEs in total), non-parametric permutation tests (N = 10,000) were performed using PALM [370] in FSL. The design file used was the same as Method 1 in Chapter 2, as shown in Figure 2.2. Data visualisation was conducted in Python.

Task FC analysis (psychophysiological interaction) for the task seed

The seed for all connectivity analysis A 5mm-sphere, task-relevant seed mask was created, centring the peak deactivation voxel observed during anticipation (MNI: 22, -3, -19; voxel: 68, 123, 53), which I will refer to as the BLA seed mask. I chose not to create a separate seed mask for the cluster identified during resistance for two reasons. Firstly, the deactivation clusters for anticipation and resistance were highly overlapping. In the standard MNI 1mm^3 space, the intersection of the deactivation clusters for resistance and anticipation comprised 577 voxels, accounting for approximately 41.2% of the resistance mask (1401 voxels) and 66.3% of the anticipation mask (870 voxels). Secondly, the peak voxels of these clusters were spatially close, and the 5-mm spheres centred on these peaks encompassed nearly identical

regions, both located within the BLA. Specifically, the distance [5] between the peak voxel for resistance (voxel: 66, 120, 57) and that for anticipation (voxel: 68, 123, 53) was just 5.39 mm. Given the significant overlap in both spatial extent and peak localisation, it is justified to use a single BLA seed for subsequent connectivity analyses, ensuring consistency and simplifying interpretation across tasks.

After defining the BLA seed, FC between the seed and the rest of the brain during the anticipation and resistance task conditions was examined using a psychophysiological interaction (PPI) analysis [127] [264]. PPI analysis is a method used to investigate task-specific changes in the relationship between activity in different brain regions, identifying voxels where activity correlates more strongly with a seed region (e.g., the BLA seed) in a specific context (i.e., anticipation or resistance).

Specifically, I first transformed the 5-mm mask from MNI 1 mm^3 space to each subject's functional EPI 2 mm^3 space. The mean timeseries for the BLA seed was then extracted by computing the voxel-wise mean within each subject-specific functional mask at each time point. This mean timeseries was subsequently entered into two separate general linear models (GLMs) in *FEAT*. Each model included an interaction term between the task regressor of interest and the seed timeseries. The task regressors represented either the anticipation of breathlessness (anticipation $>$ no anticipation) or the perception of breathlessness (perception $>$ baseline). This interaction term, known as the PPI, quantifies the task-specific modulation of connectivity between the BLA seed and other brain regions. Finally, a mixed-effects group analysis (based on the GLM shown in Figure 2.2) was conducted to assess the relationship between the PPI, group means, behavioural scores, and residual motion (confounding variable) associated with the PPI regressor.

Resting-state FC analysis for the task seed

FC between the same BLA seed and the rest of the brain during rest was subsequently examined. Mean timeseries within the BLA seed were calculated from the subject-specific functional EPI space masks and fed into a voxel-wise, single-subject analysis. This analysis included confounding regressors for the mean timeseries of the cerebrospinal fluid (CSF), white matter (WM), and a control seed located in the primary auditory cortex (see details in Figure 2.3). All explanatory variables (EVs), representing timeseries, were extracted from each subject's preprocessed functional data without the need for convolution. To account for small temporal delays in connectivity between brain regions, a temporal derivative was added for each regressor. A mixed-effects group analysis (same GLM as shown in Figure 2.2)

[5] The distance between the peak voxels of anticipation and resistance was calculated as $\sqrt{(x_1-x_2)^2+(y_1-y_2)^2+(z_1-z_2)^2}$.

was then performed to assess group means, behavioural scores, and residual motion, with a pre-threshold grey matter mask applied to constrain the analysis to the connectivity between the BLA seed and the rest of the brain grey matter.

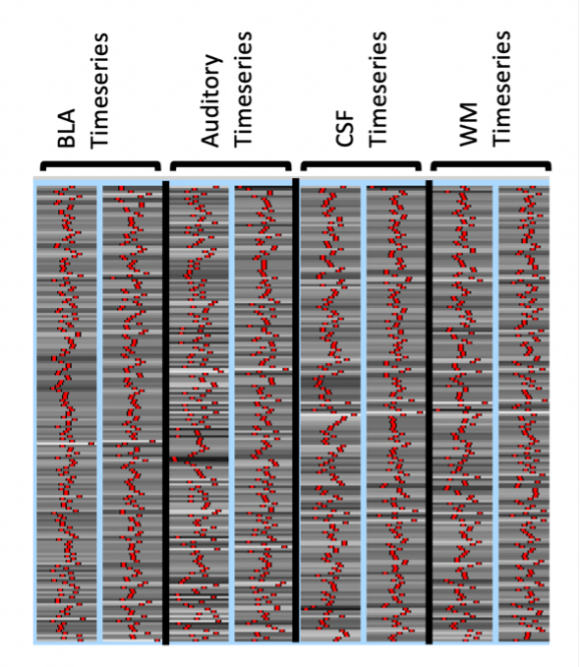


Fig. 2.3 Design Matrix of subject-level resting-state GLM within FEAT. The confounding timeseries of no interest for the CSF, WM and a control auditory region were regressed out.

2.4 Result

The following section reports three metrics in sequence:

1. Mean task-related activity in the amygdala, both voxel-wise and the complementary ROI-based methods.

2. FC of the BLA seed with the rest of the brain grey matter during the task.

3. FC of the BLA seed with the rest of the brain grey matter at rest.

For the task-related analyses (metrics 1 and 2), both mean activity and FC were reported separately for the two contrasts: anticipation of resistance (*anticipation of resistance* > *anticipation of no resistance*, $CS+ > CS-$) and resistance (*during resistive loading* > *baseline*). These results were further analysed in relation to self-reported breathlessness perception ('intensity' and 'anxiety') and the confounding variable of 'exercise.' Finally, resting-state

connectivity was examined to assess its relationship with breathlessness perception and exercise as a confounding factor.

For Metric 1, the voxel-based analysis was on a small-volume mask for the entire amygdala. I employed permutation testing with TFCE and set a family-wise error (FWE) corrected significance threshold of p<0.05, utilising the whole amygdala as a priori area of interest. This analysis was conducted using Randomise. TFCE eliminates the need for setting an arbitrary cluster-defining primary threshold by combining voxel-wise statistics with local spatial support underneath the voxel. The values at each voxel reflect the extent of local spatial support, emphasizing significant reductions in BLA activity while maintaining rigorous false positive control through permutation-based FWE correction. It enables more sensitive detection of voxel-wise activity changes.

For Metrics 2 and 3, the analysis was on the whole brain. I applied the conventional clustering method with a stringent voxel-wise primary threshold of Z > 3.1 and an FWE-corrected cluster significance threshold of p < 0.05, using the FEAT GUI.

The Harvard-Oxford atlas and the Jülich Histological Atlas [13] were utilised to aid interpretation throughout the analysis.

2.4.1 Functional activity of the amygdala during task

Anticipation of resistance

A significant decrease in BOLD activity (FWE $P < 0.05$) was observed in the amygdala bilaterally, identified using non-parametric statistics with TFCE and small volume correction for multiple comparisons. In the right hemisphere, the cluster encompassed areas of the BLA and possibly extended into the superficial group of the amygdala. In the left hemisphere, the cluster consisted of a smaller region (12 voxels), potentially located within the superficial region of the amygdala. A summary of the cluster maxima (peak voxel) is provided in Table 2.1, with an illustration of the activated columns shown in Figure 2.4.

Condition	Cl.	Vox.	Max Z	Maxima Coordinates (mm)		
				max(x)	max(y)	max(z)
Resistive loading	2	1047	6.23	66	120	57
vs. baseline	1	354	4.57	121	121	49
Anticipation	2	858	5.75	68	123	53
vs. no anticipation	1	12	3.99	106	116	58

Table 2.1 Summary of conditioned breathlessness task clusters and maxima within the amygdala. Acronyms: Cl. = Cluster, Vox. = Number of voxels, Max Z = Maximum Z-statistics, max(x), max(y), max(z) = Maxima coordinates in the X, Y, and Z dimensions.

During resistance

Similarly, a significant decrease in BOLD activity was observed in clusters of the amygdala columns in both hemispheres during resistive breathing, as identified using TFCE. In the right hemisphere, the cluster encompassed regions of the BLA, extending into the superficial area and possibly involving the entorhinal cortex of the hippocampus, situated more anteriorly, medially, and inferiorly within the amygdala, in comparison the the cluster found during anticipation. In contrast, the cluster in the left hemisphere was restricted to a small region within the BLA (refer to Table 2.1 and Figure 2.4 for a summary of the cluster maxima).

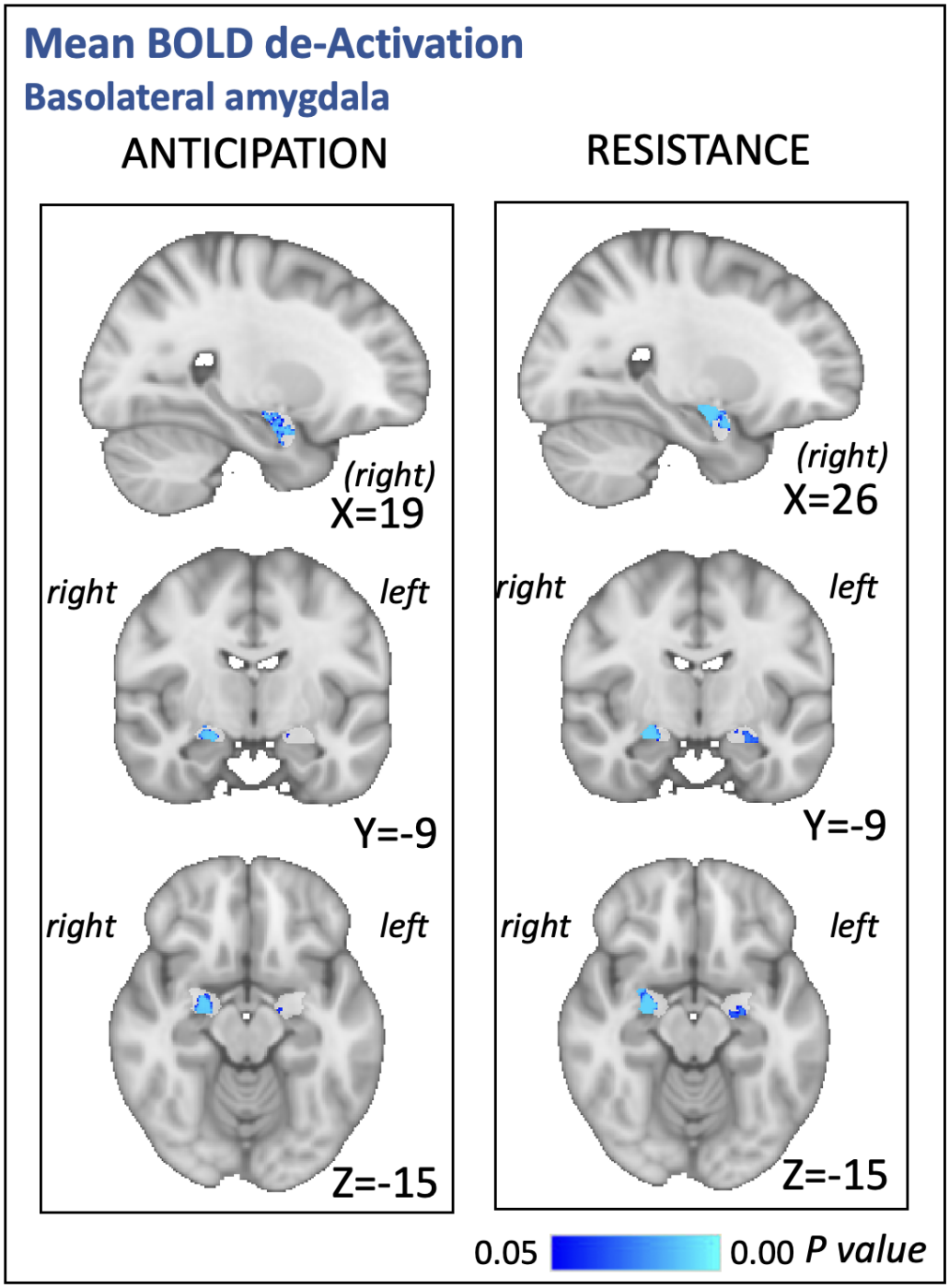


Fig. 2.4 Amygdala task response during anticipation and resistance phases of the task. Statistical maps are overlaid on a standard MNI 1 mm^3 standard brain. The light grey region delineates the whole amygdala, with significant clusters shown at $p < 0.05$, corrected using non-parametric threshold-free cluster enhancement (TFCE) and small volume correction based on an anatomically defined amygdala mask. Spatial smoothing was applied using a Gaussian kernel with a full-width at half-maximum (FWHM) of 2 mm.

Relationship to intensity and anxiety ratings

No significant clusters were identified within the amygdala that correlated with self-reported anxiety or intensity scores during either the anticipation or perception of breathlessness.

Relationship to exercise

No significant association was observed between exercise status and amygdala activity, as determined by contrasting athletes with sedentary controls.

Supplementary ROI-based analysis with nine amygdala masks (subnuclei)

To explore potential nuances not captured by the voxel-based analysis, I conducted a supplementary analysis using a region-of-interest (ROI)-based approach across nine subnuclei and regions of the amygdala.

Subject-Specific segmentation of the amygdala Segmentation of the amygdala was performed on each subject's T1-weighted (T1w) anatomical brain image, acquired at a resolution of 0.7 mm^3. The voxel counts for the 18 left and right sub-region masks are summarised in Table 2.2. These values also correspond to volumes in cubic millimetres, as the images were resampled to 1 mm^3 resolution during the Freesurfer pre-processing pipeline.

While it is conventionally recommended to erode each mask by one voxel to improve the accuracy of ROI delineation, this approach resulted in extremely small mask sizes for some regions, particularly in the central, medial, and anterior areas. As shown in Table 2.2, erosion significantly reduced the voxel count in these regions. Therefore, the bilateral uneroded masks were retained for the subsequent analyses.

Region	Voxel Number	Eroded
Left Hemisphere		
Basolateral complex		
accBA (accessory basal nuclei)	276	110
BA (basal nuclei)	491	207
LA (lateral nuclei)	728	365
Centromedial complex		
CenA (central nuclei)	37	0
CortA (cortical nuclei)	18	0
MA (medial nuclei)	1	0
Other areas		
AAA (anterior amygdala area)	36	0
CATransA (cortical-amygdaloid transition area)	183	20
ParaA (Paralaminar nuclei)	47	0
Right Hemisphere		
Basolateral complex		
accBA (accessory basal nuclei)	301	121
BA (basal nuclei)	489	205
LA (lateral nuclei)	749	372
Centromedial complex		
CenA (central nuclei)	38	0
CortA (cortical nuclei)	17	0
MA (medial nuclei)	7	0
Other areas		
AAA (anterior amygdala area)	34	0
CATransA (cortical-amygdaloid transition area)	180	19
ParaA (paralaminar nuclei)	49	0

Table 2.2 Summary of group mean mask sizes after Amygdala segmented into 9 sub-regions per hemisphere using Freesurfer. Voxel number equals to cubic mm.

As illustrated in Figure 2.5 and Figure 2.6, the result of the 18 (9 on the right and 9 on the left hemisphere) segmentation of the amygdala on each subject's T1w anatomical brain image were successful.

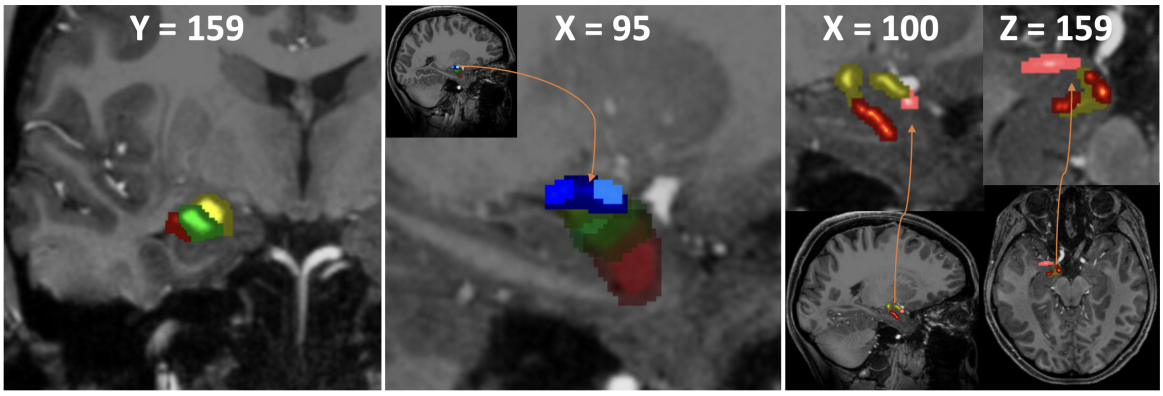


Fig. 2.5 An illustration of the amygdala segmentation using Freesurfer's atlas for 'subj015'. This shows the segmentation of the right amygdala on the native anatomical brain image of one subject. Each subject had a unique segmentation in their own native anatomical space. Left: the coronal view of the basolateral complex superimposed on the T1w image at 0.7 mm^3. accBA – yellow, BA – green, LA – red. Middle: the sagittal view of the centromedial complex superimposed on the same subject-specfic anatomical image. CenA –dark blue, CortA – mid blue, MA - light blue. The green BA and red LA masks are presented at the background. Right: for the other areas. AAA – coral, CATransA - yellow, ParaA – red.

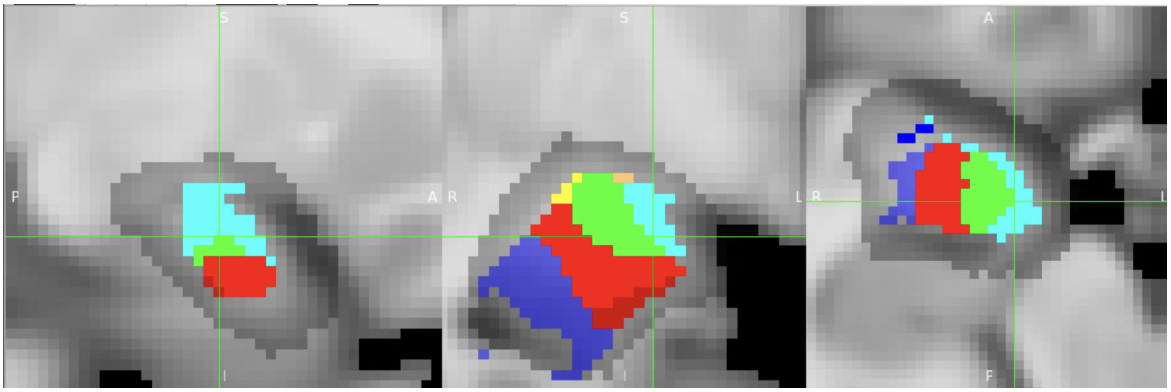


Fig. 2.6 This illustration shows the amygdala segmentation on an standard (MNI $1mm^3$) brain using Freesurfer's atlas. Freesurfer's segmentation defines more detailed amygdala subregions compared to the Harvard-Oxford atlas mask (in darker grey), which is thresholded at 50% and was used in the main chapter.

Functional task fMRI for the nine amygdala subnuclei Similar to the main voxel-wise method, the two primary contrasts of interest were BOLD activity during resistive loading (resistive loading > baseline) and during its anticipation (anticipation of resistance > anticipation of no resistance). An additional contrast (anticipation of resistance > baseline) was included for exploratory purposes.

As shown in Table 2.2, the basolateral complex of the amygdala—including the accessory basal nuclei (accBA), basal nuclei (BA), lateral nuclei (LA), and paralaminar nuclei (ParaA)—exhibited significant deactivation across all three contrast conditions after Bonferroni correction ($p < 0.05/27$).

The central amygdala nuclei (CenA) and anterior amygdala area (AAA) demonstrated unique deactivation in the 'resistance $>$ baseline' contrast, also surviving Bonferroni correction.

The cortical-amygdaloid transition area (CATran) showed deactivation during the anticipation period. However, this was significant post Bonferroni correction only when comparing anticipation to baseline ($CS+ >$ baseline) and not when comparing anticipation to the no-anticipation condition ($CS+ > CS-$).

No significant results were found for the cortical nuclei (CortA) or medial nuclei (MA), likely due to their extremely small size, as outlined in Table 2.2.

Region	Resistance > Baseline			Anticipation > No Anticipation			Anticipation > Baseline		
	Mean	t-stat	p-val	Mean	t-stat	p-val	Mean	t-stat	p-val
accBA	-0.562668	-3.61608	0.000846*	-0.443521	-4.56205	0.000049*	-0.510884	-4.90448	0.000017*
BA	-0.503329	-4.54038	0.000053*	-0.363429	-4.81310	0.000023*	-0.431350	-5.42505	0.000003*
LA	-0.455396	-4.74034	0.000028*	-0.299624	-4.26045	0.000125*	-0.320069	-4.60922	0.000043*
CenA	-0.557397	-4.21109	0.000145*	-0.278404	-3.07848	0.00380	-0.293763	-3.07255	0.00386
CortA	-0.445670	-2.68609	0.01057	-0.278292	-2.46087	0.01839	-0.295356	-2.42666	0.01996
MA	-0.444676	-3.09115	0.00367	-0.270145	-2.72403	0.00960	-0.269043	-2.59387	0.01330
AAA	-0.464663	-3.38313	0.001643*	-0.295916	-2.61983	0.01247	-0.344260	-2.98287	0.00491
CATranA	-0.312529	-2.27886	0.02823	-0.302197	-3.29401	0.00211	-0.364275	-3.61303	0.000854*
ParaA	-0.506816	-4.34130	0.000097*	-0.308777	-3.82635	0.000459*	-0.337641	-4.22722	0.000138*

Table 2.3 Summary of mean differences, t-statistics, and p-values for the 9 amygdala regions across three contrasts: resistance > baseline, anticipation > no anticipation, and anticipation > baseline. Significant p-values passing Bonferroni correction (p < 0.05/27) were marked with an asterisk (*). The basolateral complex includes the accessory basal nuclei (accBA), basal nuclei (BA), and lateral nuclei (LA). The centricortical complex consists of the central nuclei (CenA), cortical nuclei (CortA), and medial nuclei (MA). Other areas include the anterior amygdala area (AAA), cortical-amygdaloid transition area (CATranA), and paralaminar nuclei (ParaA). In addition, caution must be exercised when interpreting results related to the MA and CortA, given their limited voxel counts, as detailed in Table 2.2.

Relationship to intensity and anxiety score for the nine amygdala subnuclei None of the sub-regions identified through segmentation exhibited a significant association with either intensity or anxiety ratings.

Relationship to exercise No significant associations were observed between exercise status and amygdala activity when comparing athletes with sedentary controls.

Due to the small size of the masks and the challenges in creating a unified seed mask in the MNI brain space for further connectivity analysis, I did not explore the FC profiles for ROIs.

2.4.2 Functional task connectivity of the BLA seed

A PPI analysis [127] [264] was conducted for the active column during both anticipation and breathlessness.

Anticipation of resistance

No significant clusters were identified as co-activating with the BLA seed during the anticipation phase of breathlessness.

During resistance

As illustrated in Figure 2.7, connectivity between the contralateral (left) mediodorsal nucleus (MD) of the thalamus and the BLA seed exhibited a significant increase during resistive inspiration compared to baseline.

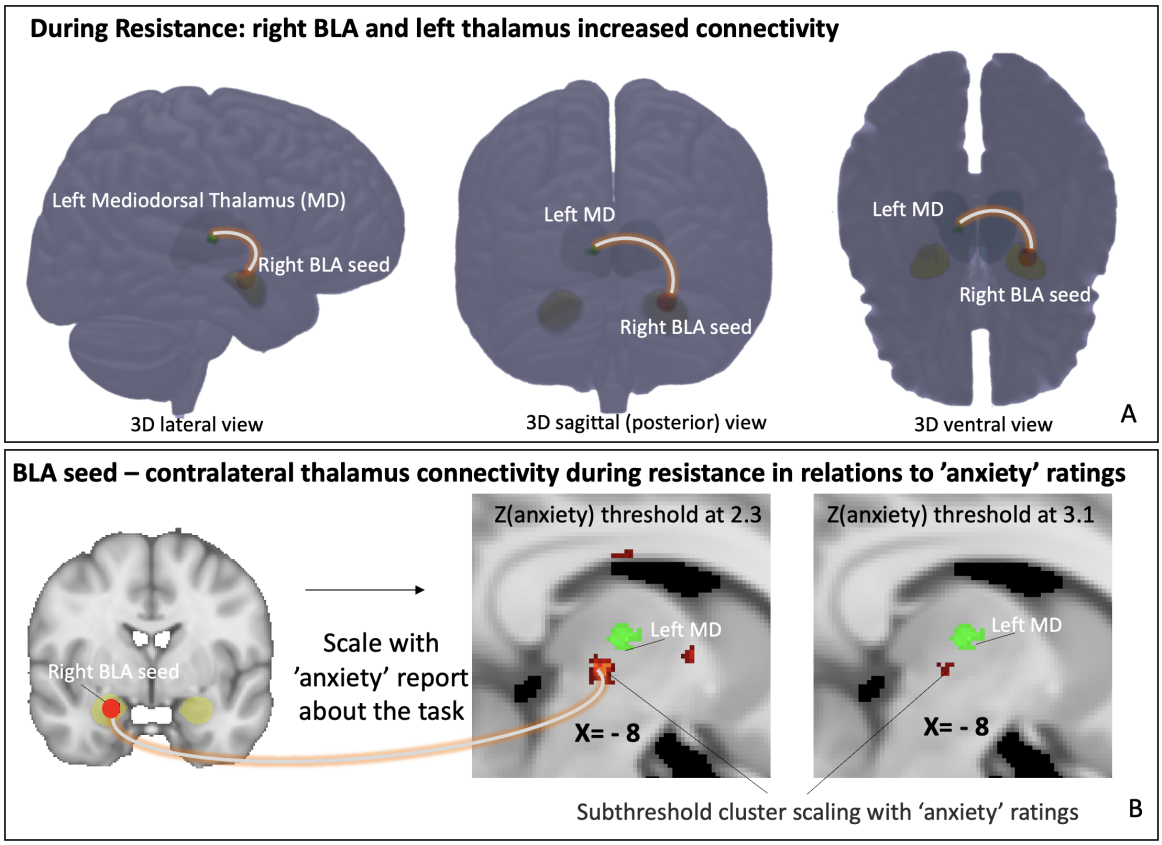


Fig. 2.7 BLA-thalamus FC during resistance and relationship to anxiety. Plane A illustrates the FC between the deactivated BLA seed (red) and the rest of the brain during the resistance phase of the task. A significant cluster was identified in the left mediodorsal thalamus (MD, green) with a threshold of $Z > 3.1$ and a cluster probability threshold of $p < 0.05$, corrected for multiple comparisons. The cluster and seed are visualised in three dimensions (3D), superimposed on a semi-transparent 3D standard brain (MNI 1 mm^3).
In Plane B, the left image displays the BLA seed's location in a sagittal view. The right two images show the location of the left thalamus (dark red) in the whole-brain statistical map, thresholded at $Z > 2.3$ and $Z > 3.1$. These maps highlight voxels exhibiting connectivity with the BLA seed during resistance, which scales with subjective anxiety ratings about the task. For reference, the green cluster corresponding to the MD is included to indicate its precise location.

Relationship to intensity and anxiety ratings

No significant clusters were identified where FC with the BLA seed during either the resistance phase or its anticipation scaled with anxiety or intensity scores.

However, anxiety scores showed a positive association with FC between the BLA and a group of voxels in the contralateral thalamus. Although these voxels exhibited Z-statistics exceeding 3.1, the cluster did not reach significance under a non-parametric TFCE test with

FWE correction ($p > 0.05$). This subthreshold cluster is located near the ventral border of the MD cluster identified in Section 2.4.2, as depicted in Plane B of Figure 2.7.

Relationship to exercise

No significant association was found for the effect of exercise by contrasting the athletes vs. sedentary controls.

2.4.3 Functional resting-state connectivity of the BLA seed

The resting state functional magnetic resonance imaging (rs-fMRI) FC associated with the same BLA seed were examined to explore their relationship with subjective breathlessness perception ratings. To validate the connectivity profile of the deactivated seed identified as the BLA, I found significant connectivity between the BLA seed and several regions, including the bilateral temporal pole, temporal occipital fusiform cortex, precuneus cortex, posterior cingulate cortex, ipsilateral frontal orbital cortex, superior frontal gyrus, subcallosal cortex, putamen, angular gyrus, lateral occipital cortex, as well as the contralateral frontal pole, frontal medial cortex, superior temporal gyrus (posterior), and middle temporal gyrus (see Figure 2.8). This FC profile support the seed's location within the BLA, which is characterised by its projections to and from the limbic system and higher-order cortices, rather than the CMA, which predominantly connects with the brainstem and pons.

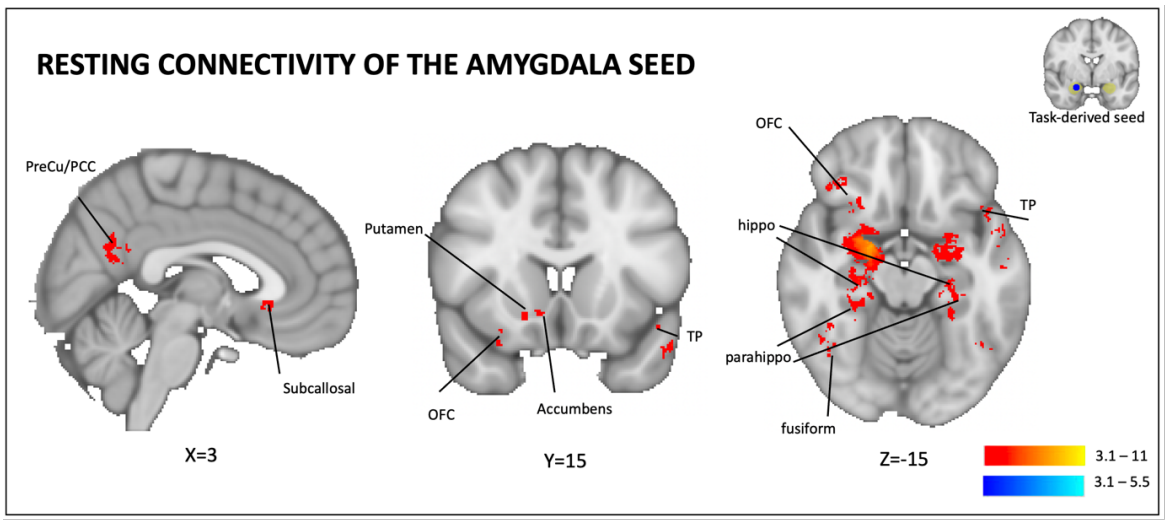


Fig. 2.8 Mean rs-fMRI FC to the de-active seed located at the BLA. Top-right corner: seed placement within the amygdala based on the task fMRI results. The images consist of a colour-rendered statistical map superimposed on a standard (MNI 1mm^3) brain. Significant regions are displayed with a threshold $Z > 3.1$, with a cluster probability threshold of $p < 0.05$ (corrected for multiple comparisons). Acronyms: TP, temporal pole; FP, frontal pole; hippo, hippocampus; parahippo, parahippocampal gyrus; fusiform, temporal occipital fusiform Cortex; PCC, posterior cingulate gyrus; precuneus cortex, PreCu; frontal orbital cortex, OFC.

Relationship to intensity and anxiety ratings

The rs-fMRI FC of the right temporal pole and the amygdala seed was found to be positively associated with the subjective ratings of intensity from the participants. The resting-state connectivity of the left precuneus cortex was found to be negatively associated with the intensity scores (See Figure 2.9). For anxiety ratings, no clusters survived the $Z > 3.1$ and FWE correction for cluster significance at $p < 0.05$.

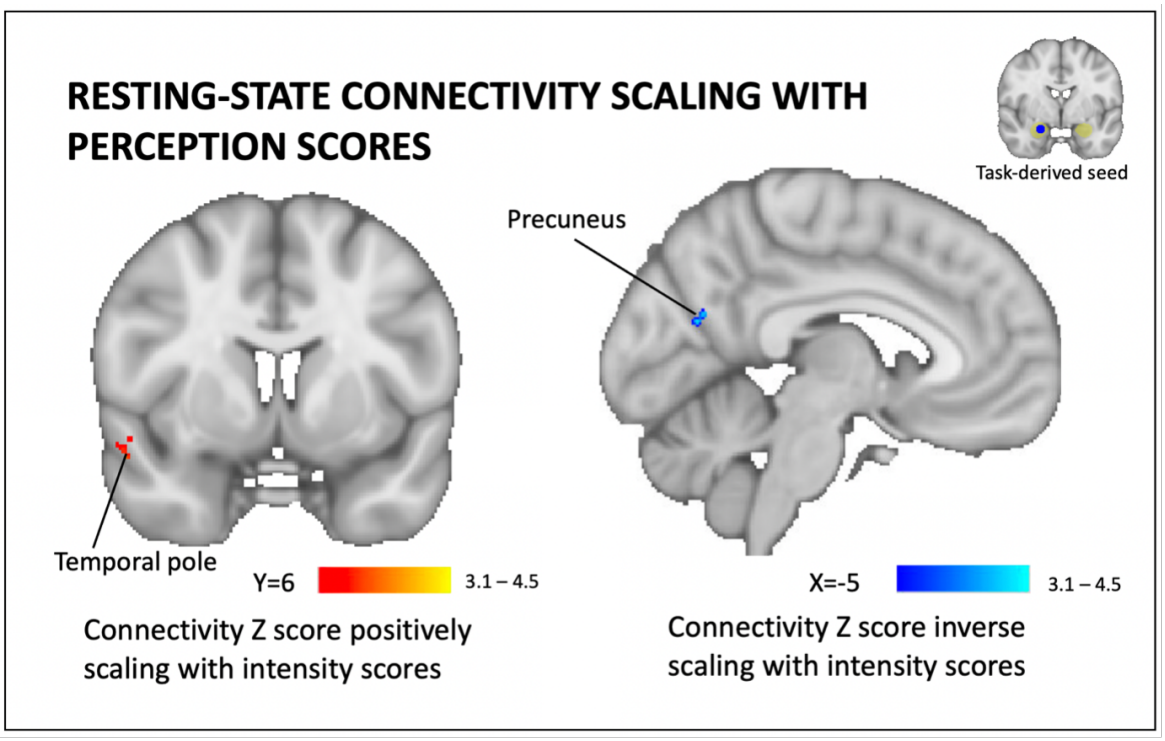


Fig. 2.9 Regions where rs-fMRI FC to the BLA seed scaled with intensity rating scores. The image presents a colour-rendered statistical map superimposed on a standard (MNI 1 mm^3) brain. Significant regions are displayed with a threshold of $Z > 3.1$, with a cluster significance threshold (corrected for multiple comparisons) of $p < 0.05$. The resting-state connectivity between the BLA seed and the ipsilateral temporal pole was positively associated, while the BLA connectivity with the contralateral precuneus cortex was negatively associated with subjective perception of 'Intensity' of respiratory threats. No clusters were found to correlate with anxiety scores.

Relationship to exercise

No significant differences were observed when comparing athletes and sedentary controls, indicating no measurable effect of exercise on the investigated parameters.

2.5 Discussion

Summary of Results In this chapter, I investigated amygdala activity during both the anticipation and experience of conditioned breathlessness, and examined how its task-related and resting-state activity and connectivity with other brain regions relate to subjective ratings of anxiety and intensity. Our findings partially support our initial hypotheses regarding the distinct spatial and temporal involvement of amygdala subregions during the breathlessness

task. Specifically, deactivation centred around the BLA was associated with both the anticipation and resistance phases of breathlessness, as revealed by both the main voxel-wise analysis and the supplementary ROI-based analysis using nine amygdala subnuclei.

The role of the BLA was evident not only through task-related deactivations but also through connectivity patterns observed during the resistance phase, where increased coupling with the contralateral mediodorsal thalamus (MD) underscored the BLA's role in perceptual inference.

Contrary to our hypothesis, no significant involvement of the CMA was observed during the resistance phase in the voxel-wise analysis, despite substantial literature supporting its role in active respiratory control [18, 163, 193, 66, 291, 210, 88, 115]. However, the supplementary ROI-based analysis, which used subject-specific masks obtained from the segmentation of each participant's amygdala into nine subnuclei, indicated that the central and anterior amygdala regions may have been uniquely deactivated during the resistance phase, and not during its anticipation.

At rest, self-reported intensity ratings of breathlessness were associated with stronger FC between the BLA seed and the temporal pole, and weaker FC between the BLA seed and the precuneus cortex. This finding contrasts with our hypothesis that anxiety ratings would be uniquely associated with BLA metrics and intensity ratings with CMA metrics. Moreover, no significant links were found between anxiety scores and BLA-related connectivity markers, nor between exercise and brain connectivity. Notably, a subthreshold cluster (uncorrected, $Z > 3.1$) in the left thalamus showed FC with the BLA during the resistance phase, scaled positively with anxiety ratings.

These results provide novel insights into the differential roles of amygdala subregions in conditioned breathlessness. While the BLA appears central to breathlessness regulation and perception, the role of the CMA may be more complex than our current methodology has captured, warranting further investigation.

2.5.1 BLA in the perceptual and freeze response to respiratory threats

Consistent with the literature on the amygdala's role in the freeze response to fear, the basolateral amygdala (BLA) was found to deactivate during both the anticipation and resistance phase of breathlessness. The supplementary ROI-based analysis yielded the same result, with an addition of ParaA. The BLA and ParaA serves as a gateway for sensory inputs from the neocortex and maintains bidirectional connections with affective and evaluative prefrontal areas [214]. Inhibitory circuits from the prefrontal cortex have been shown to modulate the expression of conditioned responses via the amygdala [285]. Lesions to the BLA—the frontotemporal region of the amygdala—have been shown to abolish conditioned

fear responses [107]. Overexpression of conditioned fear responses has also been proposed as a mechanism underlying the disproportionate breathlessness experienced by patients with chronic obstructive pulmonary disease (COPD) and asthma, despite the absence of clear biomedical markers [169]. The observed deactivation of the BLA during anticipation might suggest mechanisms that underlie maladaptive breathlessness in patients, where inappropriate and fearful associations with safe situations—such as seeing stairs or using an inhaler—lead to unwarranted breathlessness.

Interestingly, significant deactivation of the BLA was also observed during the experience of breathlessness (the resistance phase). This deactivation might reflect the simultaneous occurrence of both active and perceptual inference at the level of amygdala, suggesting that moment-to-moment updates of the perceived resistive loading were occurring. This finding contrasts with previous work on the PAG in the same task, where the vlPAG is uniquely activated during anticipation of resistive loading, corresponding to passive responses to inescapable stress, while the lPAG's activation is confined to the phase of resistive loading, reflecting active responses to threat [113] [114]. This discrepancy may indicate that respiratory regulation, when processed at higher levels of the neural hierarchy, involves more complex affective and belief-updating processes, as opposed to the more phylogenetically primitive mechanisms seen in the midbrain.

Despite significant BLA deactivation, no clusters within the amygdala, nor BLA-centred connectivity during task conditions, were significantly associated with subjective breathlessness ratings, despite a subthreshold finding in BLA-thalamus coupling during resistance, as further discussed in Section 2.5.2 below. This may be due to the difficulty in detecting such markers in a healthy sample, where random variance in subjective ratings could obscure subtle individual differences in amygdala responses to respiratory threats. Alternatively, these effects might only emerge when the resistive stressor reaches an individual's maximum threshold, evoking anxiety—an outcome that was not observed in the present study. Future research incorporating patient populations and matched healthy controls may provide a clearer contrast in BLA deactivation and better elucidate its role in respiratory symptom perception.

2.5.2 "Belief update" - task BLA-thalamus connectivity during resistance

The connectivity analysis during the task revealed an increase in BLA connectivity with the contralateral MD during resistive breathing. The thalamus is well established as a relay hub for both interoceptive and exteroceptive signals [337, 152]. Respiration involves interoceptive

signals, such as those from the chemoreceptors in the pons and possibly affective efferents from higher-order cortex, and exteroceptive signals, such as the mechanical feedback from diaphragm contraction and windpipe airflow [229]. Previous studies have consistently demonstrated thalamic activity during volitional breathing [61], exercise-induced hyperpnea [120, 111], and in the current breathlessness task [114] (see Figure 2.10 for whole-brain activity during the task [114]).

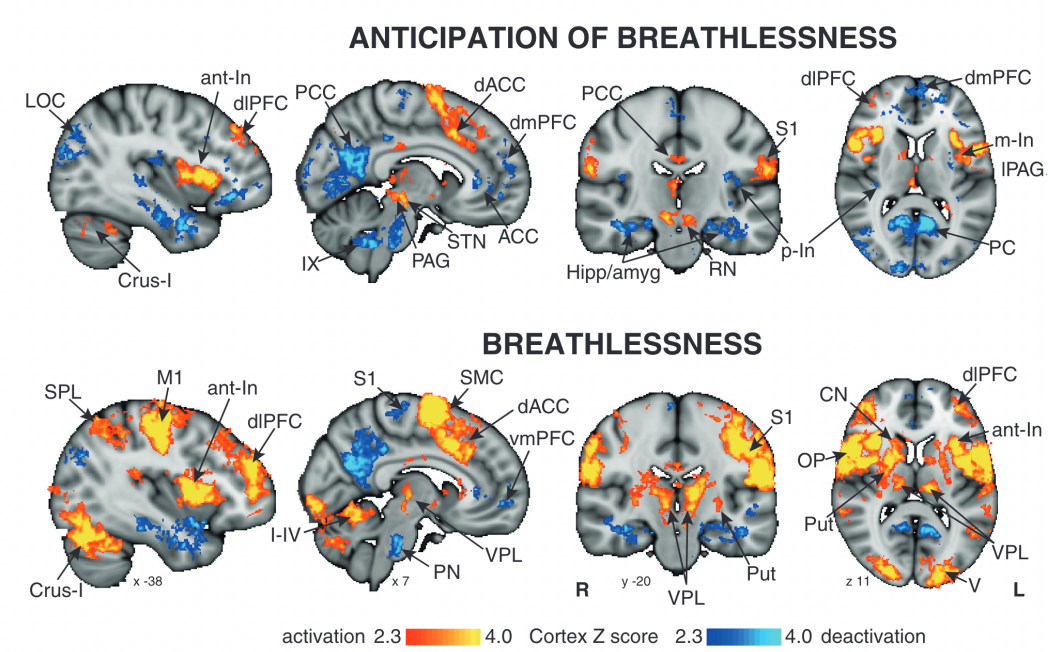


Fig. 2.10 Reproduction of whole-brain activation during the conditioned breathlessness task at two contrasts of interest—anticipation and breathlessness—as reported by Faull and colleagues [114]. A Z-threshold of 2.3 was applied (rather than 3.1), using FWE cluster correction instead of TFCE. Activity is emphasised in the PAG rather than the amygdala. This figure is presented for background information only. Acronyms: PAG, periaqueductal grey; vlPAG and lPAG, ventrolateral and lateral PAG; M1, primary motor cortex; S1, primary somatosensory cortex; CN, caudate nucleus; SMC, supplementary motor cortex; Put, putamen; ACC, anterior cingulate cortex; dACC, dorsal ACC; PCC, posterior cingulate cortex; PC, precuneus; dlPFC, dorsolateral prefrontal cortex; dmPFC, dorsomedial PFC; vmPFC, ventromedial PFC; Hipp, hippocampus; amyg, amygdala; a-In, anterior insula; m-In, middle insula; p-In, posterior insula; LOC, lateral occipital cortex; SPL, superior parietal lobule; STN, subthalamic nucleus; RN, red nucleus; OP, operculum; V1, primary visual cortex; IX, I–IV and Crus-I, cerebellar lobes; thalamic nuclei: VPL, ventral posterolateral nucleus; VIN. Activation denotes an increase in BOLD signal; deactivation, a decrease.

The MD has been linked to various pathological respiratory conditions. For instance, Cheyne-Stokes breathing (CSB), a condition resulting from impaired integration of sensory information with respiratory motor output, has been associated with increased MD activity during episodes of obstructive sleep apnoea, as observed in fMRI scans during sleep [173]. In animal studies, electrical stimulation of the MD in fetal sheep has been shown to inhibit respiratory motorneurons, resulting in prolonged expiratory times and respiratory periods [204]. Additionally, lesions in the posteromedial thalamic nuclei have been found to abolish the hypoxic inhibition of fetal breathing [202, 203]. These findings highlight the MD's role in exteroceptive processes, such as airflow-related sensory stimulation, and its involvement in motor control, evidenced by its connection with the primary motor and somatosensory cortices.

While the MD's connectivity with the respiratory motor cortex has been documented in the context of breathlessness, its interaction with limbic structures, such as the amygdala, remains unexplored. The increased MD-BLA coupling observed in this study during resistance is the first to suggest a critical role for the MD-BLA circuit in processing aversive, respiratory-related sensory signals. The MD's bidirectional connections with the prefrontal cortex (PFC) may facilitate the integration of sensory inputs, such as respiratory resistance, with higher-order cognitive and emotional processes. Notably, this basolateral limbic circuit, involving the MD, amygdala, and medial PFC, has been proposed as a triangular network supporting learning and memory processes [372], although its role in interoceptive (respiratory) processes has received less attention.

The increased MD-BLA connectivity observed in this study likely reflects the response to the salience of resistive breathing, as the MD is known to play a key role in updating cognitive states in response to novel or salient stimuli. This connectivity may reflect the active perceptual inference, such as processes of recognition and belief-updating (e.g. habituation or catastrophising), along with volitional behavioural adaptations (e.g. deepened inspiration), aiming at integrating these signals in response to respiratory threat. In this context, the BLA, crucial for emotional processing, may signal the threat or discomfort of breathing resistance, while the MD facilitates the integration of this signal into broader cortical networks for higher-order cognitive processing [274]. For example, it may be facilitating the formation of an internal belief that "This is unpleasant, but it is safe.". This interpretation aligns with the MD's role as a "Bayesian observer," integrating top-down predictions from the cortex and updating sensory representations based on unexpected inputs [292]. Thus, increased BLA-MD connectivity may represent an adaptive and phasic mechanism modulating both the perception and emotional response to respiratory discomfort.

Following this reasoning, it is plausible to hypothesise that the connectivity between the BLA and the MD during breathlessness is linked to belief-updating processes and is associated with self-reported discomfort levels. Although the primary analysis did not yield significant results after correction for FWE at $P < 0.05$ using TFCE, a neighbouring cluster of voxels located ventral to the significant MD region displayed increased FC with the BLA during resistive breathing in participants who reported higher anxiety scores at the end of the task. This finding suggests that heightened BLA-MD coupling may be particularly relevant for individuals with elevated anxiety, potentially reflecting a neural mechanism underlying breathlessness-specific catastrophising in maladaptive breathlessness. Further exploration of these subthreshold regions may provide valuable insights into the role of anxiety in modulating respiratory perceptions through the BLA-MD circuit.

Finally, the observation that BLA-MD connectivity increased during resistance but not during anticipation implies that although the deactivated areas of the amygdala overlapped in both conditions, they may play distinct roles in each phase. This hypothesis warrants further investigation.

2.5.3 Interpreting "deactivation" of BLA and its FC during task

Up to this point, the term "deactivation", or negative BOLD responses (NBRs), of the BLA during the task may be misleading. Rather than indicating disengagement of BLA neurons, it likely reflects active modulatory network inputs targeting the BLA.

Seminal work by Logothetis and colleagues [221, 222] demonstrated that BOLD responses are most strongly correlated with local field potentials (LFPs), which reflect the summed synaptic and dendritic activity of neuronal populations—i.e., inputs and local processing—rather than action potentials or axonal outputs. Attwell and Iadecola [20] estimated that approximately 74% of the brain's energy budget is allocated to postsynaptic potentials, used primarily to restore resting ion gradients via the ATP-dependent Na^+/K^+ pump. Accordingly, BOLD signals should be interpreted as representing dendritic and synaptic activity within the BLA—that is, its inputs rather than its outputs.

The BLA is predominantly composed of glutamatergic principal neurons (approximately 80%), accompanied by a population of inhibitory GABAergic interneurons [298, 329]. Of particular relevance to interpreting BOLD signals, the BLA receives primarily glutamatergic afferent projections originating from key regions such as the prefrontal cortex (including the prelimbic, infralimbic, and orbitofrontal cortices), thalamic nuclei, and sensory areas such as the dysgranular insular cortex [298, 283, 176]. These excitatory inputs predominantly target the dendrites of BLA principal neurons. In parallel, local GABAergic interneurons[283],

including parvalbumin-positive subtypes, provide inhibitory modulation that fine-tunes the excitability of these projection neurons.

In this context, the NBRs observed during the breathlessness task—both during anticipation and perception—may reflect enhanced inhibitory (e.g., GABAergic) input either directly at the BLA or indirectly at its afferent sources (e.g., PFC or thalamus), resulting in reduced excitatory (glutamatergic) drive to the BLA and thereby decreasing its metabolic demand. Given the BLA's central role in salience detection and its resting-state coupling with interoceptive regions such as the anterior insula, we propose that this deactivation reflects an active top-down regulatory mechanism modulating affective responses to aversive interoceptive stimuli (e.g., breathlessness). This adaptive suppression aligns with theoretical models of prefrontal-limbic regulation and with the concept of perceptual inference introduced in Chapter 1. It may represent the execution of a top-down cognitive instruction along the lines of: "This is unpleasant, but it is safe—because the expert or experimenter said so before I came."

It is worth noting that one may question whether inhibitory input might also increase the BOLD signal, given that GABAergic synapses also require energy consumption (e.g., via the Na^+/K^+ pump) to maintain ion gradients [280]. However, the BOLD signal reflects the net metabolic demand of both inhibitory and excitatory postsynaptic activity, which is typically reduced overall due to decreased cerebral blood flow driven by inhibitory processes [317]. Furthermore, because BOLD primarily reflects changes in cerebral blood flow and oxygenation, it is more sensitive to excitatory synaptic activity than to inhibitory input. Inhibitory activity typically results in a decrease in the BOLD signal [247, 168]. Overall, the NBRs observed in the BLA during breathlessness blocks, relative to resting-state baseline, are best interpreted as indicating a net reduction in metabolic demand.

Moreover, we observed increased FC between the BLA and contralateral MD during breathlessness blocks compared to resting state. This suggests that the deactivation dynamics of BLA and MD become more temporally synchronised under breathlessness conditions. Mechanistically, such synchrony may arise from a shared inhibitory input or from inhibition initiated at the MD and subsequently propagated to the BLA via MD–BLA glutamatergic projections. The enhanced BLA–MD coupling likely reflects a concerted gating of aversive interoceptive signals through thalamic relay pathways and limbic circuits. Importantly, the strength of this coupling appears to relate to individual anxiety levels, with more anxious participants exhibiting tighter BLA–MD synchrony (uncorrected for multiple comparisons, $P < 0.05$, TFCE). This finding supports the hypothesis that coordinated suppression of BLA and MD activity reflects subjective emotional arousal and anticipatory processing even in a non-clinical population. It may index an adaptive mechanism for maintaining emotional

homeostasis, enabling individuals to reconcile interoceptive prediction errors with learned safety predictions. Conversely, individuals with maladaptive breathlessness may lack this MD–BLA synchronisation and exhibit reduced tolerance for otherwise harmless respiratory challenges.

Finally, interpretation of NBRs in the BLA must take into account that our discussion of BOLD signal properties is grounded largely in findings from neocortical areas. Logothetis and colleagues'[221, 222] work also employed a monkey visual cortex model. There remains debate over the generalisability of BOLD signal interpretation to subcortical regions such as the BLA and MD.

Crucially, the BOLD signal is an indirect measure of local neural activity, reflecting the interplay of oxidative metabolism ($CMRO_2$), cerebral blood flow (CBF), and cerebral blood volume (CBV), which together determine changes in deoxygenated haemoglobin (dOHb)—the principal contributor to BOLD contrast [261]. The key physical principle is that dOHb is paramagnetic. In neocortical regions, the main BOLD response reflects increased neural activity leading to elevated $CMRO_2$ and CBV (both of which increase dOHb), followed by an overcompensatory increase in CBF, which brings in oxygenated haemoglobin and results in a net decrease in dOHb [45].

However, it remains debated whether such overcompensatory increases in CBF occur as reliably in subcortical regions. Neurovascular coupling—the relationship between neural activity and haemodynamic response—varies across brain regions and individuals [94]. One contributing factor is that subcortical structures typically exhibit lower capillary density, sparser vascular innervation, and a vascular architecture characterised by relatively large feeding arteries compared to their smaller peripheral branches[83]. These features, in contrast to the denser and more responsive vascular networks of cortical areas like the visual cortex, may constrain the ability of subcortical blood flow to match increases in local metabolic demand. Schridde and colleagues [305], for example, demonstrated that in the hippocampus, BOLD signals can decrease or remain unchanged during neuronal activation. Using simultaneous fMRI and neurophysiological recordings during bicuculline-induced seizures, they suggested that increased $CMRO_2$ in the hippocampus may exceed the corresponding increase in CBF, resulting in a net rise in dOHb and an NBR. Ongoing debates continue to explore these phenomena in relation to laminar structure, task engagement, and regional variability in neurovascular and metabolic responses [256, 82, 140, 313]. In general, neurovascular coupling in subcortical structures such as the BLA appears poorer or at least more variable than in cortical areas such as the visual cortex, further complicating interpretation and warranting cautious inference.

I do not discuss other explanations of NBRs that treat it as hemodynamic phenomenon that is not driven by neural activity, such as vasoconstriction [315] and "vascular steal" [162, 377][6]—for two reasons. First, more recent work using simultaneous electrophysiological recordings and BOLD-based fMRI suggested that neural activity remains the major contributor to NBRs (>60%) [316, 195, 270], and NBRs are more consistently associated with decreases in both CBF and $CMRO_2$, in both human [270, 317, 332] and monkey [316, 36, 195] visual and somatosensory/motor cortices. Second, these haemodynamic explanations are all based on cortical models, and thus their generalisation to subcortical regions is limited.

Together, based on current evidence regarding the neurophysiological basis of (negative) BOLD signals and the biological architecture of BLA, it is highly plausible that, during the breathlessness task, the BLA received inhibitory inputs or top-down suppression—either directly via recruitment of its local GABAergic interneurons, or indirectly through reduced excitatory input from its prefrontal and thalamic afferents. In particular, during the perception phase of breathlessness, this inhibition may selectively target the glutamatergic MD→BLA pathway, as reflected by the observed increase in the BLA-MD FC. While alternative explanations for the observed NBR and connectivity patterns remain possible, they should be interpreted with caution. Future research aimed at characterising the specific neurovascular properties of the amygdala and mapping its region-specific hemodynamic response function (HRF) will be essential to validate and refine this interpretation.

2.5.4 Lack of evidence for CMA's role in breathlessness

The CMA, known for its connections to respiratory centres in the pons and brainstem, has been indicated to play a well-established role in modulating respiratory patterns [385, 131, 380, 259]. Direct stimulation of the central nuclei of amygala has been shown to induce apnea in both animal and human studies [18, 163, 193, 66, 291, 210, 88], and lesions in this area have been found to alter autonomic functioning [115]. However, the main voxel-wise analysis did not reveal any significant CMA activity or connectivity during the anticipation or perception of breathlessness.

One plausible explanation for this lack of evidence is that the dynamic CMA involvement in respiration was not captured by BOLD signals. In previous animal research, activation or stimulation of CMA in relation to breathing is confined to only the inspiratory phase and

[6]Vasoconstriction refers to the narrowing of blood vessels due to contraction of smooth muscle in their walls, thereby reducing blood flow to specific areas and potentially preserving perfusion in vital regions. "Vascular steal" describes a phenomenon in which blood is diverted away from a target region towards neighbouring areas with increased CBF, effectively "stealing" the available supply. This typically occurs when the affected region has limited vasodilatory capacity and cannot adequately increase its own blood flow in response to demand.

may only be nasal-breathing dependent[385, 380, 259]. As all participants were breathing through a mouth-piece, the CMA may simply not activate due to the lack of nasal-breathing and olfaction involvement. Furthermore, human inspiration may alias with the BOLD signals. Typically, normal resting breathing falls between 0.15–0.4Hz. However, it has been found that during experimental settings, such as biofeedback studies, participants breath slower - with 4.5 to 7.0 breaths per minute (0.08–0.12 Hz) [333]. These lower frequency physiological oscillations are precisely where the BOLD signals occupy(0.01 - 0.15 Hz)[349] - e.g. 6 breaths per minute is equal to 0.1Hz, which is within the range of the frequency of the BOLD signal. Conventionally, respiratory signals have been considered noise in fMRI analyses [184, 57], and removing these components from fMRI time series has been shown to significantly improve data quality, allowing for a more reliable interpretation of the BOLD signal [51, 349]. This correction is particularly important for reducing susceptibility artifacts near regions such as the vertebrobasilar artery and adjacent brainstem structures - key to the current study[73]. Hence, I have employed physiological noise correction (PNM). PNM may have further masked any subtle CMA involvement in respiratory processing. This suggests that standard fMRI sequences may not be the most suitable tool for capturing the dynamic interactions between the CMA and the brainstem during respiration. Future studies might benefit from the use of experimental design with intentionally manipulated inspiratory pattern, to detect these dynamics in CMA during breathing more effectively.

Another likely reason for the lack of evidence may stem from the heterogeneity in the location, size, and distribution of subnuclei within the amygdala. By using a unitary whole amygdala mask based on an average standard (MNI $1mm^3$) brain as an a priori region of interest, I may have overlooked critical details. Given that the medial and central nuclei of the amygdala are particularly susceptible to signal dropout and distortion, such nuances may have been too noisy to detect as distinct clusters in our voxel-wise analyses.

The supplementary method using the pre-segmented amygdala subnuclei may have advantages over the issue of heterogeneity amygdala location and structure. This supplementary ROI-based analysis, utilising subject-specific amygdala subnuclei and regions obtained directly from ultra-high-resolution anatomical MRI images, yielded results consistent with our hypotheses, although these may be sporadic due to the extremely small size of the masks. The CMA, particularly the anterior and central amygdala areas (AAA and CenA), exhibited deactivation solely during the perception of breathlessness, and not during the anticipatory phase, in line with our predictions. Supporting our hypothesis, the phylogenetically older CMA may uniquely deactivated during the regulatory phase of breathlessness perception, but not during its anticipation. This effect was not detected in the voxel-wise analysis described above. In fact, these more superficial regions were initially grouped within the same cluster

but did not emerge as peaks among the majority of voxels in the BLA. Although the BLA and CMA appear to coactivate during the task, they may play distinct roles. Prior animal studies have long linked the CMA to active respiratory processes, yet this study is the first to show that in humans, the CMA—specifically the AAA and CenA—deactivates during regulatory responses to respiratory challenges. The absence of significant correlations between CMA deactivation and subjective ratings of intensity or anxiety may suggest that this regulatory response to experimentally induced breathlessness is adaptive and phasic, particularly in healthy volunteers.

2.5.5 "Attention deployment" - resting-state BLA-precuneus connectivity

Amygdala-precuneus connectivity has been implicated in the ability to deploy attention away from arousing or unpleasant cues and in the construct of 'trait reappraisal', which evaluates an individual's tendency to reappraise and suppress emotions in daily life [117]. This aligns with the findings of the current study, where individuals exhibiting stronger amygdala-precuneus connectivity at rest reported lower intensity ratings. The reduced subjective perception of the stimulus intensity may reflect an individual's capacity for perceptual reappraisal, rather than more effective action control (e.g., deeper and faster breathing) in response to a threatening environment. Notably, the amygdala-precuneus connectivity is linked more to the 'factual' aspects of perception ratings—namely, 'intensity'—rather than the 'emotional' aspects, such as 'anxiety'. This suggests that patients' reports of dyspnoea symptom burdens are not merely reflections of trait anxiety or tendencies to complain; instead, they may represent a factual experience of respiratory difficulties.

2.5.6 'Trait anxiety' - resting-state BLA-temporal pole connectivity

The connectivity between the amygdala and temporal pole has been implicated in emotional dysregulation, neuroticism, and trait anxiety, with increased resting-state functional connectivity (rs-fMRI) observed in populations with generalised anxiety disorders [8] [246] [218]. The temporal cortex is suggested to play a role in coordinating complex perceptual inputs into visceral emotional responses [262]. While the precise function of the temporal pole remains to be fully elucidated, its position at the end of the central visual stream, coupled with its extensive interconnections with the amygdala, may enable it to modulate affective responses to threatening stimuli.

Our finding that stronger connectivity between the BLA and temporal pole at rest correlates with higher 'intensity' scores aligns with existing literature. However, the seemingly

more relevant ratings of 'anxiety' in our experiment did not show significant associations with the rs-fMRI between the amygdala and temporal pole. This may indicate that rs-fMRI is more reflective of trait-like anxiety rather than state-like anxiety, which was measured following the task. Furthermore, the variability in anxiety scores within this healthy population might be substantial enough that subtle differences in temporal pole-amygdala connectivity remain undetected when regressing against such highly varied data.

2.5.7 Limitations

The amygdala is a small structure located deep within the medial ventral region of the brain, in close proximity to veins, bones, and sinuses. These anatomical features pose significant challenges for fMRI research, primarily due to the amygdala's low signal-to-noise ratio (SNR), susceptibility to signal dropout, and magnetic field inhomogeneities [321]. Although the use of ultra-high-resolution 7T MRI improves SNR and advanced physiological noise correction techniques were applied, the current study remains limited in its ability to reliably detect distinct activation patterns across amygdala subnuclei, due to constraints inherent to the imaging sequence of the historical dataset.

It is important to note that the cluster identified during both the anticipation and resistance phases occupied a relatively large portion of the amygdala. The classification of the BLA as the primary deactivated region was based on the location of the cluster peak and the majority of voxels. However, part of the cluster extended into more superficial areas of the amygdala - although it did not overlap with the central or medial nuclei - warranting further investigation. The supplementary method using ROIs partially addresses this issue by predefining subnuclei and regions within the amygdala prior to conducting statistical tests. However, it is limited by reduced statistical power due to small mask sizes and the application of a stringent Bonferroni correction. Additionally, because these are subject-specific masks, they lack external validity. Future research aiming to delineate the distinct roles of amygdala nuclei in respiratory processes may benefit from more sophisticated imaging techniques (e.g. clustering for the connectivity profile of all voxels within the task evoked cluster) and larger datasets, such as those from the recently published Human Connectome Study by Klein-Flügge and colleagues [200].

Additionally, the size of the amygdala varies considerably among individuals, ranging from 1 to almost 4 cm^3 [39], with differences in both location and shape. This variability makes the registration of the amygdala to a standard brain template (e.g., MNI152) particularly prone to errors, contributing to the poor replicability seen in amygdala research [38, 14]. To address this issue, the supplementary method was used to segment each participant's amygdala into nine columns based on high-resolution anatomical images (0.7 mm^3), follow-

ing an existing atlas for automatic segmentation of the amygdala in high-resolution MRI [302]. However, the reliability and quality of these subject-specific subnuclei were still poor, with some nuclei containing fewer than five voxels and most identified as part of the lateral nuclei. Consequently, no further connectivity analyses were pursued. Future studies may benefit from optimised imaging sequences tailored to the amygdala, manual segmentation of its subnuclei, or diffusion/functional network-based subnuclei to improve reliability.

Lastly, as with other fMRI studies, the results concerning amygdala deactivation and connectivity to other brain regions during task and rest conditions should not be considered in isolation, nor should causality be inferred from these findings.

2.6 Conclusion

This study advanced our understanding of the amygdala role in the anticipation and perception of breathlessness, as well as its FC with other brain regions in relation to breathing perceptions. My results revealed significant deactivation of BLA during both the anticipation and resistance phases of breathlessness. It suggests that the BLA may primarily engage in modulation of perceptual processes in a moment-to-moment manner. This notion is further bolstered by its increased coupling with the contralateral thalamus during resistance, suggesting a vital mechanism for integrating sensory inputs related to respiratory threats and updating cognitive states. In addition, its intrinsic FC at rest possibly underscores the contributions of the BLA to various cognitive and emotional processes during breathlessness intensity perception, particularly through its connectivity with the temporal pole and precuneus. The former appears to correlate with trait-like anxiety, while the latter is associated with the capacity for perceptual reappraisal, shedding light on how individuals experience and interpret breathlessness.

The unexpected absence of significant involvement from the CMA challenges existing literature, indicating that its role in respiratory control might be more intricate than previously understood. This lack of observed activity could stem from methodological constraints, such as the limitations of fMRI in capturing the rapid dynamics of respiratory-related neural responses.

Given the intricate and potentially divergent roles of the amygdala subregions in breathlessness, future research should aim to employ more targeted methodologies that could enhance our understanding of these dynamics. Innovative breathing-related imaging study design and inclusion of clinical populations may offer further insights into the mechanisms underlying breathlessness and its associated emotional responses. Overall, these findings contribute to a deeper understanding of the neural correlates of phasic breathlessness and

the emotional processes involved, providing a foundation for future investigations into therapeutic strategies for individuals experiencing chronic respiratory conditions.

Chapter 3

Methods and pre-processing of post-COVID brain imaging data

3.1 Background

This chapter outlines the methods and MRI pre-processing techniques applied to the anatomical and functional MRI data for the entire post-COVID cohort. The purpose of this standalone chapter is to avoid repetition in Chapter 5 and Chapter 6, thereby ensuring a smoother flow in the subsequent chapters.

After applying the same pre-processing steps for the anatomical and functional data, 2 distinct pipelines were used to process brain-derived measures (BMs):

- Chapter 5 employed a node-based (NB) or regions of interest(ROI)-based approach to investigate allostasis-interoception-specific pathways, centred on seed regions in the amygdala, PAG, olfaction, along with a selection of visceromotor, interoceptive, sensorimotor structures.
- Chapter 6 used a voxel-based (VB) approach to derive large-scale brain networks associated with subject measures (SMs).

This chapter details the preparation of the "cleaned data". For the NB method, the output consists of pairwise connections between predefined ROIs (or nodes). For the VB method, the output consists of hierarchical brain maps. The VB approach is entirely data-driven, whereas the NB method is based on prior knowledge of ROIs involved in respiratory control(allostasis) and perception (interoception).

3.2 MRI scanning sequence

The 7-Tesla (7T) resting-state fMRI runs lasted 10 minutes, with a TR of 1.5s (400 time points), TE of 25ms, flip angle 65°, isotropic resolution of 1.5mm, 96 slices, a multi-band factor of 4. A single-band whole brain high-contrast Echo-planar imaging (EPI) scan was acquired to aid registration of the functional scan. To aid distortion-correction, fieldmap scans of the B0 field were also acquired: TR, 620.0ms, TE1, 4.08ms, TE2 5.1ms; flip angle 39°; voxel size, 2 x 2 x 2 mm.

The T1-weighted (T1w) MP_2RAGE anatomical images were collected with 0.7mm isotropic voxels, echo time 2.64ms, TR of 3500ms, bandwidth of 300 Hz/pixel, inversion times at 725ms and 3150ms, nominal flip angles $5^\circ/2^\circ$ and matrix size of 224x224x224, for anatomical localisation and registration.

3.3 Image preprocessing

Image preprocessing was conducted using the Oxford Centre for Functional Magnetic Resonance Imaging of the Brain Software Library (FSL, version 6.0.7.6; http://www.fmrib.ox.ac.uk/fsl), MATLAB R2022b, Python 3.11.6, advanced normalization tools (ANTs) v2.2.0 and statistical parametric mapping library (SPM12) v7219. Functional MRI data were processed with FEAT (FMRI Expert Analysis Tool), also version 6.0.7.6, which is part of the FSL suite.

3.3.1 Anatomical data preprocessing

For the anatomical data, MP_2RAGE images from the two inversion-time were combined using Phase Sensitive Inversion Recovery (PSIR [59]). A liberal brain extraction were applied used to aid registration, followed by bias field correction and segmentation for the grey matter (GM), white matter (WM), and cerebrospinal fluid (CSF).

3.3.2 Resting-stage functional data preprocessing

Registration Resting-state functional MRI (rs-fMRI) data, acquired using functional echo-planar imaging (EPI), underwent the following preprocessing. This included brain extraction, head motion correction, and high-pass temporal filtering with a 100-second cutoff [326]. No spatial smoothing was applied during initial preprocessing to allow accurate identification

of subject-specific independent components (ICs)[1]. Functional images were registered to a high-contrast single-band reference image, then aligned to the individual anatomical scan using FLIRT (6 degrees of freedom)[190], and non-linearly transformed to MNI152 standard space (1 mm^3 resolution) via FNIRT[16]. EPI distortions were corrected using FUGUE and Boundary-Based Registration (BBR)[145]. The MNI brain is an averaged T1 brain image constructed from 152 normal subjects at the Montreal Neurological Institute (MNI), Montreal, QC, Canada.

ICA I employed ICA+FIX (Independent Component Analysis followed by FMRIB's ICA-based X-noiseifier) to remove structured artefacts from the data. This process began with the application of MELODIC (Multivariate Exploratory Linear Decomposition into Independent Components) on the EPI data of each participant, which decomposed the 4D dataset into approximately 200–240 spatial and temporal components. For classifier training, I manually labelled the independent components (ICs) from a subset of twenty participants, classifying the ICs as signal, motion-related, cerebrospinal fluid (CSF), blood arteries and veins, or scanner-related noise components. The labelling was based on spatial patterns and the power spectra of each component, following guidelines [146]. Participants for the training set were randomly selected to ensure balanced representation across hospitalised and non-hospitalised individuals, as well as equal distribution across the two scanning sites (50:50 ratio).

PNM The physiological data of respiration and cardiac pulses collected along with the EPI triggers (two software package used: BioPac in the Oxford site, ADI setup with ADI pulseox and a custom respiratory belt in the Cardiff site) are used to determine the phases of the respiratory and cardiac processes at each acquired slice. The phase data is then fed into a low-order Fourier expansion [42] [139] [167] that are set to provide output variables of 4 respiratory, 3 cardiac and 1 interaction regressors [114] [167]. These regressors represent potential signal changes associated with the respiratory and cardic processes.

Following the FEATs PNM (Physiological Noise Modelling) tool [139], results of each subject's cardiac and respiratory phase identification (PNM stage 1) were manually checked and adapted with different parameters to obtain optimal extraction, before entering the stage 2 and 3 of PNM.

The cleaned data (nuisance regression) I first combined the ICA noise component and each subject's time series of WM and CSF into one regressor, followed by the ICA-PNM

[1] A minimal spatial smoothing kernel of 1.5 mm was applied later during the FEAT analysis with nuisance regression.

de-noising pipeline to regress out both the ICA(+WM & CSF) and PNM noise components in a single FEAT model. It is superior than performing them separately, which avoids reintroducing variance into the 'cleaned' data when PNM and ICA have overlapping components of interest.

The temporal signal-to-noise ratio has improved drastically after the PNM+ICA preprocessing (see details in the section 3.4.4).The final result from this step for each subject will be called 'cleaned data' hereafter in the thesis.

3.4 ROIs selection

For Chapter 5, I identified 18 ROIs believed to be central to the interoceptive and allostatic network associated with respiratory processes[199]. Specifically, these encompass the anterior cingulate cortex (ACC) for visceromotor control, subcortical and brainstem visceromotor structures such as the periaqueductal gray (PAG) and hypothalamus for autonomic functions, and the insula as the primary interoceptive sensory cortex.

Furthermore, my analysis includes the amygdala, ventromedial and dorsomedial prefrontal cortex (vmPFC and dmPFC) as part of the extended limbic system, the primary sensory and motor cortices (S1 and M1) to account for the secondary exteroceptive interactions.

There is a special inclusion of the piriform cortex. The olfactory network, with its evolutionary significance in the fight-or-flight response, has been highlighted for its coactivation with the central nucleus of the amygdala during inhalation [122, 380, 259]. Notably, the piriform cortex, a key component of this network, has been identified as one of the most significantly altered cortical regions in post-COVID condition analyses [89]. This makes the piriform cortex particularly relevant to the current thesis.

3.4.1 ACC and insula

The anterior cingulate cortex (ACC) and insula regions were initially delineated using the Harvard-Oxford atlas Cortical and subcortical atlases(HO-atlas, part of fsleyes) and the atlas published by Glasser and colleagues [138], with subsequent refinement based on MNI coordinates cited in the work on the allostatic-interoceptive network by Kleckner and colleagues [199]. Spheres with a 4-mm radius centered on the MNI coordinates identified by Kleckner and colleagues [199] were generated.

The general guideline for ROI selection was to cover all meaningful sub-regions of the ACC and insula, prioritising the more precise 4mm sphere seeds described by Kleckner and colleagues ([199]). For instance, if the 4mm seed overlapped with a larger mask

generated from the atlas, the seed was retained, and the larger mask discarded. Any regions within the published ACC or insula domains not encompassed by Kleckner's 4mm seeds were included in my analysis to ensure comprehensive coverage of these critical areas. Ultimately, the following ROIs were selected for the next step: subgenual ACC (sgACC, 4mm), pregenual ACC (pACC, 4mm), dorsal ACC (dACC, 4mm), medial and lateral regions of the ventral anterior insula (mvaIns and lvaIns, 4mm), dorsal medial insula (dmIns, 4mm), dorsal posterior insula (dpIns, 4mm), and the posterior insula (PoI1 and PoI2 from Glasser's atlas segmentation).

Atlas segmentation The exact procedure for defining the insula regions from the atlas is detailed below:

Anterior Insula: Represented by the "Anterior Ventral Insular area (AVI)" and the "Anterior Agranular Insular Complex (AAIC)". These areas correspond to the anterior part of the insula, characterised by a lack of granular layers (agranular).

Middle Insula: Directly referred to as the "Middle Insular area (MI)" in Glasser and colleagues ([138]). This region represents the intermediate section of the insula, which may contain dysgranular layers.

Posterior Insula: This includes the "Posterior Insular areas PoI1 and PoI2" region, corresponding to the ventral posterior and dorsal anterior portions of the posterior insula (see Figure 3.1). These areas are located at the posterior part of the insula. The "Ig" region, suggested to contain granule cells typical of the posterior insula, conceptually overlaps with the granular 'dpIns' 4mm seed and was therefore excluded from the analysis.

3.4.2 Subcortical regions

The subcortical regions of the dorsal PAG, ventrolateral PAG, and basolateral amygdala are derived from inherited segmentation or masks based on findings from breathlessness-related tasks conducted in our lab [114] [113] and Chapter 2. It is important to note that the 2mm sphere seed labelled as 'lPAG' ([114] [113]) is included within my dPAG mask (see Figure 3.1).

The ROI for the hypothalamus was obtained through direct segmentation of each participant's anatomical brain, using the Freesurfer Segmentation of hypothalamic subunits tool (FreeSurfer 7.2) [33].

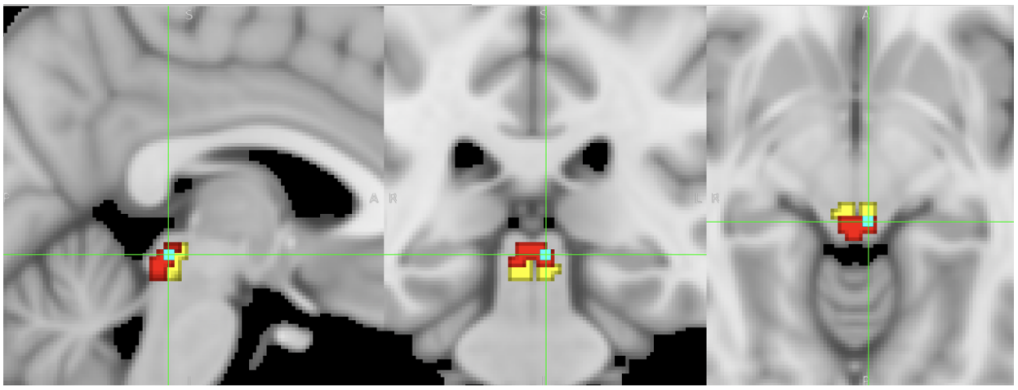


Fig. 3.1 Illustration of the PAG seeds. The 2mm sphere labelled as 'lPAG' in Faull and colleagues (2017 [114]) was highlighted in blue. Seed location of lPAG in MNI space: X = -3 , Y = -32, Z = -8. Despite its label 'lPAG', it fell under the conventional dPAG mask, which is used in the current chapter.

3.4.3 Other cortical regions

The ROIs of S1, M1, vmPFC and dmPFC were obtained using the HO-atlas. Details of how ROIs were defined are in Table 5.2.

No	Region	ROIs	Source	x	y	z
1	subcortical	BLA	inherited mask	22	-3	-19
2		Piriform	4mm sphere	16	-2	-14
3		dPAG	inherited mask	–	–	–
4		vlPAG	inherited mask	–	–	–
5		hypothalamus	T1w segmentation	–	–	–
6	ACC	sgACC	4mm sphere	2	14	-6
7		pACC	4mm sphere	13	44	0
8		dACC(aMCC)	4mm sphere	9	22	33
9	Insula	dpIns	4mm sphere	36	-32	16
10		dmIns	4mm sphere	41	2	3
11		vaIns (m and l)	4mm sphere	(m)30	16	-14
12			4mm sphere	(l)44	6	-15
13		PoI1	Atlas seg (Glasser)	–	–	–
14		PoI2	Atlas seg (Glasser)	–	–	–
15	dmPFC		Atlas seg (Harvard-Oxford)	–	–	–
16	vmPFC		Atlas seg (Harvard-Oxford)	–	–	–
17	S1		Atlas seg (Harvard-Oxford)	–	–	–
18	M1		Atlas seg (Harvard-Oxford)	–	–	–

Table 3.1 Information about ROIs identification. Subcortical regions include the basolateral amygdala(BLA), dorsal and ventroateral periaqueductal gray (dPAG and vlPAG) obtained from conditioned breathlessness task, piriform cortex due to its high relevant in COVID outcomes, hypothalamus due to its important role in interoception. The anterior cingulate cortex (ACC) includes its subgenual(sgACC) and pregenual (pACC) sections, and anterior midcingulate cortex (also known as dorsal ACC)as they are considered to be the visceromotor hubs of the cortex. The insula includes the posterior insula (PoI1 and PoI2), the dorsal posterior and dorsal medial (dpIns/dmIns) sections that are hypothesised to be the primary interoceptive sensory cortex, and the ventral anterior section which functions together with the ACC. Finally, the dorsal medial prefrontal cortex (dmPFC), ventral medial prefrontal cortex (vmPFC) comprises the cortical regions of interest.

3.4.4 Quality control of ROIs

The masks of the ROIs were transformed to each subject's functional EPI space, followed by steps to make sure the ROIs are valid and meaningful.

Visual inspection Each mask underwent visual inspection to confirm its alignment with the standard MNI brain template and ensure accurate placement within the subject-specific functional EPI space following transformation. The positioning of all masks is consistent with the established literature, with the exception of the dpIns.

The dpIns mask [199] is located more dorsally and posteriorly compared to conventional insula masks obtained from atlases. It may correspond to the planum temporale and appears to include some white matter, according to the HO-atlas (see Figure 3.2 for a comparison of the dpIns seed and the posterior insula masks from Glasser [138]). To ensure relatively full coverage of the insula while maintaining consistency with previous literature, I included the two posterior insula masks from Glasser's atlas ([138]) in addition to the dpIns mask of Kleckner and colleagues' [199].

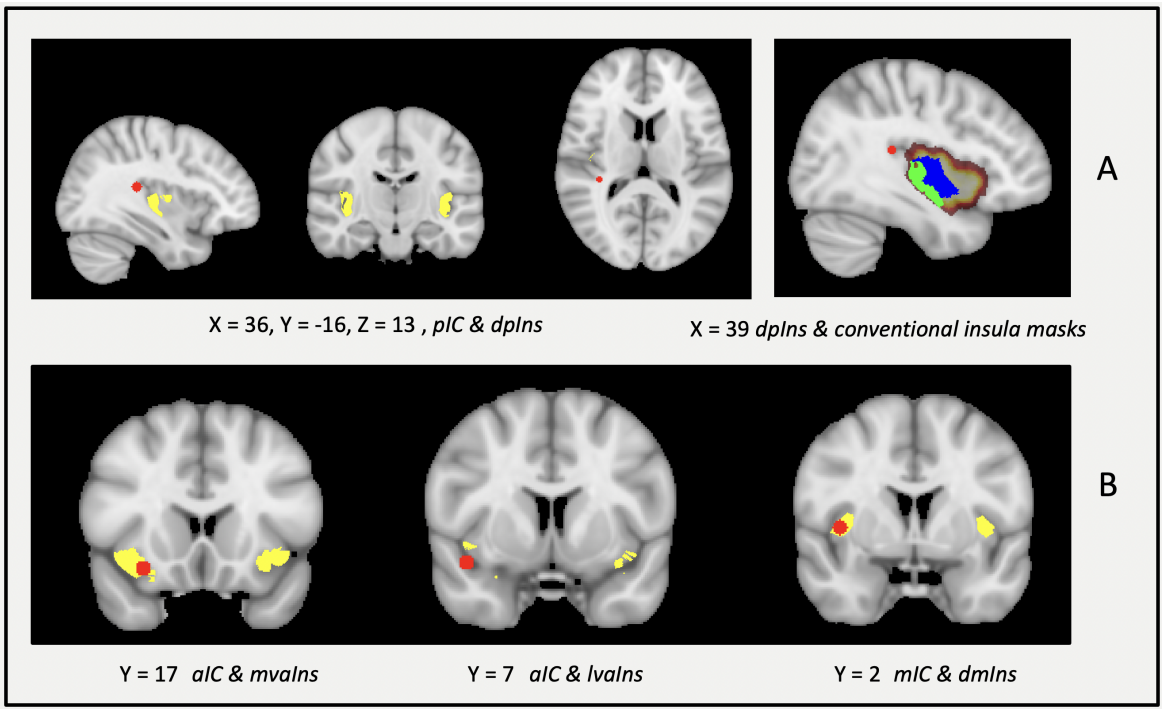


Fig. 3.2 Seed choice of insula regions based on atlas and coordinate-derived spheres. Panel A (left): the lateral, sagittal and horizontal view of the dpIns and combined posterior insula (pIC) masks superimposed on a 1mm MNI brain. These images show that the dpIns seed, created from the coordinates provide by Kleckner and colleagues[199], shown in red, is possibly located outside of the conventional cortical insula region. The pIC shown in yellow was created from the established atlas[138] with more details on the right. The whole insula mask of HO-atlas at the background are shown here fore reference. Panel A (right): the dpIns seeds and the other pIC ROIs extracted from established atlas, posterior insula 1 (PoI1) and posterior insula 2 (PoI2)[138], which were added in the ROIs to cover the posterior regions of insula. Colour green represents 'PoI1'; colour blue represents 'PoI2'; Panel B: The mvaIns and lvaIns (left and middle) locates inside or near the anterior insula mask of the atlas. The dmIns locates inside ofthe middle insula from the atlas (right). The co-ordinates are kept to represents the more specific seeds.

Mask volume The mask volume, voxel number (volume$/1.5 \times 1.5 \times 1.5\,\mathrm{mm}^3$), and the standard deviation (std) of the volume are reported in Table 3.2. Only one ROI (vmPFC) of subject007 contains less than 100 mm^3, due to great signal loss at the ventromedial region.

Region	Volume (mm^3)	Std	Voxel Number
vlPAG	311	39	92
dPAG	367	39	109
piri	244	59	72
Hyp	845	222	250
amyg	230	57	68
sgACC	228	42	67
pACC	230	63	68
dACC	217	61	64
mvaIns	241	50	71
lvaIns	262	62	77
dmIns	229	40	68
PoI1	4422	593	1310
PoI2	6584	859	1951
dpIns	198	42	59
dmPFC	17572	4459	5207
vmPFC	1327	829	393
S1	24878	4336	7371
M1	27298	4192	8088

Table 3.2 Volume and voxel number for each ROI. Mean and standard deviation of volume for each ROI, Along with voxel numbers, calculated based on the resolution of functional EPI data at 1.5 mm^3.

Temporal signal-to-noise ratio (tSNR) The mean tSNR for all masks across subjects was acceptable at above 40 (See Figure: 3.3). There was 3-6 folds increase of tSNR. See Table 3.3 for comparison between the raw EPI functional data and the cleaned data after PNM and FIX. All ROIs are acceptable to be entered into the model.

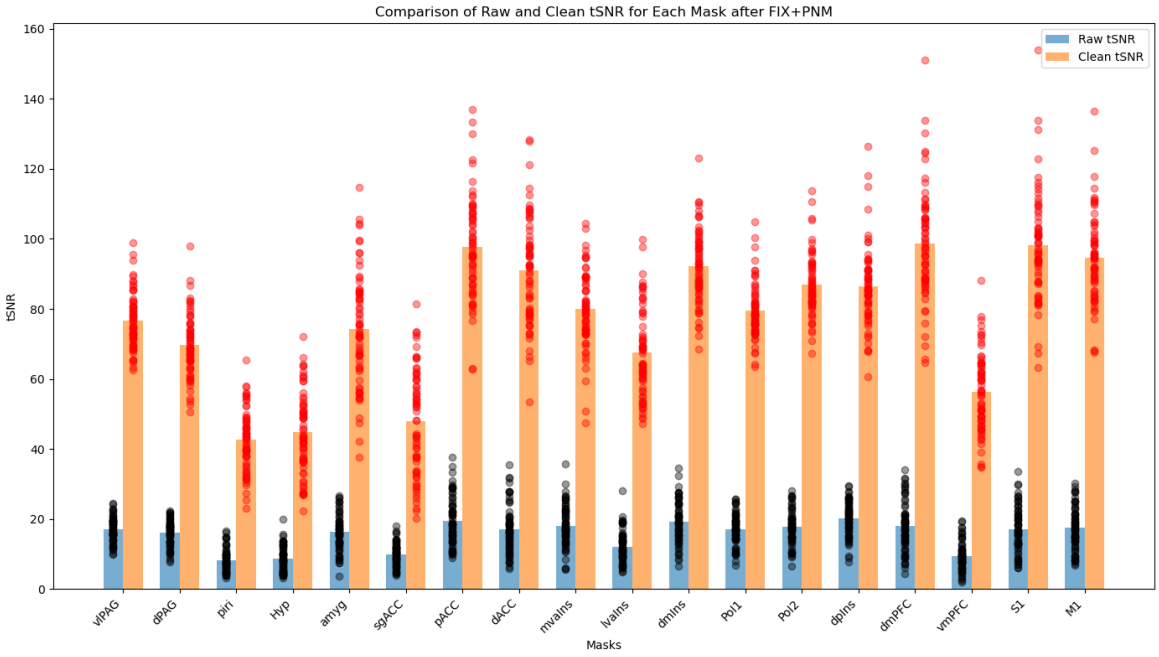


Fig. 3.3 Improvement of tSNR after FIX+PNM pre-processing. Despite having looked outside of grey matter on the averaged MNI brain, the tSNR of dpIns reveals that it has in fact meaningful signal similar to PoI1 and PoI2, with higher variance.

Mask	Percentage Increase (%)
vlPAG	364.59%
dPAG	357.94%
piri	484.22%
Hyp	481.74%
amyg	396.71%
sgACC	424.97%
pACC	461.86%
dACC	503.30%
mvaIns	386.28%
lvaIns	510.14%
dmIns	427.57%
PoI1	399.76%
PoI2	427.34%
dpIns	354.13%
dmPFC	532.65%
vmPFC	606.59%
S1	559.47%
M1	508.85%

Table 3.3 Percentage increase in tSNR for each ROI

3.5 Group-level ICA

These are the pre-processing steps for the voxel-based analysis presented in Chapter 6.

3.5.1 Group ICA parcellation

The cleaned single-subject rs-fMRI data were temporally demeaned and variance-normalised before being entered into group ICA using FSL's MELODIC tool. Group ICA dimensionalities of D=10, 25, 50, and 100 were applied and tested to identify an appropriate level of clustering that is both interpretable and as small as possible, in order to avoid overfitting in subsequent analyses due to the small sample size. The group ICA produces a set of ICA maps, which can be considered parcellations (or nodes), containing non-binary values for each voxel across all subjects (hence, group ICA). For conciseness, the following chapters will assume a group ICA dimensionality of D=25.

3.5.2 Subject time series for each ICA component

I next derived each subject's 'involvement' in each of the group ICA component (nodes) by regressing the ICA maps spatially onto the 4D rs-fMRI data for each subject. I got one time series per ICA component per subject. This represents the stage 1 of Dual-regression.

3.5.3 Dimension reduction for BM

Firstly, a 25x25 functional connectivity matrix were generated by calculating Tikhonov-regularized [348] partial correlation for every pair of the time series for each subject. Each entry represents an edge between two ICA regions.

Secondly, instead of reducing the dimension directly on the whole data space, the BMs will be grouped into the 25 ICA regions, for which each contains 25 edges. The domain-driven dimension reduction (DDR [220]) approach is an optimised pipeline for brain-behaviour dimension reduction based on conventional principal component analysis (PCA) for both SMs and BMs followed by canonical-correlation analysis (CCA), such as the Smith and colleagues[325]' paper. It is superior with higher interpretability and stability, and, importantly for the current study, cope with small sample size to variable number ratio because the dimension reduction step is within a sub-domain.

Thirdly, these estimates (node time series) were input into network modelling using the FSLNets Toolbox. For each subject, Netmats were estimated and converted from Pearson correlation scores (partial correlation) to z-statistics using Fisher's transformation. This resulted in one partial correlation z-statistics Netmat for each subject. The resulting network representations were compared to the existing literature [325] and should be identifiable as large brain networks at a higher hierarchical level, such as the Default Mode Network, Sensorimotor Network, and Attention Network.

Based on the D value (here assumed to be an ideal case of D=25) chosen in the previous steps, an additional PCA with 'Varimax' rotation was conducted to further reduce components before entering the CCA analysis.

3.6 Conclusion

In summary, this chapter described the preprocessing of anatomical and functional MRI data using FIX and PNM at the subject level, followed by ROI definition and group-level ICA. These procedures support the node-based analyses presented in Chapter 5 and the voxel-based analyses in Chapter 6. The following chapter, Chapter 4, will first investigate all the SMs —including demographic, clinical, and post-COVID behavioural outcomes across

psychological, physiological, and cognitive domains—prior to exploring their associations with BMs in Chapters 5 and 6.

Chapter 4

Characteristic of the behavioural outcomes of the post-COVID sample

4.1 Abstract

This exploratory chapter investigates the representativeness and latent clustering of a post-COVID cohort ($N = 118$) in relation to the broader population, drawing on published literature involving large-scale samples. The analysis focuses on demographic, clinical, and post-COVID behavioural outcomes, with the aim of evaluating the cohort's informational richness and its potential utility for stratifying patients in subsequent brain-behaviour analyses.

The cohort predominantly comprised older, overweight, female, and Caucasian individuals. Substantial heterogeneity was evident across several dimensions, including age, gender, disease severity, medical history, and the time elapsed since infection. Subjective cognitive impairment and fatigue emerged as the most discriminative features among the hospitalised, non-hospitalised, and control groups. Notably, the control group exhibited an atypical profile, characterised by low functional capacity in the absence of self-reported symptoms, alongside younger age and indicators of lower socioeconomic status.

To address the challenges posed by a limited sample size and substantial inter-group variability, eleven behavioural domains were identified: breathlessness, fatigue, negative mood, lack of motivation, stress, anxiety, pain, poor function, poor sleep, objective cognitive impairment, and subjective cognitive impairment. These domains facilitated dimensionality reduction while retaining clinical interpretability.

This chapter further highlights the methodological challenges associated with control group selection, including evidence of selection bias. Nevertheless, the relative homogeneity

in symptom severity among patient groups provides a rationale for employing correlational analyses in later brain connectivity studies.

In summary, this chapter emphasises the importance of addressing sample heterogeneity, selection bias, and appropriate dimensionality reduction when interpreting behavioural and neurobiological data in long COVID research.

4.2 Introduction

There has been a great effort to phenotype patients suffering from post-acute sequelae of SARS-CoV-2 infection (long COVID) based on large non-imaging datasets in the past three years post-pandemic [81] [76] [288] [282] [383] [104] [196] [243]. However, knowledge of how these behavioural domains, especially neurophysiological symptoms such as breathlessness, anxiety, fatigue, and cognitive impairment were driven by neural vulnerabilities or alterations in the brain is scarce.

Research in brain-behavioural stratification requires well-defined features for the behavioural domain. Ideally, the behavioural data shall be homogeneous (no demographic information is selectively correlated with certain symptom outcomes), cover a wide range of symptom types and levels of severity that are associated to known brain functional networks, and contain a large sample size. Additionally, the taxonomy shall be realistic to the nature of the dataset and comparable to the published literature.

The current dataset includes a unique sample of post-COVID patients, with both imaging and non-imaging data collected between 125 and 914 days post-infection, who recovered from varied levels of severity. I acknowledge that the dataset was collected during the challenging and dynamic period of the COVID-19 pandemic, in which the ability to recruit different groups of COVID-related participants fluctuated over time. For instance, early patient recruitment from 2020 to 2021 was predominantly comprised of post-hospitalised individuals, yet we managed to recruit a substantial number of non-hospitalised patients at a later stage, particularly at the Cardiff site, thanks to the establishment of long COVID clinics in local hospitals. Healthy controls, on the other hand, were initially reluctant to participate due to the fearful environment surrounding the virus and strict social distancing policies and few individuals remained uninfected by the later stages of the pandemic.

Another difficulty arose from the stringent screening for the 7T MRI scanner safety. This process had not only excluded many potential patients and controls, but also significantly increased the drop-out rate due to the numerous contact points involved in detailing the concerns (such as the brand of contraceptives). Despite the reduced efficiency of recruitment, we ultimately achieved 68 participants with a full set of uncompromised MRI scans and 118

participants with only behavioural data. While this is a respectable size for a typical ultra-high resolution MRI study, it remains underpowered for effective analysis of high-dimensional data, such as the whole-brain Connectomes in Chapter 6.

Before delving into the imaging data, this chapter utilised the entire behavioural dataset (N=118) from individuals who completed the questionnaires and tasks, including those later excluded due to 7T MRI scan safety concerns, to explore the demographic and clinical background, post-COVID outcomes, and their relationships. This exploration will provide a foundation for future analyses, ensuring that the chosen methodologies are well-suited to identifying meaningful long COVID phenotype through brain-behaviour correlations. It will also help the interpretation of subsequent analyses to be more appropriated grounded by highlighting caveats and biases of this particular pool of participants. Specifically, this chapter contains the following aspects:

1. Contextualizing the sample: The demographic information was explored, with particular attention to identifying biases and confounding factors within the current sample.

2. Disambiguating patient heterogeneity and Differences of Controls: In this larger sample pool, the post-COVID outcome measures were thoroughly examined to identify patterns, correlations, clusters, and group differences (hospitalised, non-hospitalised, and control).

3. Behavioural data dimension reduction: Based on the exploratory analysis and existing literature, distinct behavioural domains were defined to comprehensively capture clinically meaningful post-COVID outcomes, followed by dimension reduction within each domain ensuring that the data is suitable for the final Canonical Correlation Analysis (CCA) with brain connectivity features in Chapter 6. This step is essential given the small sample size, and care was taken to avoid over-fitting while preserving the integrity of the data.

4.3 Methods

4.3.1 Participants

The study was approved by the North West - Preston Research Ethics Committee. All participants provided informed consent either for the sub-study 'CMORE-NEURO' of the 'CMORE' project, titled Assessing the Effects of Coronavirus Disease (COVID-19) on Multiple Organ Systems and Impact on Quality of Life, Functional Capacity, and Mental Health (REC reference: 20/NW/0235, IRAS project ID: 282608), or for the BBB-COV study,

titled Brain and Brainstem Basis of Persistent Symptoms in COVID-19 (REC reference: 21/NW/0090, IRAS project ID: 297314).

Behavioural data of 91 patients with a medical history of COVID-19 and 27 healthy volunteers were collected. The patients were recruited from two sites: 1) the Wellcome Centre for Integrative Neuroimaging (WIN, Oxford, UK), referred from the John Radcliff hospital or the Churchill post-COVID clinic (Oxford, UK); and 2) Cardiff University Brain Research Imaging Centre (CUBRIC, Cardiff, UK), referred by the Cardiff and Vale University Health Board (Cardiff, UK; referred to as 'post-COVID clinic' hereafter). Healthy participants were recruited from public ads such as flyers, twitter, and Facebook.

Recruitment began with a telephone screening, aimed at identifying patients who, following referral from a hospital or clinic, were suitable and safe to be scanned at the 7T MRI. Those who were considered safe to scan completed a series of questionnaires online and undertook a cognitive task within 5 days of the scheduled MRI scan, following the consent processes.

Of note, this cohort comprised 38 hospitalised patients, 53 non-hospitalised patients, and 27 controls, of which 19, 34, and 15, respectively, completed MRI scans without compromise. This was detailed in Chapter 5.

4.3.2 Materials

For the 118 participants, we collected their demographic information, clinical measures, and post-COVID outcome data as detailed below. The questionnaires and tasks cover symptoms across respiratory, psychological, somatic, cognitive, and functional aspects of life were collected <5 days before the scan day.

Demographic and clinical measures

Clinical data from the time of medical intervention—either during hospitalisation or post-COVID clinic visits—were obtained prospectively during admission or retrospectively from NHS electronic patient records. These measures included the WHO Clinical Progression Scale, medical history of respiratory and cardiovascular conditions, acute COVID-19 symptoms, ventilator use, and peak inflammatory markers (C-reactive protein [CRP] and D-dimer). Demographic information, such as sex, age, and body mass index (BMI), was collected within five days prior to the scheduled MRI scan, regardless of whether the scan ultimately took place.

Questionnaires

The following questionnaires were selected to capture the multidimensional experience of post-COVID symptoms related to neurophysiological processes[81], encompassing physiological, psychological, and cognitive domains, as well as to assess severity levels during the acute infection phase.

Dyspnoea-12 The Dyspnoea-12 ([379], D-12) questionnaire is an instrument designed to measure the severity and impact of breathlessness in individuals with respiratory diseases. Comprising twelve items, the questionnaire captures both the physical and emotional aspects of breathlessness experiences. Each item is scored on a four-point Likert scale, ranging from "none" to "severe," allowing patients to quantify the intensity of their symptoms and the distress they cause. The total score is obtained by summing the responses to all 12 items, with higher scores indicating greater severity of dyspnoea. The Dyspnoea-12 questionnaire has been validated in various patient populations, demonstrating strong psychometric properties, including reliability and validity across different types of respiratory conditions[320, 367, 150].

Breathlessness Catastrophising Scale The Breathlessness Catastrophising Scale ([328], BCS) is a validated 13-item instrument designed to evaluate the cognitive and emotional responses to breathlessness experiences. Responses to each question on the BCS are captured using a 5-point Likert scale, ranging from 0 ("not at all") to 4 ("all the time"), allowing for a total score between 0 and 52. A higher score on this scale signifies a greater propensity for catastrophising breathlessness. Drawing inspiration from the established Pain Catastrophising Scale[342], the BCS has undergone validation in adult patient populations (Chronic Obstructive Pulmonary Disease) [342][328] and has shown a notable link with breathlessness anticipation in healthy population in other fMRI studies [340].

Fatigue Severity Score The Fatigue Severity Score ([209], FSS) evaluates the impact of fatigue on motivation, physical activity, work, and social interactions. It consists of a nine-item questionnaire rated on a seven-point scale, with higher scores indicating greater fatigue severity. Krupp and colleagues [209] conducted an initial psychometric evaluation of the FSS, finding an internal consistency of 0.88 and a test–retest reliability of 0.84.

Patient Health Questionnaire-15 The Patient Health Questionnaire somatic symptom severity scale ([207], PHQ-15) assesses psychological distress from somatic symptoms. It includes 15 questions that ask individuals to rate the frequency of various physical symptoms

they have experienced over the past four weeks, such as stomach pain, back pain, and dizziness. Each symptom is scored from 0 (not bothered at all) to 2 (bothered a lot), with higher total scores indicating greater somatic symptom burden.

Patient Health Questionnaire-9 The Patient Health Questionnaire depressive symptom severity scale ([206], PHQ-9) is a widely used screening tool for diagnosing and monitoring the severity of depression. It consists of nine questions, each corresponding to one of the DSM-IV criteria for major depressive disorder. Patients rate the frequency of symptoms such as lack of interest, low mood, and sleep disturbances over the past two weeks on a scale from 0 (not at all) to 3 (nearly every day). The total score ranges from 0 to 27, with higher scores indicating more severe depression.

Generalized Anxiety Disorder 7-item scale Generalized Anxiety Disorder 7-item scale ([331, 208], GAD-7) is a validated self-report anxiety assessment tool that consists of seven questions evaluating the frequency of anxiety symptoms over the previous two weeks. Responses to each item are scored on a four-point Likert scale ranging from 0 ('not at all') to 3 ('nearly every day'), yielding a total score between 0 and 21. This instrument identifies varying levels of anxiety severity, with total scores of 5, 10, and 15 representing thresholds for mild, moderate, and severe anxiety, respectively. A score of 10 or higher suggests the need for further clinical evaluation for Generalized Anxiety Disorder (GAD) due to its demonstrated sensitivity (89%) and specificity (82%) [331].

Perceived Stress scale The Perceived Stress Scale ([60], PSS) measures perception of stress. It consists of 10 questions that ask individuals to rate their feelings and thoughts during the last month on a scale from 0 (never) to 4 (very often). Questions cover experiences of stress, such as feeling nervous, unable to control irritations, or feeling confident in handling personal problems. Scores are summed to provide an overall measure of perceived stress.

Apathy Motivation Index The Apathy Motivation Index ([17], AMI) is an 18-item self-report scale that captures apathy in healthy people. It evaluates three distinct dimensions of apathy: behavioural engagement, emotional sensitivity, and social motivation, using 18 items to be ranked from 'Completely true' to 'Completely untrue'.

Short-Form 36 The RAND short-form 36([365], SF-36) is a widely recognized, validated instrument that comprises 36 questions, grouped into eight scaled scores: physical functioning, bodily pain, role limitations due to physical health problems, role limitations due to

personal or emotional problems, emotional well-being, social functioning, energy/fatigue, and general health perceptions. These scales provide a comprehensive measure of both physical and mental health components. The responses were scored using standard algorithms, producing a profile of scores ranging from 0 to 100, where higher scores indicate better health status.

Cognitive Failures Questionnaires The Cognitive Failures Questionnaire ([41], CFQ) is a self-report tool designed to assess cognitive function. It contains subjective ratings for common cognitive errors such as forgetfulness, distractibility, and slips of action in daily life. The CFQ consists of 25 items where respondents rate how often they experience these lapses on a scale from 0 (never) to 4 (very often). Higher scores on the CFQ indicate a greater propensity for cognitive failures.

WHO Clinical Progression Scale The World Health Organization Ordinal Scale for Clinical Improvement ([231], WHO Clinical Progression Scale) that was designed to assess the progression and outcomes of COVID-19 in patients was recorded. It categorizes the disease severity of acute-stage COVID infection on an ordinal scale ranging from 0, indicating no infection, to 8, denoting death.

Tasks

Cognitive test battery The "Cognitron" task consists of 13 tasks designed to objectively capture aspects of cognitive function post-COVID (Figure 4.1; see the Appendix A for detailed descriptions of each task). The 13 tasks can be accessed at https://fo7t.cognitron.co.uk. They were designed and programmed in HTML5 with JavaScript by Peter J. Hellyer(P.J.H.) and Trender William, and are hosted on the custom server system, *Cognitron*, developed by P.J.H. on the Amazon EC2 platform. The application of this battery in COVID-related populations has been widely documented [158, 157, 157]. These tasks were undertaken following the order of:

1. Object Memory (immediate memory)
2. Word Memory (immediate memory)
3. Spatial Span (spatial short-term [working] memory capacity)
4. Simple Reaction (concentration)
5. Motor Control (motor control)

6. Choice Reaction (concentration)
7. Target Detection (concentration)
8. Tower of London (spatial planning)
9. Verbal Analogies (semantic reasoning)
10. 2D mental Rotations (mental rotation)
11. 3D Mental Rotations (mental rotation)
12. Object Memory (delayed memory)
13. Word Memory (delayed memory)

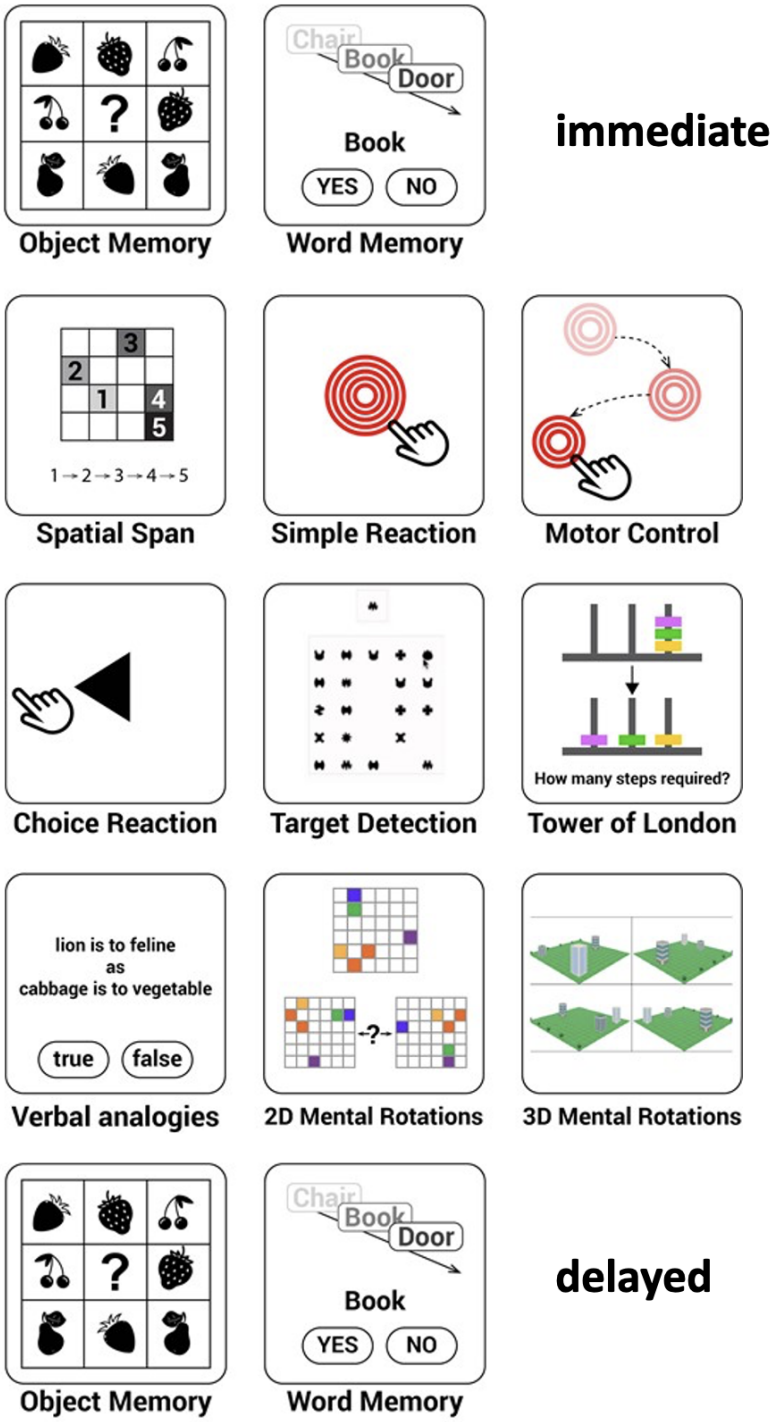


Fig. 4.1 Cognitron tasks. Details of these tasks can be found in Appendix A.

A summary of all the behavioural scales and their acronyms used through out the thesis can be found in Table 4.1.

Subscales	Explanation	Indicative of poor outcome	Final Domain
PHQ15	Patient Health Questionnaire (mainly pain measures)	High means bad	Pain
GAD7	Generalised Anxiety Disorder Assessment	high	Anxiety
PHQ9	Patient Health Questionnaire-9 (depression)	high	Mood
Fatigue	Fatigue Severity Scale (FSS)	high	Fatigue
D12	Dyspnoea 12	high	Breathlessness
BCS	Breathlessness Catastrophising Scale	high	Breathlessness
AMIBehaviouralDomain	Apathy Motivation Index Behavioural Domain	high	Motivation
AMISocialDomain	Apathy Motivation Index Social Domain	high	Motivation
AMIEmotionalDomain	Apathy Motivation Index Emotional Domain	high	Motivation
Stress	Perceived Stress Scale	high	Stress
CFQ	Cognitive Failures Questionnaire (subjective)	high	Cognition (subjective)
SF36PhysicalFunctioning	Short Form 36 - Physical Function	low	Function
SF36RoleLimitationsPhysicalHealth	Short Form 36 - Role Limitations Physical Health	low	Function
SF36RoleLimitationsEmotionalProblems	Short Form 36 - Role Limitations Emotional Problems	low	Function
SF36Pain	Short Form 36 - Pain	low	Function/Pain
SF36EmotionalWellBeing	Short Form 36 - Emotional Well-Being	low	Function/Mood
SF36Energy	Short Form 36 - Energy	low	Function/Fatigue
SF36SocialFunctioning	Short Form 36 - Social Functioning	low	Function
SF36GeneralHealth	Short Form 36 - General Health	low	Function
mmr_obj_imm	Cognitron task - Immediate Object Memory	high	Cognition (objective)
mmr_obj_delay	Cognitron task - Delayed Object Memory	high	Cognition (objective)
mmr_word_imm	Cognitron task - Immediate Word Memory	high	Cognition (objective)
mmr_word_delay	Cognitron task - Delayed Word Memory	high	Cognition (objective)
mmr_SpatialSpan	Cognitron task - Spatial Span (working memory)	high	Cognition (objective)
SRT	Cognitron task - Simple Reaction Task	high	Cognition (objective)
motor_control	Cognitron task - Motor Control	high	Cognition (objective)
CRT	Cognitron task - Choice Reaction	high	Cognition (objective)
TargetDetection	Cognitron task - Target Detection	high	Cognition (objective)
TOL	Cognitron task - Tower of London	high	Cognition (objective)
VerbalAna	Cognitron task - Verbal Analogy	high	Cognition (objective)
mentalrot_2d	Cognitron task - 2D Mental Rotation	high	Cognition (objective)
mentalrot_3d	Cognitron task - 3D Mental Rotation	high	Cognition (objective)

Table 4.1 Summary of subscales, their explanations, and corresponding domains for most items.

4.3.3 Analysis

The analysis of behavioural measures was performed in Python 6.5.2. To examine the characteristics of the current sample in terms of their demographic information, clinical profile during hospitalisation or during clinic visit, and post-COVID outcomes, exploratory analysis were followed by steps to reduce data dimension for all the behavioural outcomes.

Data exploration

Firstly, I conducted exploratory analysis to summarize the main demographic and clinical measures of the current sample, followed by further tests among three groups, to reveal key confounding factors that need to be dealt with caution in the following analysis in Chapter 5and 6. I performed ANOVA tests for the continuous variables (age, BMI, WHO clinical progression scale, cube root of brain volume, cube root intracranial volume). Tukey's HSD post-hoc tests were conducted for any significant outcomes to identify specific group differences. For the dichotomous variables (site, gender, first language, BAME, respiratory MH, cardiac MH), Chi-square tests were utilised followed by pairwise comparisons for significant variables to determine the direction and specific group differences.

Secondly, I explored the underlying structure of the current dataset based on the pair-wise correlations (heatmaps) on all raw question/task responses and their subscales. Heatmaps that show the correlational structure of the raw question/task items (150 x 150) and subscales (32 x 32) were re-ordered based on hierarchical clustering (seaborn library - clustermap) to aid visual examination of clusters. I also examined the subscale matrix after adjusting for multiple comparisons with Bonferroni correction. For the full raw item heatmap, all question/task scores were flipped so that higher score always corresponded to undesirable outcomes, e.g. bad mood, fatigue, poor function. In keeping with previous literature, the subscale heatmap was defined whereby higher scores on SF-36 (function) referred to better outcome, while higher scores on all other subscales referred to worse outcome.

Thirdly, building on the insights obtained from the heatmap visual inspection and drawing from previous literature on post-COVID outcomes, I pre-defined 11 domains of interest that balance feasibility and clinical relevance. These domains are: breathlessness, fatigue, negative mood/depression, lack of motivation, stress, anxiety, pain, poor function, poor sleep, objective cognitive impairment measured by cognitive tasks, and subjective cognitive impairment measured by self-report (acronyms: breathlessness, fatigue, negative_mood, lack_of_motivation, stress, anxiety, pain, poor_function, poor_sleep, cogimp_obj, cogimp_subj). Each question or task was manually coded into one of these 11 domains, item by item. To improve the interpretability of the final results, all ratings were adjusted so

that higher scores consistently indicate poorer outcomes, such as increased breathlessness, greater depression, or poorer cognitive function. I also applied multiple imputation, using a round-robin approach (Python: sklearn.impute.IterativeImputer), where each feature with missing data was modelled as a function of other features or summary measures.

Finally, to disambiguate the inhomogeneity within the patient group, and their differences in comparison to the controls, I took three steps: 1) simple group comparison with ANOVA followed by pairwise group comparisons with multiple comparison corrections; 2) Neighborhood Component analysis[141]; and 3). K-means Clustering[226].

The Neighbourhood Components Analysis (NCA) is a supervised machine learning algorithm that learns a linear transformation of input data (11 features of all domains) and project them into a lower dimension (n_component set to 2) for the aims of maximising the distinction between the hospitalised, non-hospitalised, and control groups. This indicates if there are important differences between these groups and what the differentiating features (or linearly combined features) are.

The K-means clustering analysis is an unsupervised machine learning algorithm that partitions a dataset into k distinct, non-overlapping clusters based on feature similarity by iteratively updating cluster centroids, in which I used a k = 3, based on the elbow method. This plots the within-cluster sum of squares (y-axis) against the number of clusters (x-axis). I later highlighted group membership of each clusters to provide a visual representation of how data-driven clustering are related to the groups.

Dimension reduction

Direct dimension reduction using methods such as PCA is highly susceptible to over-fitting in the current small sample size in comparison to the question/task numbers (118 participants, of which 90 patients; 150 questionnaire and task items). Hence I adopted the optimised Domain-based Dimension reduction (DDR) [220] method, in which clinical meaningful domains of interest were pre-defined manually and PCA was conducted within each domain, separately. This section of exploratory analysis helped inform decisions on the definition of domains.

4.4 Results

4.4.1 Basic demographic information

The current cohort consists of 118 individuals, including post-COVID-19 patients (hospitalised and non-hospitalised) and healthy controls. The participants are predominantly older

(mean age: 50.17 ± 13.88 years), Caucasian (non-BAME: 93%), and overweight (BMI range: 25.0–29.9, mean BMI: 27.58 ± 5.27). Gender distribution varies across groups: hospitalised (26% female), non-hospitalised (75% female), and controls (48% female). As indicated in Table 4.2, hospitalised patients were significantly older than both the control group (mean difference = 13.006, $p = 0.0003$) and the non-hospitalised group (mean difference = 12.3876, $p < 0.0001$), while no notable age difference was observed between the control and non-hospitalised groups.

In terms of gender distribution, significant differences were identified between non-hospitalised and control groups ($p = 0.0282$) as well as between non-hospitalised and hospitalised groups ($p < 0.0001$). However, no significant gender difference was observed between the control and hospitalised groups ($p = 0.1209$), with the hospitalised group being predominantly male and the non-hospitalised group predominantly female.

Pairwise site comparisons reveal significant differences between the non-hospitalised and control groups ($p = 0.0067$), non-hospitalised and hospitalised groups ($p < 0.0001$), and control and hospitalised groups ($p = 0.0005$), reflecting that participant recruitment was not evenly distributed across sites.

For acute infection severity, assessed using the WHO Clinical Progression Scale, substantial differences were present across all group comparisons. The hospitalised group demonstrated markedly higher severity than both the control group (mean difference = 4.7027, $p < 0.0001$) and the non-hospitalised group (mean difference = -3.7216, $p < 0.0001$). Additionally, the non-hospitalised group exhibited a slightly elevated severity level compared to the control group (mean difference = 0.9811, $p < 0.0001$).

The data collection interval from acute infection was notably longer and more variable for non-hospitalised patients ($M = 456.81$ days, $SD = 260.11$) compared to hospitalised patients ($M = 211.19$ days, $SD = 67.5$). Analyses of respiratory medical histories showed significant differences between both the hospitalised and control groups ($p = 0.0295$) and the non-hospitalised and control groups ($p = 0.0458$), with no meaningful difference between the non-hospitalised and hospitalised groups ($p = 0.9339$). Finally, in cardiac medical history, significant differences were found between the non-hospitalised and hospitalised groups ($p = 0.0043$) as well as the control and hospitalised groups ($p = 0.0147$), but not between the non-hospitalised and control groups ($p = 0.9403$).

Variable	Hospitalised	Non-Hospitalised	Control	All	N	Group diff (p-value)
Age (M, SD)	58.78 (12.87)	46.4 (11.23)	45.78 (14.96)	50.17 (13.88)	117	0.0000**
Gender (F/M, % female)	10F/28M (26%)	40F/13M (75%)	13F/14M (48%)	63F/55M (53%)	118	0.0000**
BMI (M, SD)	28.31 (5.08)	28.12 (5.77)	25.7 (4.25)	27.58 (5.27)	97	0.1298
WHO (M, SD)	4.7 (1.13)	0.98 (0.14)	0.0 (0.0)	1.95 (2.03)	116	0.0000**
days_from_acute (M, SD)	211.19 (67.5)	456.81 (260.11)	nan (nan)	341.22 (229.58)	68	
Brain Vol (M, SD)	112.18 (3.35)	111.35 (4.01)	113.0 (4.25)	111.95 (3.89)	68	0.3809
Intra Vol (M, SD)	0.92 (0.02)	0.91 (0.03)	0.92 (0.03)	0.91 (0.03)	68	0.3642
Site (Ca/Ox count % Cardiff)	0/38 (0%)	36/17 (68%)	9/18 (33%)	45/73 (38%)	118	0.0000**
First Language (count % English)	37/1 (97%)	50/3 (94%)	26/1 (96%)	113/5 (96%)	118	0.7692
BAME (count %)	3/35 (8%)	3/50 (6%)	2/25 (1%)	8/110 (7%)	118	0.9064
RespMH (count %)	9 (31%)	10 (27%)	0 (0%)	19 (23%)	83	0.0389*
CardMH (count %)	13 (45%)	4 (11%)	1 (6%)	18 (22%)	83	0.0008**

Table 4.2 Summary of key demographic and clinical characteristics. Values are presented as mean ± SD for continuous variables or as counts and percentages (n, %). Group differences were assessed using ANOVA for continuous variables and the Chi-Square test for categorical variables. Significant differences are indicated as follows: ** for $P < 0.01$ and * for $P < 0.05$ (unadjusted). BMI - body mass index in units of kg/m², calculated by dividing body weight by the square of the body height. WHO - WHO clinical progression scale. days_from_acute - days from the acute infection to the consent day, which is within 5 days of the MRI scan. Brain Vol - cube-root of total brain volume, including ventricles. Intra Vol—cube-root of total intracranial volume. Ca/Ox - Cardiff site or Oxford site. BAME - Black, Asian, and Minority Ethnic. Resp MH - medical history of respiratory conditions. Card MH - medical history of cardiac conditions.

Regarding heterogeneity within the patient groups, the hospitalised cohort was characterised by older males, more severe acute-phase infection (456.81 ± 260.11 vs. 211.19 ± 67.5), a shorter interval between acute infection and study participation (0.98 ± 0.14 vs. 4.7 ± 1.13 months), and a higher prevalence of cardiac disease (45% vs. 11%) compared to the non-hospitalised group. However, the prevalence of respiratory disease was similar between the two groups (31% vs. 27%). No significant differences were observed in BMI, ethnicity (BAME), first language (English), brain volume, or socioeconomic status.[1] See Table 4.2 and Table 4.3 for further details. All participants in the hospitalised group were recruited and assessed in Oxford, whereas the majority of the non-hospitalised group were studied in Cardiff.

In comparison to the patient groups, the control group was younger, exhibited a more balanced gender distribution, and had a lower prevalence of respiratory and cardiac medical history. No significant group differences were observed in BMI (controls had lower values on average, but remained in the overweight range), brain volume, ethnicity (BAME), or first language (English). Participants were predominantly employed and displayed the highest level of educational attainment, with 65% holding university degrees—including 15% with doctoral qualifications—and a predominantly middle-class income profile (42% earning £20–40K annually), based on available data.[2].

[1]The hospitalised group had a high proportion of missing data, with many participants selecting "unknown" or "prefer not to say".

[2]Caution is warranted when interpreting group comparisons due to substantial missing data, particularly within the hospitalised group.

Occupation	**Hosp**	**Non-Hosp**	**Control**	**All**
Total Group N	**38**	**53**	**27**	**118**
Worker	9 (29%)	45 (87%)	17 (74%)	71 (67%)
Student	NaN	2 (4%)	NaN	2 (2%)
Homemaker	NaN	NaN	NaN	NaN
Retired	4 (13%)	4 (8%)	1 (4%)	9 (8%)
Unemployed/Looking for work	NaN	NaN	2 (9%)	2 (2%)
Disabled/Not applicable/Sheltered employment	NaN	1 (2%)	NaN	1 (1%)
Unknown	18 (58%)	NaN	3 (13%)	21 (20%)
based on non-missing N of:	31	52	23	106
Income	**Hosp**	**Non-Hosp**	**Control**	**All**
£0-10K	1 (7%)	6 (12%)	NaN	7 (8%)
£10-20K	NaN	2 (4%)	3 (16%)	5 (6%)
£20-30K	1 (7%)	14 (27%)	5 (26%)	20 (24%)
£30-40K	1 (7%)	11 (21%)	3 (16%)	15 (18%)
£40-50K	2 (14%)	4 (8%)	2 (11%)	8 (9%)
£50-60K	1 (7%)	4 (8%)	1 (5%)	6 (7%)
£60-70K	NaN	2 (4%)	1 (5%)	3 (4%)
£70-80K	NaN	NaN	1 (5%)	1 (1%)
£80-90K	1 (7%)	NaN	NaN	1 (1%)
£90-100K	NaN	NaN	NaN	NaN
>100K	2 (14%)	2 (4%)	NaN	4 (5%)
Prefer not to say	5 (36%)	7 (13%)	3 (16%)	15 (18%)
based on non-missing N of:	14	52	19	85
Education	**Hosp**	**Non-Hosp**	**Control**	**All**
No schooling	NaN	NaN	NaN	NaN
Primary/Elementary school	NaN	1 (2%)	NaN	1 (1%)
Secondary school/High school diploma	14 (56%)	12 (23%)	7 (35%)	33 (34%)
University degree	9 (36%)	38 (73%)	10 (50%)	57 (59%)
PhD	2 (8%)	1 (2%)	3 (15%)	6 (6%)
based on non-missing N of:	25	52	20	97

Table 4.3 Occupation, Income, and Education by Group. This table displays the count and percentage within each group, specifically the hospitalised group (n = 38), non-hospitalised group (n = 53), control group (n = 27), and the overall total (n = 118). Percentages are calculated based on available (non-missing) data within each category. Please note that groups with substantial missing data, such as income for the hospitalised group, require cautious interpretation of percentage values.

4.4.2 Post-COVID outcomes

Raw Data and Subscales Exploration

The raw data correlational heatmap (150 x 150 question/task items, scaled) showed approximately 4-7 clusters at the lower level, as shown in Figure 4.2. Four bigger clusters from the top left and bottom right corner off diagonal indicated domains of respiratory-related questions, pain and fatigue, self-report cognitive function impairment, and depression-related questions, which can be further segmented into anxiety, stress, negative mood, poor sleep and lack of motivation. Three smaller clusters at the two ends of the diagonal showed items reflecting specifically function, cognitive task performance, and possibly certain aspects of pain, respectively,

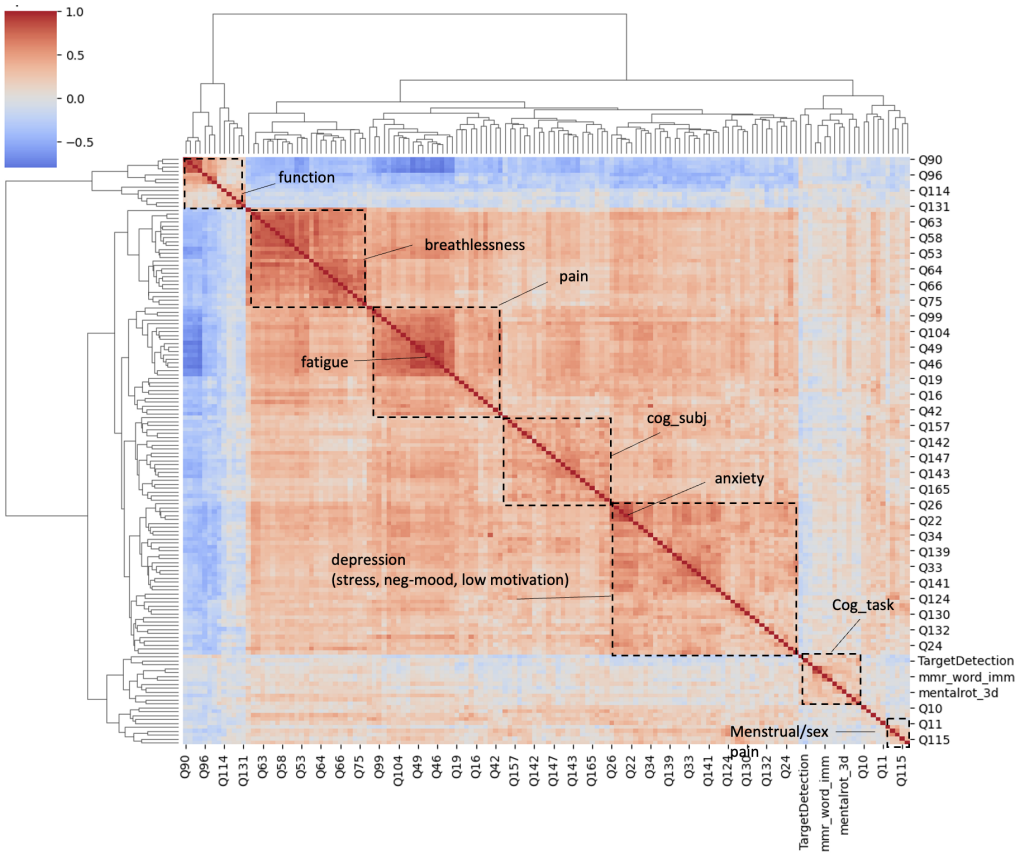


Fig. 4.2 Heatmaps of all raw question/task items. This figure presents a clustered correlation heatmap illustrating the relationships among all raw question or task items, with hierarchical clustering applied to both rows and columns. The dendrograms along the top and left edges represent the clustering results, aiding in the visualization of similar item groupings. Key clusters, examined and interpreted based on item content, are marked with black dashed boxes and annotated for clarity. The heatmap is color-coded using a "coolwarm" palette: warmer colors (reds) indicate positive correlations, cooler colors (blues) denote negative correlations, and the midpoint (0) represents neutral correlations. This color scheme enables quick identification of both strong positive and negative relationships across items, helping to visually highlight potential clusters and relational patterns among them.

A complementary exploratory analysis for all existing subscales (32 x 32 summary scores, scaled; See Table 4.1) indicated a similar, yet less granular, result.

In the top panel of Figure 4.3, which displays the raw Pearson correlations of the subscales organized by hierarchical clustering analysis, three clusters can be visually identified: two smaller clusters at the top left and bottom right corner off diagonal, and one large cluster in the middle section. The two small clusters correspond to poor general function dominated by the SF-36 questionnaires, or the objective cognitive impairment measured by the Cognitron tasks. The middle larger cluster correspond to most of the psycho-physiological outcomes, which

can possibly be further separately into four sub-clusters (ordered from left top to right bottom): breathlessness, fatigue & pain, subjective cognitive impairment, anxiety&depression). This cluster also includes cognitive tasks related to motor control and reaction speed (SRT, CRT).

In the bottom panel of Figure 4.3, after limiting the correlations to those that survived Bonferroni correction, a distinct cluster of cognitive tasks (orange, bottom right corner) remained. Additionally, there appears to be a stronger cluster among psychological and physiological measures (top left corner) and a clearer connection between these psycho-physiological ratings and cognitive tasks (bottom left), which was not as evident in the uncorrected heatmap on the left. The prominence of SF-36 related functioning was reduced in this filtered view. Overall, unstable (before vs. after statistical tests) clustering around the self-report psychological and physiological measures, including the GAD7, PHQ9, PHQ15, D12, BCS, CFQ, Stress, etc., and their associations with the cognitive functional measures, may suggest higher heterogeneity between individuals.

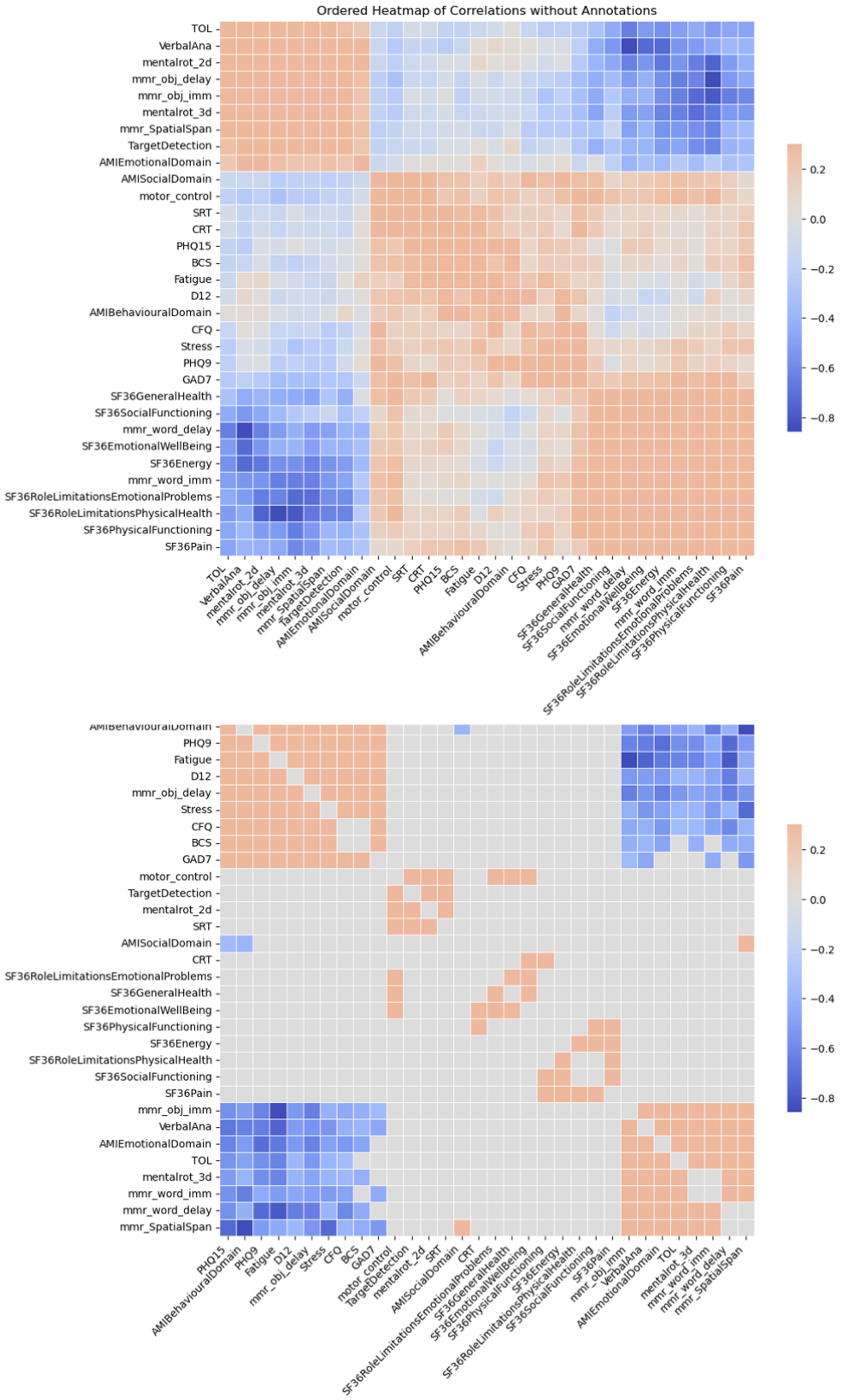


Fig. 4.3 Heatmaps of all subscales. These clustered correlation heatmaps illustrate relationships among all subscales, with hierarchical clustering applied to both rows and columns. Significant correlations (Bonferroni-corrected) are highlighted in the bottom figure. Refer to Table 4.1 for acronym details. The "coolwarm" color scheme indicates correlation strength and direction: reds for positive correlations, blues for negative correlations, with zero (neutral) at the center, allowing quick identification of strong relationships among subscales.

Defining key domain Based on the nature of the current dataset and published literature in long COVID symptoms, I have identified 11 domains of interest in the current chapter and further analysis in this thesis. Each item from the questionnaires and tasks was categorized into one of these 11 domains: breathlessness, fatigue, negative mood/depression, lack of motivation, stress, anxiety, pain, poor function, poor sleep, objective cognitive impairment measured by cognitive tasks and subjective cognitive impairment measured by self-report (acronyms: breathlessness, fatigue, negative_mood, lack_of_motivation, stress, anxiety, pain, poor_function, poor_sleep, cogimp_obj, cogimp_subj). A summary of how these domains fall under each subscales is provided in Table 4.1. For ease of interpretation, all items were flipped so that higher scores consistently represent more undesirable outcomes.

I took the mean of all question/task items (z-scored) in each domain to form 118 x 11 summary scores matrix, based on which I conducted exploratory analysis to establish the impact of groups.

Relationship between demographic background and COVID Outcomes

To contextualise the 'risk factors' for developing long COVID, Pearson correlations were calculated between demographic and clinical background information and 11 domains of post-COVID outcomes for all 91 patients (38 hospitalised, 53 non-hospitalised). These results are presented in Figure 4.4.

In the full patient group, variables such as study site, group (hospitalised vs. non-hospitalised vs. control), gender, and the WHO Clinical Progression Scale showed strong correlations with fatigue, pain, negative mood, and subjective cognitive impairment. However, the gender effect diminished when the hospitalised and non-hospitalised groups were analysed separately. The WHO Clinical Progression Scale remained strongly correlated with poor overall function but not with specific symptoms.

The number of days from acute infection to the study was significantly correlated with negative mood and stress in the hospitalised group but not in the non-hospitalised group. Age was primarily associated with objective cognitive function, while a history of respiratory conditions was strongly linked to breathlessness. In the non-hospitalised group, participants from BAME backgrounds showed a high correlation with breathlessness, although this may reflect bias due to the small sample size (N=3), some of whom had asthma or COPD as comorbidities.

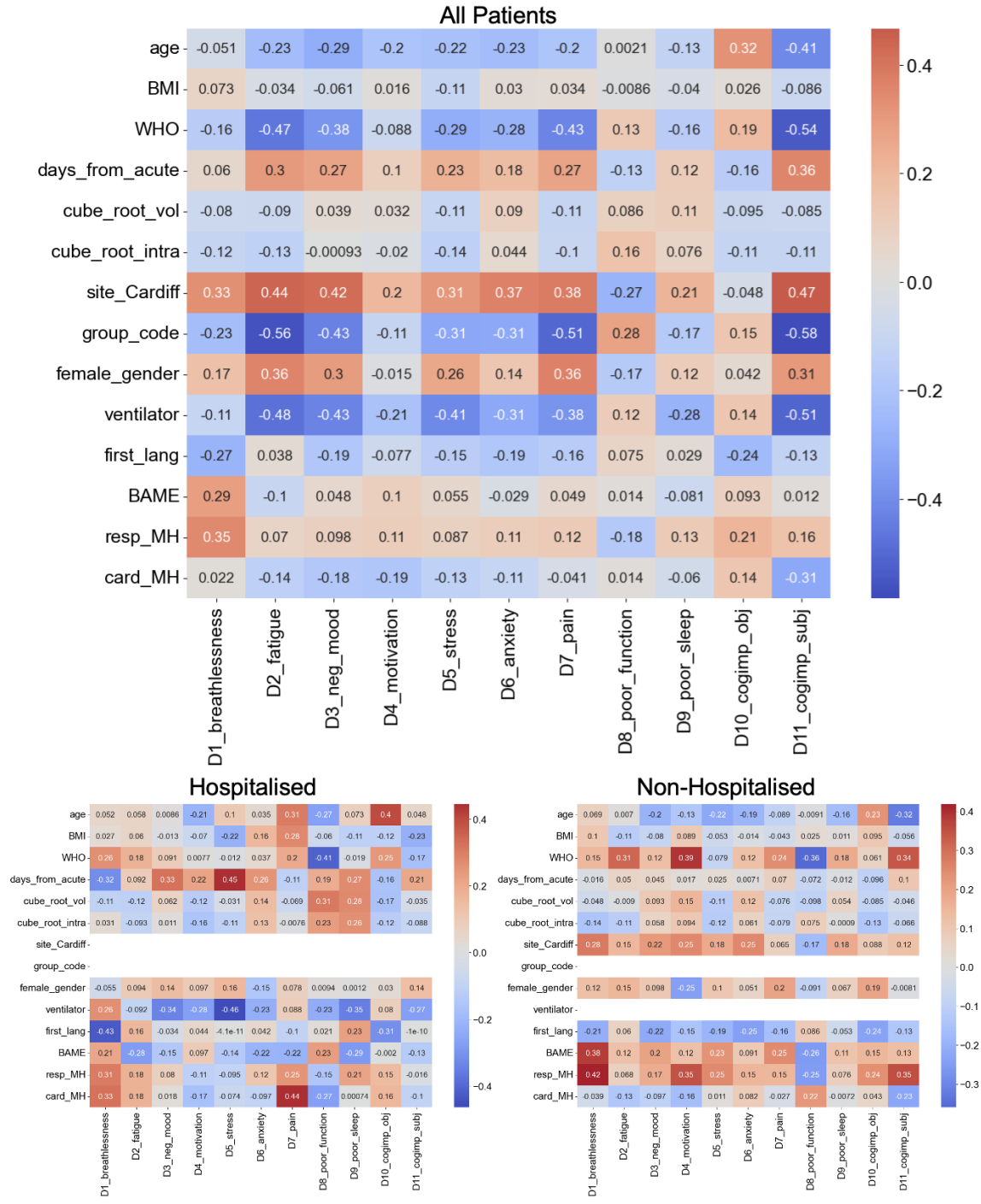


Fig. 4.4 Correlations between demographic and clinical characteristics and COVID-19 outcomes. These were displayed as heatmaps illustrating correlations between demographic and clinical characteristics and COVID-19 outcomes for all patients, hospitalised patients, and non-hospitalised patients. The "coolwarm" colour scheme represents correlation strength and direction: reds indicate positive correlations, blues indicate negative correlations.

Simple Group Comparison

As shown in Figure 4.5, significant differences between the hospitalised and non-hospitalised groups were found in the domains of subjective cognitive impairment, breathlessness, fatigue, negative mood, stress, anxiety, pain, and poor sleep. Specifically, the non-hospitalised group reported worse outcomes in these domains compared to the hospitalised group.

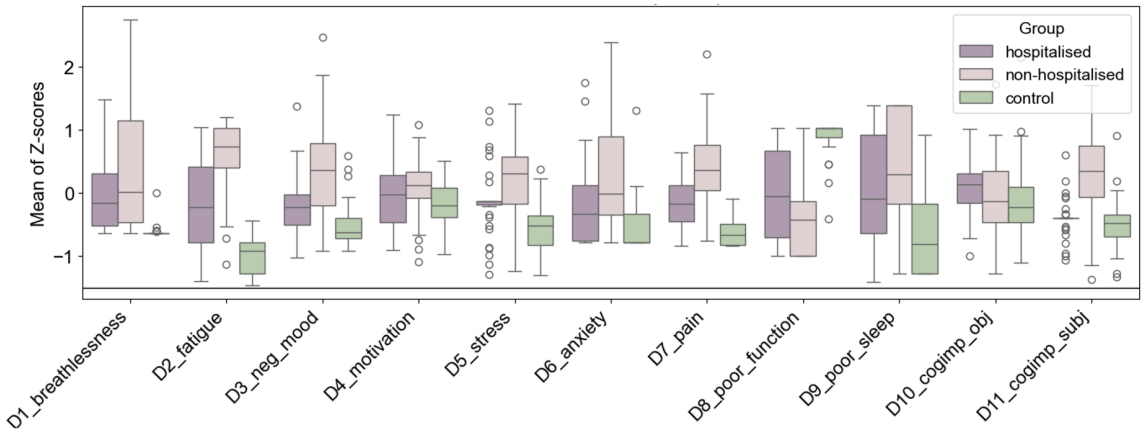


Fig. 4.5 Boxplot of domain means by group. This plot is based on all 118 participants. Note that there were considerable missing data for the domains for subjective cognitive task and Stress for hospitalised patients.

When comparing the non-hospitalised group to the control group, significant differences were observed in the same domains —subjective cognitive impairment, breathlessness, fatigue, negative mood, stress, anxiety, pain, poor function, and poor sleep—with the non-hospitalised group showing higher levels of impairment or distress.

Comparisons between the hospitalised group and the control group revealed significant differences in breathlessness, fatigue, pain, poor function, and poor sleep, with the hospitalised group showing worse outcomes in these domains.

No significant differences were observed between groups for objective cognitive impairment and motivation after Bonferroni correction, even though the control group showed a trend of high levels of objective cognitive impairment and low levels of subjective cognitive impairment. The hospitalised group has shown highly varied levels of fatigue and pain.

NCA Based on 11 Domains

We then conducted a NCA to assess the extent to which these 11 behavioural domain summary scores could differentiate between the initial groups: non-hospitalised, hospitalised, and control. The results of the NCA with two dimensions are shown in the left panel of Figure 4.6.

NCA Component 1 primarily contrasts perceived cognitive difficulties and fatigue with physical function and sleep quality. NCA Component 2 contrasts breathlessness and poor sleep with perceived cognitive difficulties, as shown in the right panel of Figure 4.6.

The three groups, hospitalised, non-hospitalised, and control, differed more substantially on the first component, which primarily reflexes self-reported cognitive difficulties and fatigue. The non-hospitalised group exhibited the most severe symptoms, followed by the hospitalised group, while the control group showed the least severity, with some overlap. The groups showed minimal variation on the second component, which reflexes breathlessness and poor sleep.

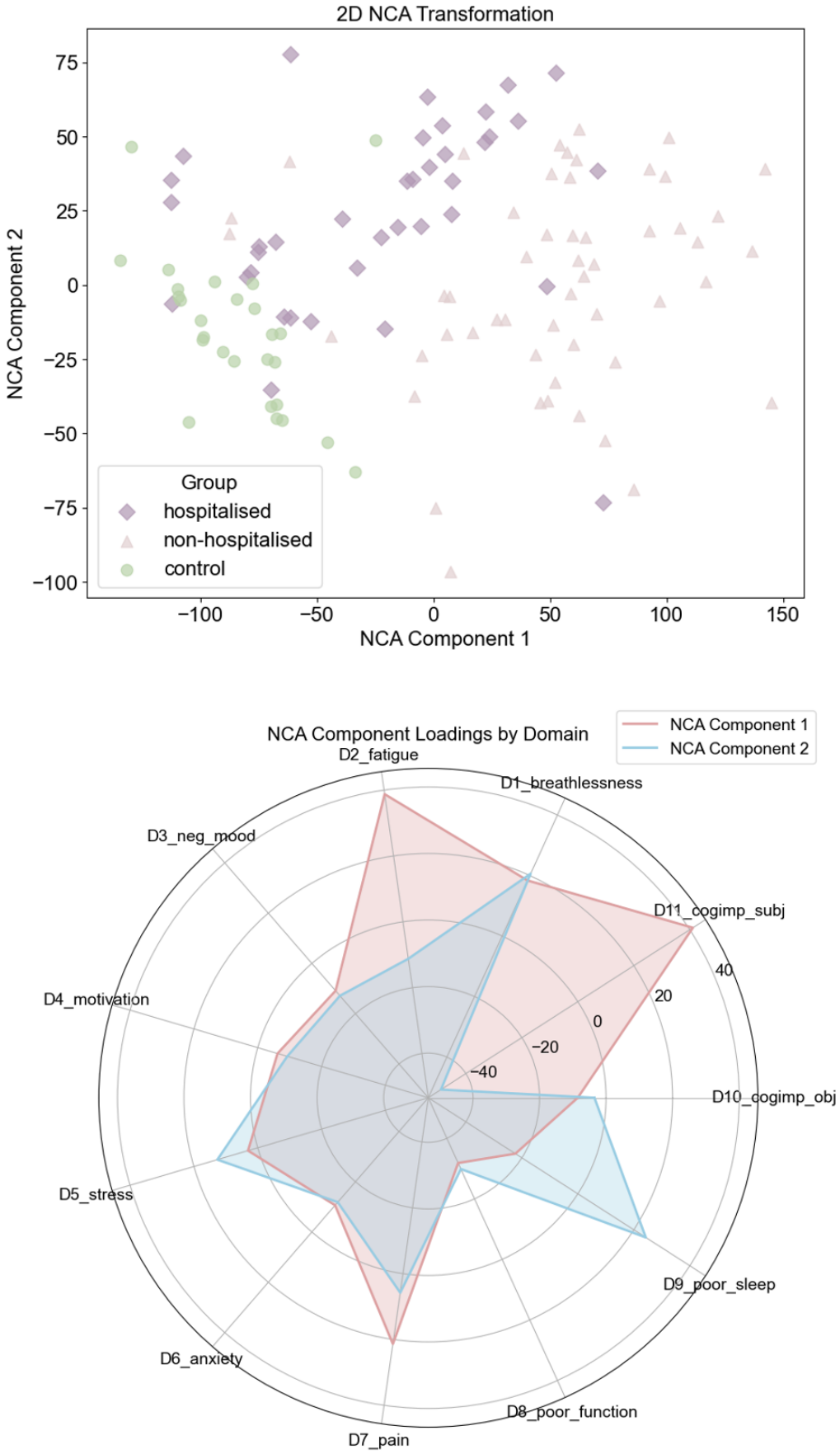


Fig. 4.6 Scatter plot of the three groups—hospitalised, non-hospitalised, and control—plotted on the two NCA components, alongside a radar plot showing the loadings of the 11 behavioural domain summary scores on these components.

K-means Clustering Based on 11 Domains

Three clusters decided by the elbow method (see top plane of Figure 4.7) were identified pulling all individuals' 11 domain means together. As shown in Figure 4.7 and Figure 4.8, they are:

1. *"Cluster of High symptom burden yet functioning well" (Cluster 0, marked by blue 'x')*: This cluster is characterised by a high overall symptom burden, yet participants demonstrate relatively good functioning in daily life and maintain good objective cognitive performance. It consists solely of patients, particularly non-hospitalised individuals.

2. *"Cluster of No symptoms but poor function" (Cluster 1, marked by orange squares)*: Individuals in this cluster exhibit few or no symptoms but experience significant difficulties in daily functioning. It is predominantly composed of controls, with a smaller proportion of hospitalised patients.

3. *"Cluster of Mild symptoms and tired" (Cluster 2, marked by green dots)*: This cluster represents individuals with mild symptoms, with fatigue being the most prominent complaint. It includes roughly equal numbers of non-hospitalised and hospitalised patients.

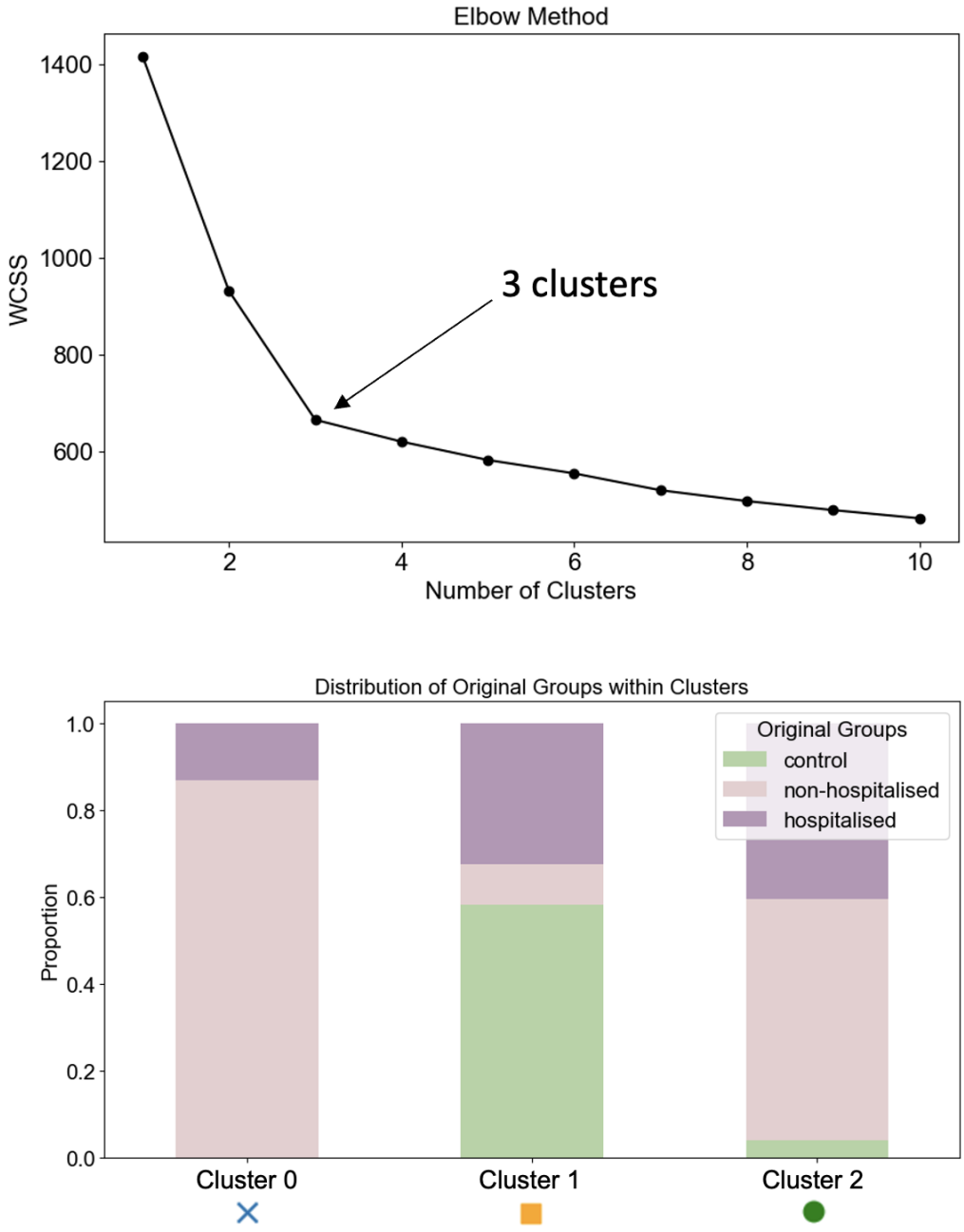


Fig. 4.7 K-Means Clustering and distribution among clinical groups. Using the elbow method, I identified three clusters by plotting the within-cluster sum of squares (y-axis) against the number of clusters (x-axis), as shown in the top figure. The bottom figure displays the distribution of original clinical groups across the three data-driven clusters.

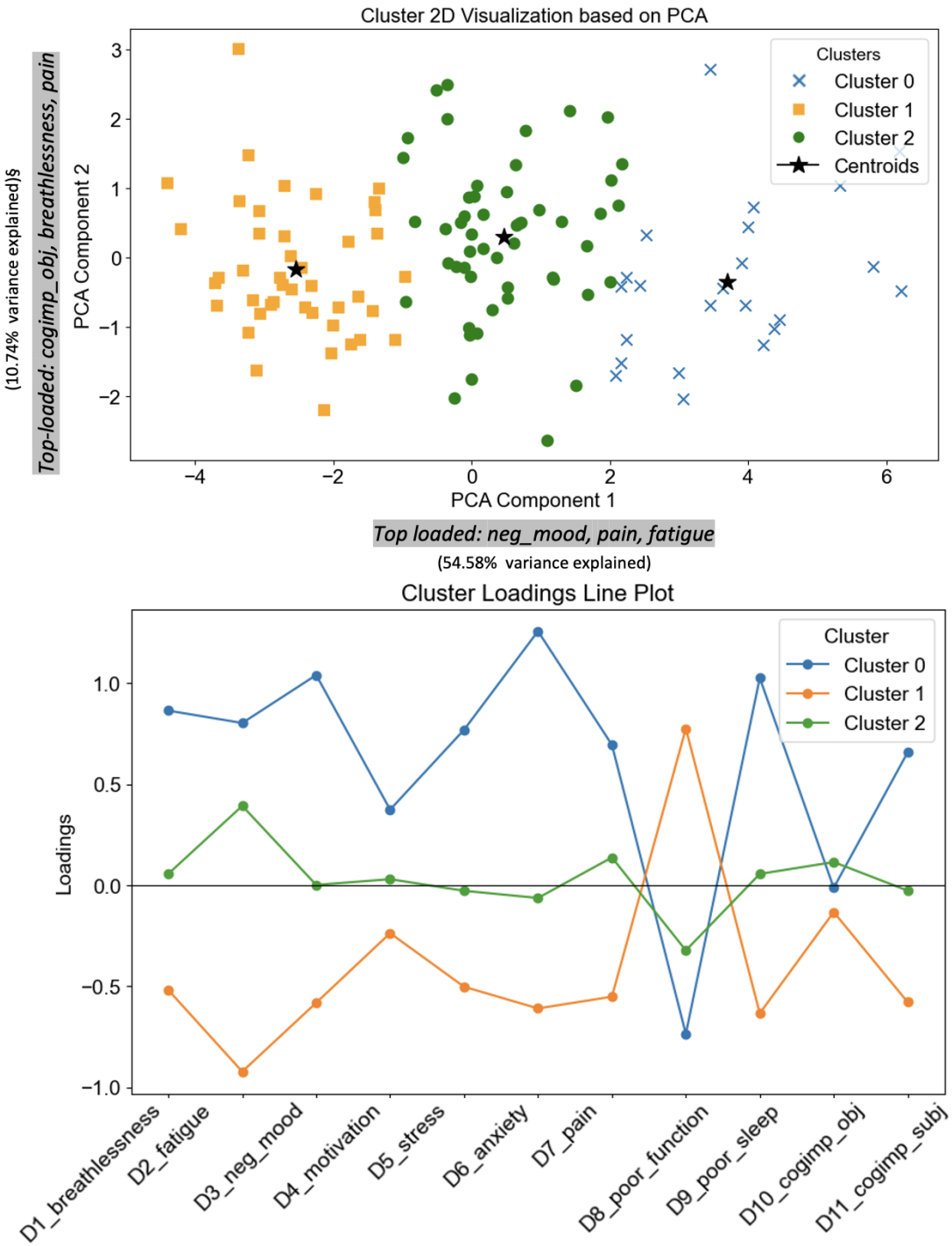


Fig. 4.8 Scatterplort of K-Means Clusters and loadings. The top figure visualizes the clustering results of K-Means on the first two PCs of the 11 domains. Principal Component Analysis (PCA) is used here solely for the purpose of providing a 2-dimensional representation of the clusters, and the PCA transformation is not utilised in the main analysis of the study. Each cluster is shown in different colours, with the centroids represented as black stars. The bottom figure displays the detailed loadings of each cluster on the original feature domains. These loadings represent how much each original feature contributes to the clusters and provide insight into the characteristics of each group based on the original data dimensions.

4.4.3 Domain-based dimension reduction

For the purpose of dimension reduction on all patients' brain-behaviour analysis, data for control subjects were excluded, focusing the subsequent analysis solely on patient data (N=90).

Following this, Domain-Based Dimension Reduction was conducted using Principal Component Analysis (PCA). For each domain, principal components (PCs) explaining at least 50% of the variance were retained. Specifically, the first PC was retained for the domains of breathlessness, fatigue, negative mood, anxiety, function, and poor sleep. For the stress domain, the first two PCs were retained, while for the domains of lack of motivation, pain, subjective cognitive impairment, and objective cognitive impairment, the first three PCs were kept. In total, 20 PCs across all behavioural measures were retained for further consideration (see Figure 4.9, and Table 4.4).

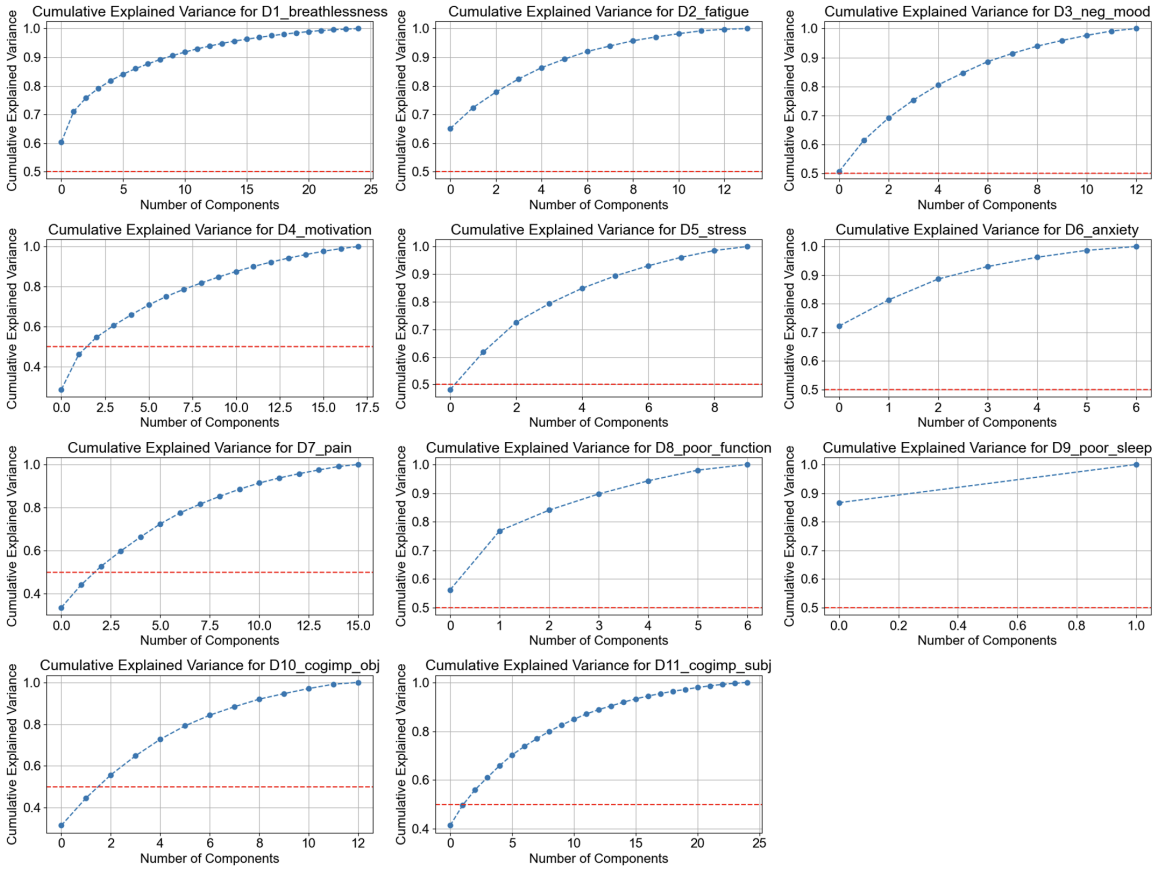


Fig. 4.9 Domain-based PCA:Cumulative Explained Variance. Plots of the cumulative explained variance by number of components for each of the 11 domains. The red dashed line represents the 50% threshold.

Domain	No. of PCs	Cumulative Var. Explained	1st PC Var. Explained
D1_breathlessness	1	60%	60%
D2_fatigue	1	65%	65%
D3_neg_mood	1	51%	51%
D4_lack_motivation	3	55%	29%
D5_stress	2	62%	48%
D6_anxiety	1	72%	72%
D7_pain	3	53%	34%
D8_function	1	56%	56%
D9_poor_sleep	1	87%	87%
D10_cog_obj	3	56%	31%
D11_cog_subj	3	56%	41%

Table 4.4 Principal components and variance explained for each Domain

Principal Component Loading To clarify the role and necessity of each PC retained in the model for domains where more than one PC was retained after PCA dimension reduction, I examined the loadings and interpretations of each PC.

- Motivation: PC1 represents general motivation, such as initiating activities and social interactions, while PC2 is linked to interpersonal relationships, including feelings of guilt and concern for others. For example:

  PC1 - I suggest activities for me and my friends to do. (q117) I enjoy doing things with people I have just met.(q116) When I decide to do something, I am motivated to see it through to the end(q125). I enjoy choosing what to do from a range of activities. (q130)

  PC2 - If I realise I have been unpleasant to someone, I will feel terribly guilty afterwards (q131). I feel bad when I hear an acquaintance has an accident or illness (q129). Based on the last two weeks, I would say I care deeply about how my loved ones think of me. (q120)

- Stress: PC1 reflects feelings of being overwhelmed, while PC2 includes an emotional component, focusing on anger and irritation due to uncontrollable events. For example:

  PC1 - In the last month, how often have you felt that you were unable to control the important things in your life? (q133). In the last month, how often have you felt difficulties were piling up so high that you could not overcome them? (q141)

  PC2 - In the last month, how often have you been angered because of things that happened that were outside of your control? (q140) In the last month, how often have

you been upset because of something that happened unexpectedly? (q132) In the last month, how often have you been able to control irritations in your life? (q138)

- Pain: PC1 captures overall pain intensity and its impact on daily activities. PC2 and PC3 focus on specific types of pain, such as limb pain and menstrual pain. For example:

  PC1 - How much pain have you had during the past 4 weeks? (q98) How much did pain interfere with your normal work (including both work outside the home and housework)? (q99) Feeling your heart pound or race (q16)

  PC2 - How much did pain interfere with your normal work (including both work outside the home and housework)? (q99) stomach pain (Q5, negative loading)

  PC3 - Pain in your arms, legs, or joints (knees, hips, etc). (q7, negative loading) Menstrual cramps or other problems with your periods (q10)

- Objective (Task) Cognitive Impairment: PC1 emphasises overall cognitive impairment with a focus on memory tasks. PC2 emphasises reaction/motor control possibly associated with attention. PC3 contrasts immediate recall abilities with working memory and language processing-related cognitive tasks (detailed loadings in Table 4.5) .

- Subjective (Self-Reported) Cognitive Impairment: PC1 relates to daily cognitive slips and forgetfulness. PC2 highlights communication difficulties, like confusion in giving directions, while PC3 is associated with distractibility and retrieval issues.

  PC1- Do you find you forget what you came to the shops to buy? (q164) Do you fail to see what you want in a supermarket (although it is there)? (q154) Do you find you accidentally throw away the thing you want and keep what you meant to throw away as in the example of throwing away the matchbox and putting the used match in your pocket? (q159)

  PC2 - Do you find you confuse right and left when giving directions? (q145) Do you find you can't think of anything to say? (q166, negative loading) Do you find yourself suddenly wondering whether you've used a word correctly? (q155, negative loading)

  PC3 - Do you start doing one thing at home and get distracted into doing something else (unintentionally)? (q162) Do you find you can quite remember something although it is on the tip of your tongue? (q163)

PC	Task	Domain	Loading
PC1	Object Memory (delayed)	Memory	0.3314
	Object Memory (immediate)	Memory	0.3277
	Word Memory (delayed)	Memory	0.3202
	Word Memory (immediate)	Memory	0.3051
PC2	Choice Reaction	Concentration	0.4556
	Target Detection	Concentration	0.4099
	Motor Control	Motor Control	0.3973
	3D Mental Rotations	Mental Rotation	-0.3366
PC3	Word Memory (immediate)	Memory	0.4062
	Object Memory (immediate)	Memory	0.3777
	Verbal Analogies	Reasoning	-0.3420
	Spatial Span	Working Memory	-0.3267

Table 4.5 Top 4 tasks for each principal component in objective cognitive impairment. Details of these tasks can be found in Appendix A.

4.5 Discussion

4.5.1 Summary

Assessing the representativeness of the current sample in the context of published literature, particularly large population databases, is crucial before conducting well-designed and appropriately interpreted brain-behaviour analyses for long COVID. This chapter begins with an extensive exploration and visualisation of data, focusing solely on demographic and clinical backgrounds alongside post-COVID behavioural (non-imaging) outcomes. It revealed that this larger sample (N=118), including those excluded due to 7T MRI scan safety concerns, recruited from two study sites with a high overlap in patient group allocations, consisted of an older, predominantly female, Caucasian population with a high prevalence of overweight individuals. A high degree of heterogeneity was observed within the patient groups (hospitalised vs. non-hospitalised), particularly in terms of age, gender, disease severity, medical history of cardiac conditions, and time from acute infection to the study. Subjective cognitive impairment and fatigue emerged as the most distinct outcomes to differentiate the pre-existing groups (hospitalised vs non-hospitalised vs control). The control group exhibited a more sporadic profile, characterised by a distinct “low function but no

symptom" pattern. This group tended to be younger, had lower (yet still overweight) BMI, and presented with lower socioeconomic status.

Given the constraints of a large number of behavioural features with a small sample size, compounded by the high heterogeneity within the patient group, I defined 11 domains of behavioural outcomes, within which dimension reduction was conducted. These domains strike a balance between covering clinically important aspects of long COVID and remaining statistically feasible given the nature of the data. The 11 domains are as follows: breathlessness, fatigue, negative mood/depression, lack of motivation, stress, anxiety, pain, poor function, poor sleep, objective cognitive impairment measured by cognitive tasks and subjective cognitive impairment measured by self-report (acronyms: breathlessness, fatigue, negative_mood, lack_of_motivation, stress, anxiety, pain, poor_function, poor_sleep, cogimp_obj, cogimp_subj).

4.5.2 Contextualising the current sample within the post-COVID population

The sample of post-COVID patients, drawn from both discharged hospitalised individuals and non-hospitalised patients who sought outpatient care due to long COVID symptoms, presents several important biases and characteristics. Firstly, this sample does not represent the full spectrum of post-COVID patients. Instead, it comprises two 'special' subgroups: those who experienced severe acute COVID-19—such as those who were hospitalised and may have received invasive mechanical ventilation—and those who were not severely ill during the acute phase but developed a significant symptom burden afterwards. The majority of COVID patients who were not hospitalised and did not develop significant levels of post-COVID symptoms, were not included in this sample.

As a result, the hospitalised group appears to have better post-COVID outcomes compared to the non-hospitalised group, as indicated by the simple group comparisons, NCA, and K-means clustering results. However, this may simply reflect that some hospitalised patients did not develop long COVID. Therefore, caution is needed when drawing conclusions from this sample about the relationship between acute severity and post-COVID outcomes.

Secondly, it is important to note that the variable "group" is highly correlated with site, acute phase severity (WHO clinical progression scale), and even sex. Non-hospitalised patients were predominantly recruited from Cardiff, while hospitalised patients were exclusively recruited from Oxford. The non-hospitalised group was also predominantly female, which aligns with published literature indicating that females are more likely to develop long COVID, whereas males are more likely to be hospitalised or die from COVID-19 [104]

[232] . This complex interplay of factors underscores the importance of controlling for the group effect and avoiding the risk of multicollinearity by combining site, sex (female), and severity into a single model. Caution is also necessary when considering the effects of group-related variability. For instance, while female sex was strongly correlated with major post-COVID symptoms when analysing the patient group as a whole - in consistency of the published literatures[104, 232] this effect diminished when examined within the hospitalised and non-hospitalised groups separately. This may correspond to the inconsistent findings on sex as a risk factor for developing long COVID, as highlighted in several previous studies [260].

4.5.3 Patient heterogeneity

Using simple group comparison, NCA, K-means and correlations between demographic background and COVID outcomes, I have comprehensively explored and identified several aspects of heterogeneity of hospitalised and non-hospitalised group.

Firstly, the non-hospitalised group was primarily composed of younger females, mostly from the Cardiff site, while the hospitalised group tended to be older males, with higher educational and economic status, predominantly white British (non-BAME), more English-speaking, and with a greater history of respiratory and cardiac conditions.

Secondly, patients from long COVID clinics (non-hospitalised) exhibited a higher symptom burden, especially in terms of subjective cognitive performance. Hospitalised patients, on the other hand, showed a broader range of symptoms, including fatigue and pain. To determine if there were any defining or signature symptoms distinguishing the groups, I manually set NCA components to two. The first component was associated with self-reported cognitive difficulties and fatigue, while the second was related to breathlessness and poor sleep. These components helped differentiate the two patient groups, suggesting that the non-hospitalised group experienced slightly worse cognitive difficulties and fatigue but somewhat better breathlessness and sleep quality compared to the hospitalised group, possibly due to its overall younger population. Overall, it was challenging to clearly differentiate the two groups based on these outcomes, indicating no significant bias in symptom-group coupling (e.g., hospitalised patients all have breathlessness while non-hospitalised patients do not).

The results suggest that this patient cohort is relatively homogeneous, with demographic factors not being strongly correlated with specific symptom outcomes, except for perhaps age effect. This supports the rationale for conducting further brain-behaviour analyses by pooling the entire cohort, enabling the association of symptom severity with brain network measures. Specifically, if an association is found between breathlessness severity and the strength of a brain network, it is crucial that this relationship reflects the true severity of

breathlessness, rather than differences between groups. Since breathlessness, for instance, did not significantly differentiate the groups in the NCA, we can be confident that factors such as group allocation, hospitalisation status, age, sex, or the site of data collection are unlikely to significantly influence the results.

Thirdly, to explore how our subjects naturally clustered based on behavioural measures, K-means clustering revealed three groups: "mild symptom and tired," consisting mainly of hospitalised patients; "no symptom but poor function," which included controls and a small number of patients; and "high symptom burden yet functioning well," primarily made up of non-hospitalised patients. Unlike many previous studies with larger, more sophisticated samples and methods [81] [76] [288] [282] [383] [104] [196] [243], my analysis highlighted the critical role of function in distinguishing clusters. This aligns with psychological research, particularly in depression and anxiety, showing that function and symptom levels can load onto distinct factors even within the same questionnaire[58], such as in the SF-36. For example, positive functional items like "carrying out normal activities" may load separately from negative items such as "feeling tired," despite both addressing health. Discrepancies between function and symptom severity (e.g. functioning well despite severe symptoms) are important in predicting recovery trajectories, potentially reflecting resilience factors like self-efficacy and coping strategies.

4.5.4 Stratification of post-COVID patients using non-imaging data

Not all individuals recover from COVID-19 in the same way. Among those who continue to experience symptoms beyond the acute phase, improved stratification of long COVID patients would support the development of more precise interventional, clinical management, and rehabilitation strategies, as evidenced by findings from large-scale studies.([81] [288] [282] [383] [104] [196] [243]).

Attempts to stratify long COVID outcomes solely on behavioural measures have been challenging. Firstly, the behavioural symptoms of COVID-19 have been predominantly descriptive, lacking a unified terminology and emphasis. A review attempted to standardise long COVID into 31 unique clinical features based on the synthesis of 303 articles according to the Human Phenotype Ontology (HPO) standard [81]. The most frequent features include: fatigue, ground-glass opacification (a hazy area on the lung visible on a CT scan), breathlessness, insomnia, decreased diffusion capacity for carbon monoxide (DLCO), difficulty walking, anxiety, depression, and cognitive impairment. This study had adhered to these definitions. Secondly, clustering and conclusions about risk factors associated with different recovery trajectories may be clinically robust only when using a large database, such as the NIH Researching COVID to Enhance Recovery (RECOVER) Initiative (for more information

on RECOVER, visit https://recovercovid.org). From a sample of 5,434,528 patients [288], this initiative identified six clusters encompassing domains of cardiovascular, constitutional, endocrine, ear, nose, and throat (ENT), eye, gastrointestinal, immunology, laboratory, neuropsychiatric, pulmonary, and skin. Risk factors including female sex, obesity, pre-existing comorbidities, and invasive mechanical ventilation were also identified as predictors of worse recovery in COVID-19 patients, as evidenced by the large sample base ([288] [104]).

The current research includes a unique sample of post-COVID patients who also underwent ultra-high resolution MRI scans. This chapter focused on the behavioural data, with no intention of competing with studies using larger datasets, or even smaller ones focusing on similar neuropsychiatric aspects (e.g. [282]). I am aware of the highly biased sampling of the current small dataset and aim to describe this data in order to contextualise it within the broader scope of long COVID phenotyping studies within the behavioural domain.

My clustering approach complements prior research, such as Evans and colleagues (2022 [104]), which identified severity-based clusters, and Reese and colleagues (2023 [288]), whose large-scale study identified six clusters across pulmonary, neuropsychiatric, cardiovascular, pain/fatigue, and multisystem categories. While I did not observe clear symptom-driven clusters, I found a role for fatigue and cognitive impairment in clusters 0 and 2. Other studies, such as Kenny et al. (2022 [196]) and Prabhakaran et al. (2023 [282]), identified more well-defined clusters, including pain, cardiovascular, and neuropsychiatric profiles. These studies highlight the diverse ways in which post-COVID symptoms manifest, with functional outcomes playing a key role in cluster differentiation.

4.5.5 The control group

Due to challenges in recruiting a sufficiently large and well-matched control group, it was anticipated that meaningful comparisons of MRI connectivity profiles might be limited. Consequently, a key aim of this chapter was to utilise the relatively larger behavioural dataset to assess whether the control group is comparable to the patient groups in terms of demographics and post-COVID outcomes, and to inform the design of subsequent analyses.

The control group exhibited a lower, yet still overweight, BMI, a more balanced sex distribution; a lower prevalence of respiratory and cardiac medical history, and relatively lower socioeconomic status. As expected, they reported a lower symptom burden across all post-COVID outcome domains. However, a substantial proportion of controls were classified within a cluster labelled “no symptoms but poor function,” possibly suggesting that this group may not be representative of the broader population unaffected by COVID-19.

These findings underscore the need for caution when making direct comparisons between this control group and the patient cohort. Based on these observations, it is concluded that

future comparisons of brain-behaviour relationships between these groups may lack clinical validity.

4.5.6 Dimension reduction

As previously discussed, the dataset presents analytical constraints due to the large number of features ($f = 150$) relative to the small and heterogeneous sample size ($n = 118$). This situation may impede the identification of significant patterns and clusters in the correlation matrix (heat map) or lead to sporadic clusters, potentially indicating over-fitting. To address this, I first manually examined the heat maps of both the raw items and the subscales to better understand the dataset's underlying structure. My analysis suggested that individual items, rather than subscale summary scores, may capture more nuanced dimensions of behavioural data.

Integrating insights from existing literature [81] [288] [282] [383], I have struck a balance by determining the content and number of domains that encompass critical aspects of long COVID from a clinical perspective, while remaining statistically feasible given the nature of my data structure. For example, constructs such as "pain" and "sleep" were not direct subscales in all of our questionnaires. However, they have been repeatedly identified in large post-COVID clustering studies. I manually selected questions that corresponded to these constructs; for instance, items related to pain from the PHQ-15 were chosen to represent the pain domain. Ultimately, I defined 11 domains: breathlessness, fatigue, negative mood/depression, lack of motivation, stress, anxiety, pain, poor function, poor sleep, objective cognitive impairment measured by cognitive tasks and subjective cognitive impairment measured by self-report (acronyms: breathlessness, fatigue, negative_mood, lack_of_motivation, stress, anxiety, pain, poor_function, poor_sleep, cogimp_obj, cogimp_subj).

The domain-based dimension reduction approach [220] is adapted from strategies used in brain-behaviour CCA. This approach addresses challenges associated with traditional CCA, which typically requires large datasets and can be difficult to interpret due to the purely data-driven nature of its components. For each of the 11 domains, I performed PCA. I then assessed the meaning of each retained PC within its domain and retained those that are potentially distinguishable in the context of brain connectivity.

I observed that the differences among multiple PCs in the motivation, stress, and pain domains are minimal and may not yield meaningful insights when analysed with brain markers. Consequently, I have reduced these domains to their first PCs to avoid unnecessary complexity. The top three PCs in both objective and subjective cognitive impairment domains exhibit interesting loading patterns; however, it is unlikely that these patterns can be

distinguished in large brain networks. Future research should focus on cognition-oriented analyses to capture the data's nuances more effectively.

In summary, the multiple PCs in the motivation, stress, and pain domains show too subtle distinctions to offer significant insights with brain markers, leading me to retain only the first PC for each domain. While the top three PCs in objective and subjective cognitive impairment domains display interesting patterns, their relevance to large brain networks is uncertain. Future research should focus on cognition-oriented analyses for better data understanding. This resulted in 11 PCs in total, with only the first PC for each domain retained.

4.6 Conclusion

This chapter employed extensive data exploration and analytical methods to uncover the underlying structure of a specific cohort of post-COVID patients and controls. The aim was to situate this small sample within the broader post-COVID population, thereby guiding decisions for subsequent analyses. The results indicated significant heterogeneity within the patient group, underscoring variability in symptom presentation and the need to control for the confounding factor of "group". Nevertheless, the findings suggested that post-COVID outcomes, in terms of symptom severity, were sufficiently homogeneous across groups, justifying the use of correlation analyses to investigate the relationship between symptom severity and brain connectivity measures.

The chapter also highlighted the limitations of direct comparisons with the control group due to selection bias, particularly concerning their poorer objective cognitive function and the atypical profile of impaired function in the absence of symptoms. Despite these limitations, 11 domain-based features were identified, which balanced insights from data exploration with the existing literature. This provided a solid foundation for dimensionality reduction and subsequent analysis of brain connectivity.

In response to the fluctuating pandemic conditions, I adopted an opportunistic and flexible recruitment strategy, which enabled the achievement of a well-sized sample. I acknowledge the limitations imposed by the sample size, the small and potentially mismatched control group, and the heterogeneity observed within the patient group. These factors must be carefully considered in the following chapters when linking behavioural data to brain measures. A comprehensive understanding of the dataset, alongside judicious dimensionality reduction, will be essential to ensure robust and interpretable findings.

Chapter 5

Node-based allostatic-interoceptive network and breathlessness post-COVID

5.1 Abstract

An estimated 20% to 50% of individuals suffer from breathlessness post-COVID[136, 47, 55, 156] despite only a small percentage exhibiting measurable pulmonary injury[338, 1, 9, 279, 366], prompting hypotheses regarding alterations in the central nervous system.

In this study, I collected resting-state functional magnetic resonance imaging (rs-fMRI) data at 7 Tesla (7T) ultra-high-field from 53 post-COVID patients, all of whom experienced varying levels of breathlessness despite limited evidence of pulmonary dysfunction. The primary aim was to investigate the specific brain networks underlying this maladaptive and tonic respiratory experience, as hypothesised in the context of interoceptive and allostatic control.

I assessed the predictive ability of 153 resting-state functional connectivity (rs-FC) measures between 18 brain regions of interest and breathlessness outcomes, using robust regression models with false discovery rate correction. Functional decoupling between the dorsal periaqueductal gray and posterior insula (dPAG–PoI1), alongside coupling between the basolateral amygdala and dorsal anterior cingulate cortex (BLA–dACC), was associated with higher breathlessness catastrophizing scores. The contribution of dPAG–PoI1 connectivity to breathlessness remained significant after adjusting for general anxiety scores, acute infection severity, and ventilator use, whereas the effect of BLA–dACC did not. Notably, dPAG–PoI1 exhibited even greater explanatory power for breathlessness in ventilated patients.

Tonic breathlessness may stem from a dual-component neural model: first, reduced integration of afferent visceral signals, potentially resulting from brainstem damage in

severely affected individuals or predisposition to such damage, which impairs the learning of safety signals; and second, an exaggerated efferent anticipatory bias towards adverse respiratory experiences, potentially driven by the psychologically traumatic acute infection phase.

5.2 Introduction

5.2.1 Breathlessness in long-COVID

Breathlessness is a hallmark symptom of post-acute sequelae of SARS-CoV-2 infection (long-COVID), estimated to affect 20% to 50% of patients at 60 to 100 days post-infection [136, 47, 55, 156], and more than half of patients discharged from the ICU at a 90-day follow-up [134].

Patients with long-COVID report breathlessness for periods ranging from months to over a year following the acute phase of infection, regardless of their viral status, as demonstrated in several cohorts [47, 116, 158]. A key feature of long-COVID breathlessness is the frequent mismatch between patients' subjective experiences and objective clinical markers, possibly representing a state of maladaptive breathlessness, as defined in the theoretical framework of Section 1.4 in Chapter 1.

Only a small proportion of patients with more severe COVID-19 infections develop long-term pulmonary sequelae, such as fibrotic interstitial lung disease (ILD) and progressive pulmonary fibrosis [245, 388]. Persistent radiological abnormalities—including ground-glass opacities and fibrotic changes—have been observed in up to 7% of hospitalised patients within 12 months, with a higher prevalence reported among those admitted to intensive care units [338]. Pulmonary embolism, defined as obstruction or blockage in a pulmonary blood vessel, has been reported in 0.9–3.4% of hospitalised patients, with incidence rising as high as 59% in critically ill individuals requiring extracorporeal membrane oxygenation (ECMO) [1, 9, 279, 366].

Recent research using hyperpolarised Xenon Magnetic Resonance Pulmonary Imaging (Xe-MRI), along with normal respiratory investigations (chest imaging and lung function tests), has found no evidence of functional deficits at the alveolar-capillary membrane level as the cause of long-COVID breathlessness (Fraser et al., 2025, in preparation) in long-COVID patients recruited from post-COVID clinics. This absence of identifiable peripheral deficits among less severely infected COVID patients strengthens the rationale for investigating brain-based mechanisms underlying maladaptive breathlessness in long-COVID, making such research both timely and necessary.

Non-hospitalised patients exhibit significantly lower incidences of these complications [244]. While earlier studies raised concerns about possible alveolar-capillary diffusion impairments not detectable via standard CT imaging in both hospitalised [147] and non-hospitalised individuals [148], subsequent investigations involving a larger cohort of non-hospitalised long-COVID patients (N = 217) found no evidence of functional abnormalities at the alveolar-capillary membrane that could explain persistent breathlessness [Fraser et al.]. These findings are consistent with results from a separate study involving 34 patients [235].

5.2.2 The "anxiety hypothesis" for breathlessness

The experience of respiratory distress is traditionally conceptualised within a dualistic "sensory-affective" framework, which distinguishes between the sensory dimension—representing the perceived "intensity" of breathlessness—and the affective dimension, linked to its "unpleasantness" [362]. This model suggests the presence of two distinct neural pathways: one involving the ventroposterior thalamus and sensorimotor cortices, which processes the sensory attributes of breathlessness, and another comprising the mediodorsal thalamus, insula, amygdala, and cingulate cortex, which governs the emotional and affective responses. It has been suggested that affective engagement may modulate or distort how individuals interpret respiratory sensory signals, potentially amplifying the subjective experience of breathlessness.

Psychological constructs such as anxiety, neuroticism, negative affectivity, and catastrophising have been considered factors that exacerbate perceptions of breathlessness [166, 93, 40, 340, 160] and underpin maladaptive breathlessness. In research, anxiety as a general trait has been commonly used to explain clinical outcome of chronic obstructive pulmonary disease (COPD) [188] above and beyond the "bodily" dysfunction. This "anxiety hypothesis" of maladaptive breathlessness forms the foundation of current treatment approaches for patients exhibiting post-COVID breathlessness without pneumonia or presenting with "medically unexplained" conditions. Indeed, pulmonary rehabilitation, a well-established, evidence-based treatment for COPD [237], has been shown to improve patients' well-being without significantly affecting lung function [48], but by reducing negative emotions [363].

However, the link between maladaptive breathlessness and anxiety appears not robust[257]. For instance, trait anxiety has not proven to be a strong predictor of breathlessness responses under experimentally induced respiratory threats such as breath-holding or a carbon dioxide (CO_2) challenge [287, 239, 346], compared to the 'anxiety sensitivity' scores [290]. Further research has demonstrated that 'suffocation fear' is an even stronger predictor of anxious responses and self-reported bodily sensations following breath-holding than anxiety sensitivity

[240]. This list goes on: from the Catastrophizing about Asthma Scale to the Breathlessness Beliefs Questionnaire [79, 78], with more narrowed defined constructs.

Although refining descriptive measures of breathlessness has utility, particularly in providing a quick and simple tool for quantifying the efficacy of rehabilitation treatments [188], it contributes little to our understanding of the mechanisms underlying maladaptive breathlessness, nor does it account for the potential heterogeneity among patients. Additionally, the observation in some individuals that have low trait anxiety and report fear in response to respiratory challenges could simply reflect an adaptive affective inference, rather than a pathological response. Treating such cases based solely on anxiety may not be appropriate.

Here, I contend that the "anxiety hypothesis", which equates maladaptive breathlessness to purely affective breathlessness, oversimplifies the complexity of this condition. Furthermore, neuroimaging data may provide clearer insights into the neural mechanisms associated with maladaptive breathlessness.

5.2.3 Explain breathlessness using Active Inference

As elaborated in the theoretical framework for conceptualising respiratory perception and regulation as the Active Inference of gas-exchange information within a cortical hierarchy (Section 1.4, Chapter 1), this chapter utilises mechanistic evidence, as detailed in the Embodied Predictive Interoception Coding (EPIC) model [27, 199, 384], to examine which brain regions within the cortical hierarchy contribute to the interoceptive experience of breathlessness post-COVID.

This theoretical framework understands the brain as an inferencing organ. It makes predictions by exerting actions to generate sensory evidence that aligns with homeostatic set points and that it engages in perception as a process of hypothesis testing, or as the inverse of a generative model of the "world" it inhabits [126, 311, 27, 310, 125].

The EPIC model proposes that the more differentiated regions of the insula (granular and dysgranular), which receive afferent signals from the brainstem, serve as the primary interoceptive sensory cortex. In contrast, the less differentiated (agranular) anterior cingulate cortex (ACC), which projects predictive signals to the insula, functions as the visceromotor cortex [199]. See more details in Section 1.4.4.

As detailed in Section 1.4.3 of Chapter 1, I propose that post-COVID breathlessness may represent a state of maladaptive breathlessness, characterised by the inability to resolve prediction errors related to gas exchange within the reflex arcs of the brainstem, despite prolonged attempts to minimise them. Notably, I suggest that an affective response is not always a necessary component of this breathless state.

To challenge the "anxiety hypothesis" of breathlessness, I formulated hypotheses suggesting that maladaptive breathlessness is characterised by excessive top-down limbic regulation of the inferential processes underlying respiratory perception. Specifically, I predict heightened connectivity involving the visceromotor cortex, the agranular ACC, and the amygdala. In attempting to falsify the "anxiety hypothesis" of breathlessness, I formulated hypotheses predicting that maladaptive breathlessness is characterised by excessive top-down limbic regulation of the inferential processes involved in respiratory perception. Specifically, the visceromotor cortex, along with the agranular ACC and the amygdala, may exhibit heightened connectivity.

5.2.4 Why resting-state

There are several reasons why resting-state functional MRI (rs-fMRI) data was used instead of implementing tightly controlled task-based paradigms.. First, rs-fMRI offers a more tolerable and accessible approach for post-COVID populations [123, 144, 314], who were often older and had pre-existing medical conditions—particularly relevant during the early phases of our study in 2020. From a respiratory standpoint, employing tasks involving breathing challenges, such as the resistive loading paradigm described in Chapter 2, would have posed feasibility and ethical challenges during the COVID-19 pandemic. Second, rs-fMRI was more practical to deploy under the rapidly evolving pandemic conditions. Given time constraints and limited access to high-field MRI (e.g., 7T), we could not scan a large enough patient cohort using task-based designs, as discussed in the Introduction of Chapter 4. Third, resting-state networks (RSNs) are now widely accepted as reflecting intrinsic patterns of functional connectivity, offering a robust alternative for studies focused on traits such as heritability or enduring vulnerability [97, 137]. Fourth, many functional brain networks identified through task-based fMRI—such as those catalogued in the BrainMap meta-analysis database [211]—can also be reliably detected in rs-fMRI data [323, 326]. Finally, rs-fMRI findings may offer greater translational potential for clinical application, as resting-state data can be more easily acquired across diverse populations, including children, the elderly, and those with psychiatric or neurological conditions [123, 144, 314]. Importantly, while task-based paradigms are useful for probing acute and adaptive brain responses to a genuine respiratory challenges, rs-fMRI may more effectively capture the intrinsic neural vulnerability associated with maladaptive breathlessness—an issue particularly relevant to clinical populations where breathlessness persists in the absence of overt physiological threat.

Despite the prevalent use of large-scale network analyses in resting-state studies (e.g. [325]), and what I have done in the following Chapter 6, this chapter investigates the rs-FC between a set of highly precise brain regions, building on previous literature on the EPIC

model and those found to be relevant to breathlessness (e.g. BLA and periaqueductal grey [PAG]) [114]) and COVID-19 infection (e.g., piriform cortex [89]). This approach leverages recent advancements in interoception and allostasis to not only validate the EPIC model within a realistic patient cohort, but also generate hypotheses for future studies, and identify potential targets for neuromodulatory or pharmacological interventions.

5.2.5 Hypotheses

In this study I used ultra-high field 7 Tesla (7T) functional MRI functional connectivity (FC) data to investigate the neural mechanisms, either as predisposed neurophysiological vulnerability or as COVID infection-induced neural alternations, underlying maladaptive breathlessness post-COVID, based on the recently developed model of the interoceptive network [199]. I hypothesised that:

1. Breathlessness symptom levels post-COVID are strongly correlated with the severity of the acute infection, particularly in cases where symptoms of breathlessness and olfactory loss were present during the acute COVID-19 phase.

2. Consistent to the "anxiety hypothesis" for maladaptive breathlessness, persisting post-COVID breathlessness symptoms are associated with an over-dominance of top-down regulation (prior expectations) within the interoceptive brain network for respiration. This manifests as stronger rs-FC centred on the limbic and prefrontal cortex (PFC) regions, as well as agranular areas of ACC and insula, which focus on prediction, as predicted in the EPIC model.

3. If the "anxiety hypothesis" were the sole mechanism underlying maladaptive breathlessness, persisting post-COVID breathlessness symptoms would be expected to reflect an over-dominance of bottom-up regulation (i.e., prediction errors) within the interoceptive brain network for respiration. This would manifest as stronger resting-state functional connectivity centred on lower-level structures such as the PAG, hypothalamus, and granular regions like the posterior insula, which are primarily involved in processing afferent respiratory signals, as proposed by the EPIC model.

4. These top-down regulation FC markers are linked to negative affectivity, whereas the bottom-up FC markers are not. Introducing the anxiety levels into the model may attenuate or eliminate the association between the top-down FC markers and breathlessness (in hypothesis 2), but not for the bottom-up markers (hypothesis 3).

5. Patients with higher levels of breathlessness may rely more on voluntary motor and proprioceptive input from respiratory muscles due to the effortful nature of breathing. This is reflected by higher FC centred on the primary motor (M1) and somatosensory (S1) cortices.

6. Loss of olfactory sensory input during the acute phase of COVID-19 may alter the interoceptive 'model of the world' concerning gas exchange. This is likely reflected in altered piriform cortex-centred connectivity during the acute infection, particularly in cases where olfactory loss was experienced. These alterations may be associated with respiratory symptoms, as measured by the D-12 and BCS scales, in the post-COVID phase.

5.3 Methods

5.3.1 Subjects

The recruitment followed the same protocols as described in Chapter 4. The study was approved by the North West - Preston Research Ethics Committee. All participants provided informed consent either for the CMORE sub-study, titled 'CMORE-NEURO' (REC reference: 20/NW/0235, IRAS project ID: 282608), or for the BBB-COVID study, titled Brain and Brainstem Basis of Persistent Symptoms in COVID-19 (BBB-COV) (REC reference: 21/NW/0090, IRAS project ID: 297314).

Fifty-three patients (32 or 60% female, age 50 ± 14 y.o., BMI 28 ± 5) with a medical history of COVID-19 (see details in Table 5.1) were recruited in this study and underwent 7T MRI scans at two sites. 1) the Wellcome Centre for Integrative Neuroimaging (WIN, Oxford, UK) scanned twenty hospitalised and subsequently discharged patients and eight non-hospitalised patients who were referred by the Oxford Post-COVID Service at the Churchill Hospital. 2) Cardiff University Brain Research Imaging Centre(CUBRIC, Cardiff, UK) scanned twenty-five non-hospitalised patients who were referred by the Cardiff and Vale University Health Board (Cardiff, UK). Recruitment began with a telephone screening process, aimed at identifying patients who, following referral from a hospital or clinic, were suitable and safe to be scanned at the 7T MRI. All participants received MRI scans at 334 ± 213 days following the acute COVID-19 infection. They completed a series of questionnaires online and performed a cognitive task scheduled within five days of the MRI scan, after consent.

Table 5.1 Demographic Information of Participants

Demographic Variable	Value
Participants	53 patients
Hospitalisation (count, percentage)	19, 36%
Age at consent in years (Mean, SD, range)	$50 \pm 14\,(20-79)$
Gender (female count, percentage)	32, 60%
BMI (Mean, SD, range)	$28 \pm 5\,(18-43)$
WHO clinical progression scale (Mean, SD, range)	$2.4 \pm 2.0\,(0-7)$
FEV1%pred (Mean, SD, range)	$95 \pm 18\,(61-127)$
FVC%pred (Mean, SD, range)	$104 \pm 18\,(61-139)$
FEV1/FVC (Mean, SD, range)	$79 \pm 6\,(64-92)$
Days from infection to scan (Mean, SD, range)	$334 \pm 213\,(125-806)$

5.3.2 Questionnaires

The questionnaires used in this chapter were: Dyspnoea-12 ([379], D-12), The Breathlessness Catastrophising Scale([328], BCS), Generalized Anxiety Disorder 7-item scale([331, 208], GAD-7), and World Health Organization Ordinal Scale for Clinical Improvement ([231], WHO clinical progression scale). Details for all questionnaires can be found in Chapter 4.

5.3.3 Clinical Measures

I retrospectively collected clinical measures reflecting the physiological status during the acute stage using the NHS Electronic Patient Records. These measures included the infection date, acute stage symptoms, severity at discharge (as indicated by the WHO clinical progression scale for hospitalised patients) [231], as well as markers of inflammation, specifically D-dimer and C-reactive protein (CRP). For assessing objective pulmonary impairment, spirometry test results recorded in the NHS Electronic Patient Records were analysed, including forced expiratory volume in one second (FEV1) [71], forced vital capacity (FVC)[71], and their predicted values based on gender, age, height, and ethnicity, according to the Global Lung Function Initiative (GLI-2012) equations. The FEV1/FVC ratio was also calculated[1]

[1]Forced vital capacity (FVC) is the volume of air that can be forcibly exhaled after full inspiration, measured in litres. Forced expiratory volume in one second (FEV1) is the volume of air that can be forcibly exhaled in one second following full inspiration.

5.3.4 Analysis

The MRI scanning sequence, preprocessing steps, and the selection of regions of interest (ROIs) are detailed in Chapter 3. For ease of reference, the list of ROIs is also provided in Table 5.2 to maintain the flow of the text.

No	Region	ROIs	Function	Cortical Lamination
1	subcortical	BLA	N/A	N/A
2		Piriform	N/A	N/A
3		dPAG	N/A	N/A
4		vlPAG	N/A	N/A
5		hypothalamus	N/A	N/A
6	ACC	sgACC	Visceromotor control	Agranular
7		pACC	Visceromotor control	Agranular
8		dACC (aMCC)	Visceromotor control	Agranular
9	Insula	dpIns	Primary interoceptive cortex	Granular
10		dmIns	Primary interoceptive cortex	Dysgranular
11		mvaIns	Visceromotor control	Agranular
12		lvaIns	Sensory integration	Agranular
13		PoI1	Primary interoceptive cortex	Granular
14		PoI2	Primary interoceptive cortex	Granular
15	dmPFC		N/A	N/A
16	vmPFC		N/A	N/A
17	S1		N/A	N/A
18	M1		N/A	N/A

Table 5.2 Information about ROIs identification. Subcortical regions include the basolateral amygdala(BLA), dorsal and ventroateral periaqueductal gray (dPAG and vlPAG) obtained from conditioned breathlessness task, piriform cortex due to its high relevant in COVID outcomes, hypothalamus due to its important role in interoception. The ACC includes its subgenual(sgACC) and pregenual (pACC) sections, and anterior midcingulate cortex (also known as dorsal ACC)as they are considered to be the visceromotor hubs of the cortex. The insula includes the posterior insula (PoI1 and PoI2), the dorsal posterior and dorsal medial (dpIns/dmIns) sections that are hypothesised to be the primary interoceptive sensory cortex, and the ventral anterior section which functions together with the ACC. Finally, the dorsal medial prefrontal cortex (dmPFC), ventral medial prefrontal cortex (vmPFC) comprises the cortical regions of interest.

Functional connectivity (FC) extraction

For each subject, mean time courses were extracted for each ROI within the subject-specific functional Echo-planar imaging (EPI) space, forming a $18 \times 400 \times 53$ matrix (representing ROI number, time points, and subject number, respectively). These ROIs are also known as 'nodes' in neuroimaging. Following quality control procedures of all nodes, functional connectivity (FC), also referred to as 'edges', were computed. These values represent the Pearson correlation coefficients calculated between all pairs of ROIs for each individual, of which every two nodes forms one edge. From these computations, we derived a final matrix of dimensions 53×153, corresponding to the number of subjects and unique edges (153 unique connections), respectively.

Statistics

To evaluate the predictive value of each FC on post-COVID breathlessness outcomes, including D-12 [379] and BCS [328], robust regression models (the Robust Linear Model (`RLM`) function in `statsmodels` library in Python 3.11.6) were employed. These models are particularly advantageous as they provide estimates that are less sensitive to outliers in the data, thereby offering a more reliable analysis in the presence of non-normal error distributions or heteroscedasticity.

In the regression model, D-12/BCS, separately, were set as the dependent variable, while the FCs or edges between different brain regions serves as the explanatory variables. To explore the associations between the D-12/BCS and other clinical and demographic information, including the acute infection severity, the objective lung impairment, MRI-related variables, age, gender, BMI, etc., a preliminary correlational analysis (Spearman correlation for continuous variables and point-biserial correlation for binary categorical variables) was conducted. Those that were not correlated to the D-12/BCS, and contain considerable missing data, were excluded from the final regression models. Eventually, the following confounding variables were retained in the analysis: gender, age, body mass index (BMI), mean framewise displacement (both relative and absolute), the cube root of total intracranial brain volume, and the cube root of total brain volume, including ventricles. All variables were z-scored. Blood pressure was conventionally used as a confounding variable for MRI studies [325], however due to high percentage of missing data and different time points of the measurements in hospitalised and non-hospitalised patients, I did not include it in the model. Site and group (hospitalisation) were also not included in the default regression model for two reasons: first, they were not significantly correlated with the breathlessness outcome measures; second, their inclusion would account for variance that is exactly what our

research questions try to delineate —specifically, the explanatory power of brain connectivity over breathlessness and its relationships to acute severity levels —given that both variables are strongly correlated with severity, the use of mechanical ventilation, and gender.

To evaluate whether general anxiety, as measured by the Generalized Anxiety Disorder 7-item scale (GAD-7[331]; see Chapter 4 for details), could account for the observed FC associations with D-12/BCS, I included GAD-7 scores as a covariate in the default regression model. This analysis tested whether the significant FC associations remained after accounting for general anxiety.

To investigate whether the identified significant FC represents a predisposed neurophysiological vulnerability (e.g., neurotic personality) or a brain network alteration caused by the acute, and potentially psychologically traumatic, COVID-19 experience, I examined the regression function for the significant FC after incorporating clinical covariates from the acute stage of infection. These covariates were carefully selected based on data completeness and their correlation with D-12/BCS, ultimately including the WHO Clinical Progression Scale and the dichotomous use of ventilatory support.

To validate the relevance of group (hospitalised vs. non-hospitalised) and recruitment site, these two covariates were also added to the regression models for the edges of interest.

To address concerns about multiple comparisons, I applied a False Discovery Rate (FDR) control procedure with a threshold of $\alpha = 0.05$. This approach minimised the risk of Type I errors while preserving the ability to detect true effects.

Finally, although some FCs lack direct evidence of connection based on prior human cytoarchitectonic mapping or animal trace-tracking studies within the interoceptive network, I included all 153 FCs in the regression and FDR correction. While this increased the likelihood of Type II errors, it ensured comprehensive coverage of FCs that may be indirectly connected.

5.4 Results

5.4.1 Behavioural data

Chapter 4 provides a comprehensive description of the post-COVID outcome measures, alongside the relevant clinical and demographic data of the current sample.

Spirometry

I wish to investigate the extent to which the respiratory symptoms observed in this sample were a result of neurological factors, as opposed to actual pulmonary impairment. To address

this, I examined the spirometry test results. The available data (N=33) revealed an average FEV1/FVC ratio[2] of 0.79 ± 0.06, as shown in Figure 5.1 and detailed in Table 5.1. The expected FEV1 and FVC values were 98 ± 19 and 103 ± 22, respectively, based on data from N=12 hospitalised patients, also shown in Figure 5.1.

Given the data from patients who underwent spirometry testing—predominantly hospitalised individuals—this sample does not indicate significant pulmonary dysfunction, with possibly the exception of one 76-year-old male who had an FEV1/FVC ratio of 64.4, which was deemed acceptable.

Due to the large amount of missing data, spirometry results were not included as a confounding variable in the final regression models. All patients in our sample were considered to have relatively normal lung function, consistent with the broader long-COVID population as reported in the Xe-MRI study (Fraser et al., 2025, in preparation), and post-COVID pulmonary structural and functional studies in large cohorts[338, 1, 9, 279, 366].

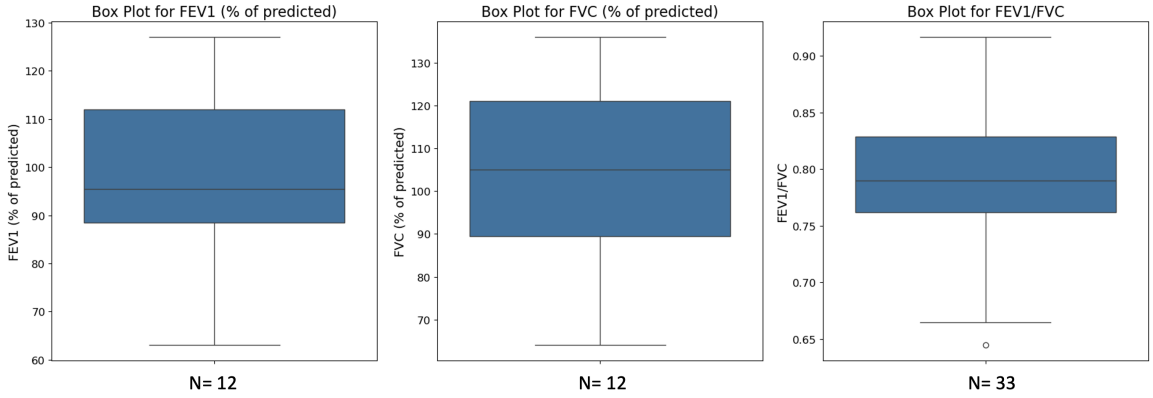


Fig. 5.1 Boxplot of spirometry data showing predicted FEV1, predicted FVC, and the FEV1/FVC ratio.

Information of the D-12, BCS, and GAD-7

Spearman's rank correlation analysis was conducted to assess the relationships among the three measures: D-12, BCS, and GAD-7. As expected, the results revealed significant correlations between all pairs of measures. Specifically, a strong positive correlation was found between D-12 and BCS ($\rho = 0.788$, $p < 0.00001$). A moderate positive correlation was observed between D-12 and GAD-7 ($\rho = 0.337$, $p = 0.014$), and between BCS and GAD-7 ($\rho = 0.391$, $p = 0.004$).

[2]Forced vital capacity (FVC) refers to the volume of air that can be forcibly exhaled after a full inspiration, measured in litres. Forced expiratory volume in one second (FEV1) represents the volume of air forcibly exhaled in the first second following full inspiration.

Hospitalised vs. non-hospitalised for post-COVID outcomes Comparisons of post-COVID outcomes, as well as clinical and demographic information between groups, were conducted in details in Chapter 4. In the current patient sample, the results of the non-parametric Mann-Whitney U test indicated no statistically significant difference between the hospitalised and non-hospitalised groups in terms of D-12 scores ($U = 218.0$, $p = 0.055$) and BCS scores ($U = 242.0$, $p = 0.143$). However, there was a statistically significant difference in GAD-7 scores between the two groups ($U = 199.0$, $p = 0.023$), with the non-hospitalised group exhibiting higher levels of generalized anxiety (median = 5.5) in comparison to the hospitalised group (median = 2.0).

Correlations between post-COVID outcomes and subject information

Contrary to the hypothesis, none of the D-12, BCS, GAD-7 were associated with the severity levels of COVID during the acute stage, qualified by the World Health Organization [231] Ordinal Scale for Clinical Improvement (WHO clinical progression scale), nor the presence of breathlessness and olfactory loss symptoms during acute COVID infection, nor the inflammatory markers of D-dimer and CRP [3].

Further, to provide an overview of the relationships between post-COVID symptom outcomes (D-12, BCS, GAD-7) and demographic and clinical measures during the acute phase of infection, I present data from 53 patients in Figure 5.2 and Table 5.3. Spearman's Rank Correlation Coefficient (Spearman's rho) was employed to assess continuous variables, including age, body mass index (BMI), absolute and relative motion during scanning (motionabs, motionrel), WHO clinical progression scale, systolic and diastolic blood pressure (BPSystolic, BPDiastolic), D-dimer, CRP, days from acute infection to the scan (days_from_acute), and spirometry information, including the FEV1/FVC ratio (spiro_ratio; the ratio of forced expiratory volume in one second to forced vital capacity, indicating airflow limitation), FEV1%pred (the percentage of predicted FEV1 based on reference values for age, sex, and height), FVC%pred (the percentage of predicted forced vital capacity). For categorical variables—such as site (siteCardiff being 1), group (hospitalisation being 1), gender (female being 1), medical history of respiratory or cardiac disorders (resp_MH, card_MH), presence of acute respiratory symptoms (acuteresp), and acute olfactory symptoms (acuteolf)—the Point-Biserial Correlation Coefficient was applied.

[3] It is important to exercise caution when interpreting the inflammatory markers D-dimer and CRP, as well as blood pressure measurements, due to differences in the timing of data collection. For hospitalised patients, these measures were obtained during hospitalisation amidst the acute phase of infection. For non-hospitalized patients, the same measures were recorded around their scan dates. Consequently these measures were not used in further analysis as confounding variables or co-variates.

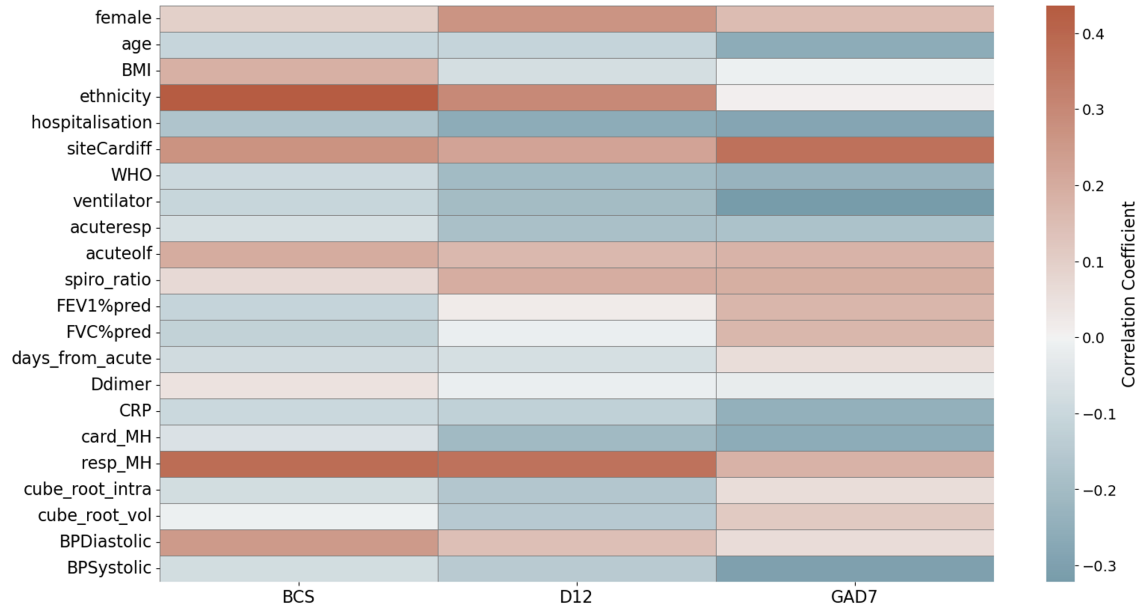


Fig. 5.2 Correlations of demographic and clinical information with D-12, BCS and GAD-7. No significant association after FDR correction for multiple comparison.

The analysis revealed that no demographic or clinical measures were significantly associated with post-COVID outcomes of breathlessness (D-12, BCS) and anxiety (GAD-7) after correction for false discovery rate (FDR) due to multiple comparisons. However, several notable associations were observed, with significance levels close to or at $P < 0.05$ prior to adjustment. Specifically, female gender was associated with higher D-12 scores. A history of respiratory disease and non-Caucasian ethnicity were associated with elevated scores on both the D-12 and BCS. It is important to note that the non-Caucasian ethnicity variable applies to only five participants, of whom two reported a history of respiratory diseases yet exhibited normal FEV1/FVC ratios, and anther two received ventilator support during hospitalisation. Thus, there are no definitive conclusions regarding the COVID-19 outcome characteristics in non-Caucasian individuals, as they represent a special profile of people with basic respiratory disease or high severity of COVID infection. Furthermore, participants from Site 2 (Cardiff, which included only non-hospitalised individuals) and who are non-hospitalised exhibited higher GAD-7 scores. Counter-intuitively, those who received mechanical ventilation during acute infection (indicative of hospitalised individuals scanned at Oxford) displayed lower GAD-7 scores.

It is noteworthy that the highly inter-correlated cluster of variables—site, gender, group (hospitalised or non-hospitalised), ventilator use, and severity—identified in the larger behavioural dataset (as discussed in Section 4.5.2 of Chapter 4) is also evident in this MRI sample, which includes only patients. Specifically, non-hospitalised patients, predominantly

recruited from the Cardiff site, were more likely to be female and exhibited elevated general anxiety levels, despite reporting less severe symptoms during the acute phase of infection.

Crucially, for this chapter, the key breathlessness outcome measures were not associated with site or group, even at unadjusted levels.

Clinical/demo	Outcome	Correlation	P-value	Note	N
female	D12	0.266	0.055	on all data	53
female	BCS	0.098	0.486	on all data	53
female	GAD7	0.154	0.270	on all data	53
age	D12	-0.112	0.425	on all data	53
age	GAD7	-0.261	0.059	on all data	53
age	BCS	-0.111	0.429	on all data	53
BMI	GAD7	-0.009	0.954	on non-missing data	46
BMI	BCS	0.190	0.205	on non-missing data	46
BMI	D12	-0.078	0.605	on non-missing data	46
ethnicity	GAD7	0.010*	0.945	on all data	53
ethnicity	BCS	0.436	0.001	on all data	53
ethnicity	D12	0.298	0.030	on all data	53
hospitalisation	D12	-0.260	0.060	on all data	53
hospitalisation	BCS	-0.173	0.216	on all data	53
hospitalisation	GAD7	-0.286	0.038*	on all data	53
siteCardiff	BCS	0.269	0.051	on all data	53
siteCardiff	GAD7	0.371	0.006*	on all data	53
siteCardiff	D12	0.221	0.112	on all data	53
WHO	GAD7	-0.232	0.095	on all data	53
WHO	D12	-0.204	0.142	on all data	53
WHO	BCS	-0.092	0.512	on all data	53
ventilator	BCS	-0.108	0.501	on non-missing data	41
ventilator	GAD7	-0.321	0.041*	on non-missing data	41
ventilator	D12	-0.200	0.209	on non-missing data	41
acuteresp	BCS	-0.071	0.676	on non-missing data	37
acuteresp	GAD7	-0.178	0.291	on non-missing data	37
acuteresp	D12	-0.185	0.273	on non-missing data	37
acuteolf	GAD7	0.178	0.291	on non-missing data	37

Continued on next page

Table 5.3 Correlation between Post-COVID outcome and Clinical/Demographic Variables

Outcome	Clinical/demo	Correlation	P-value	Note	N
acuteolf	BCS	0.198	0.240	on non-missing data	37
acuteolf	D12	0.167	0.324	on non-missing data	37
spiro_ratio	D12	0.195	0.276	on non-missing data	33
spiro_ratio	BCS	0.072	0.691	on non-missing data	33
spiro_ratio	GAD7	0.191	0.286	on non-missing data	33
FEV1%pred	D12	0.022	0.911	on non-missing data	29
FEV1%pred	BCS	-0.112	0.564	on non-missing data	29
FEV1%pred	GAD7	0.172	0.373	on non-missing data	29
FVC%pred	BCS	-0.122	0.528	on non-missing data	29
FVC%pred	GAD7	0.168	0.384	on non-missing data	29
FVC%pred	D12	-0.014	0.943	on non-missing data	29
days_from_acute	GAD7	0.060	0.713	on non-missing data	40
days_from_acute	D12	-0.076	0.643	on non-missing data	40
days_from_acute	BCS	-0.085	0.601	on non-missing data	40
Ddimer	D12	-0.016	0.927	on non-missing data	37
Ddimer	GAD7	-0.020	0.906	on non-missing data	37
Ddimer	BCS	0.044	0.796	on non-missing data	37
CRP	BCS	-0.101	0.534	on non-missing data	40
CRP	D12	-0.126	0.440	on non-missing data	40
CRP	GAD7	-0.246	0.126	on non-missing data	40
card_MH	D12	-0.207	0.193	on non-missing data	41
card_MH	GAD7	-0.262	0.099	on non-missing data	41
card_MH	BCS	-0.059	0.716	on non-missing data	41
resp_MH	D12	0.364	0.019*	on non-missing data	41
resp_MH	BCS	0.381	0.014*	on non-missing data	41
resp_MH	GAD7	0.183	0.252	on non-missing data	41
cube_root_intra	BCS	-0.081	0.563	on all data	53
cube_root_intra	D12	-0.159	0.256	on all data	53
cube_root_intra	GAD7	0.060	0.669	on all data	53
cube_root_vol	GAD7	0.116	0.406	on all data	53
cube_root_vol	BCS	-0.010	0.945	on all data	53

Continued on next page

Table 5.3 Correlation between Post-COVID outcome and Clinical/Demographic Variables

Outcome	Clinical/demo	Correlation	P-value	Note	N
cube_root_vol	D12	-0.152	0.279	on all data	53
BPDiastolic	D12	0.144	0.369	on non-missing data	41
BPDiastolic	GAD7	0.061	0.707	on non-missing data	41
BPDiastolic	BCS	0.252	0.113	on non-missing data	41
BPSystolic	D12	-0.147	0.358	on non-missing data	41
BPSystolic	GAD7	-0.298	0.059	on non-missing data	41
BPSystolic	BCS	-0.081	0.614	on non-missing data	41

Table 5.3 Correlation between Post-COVID outcome and Clinical/Demographic Variables. I applied Spearman correlation for continuous variables and point-biserial correlation for binary categorical variables. Uncorrected significant P-values ($P < 0.05$) are marked with an asterisk (*). acuteresp—respiratory symptoms during acute infection/hospitalization; acuteolf—olfactory symptoms during acute infection/hospitalization; ventilator—ventilator use during acute infection; respMH—history of respiratory disease (asthma, COPD); cardMH—history of cardiac disease (e.g., hypertension); motionabs/motionrel—absolute/relative mean framewise displacement; brainvol—cube-root of total brain volume (including ventricles); intravol—cube-root of total intracranial volume; WHO - WHO clinical progression scale; BPSystolic/BPDiastolic—blood pressure; D-dimer—highest D-dimer level (during admission or clinic visit); CRP—highest C-reactive protein level (during admission or clinic visit); daysfromacute—days from infection to scan/questionnaire; Spirometry Ratio—FEV1/FVC ratio.

5.4.2 Interoceptive networks and D-12

The univariate robust regression coefficients for each of the 153 edges, regressed on the BCS scores while controlling for potential confounding variables—such as age, gender, BMI, head motion parameters (both relative and absolute), cube-root brain volume (including CSF), and cube-root intracranial volume—are presented in the heatmap in Figure 5.4.

In examining the relationship between the edges (X) and D-12 scores (y), our univariate robust regression analysis found no statistically significant results after FDR correction, controlling for potential confounding variables of age, gender, BMI, head motion parameters (both relative and absolute), cube-root brain volume (including CSF), and cube-root intracranial volume. The top 10 edges with the highest regression coefficients and their unadjusted P-value are shown in Table 5.4. Heatmap of regression coefficients for all edges (nodes pairs) on which D-12 was regressed is shown in Figure 5.3.

Edge	Coefficient	P-value
dpIns_dmIns	4.35	0.0139
vlPAG_dpIns	4.08	0.1069
dPAG_PoI1	-3.72	0.0157
BLA_dACC	3.70	0.0445
Hyp_M1	-3.49	0.0069
dPAG_dpIns	3.49	0.1637
BLA_mvaIns	3.35	0.0279
dPAG_lvaIns	-3.21	0.0468
pACC_dpIns	-3.12	0.1575
dPAG_PoI2	-3.10	0.0848

Table 5.4 Top ten edges with the highest coefficients where D-12 was regressed. No edges were found to be significant after FDR correction. dpIns—dorsal posterior insula; dmIns—dorsal medial insula; vlPAG—ventrolateral periaqueductal gray; dPAG—dorsal periaqueductal gray; BLA—basolateral amygdala; PoI1, PoI2—posterior insula (sections 1 and 2); dACC—dorsal anterior cingulate cortex; sgACC—subgenual anterior cingulate cortex; pACC—pregenual anterior cingulate cortex; lvaIns—lateral ventral anterior insula; M1—primary motor cortex.

Although not withstanding FDR correction, I observed a trend of positive association with D-12 in edges centering regions that were hypothesised to conduct top-down viscero-motor control and negative association in edges centering regions in bottom-up 'primary interoceptive cortex'. In specific, intra-dorsal insula connectivity between dorsal posterior Insula (dpIns) and dorsal medial Insula (dmIns), and basolateral amygdala (BLA)'s connectivity with visceromotor control regions such as medial ventral anterior insula (mvaIns) and dorsal anterior cingulate (dACC), appeared to be positively associated with D-12. Negative links with D-12 were found in FC between (dPAG) and primary interoceptive cortex such as posterior insula (PoI1) and lateral ventral anterior insula (lvaIns), or between the the hypothalamus (Hyp) and the primary Motor Cortex (M1). No prominent edges centering cortical regions such as vmFFC, dmPFC, S1, and majority sub-regions of ACC are shown, even counting in the unadjusted results.

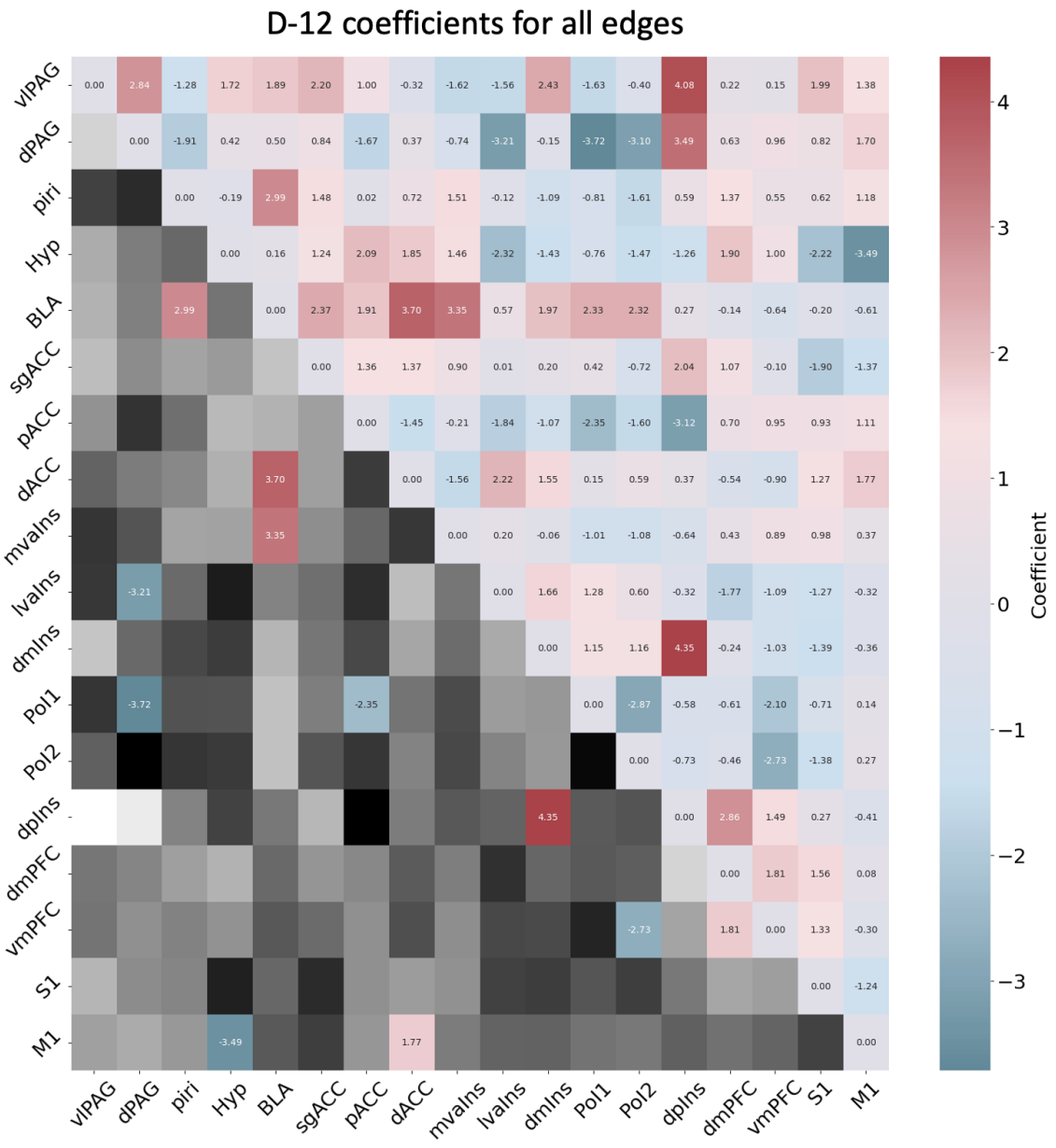


Fig. 5.3 Heatmap of D-12 regression coefficients for all edges. Each cell represents a univariate robust regression coefficient obtained by regressing D-12 on the FC(or edge) between the two ROIs (or nodes) from x and y axis. The upper triangle displays all coefficients, while only coefficients with an unadjusted P-value < 0.05 are shown in colour in the lower triangle. Brain nodes are organized by region: subcortical areas, ACC, insula, and cortical regions. No FC remained significant after false discovery rate (FDR) correction. Please refer to Table 5.2 for the details of all ROIs acronyms.

5.4.3 Interoceptive networks and BCS

The univariate robust regression coefficients for each of the 153 edges (X), regressed on the BCS scores (y) while controlling for the same set of confounding variables of D-12 are presented in the heatmap in Figure 5.4. Following correction for multiple comparisons using the FDR, two edges remained significant: the coupling between the basolateral amygdala and the dorsal anterior cingulate cortex (BLA-dACC), and the decoupling between the dorsal periaqueductal grey and the posterior insular cortex (dPAG-PoI1). The top ten edges exhibiting the highest absolute regression coefficients, along with their unadjusted p-values, are shown in Table 5.5.

Similar to the findings for D-12, connectivity within the intra-dorsal insula (dpIns-dmIns) and functional connectivity in regions related to visceromotor control, such as BLA, dACC, sgACC, and vlPAG (BLA-dACC, vlPAG-sgACC), displayed a positive correlation with BCS scores. In contrast, functional connectivity involving the primary interoceptive cortex, including the dPAG and posterior insular regions (PoI1/PoI2) (dPAG-PoI1/PoI2), as well as the sensory integration area (lvaIns) (dPAG-lvaIns), demonstrated a negative correlation with BCS scores, although these findings were not statistically significant following FDR correction.

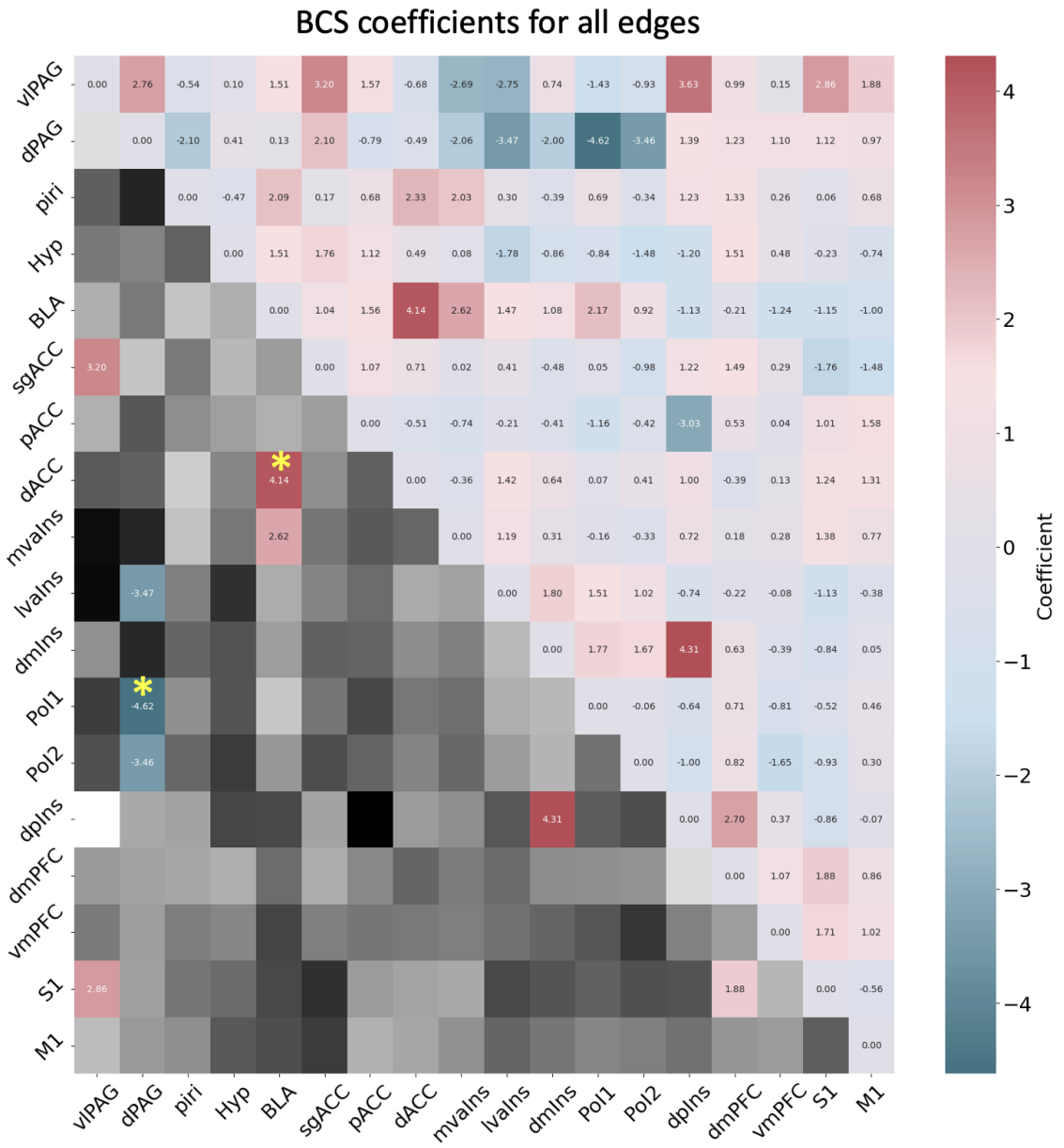


Fig. 5.4 Heatmap of BCS regression coefficients for all edges. Each cell represents a univariate robust regression coefficient obtained by regressing D-12 on the FC(or edge) between the two ROIs (or nodes) from x and y axis. The upper triangle displays all coefficients, while only coefficients with an unadjusted P-value < 0.05 are shown in colour in the lower triangle. Brain nodes are organized by region: subcortical areas, ACC, insula, and cortical regions. Statistically significant edges, specifically the dPAG–PoI1 and BLA–dACC, are marked with an asterisk (*) to indicate significance after false discovery rate (FDR) correction. Please refer to Table 5.2 for the details of all ROIs acronyms.

Edge	Coefficient	P-value
dPAG_PoI1	-4.62	0.0001*
dpIns_dmIns	4.31	0.0048
BLA_dACC	4.14	0.0005*
vlPAG_dpIns	3.63	0.0833
dPAG_lvaIns	-3.47	0.0179
dPAG_PoI2	-3.46	0.0110
vlPAG_sgACC	3.20	0.0465
pACC_dpIns	-3.03	0.0870
vlPAG_S1	2.86	0.0458
dPAG_vlPAG	2.76	0.0758

Table 5.5 Top ten edges with the highest coefficients where BCS is regressed. The functional connectivity (FC) between dPAG_PoI1 and BLA_dACC remained significant after FDR correction, showing a negative and positive association with BCS scores, respectively. These edges are marked with an asterisk (*) next to the corresponding p-values. dPAG—dorsal periaqueductal gray; PoI1, PoI2—posterior insula (sections 1 and 2); dpIns—dorsal posterior insula; dmIns—dorsal medial insula; BLA—basolateral amygdala; dACC—dorsal anterior cingulate cortex; vlPAG—ventrolateral periaqueductal gray; lvaIns—lateral ventral anterior insula; sgACC—subgenual anterior cingulate cortex; pACC—pregenual anterior cingulate cortex; S1—primary somatosensory cortex.

dPAG-PoI1 decoupling in predicting BCS

The dPAG-PoI1 connectivity exhibited a significant negative association with BCS scores, with a coefficient of -4.62 (95% CI: $[-6.88, -2.36]$, $p = 0.000062$), after controlling for confounding variable and applying FDR correction. As displayed in Figure 5.5, the distribution of hospitalised and non-hospitalised patients was balanced, showing no clustering along the regression line.

To validate the robustness of our model and mitigate the risk of overfitting, such as biases arising from participant selection, I conducted an ad-hoc 5-fold cross-validation (CV) with 10,000 permutations for this particular edge, as illustrated in the lower plane in Figure 5.5. This method involves randomly splitting the dataset into five subsets, training the model on four subsets while testing it on the remaining one, and repeating this process for all possible combinations of the subsets. This approach allowed us to compute the average coefficient of the robust regression model across the folds, which, combined with the permutation tests, provided a mean coefficient of -4.45 ($p = 0.003$), confirming the significance of the results.

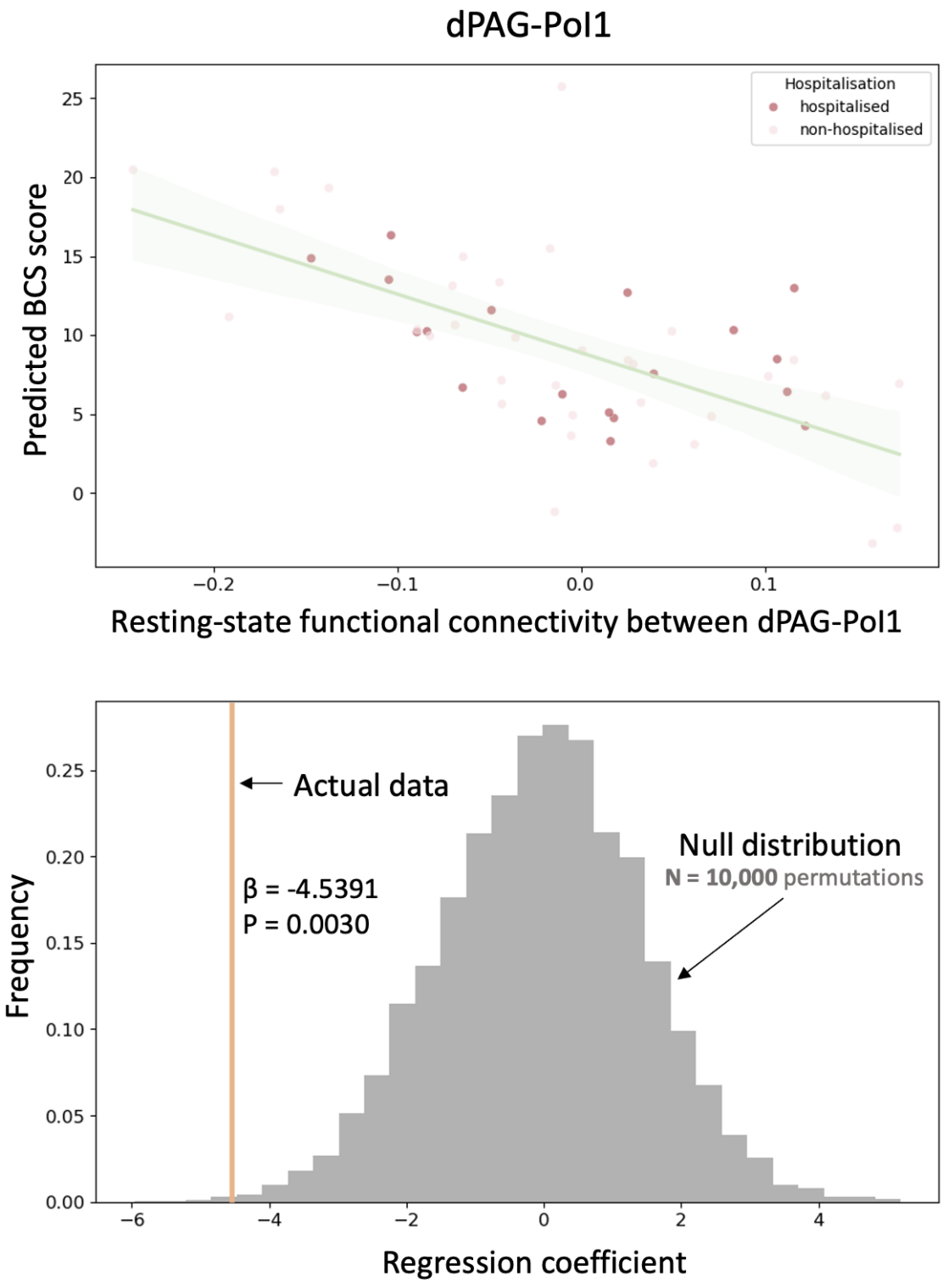


Fig. 5.5 Scatterplot and 5-fold cross-validation test for regressing dPAG-PoI1 FC on BCS. The scatterplot on the top plane represents the predicted BCS scores (y-axis) using the regression model with the FC between dPAG and PoI1 as the predictor (x-axis), while controlling for age, gender, BMI, motion parameters, and brain volume parameters. Hospitalisation profile of each individuals are highlighted in two shades of red. The green regression line represents the estimated relation between the FC and predicted BCS scores, with the shaded region indicating the 95% confidence interval for this fit. The bottom panel displays the ad-hoc permutation test with 5-fold cross-validation, with the observed coefficient value and P value highlighted in the null distribution.

Further, as shown in Figure 5.6, the negative association between dPAG-PoI1 connectivity and BCS scores remained both significant and stronger upon adjusting for anxiety levels (GAD-7), as shown by partial correlation analysis: $\beta = -5.69$, $p = 1.047 \times 10^{-7}$, 95% CI: $[-7.80, -3.60]$. Likewise, after adjusting for acute-phase severity using the WHO Clinical Progression Scale, the association remained robust ($\beta = -4.62$, $p = 0.00008$, 95% CI: $[-6.92, -2.33]$) and significant following FDR correction. These findings indicate that the predictive value of dPAG-PoI1 decoupling for BCS scores is above and beyond the contributions of anxiety or levels of acute COVID-19 severity.

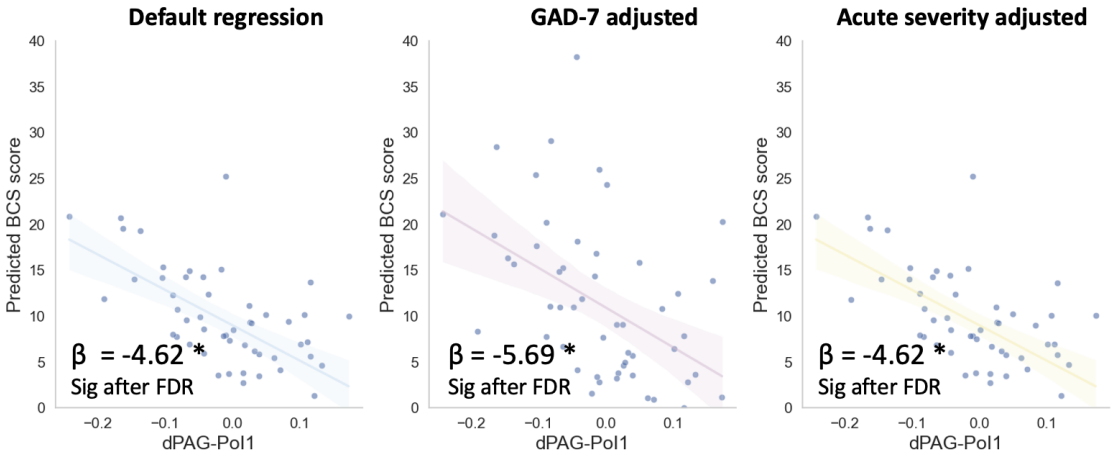


Fig. 5.6 Scatterplot of dPAG-PoI1 regression on BCS adjusted for anxiety or severity. The three scatterplots represent the predicted BCS score at y-axis by dPAG-PoI1 connectivity at x-axis, adjusted for default demographic and MRI scan-related confounding variables (left), or with an additional covariate of GAD-7 (middle), or with an additional covariate of severity levels at the acute infection phase (WHO Clinical Progression Scale) (right). The β value, significance information (with an asterisk *) after FDR correction, and a regression line with a 95% confidence interval, indicated by the shaded region, are displayed on top of each scatterplot.

Finally, as shown in Figure 5.7, the binary variable of 'ventilator use' during the acute phase was also tested within the model, which included an interaction term for ventilator use $\times$ dPAG-PoI1. Fourteen out of the 53 participants in the current sample experienced mechanical ventilation during hospitalisation. The main effect of dPAG-PoI1 connectivity on BCS scores, representing the degree to which changes in dPAG-PoI1 connectivity predict BCS outcomes in the no-ventilator subgroup, was significant ($\beta = -3.29$, $p = 0.002$). Additionally, the interaction term, ventilator use $\times$ dPAG-PoI1, was significant ($\beta = -7.24$, $p = 0.0048$), indicating that, for patients who underwent mechanical ventilation during the

acute phase, the increase in BCS associated with greater dPAG-PoI1 decoupling was more pronounced. [4].

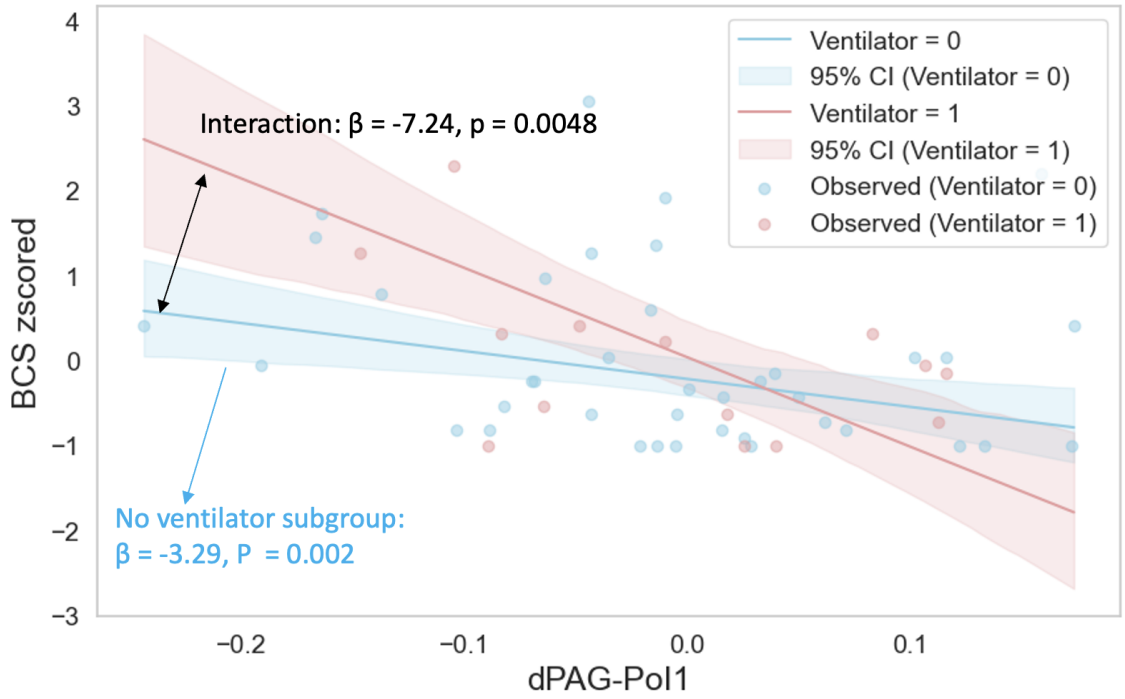


Fig. 5.7 Effect of ventilator use during the acute phase on the regression of dPAG-PoI1 on BCS. This figure displays two regression lines for the ventilator (red) and no-ventilator (blue) subgroups, with shaded regions representing the 95% confidence intervals. The scatterplot shows dPAG-PoI1 FC values on the x-axis and z-scored BCS scores on the y-axis. For the no-ventilator group, the slope of the regression line equals the coefficient of dPAG_PoI1. For the ventilator group, the slope (-10.53, not shown in the figure) reflects the combined coefficients of dPAG_PoI1 and the interaction term, as the interaction term equals dPAG_PoI1 when ventilator use is present.

BLA-dACC coupling in predicting BCS

The BLA-dACC connectivity showed a significant positive association with BCS scores, with a coefficient of 4.14 (95% CI: $[1.81, 6.47]$, $p = 0.000508$) after controlling for confounding variables and applying FDR correction (see Figure 5.8). The distribution of hospitalised

[4]The main effect for the ventilator group alone is not of primary interest and is underpowered with only 14 subjects. However, the coefficient for the 'ventilator = 1' group is calculated by combining the main effect and the interaction term: -10.53 for dPAG-PoI1 and 4.77 for BLA-dACC. These values are also shown as the slopes of the red regression lines in Figure 5.7 and Figure 5.10. For the ventilator group, the slope reflects the combined influence of both dPAG_PoI1 and the interaction term, since the interaction term equals dPAG_PoI1 when ventilator use is present. For the calculation: when ventilator =1, the interaction term becomes equal to dPAG-PoI1, modifying the main effect by adding the value of interaction coefficient to dPAG-PoI1's coefficient.

and non-hospitalised patients was relatively uniform, with no visible clustering along the regression line. An ad-hoc permutation test using 5-fold cross-validation was also performed, yielding a mean coefficient of 4.02 ($p = 0.001$), further supporting the robustness of these findings, as illustrated in the lower panel of Figure 5.8.

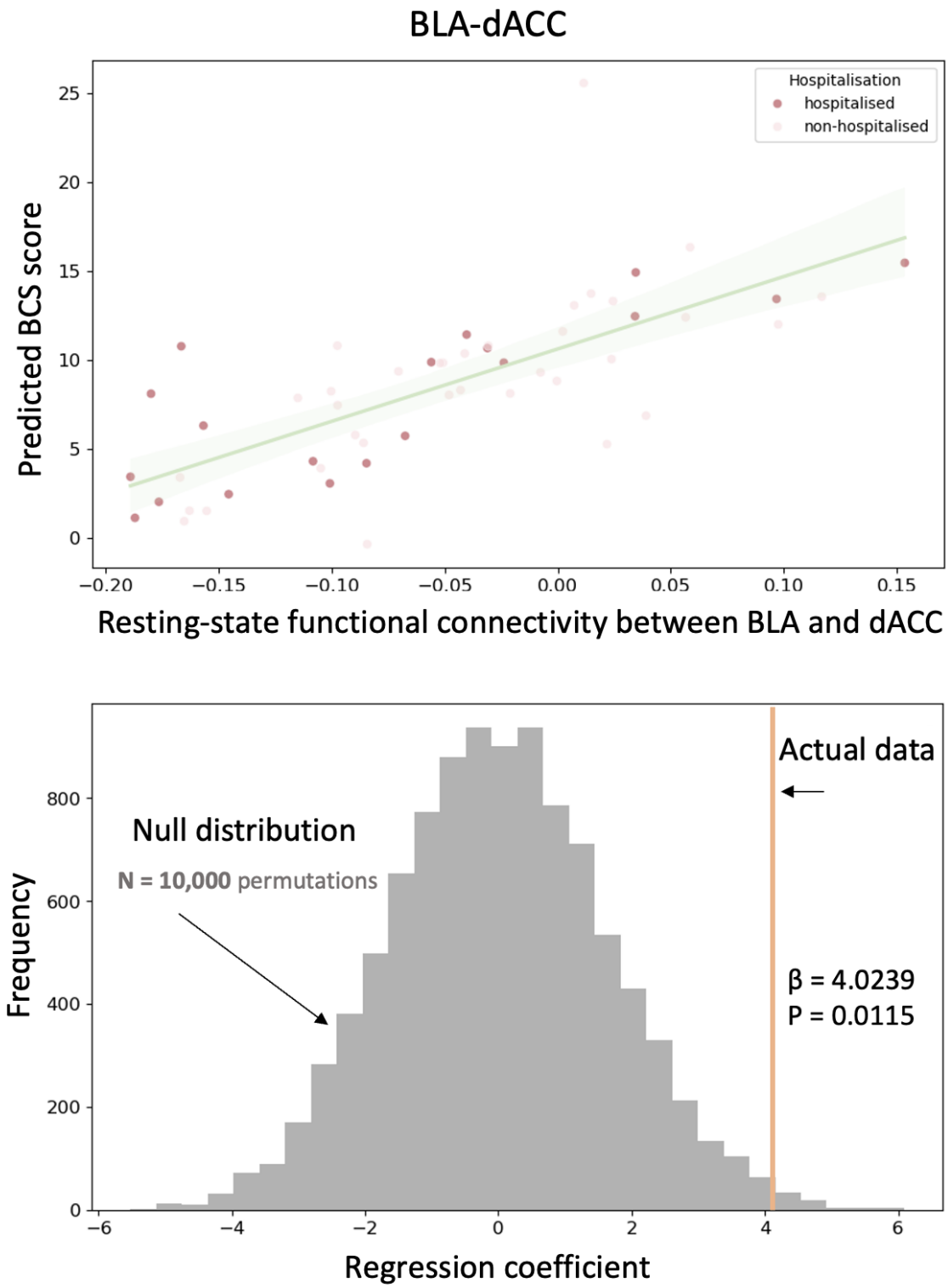


Fig. 5.8 Scatterplot and 5-fold cross-validation test for regressing BLA-dACC FC on BCS. The scatterplot on the top plane represents the predicted BCS scores (y-axis) using the regression model with BLA_dACC as the predictor (x-axis), while controlling for age, gender, BMI, motion parameters, and brain volume parameters. Hospitalisation profiles of each individual are highlighted in two shades of red. The green regression line represents the estimated relationship between the FC and predicted BCS scores, with the shaded region indicating the 95% confidence interval for this fit. The bottom panel displays the ad-hoc permutation test with 5-fold cross-validation, with the observed coefficient value and *p*-value highlighted in the null distribution.

However, when GAD-7 or the WHO Clinical Progression Scale was included as a covariate, the previously observed positive association between BLA-dACC connectivity and BCS scores diminished to a non-significant level after false discovery rate (FDR) correction: $\beta = 3.99$; $p = 0.00715$, 95% CI: $[1.08, 6.90]$ for GAD-7, and $\beta = 4.14$; $p = 0.0009$, 95% CI: $[1.70, 6.58]$ for the WHO Clinical Progression Scale, as shown in Figure 5.9. Caution is warranted, as the β values remain relatively high, and their non-significant results may be attributed to the multiple comparison correction process.

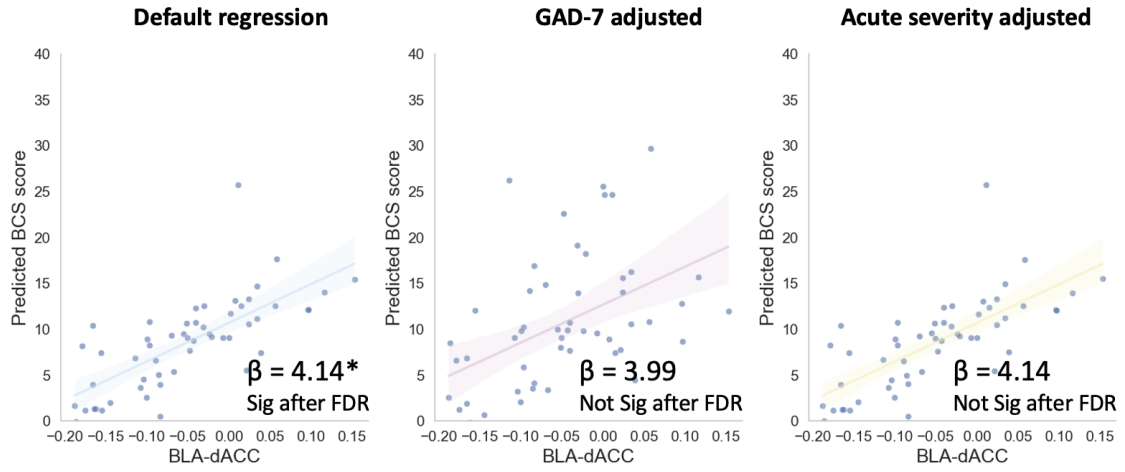


Fig. 5.9 Scatterplot of BLA-dACC regression on BCS adjusted for anxiety or severity. The three scatterplots represent the predicted BCS score at y-axis by BLA-dACC connectivity at x-axis, adjusted for default demographic and MRI scan-related confounding variables (left), or with an additional covariate of GAD-7 (middle), or with an additional covariate of severity levels at the acute infection phase (WHO Clinical Progression Scale) (right). The β value, significance information (with an asterisk *) after FDR correction, and a regression line with a 95% confidence interval, indicated by the shaded region, are displayed on top of each scatterplot.

Moreover, as shown in Figure 5.10, the association between BLA-dACC connectivity and BCS scores was completely attenuated when ventilator use was taken into account, rendering it statistically insignificant ($\beta = 2.94$; $p = 0.11$). This finding indicates that the BLA-dACC connectivity, when ventilator use equals zero, is not significantly associated with BCS scores. In other words, the relationship between BLA-dACC and BCS was not observed in individuals who had no experience of mechenical ventilation. Notably and in contrast, the main effect for dPAG-PoI1 was significant ($\beta = -3.29$; $p = 0.002$), although not surviving FDR correction. Furthermore, The interaction term between BLA-dACC and ventilator use was not significant: $\beta = 1.82$; $p = 0.51$, which also contrasts that of dPAG-PoI1.

These findings suggest that, in contrast to the dPAG–PoI1 pathway, the association between BLA–dACC connectivity and BCS was not evident among individuals who did not receive mechanical ventilation during the acute phase. Moreover, the predictive value of BLA–dACC connectivity for BCS outcomes may be limited, as it appears sensitive to covariates such as GAD-7 scores, acute illness severity as indexed by the Clinical Progression Scale, and ventilator use. These variables may share overlapping variance with BLA–dACC connectivity, potentially reflecting a common underlying construct related to affective or interoceptive processing.

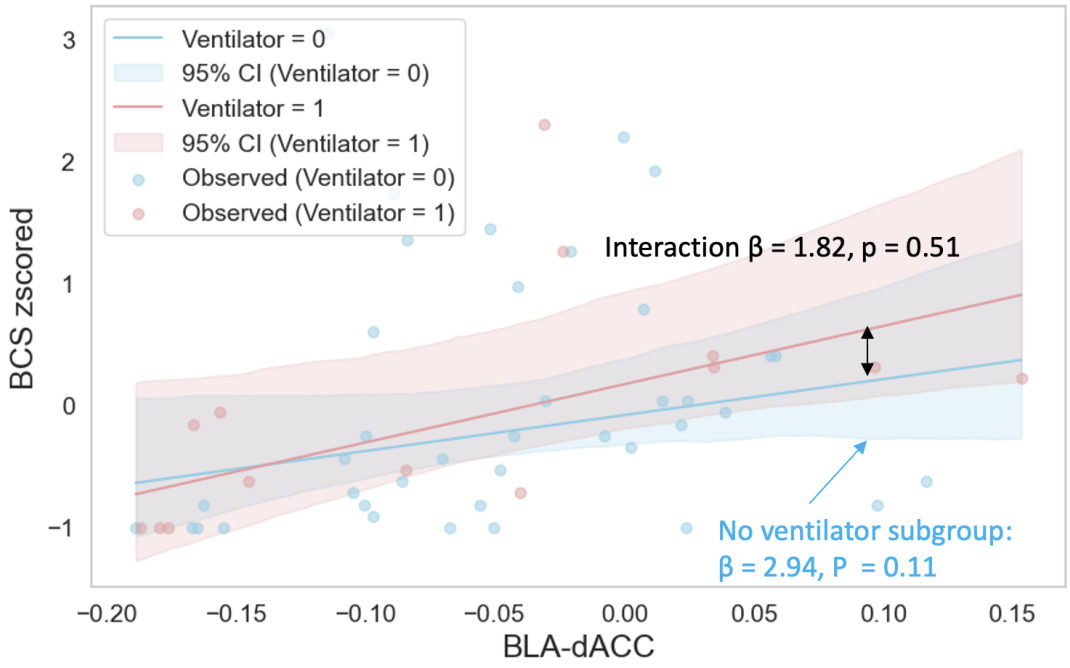


Fig. 5.10 Effect of ventilator use during the acute phase on the regression of BLA-dACC on BCS. This figure displays two regression lines for the ventilator (red) and no-ventilator (blue) subgroups, with shaded regions representing the 95% confidence intervals. The scatterplot shows BLA-dACC FC values on the x-axis and z-scored BCS scores on the y-axis. For the no-ventilator group, the slope of the regression line equals the coefficient of BLA-dACC. For the ventilator group, the slope (4.77, not shown in the figure) reflects the combined coefficients of BLA-dACC and the interaction term, as the interaction term equals BLA-dACC when ventilator use is present.

Additional examination of site and group effect

The association between dPAG-PoI1 de-coupling and BLA-dACC coupling with BCS scores remained significant with FDR correction after controlling for the 'Group' (hospitalised

vs. non-hospitalised) variable. Specifically, for dPAG-PoI1, the coefficient was $B = -4.62$, $p = 0.00008$, 95% CI: $[-6.92, -2.33]$. For BLA-dACC, the coefficient was $B = 4.18$, $p = 0.00048$, 95% CI: $[1.83, 6.52]$.

Regarding the effect of 'Site', only the association with dPAG-PoI1 remained significant: $B = -4.38$, $p = 0.00031$, 95% CI: $[-6.75, -2.00]$. The association with BLA-dACC, however, fell out of significance after FDR correction: $B = 3.97$, $p = 0.0014$, 95% CI: $[1.54, 6.40]$.

5.4.4 Role of piriform cortex

Finally, using the subsample with the spirometry rate data serving as an additional confounding variable, the relationship seem to be independent of the functioning of the lung. No significant functional connectivity was found associating with the piriform cortex when regressing on D-12 or BCS.

5.5 Discussion

5.5.1 Main findings

I investigated the rs-FC between 18 a-priori defined ROIs underlying interoceptive and allostatic processing of respiration to understand the puzzling discordant breathlessness experienced in post-COVID patients with limited evidence of long-term pulmonary damage. Our findings supported, and extended the "anxiety hypothesis" of maladaptive breathlessness. There was an increased coupling between the basolateral amygdala (BLA) and dorsal anterior cingulate cortex (dACC), indicating an intensified top-down limbic influence on interoceptive processes, corresponding to perception of greater burden of breathlessness symptoms. Additionally, I identified a distinct neural pathway involving possibly diminished bottom-up visceral signal integration, reflected in the decoupling of the dorsal periaqueductal grey (dPAG) and the posterior insula (PoI1), which was also associated with increased breathlessness. Further analysis showed that BLA-dACC connectivity's explanatory power for breathlessness depended on acute-phase severity and possibly general anxiety, and was absent in those who had not undergone ventilatory support. In contrast, dPAG-PoI1 connectivity appeared independent of general anxiety or acute-phase severity, retaining significance in patients who had not required mechanical ventilation.

At the beginning of the Chapter, I formulated five hypotheses based on the "anxiety hypothesis" for maladaptive breathlessness. I will discuss the findings accordingly.

5.5.2 Hypothesis 1

As predicted, the primary breathlessness behavioural outcomes (D-12, BCS, and GAD-7) exhibited strong correlations. However, none were associated with acute-stage severity, the presence of respiratory or olfactory symptoms during the acute infection, or inflammatory markers. There is limited evidence to suggest objective pulmonary dysfunction across all individuals for whom data were available[5]. This suggests that, at the behavioural level, breathlessness may not be a direct consequence of the clinical profile associated with acute COVID-19 infection; rather, it may reflect a result of the interactions between pre-existing or COVID-induced neurophysiological factors and the COVID-19 experience.

5.5.3 Hypothesis 2

In line with my hypothesis regarding affective top-down influences, I observed that rs-FC between the BLA and dACC correlates positively with self-reported breathlessness in post-COVID individuals.

The 4mm-sphere BLA seed was identified from the peak deactivation loci observed during both the anticipation and perception phases of a conditioned breathlessness challenge in healthy volunteers (see Chapter 2). As part of the amygdalar complex, the BLA is richly interconnected with higher-order cortical areas and maintains bidirectional connections with affective and evaluative prefrontal circuits. These connections are thought to underpin the expression of conditioned fear toward respiratory threats [214].

Notably, BLA connectivity with the mediodorsal thalamus increased during the breathlessness challenge, possibly reflecting a process of perceptual inference. In this process, cognitive and affective states are updated in response to novel or salient stimuli. The breathlessness task, detailed in Chapter 2, may partially simulate the acute infection phase, during which a genuine respiratory threat—such as reduced breathing capacity or mechanical ventilation (see Hypothesis 4)—disrupts typical respiratory models.

Importantly, animal studies suggest that the BLA is not typically involved in the regulation of reflexive breathing; this function is more closely associated with the centromedial amygdala that projects to the lower-level autonomous regulatory structures in the brainstem [385, 131]. The involvement of the BLA in post-COVID breathlessness may therefore reflect a maladaptive activation of affective pathways, whereby a "vigilant style" of respiratory inferencing—potentially established during the acute phase—persists even after the immediate threat has resolved. This sustained hypervigilance may lead to top-down inferences, such as entrenched beliefs about compromised respiratory function, overriding bottom-up sensory

[5] except for one 76-year-old male with an FEV1/FVC ratio of 64.4, which I considered acceptable

input, despite the absence of a genuine respiratory threat. Such a mechanism may underlie the persistent experience of breathlessness reported by individuals following COVID-19 infection.

The dACC, also referred to as the anterior midcingulate cortex (aMCC), is an agranular region implicated in interoception, motor functions, and attention. It acts as a "rich club" hub, interconnecting with frontoparietal, temporal, motor, and subcortical structures, including the amygdala and periaqueductal grey (PAG) [361]. Due to its high centrality, the dACC has been proposed to participate in multiple intrinsic large-scale networks, such as the salience network, allostatic-interoceptive networks, the frontoparietal network, and the ventral attention network [350].

The dACC consistently appears in fMRI studies investigating breathlessness, pain, and thirst, underscoring its role as an "alarm" centre signalling survival threats [219], or as a visceromotor cortex involved in allostasis [199]. It is also known to activate in anticipation of noxious stimuli [361], resembling the role of the BLA described in Chapter 2. In the EPIC model, the dACC is identified as a primary visceromotor cortical region responsible for regulating the body's internal milieu [199].

The agranular dACC serves as a key hub for visceromotor control, functioning alongside the broader ACC, which encompasses the subgenual (sgACC) and pregenual (pACC) regions, as well as the medial ventroanterior insula (mvaIns). Notably, a general trend of increased coupling between the BLA and the mvaIns, sgACC, and pACC was observed in association with higher D-12 and BCS scores. However, these associations did not reach significance after correction for multiple comparisons using the FDR.

Both the dACC and amygdala are key nodes within the salience network, with connectivity between these regions well-documented to correlate with trait anxiety [143]. In the post-COVID context, heightened BLA–dACC FC may reflect an affectively driven, top-down prediction of breathlessness. Within a predictive coding framework, this increased connectivity could signify an amplified influence of prior beliefs or expectations about breathlessness—beliefs likely reinforced by affective states or previous experiences of respiratory discomfort. Such top-down predictions may bias interoceptive perception, intensifying the subjective sensation of breathlessness. Specifically, the dACC is hypothesised to receive affective and salience signals from the BLA, modulating the perception of threat akin to that experienced during the acute infection phase. By integrating this information across broader networks involved in allostasis, interoception, attention, and salience, the dACC may perpetuate the experience of breathlessness, even in the absence of any actual pulmonary dysfunction.

Overall, this finding aligns with recent efforts to apply the Bayesian theoretical framework to breathlessness [357, 112, 229], which interpret maladaptive breathlessness as an over-reliance on the brain's priors in shaping the perception of breathing.

5.5.4 Hypothesis 3

Contrary to our third hypothesis based on the "anxiety hypothesis", I found that the bottom-up FC marker—decoupling between PoI1 (the posterior insula, ventral region) and the dPAG—predicts breathlessness scores. Specifically, BCS remained significant after FDR correction, while D-12 was significant without adjustment. This finding underscores the importance of the lower-order, phylogenetically older interoceptive sensory cortex, which is not reflecting higher-order affective factors.

The posterior insula comprises more differentiated granular regions that primarily receive interoceptive signals concerning the body's internal state. It may serve as the site where predictions (efferent copies from the ACC) are compared with interoceptive afferents, which are transmitted via the vagus nerve and small-diameter C and Aδ fibres from the brainstem through the thalamus [68]. This region is distinct from the anterior portion of the insula, which represents a more evolutionarily conserved system responsible for the physiological regulation of bodily functions, such as respiration, energy balance, temperature regulation, hunger, thirst, pain, and sensory homeostasis.

Evidence regarding the role of the dPAG in respiratory function and perception is limited. A human fMRI study revealed that the dPAG[6] is deactivated during the anticipation of breathlessness [114] and is functionally connected to the posterior insula at rest. In animal studies, direct stimulation of the dPAG induces tachypnoea (rapid breathing), along with excitation of both late inspiratory (late-I) and post-inspiratory (post-I) medullary neurons, which are believed to regulate the transition from inspiration to expiration [250, 297]. However, evidence supporting the involvement of the dPAG in the sensory aspects of respiration (such as the transmission of afferent signals) is scarce.

In post-COVID individuals, greater decoupling between the dPAG and PoI1 may indicate hypo-recruitment in the integration of interoceptive respiratory signals. This could lead to a more ambiguous representation of afferents if the dPAG also plays a role in respiratory sensory processing. Alternatively, the uptake of respiratory signals in the posterior insula might be less effectively translated into action to modulate respiration (as if 'body forgot to

[6] In the original paper, the seed of the peak activation during anticipation of resistive inspiration load in the PAG was labelled as 'lPAG'. However, it is located within the dPAG mask used in this chapter. See Figure 3.1 for details.

breath automatically'), particularly during the transition between inspiration and expiration, in individuals experiencing maladaptive breathlessness after COVID-19.

Together, maladaptive breathlessness could result from an inability to integrate visceral respiratory signals and update the predictive model of gas exchange in the body, which may be interpreted as a failure of safety signal learning following COVID-19.

5.5.5 Hypothesis 4

To address the fourth hypothesis, I found that the association between dACC (aMCC)-BLA coupling and breathlessness scores diminished when general anxiety scores (GAD-7) or severity scores during the acute phase were included in the model. However, the dPAG-PoI1 decoupling explained variance in breathlessness above and beyond anxiety and severity scores.

Moreover, among participants who did not require mechanical ventilation during the acute phase, dPAG-PoI1 FC remained associated with breathlessness, whereas BLA-dACC coupling did not. FC between dPAG and PoI1 exhibited a significant interaction with ventilator use in predicting breathlessness scores, with those who received mechanical ventilation reporting even higher breathlessness.

These findings further support the view that top-down dACC (aMCC)-BLA coupling is closely related to affective states, potentially reflecting the lasting impact of psychologically traumatic hospitalisation experiences. In contrast, dPAG-PoI1 connectivity may represent a pre-existing neurological factor that also interacts with experiences during the acute infection. In fact, The BLA and dACC coupling may function as a domain-general neurophysiological marker that is not specific to respiratory perception - potentially extending to other conditions like pain. Additionally, we can infer that the heightened dACC-BLA coupling in individuals experiencing more severe post-COVID breathlessness may be attributable to psychologically traumatic experiences during the acute infection phase. Factors such as the WHO clinical progression scale and the use of ventilators at the acute infection phase could account for this effect. Indeed, compelling evidence indicates that approximately one in five individuals with long COVID develops post-traumatic stress disorder (PTSD), anxiety disorders, or depression [194, 49, 50, 105]. Overall, hyper-recruitment of top-down regulatory processes during respiratory inference may manifest as increased dACC-BLA coupling, which, while linked to COVID-19 infection, may not be exclusive to respiratory function.

The underlying reasons for weaker FC between the dPAG and PoI1 in the nervous system remain unclear. However, findings regarding the interaction between dPAG–PoI1 FC and ventilator use provide a potential direction for further investigation. Specifically, the observation that dPAG–PoI1 FC is predictive of breathlessness symptom levels among individuals who

did not require ventilator support may suggest that this connectivity represents a pre-existing neurological factor. In addition, the significant interaction effect, whereby ventilated patients exhibit even higher predictability to the breathlessness symptom levels post-COVID, could indicate pathological changes in the brainstem among the most severely affected patients, as reported in recent work by Rua and colleagues [295].

Together, I propose that post-COVID maladaptive breathlessness may be a result of two neural pathway alterations. One pathway is characterised by increased dACC-BLA coupling (top-down regulation) - along with the wider network within the visceromotor structures[199], which may reflect alterations in the affective salience network stemming from the psychologically traumatic experience of acute infection. The second pathway involves greater dPAG-PoI1 decoupling (bottom-up regulation) - along with the wider network within the primary interoceptive regions[199], possibly indicating a pre-existing neurological vulnerability or brainstem damage in most severe patients[295]. It may relate to impaired signal integration and respiratory control model updating. The hyperconnectivity within the visceromotor regions and hypoconnectivity within the primary interoceptive areas may prevent the organism from returning to effortless, reflexive breathing, despite having well-functioning lungs. Notably, the explanatory power of dPAG-PoI1 decoupling for post-COVID breathlessness intensified when general anxiety was added as a covariate, supporting this interpretation. However, caution is warranted before drawing definitive conclusions, as the effect size remains high with a significant P-value prior to adjustment.

5.5.6 Hypothesis 5, 6, 7

Regarding the fifty hypothesis, which posited that patients experiencing higher levels of breathlessness may rely more on voluntary motor and proprioceptive input from the respiratory muscles was not supported by our current analysis. No significant connectivity was observed between the M1 or S1 seeds and any of the nodes defined within the interoceptive network.

Regarding the sixth and final hypothesis concerning the involvement of the olfactory system in respiratory alterations, I did not observe any significant functional connectivity (FC) related to the piriform cortex, despite findings in the large longitudinal study by Douaud et al. [89], which demonstrated structural changes in the olfactory system using UK Biobank data. One possible explanation for this discrepancy is the low signal-to-noise ratio typically associated with the piriform cortex. As a result, the grey matter loss reported in the piriform cortex of post-COVID patients [89] may not be reflected in our functional connectivity analysis.

5.5.7 Limitations

1. The univariate method used in this study was constrained by the strict multiple comparison correction, which limited its effectiveness. Attempts to apply multivariate methods, including support vector machines (SVM), linear discriminant analysis (LDA), and random forest models with leave-one-out cross-validation (LOOCV), demonstrated no predictive power across the entire network (153 edges), with prediction accuracy for the test samples falling below 50%. This highlights the potential need for the development of more sophisticated analytical methods.

2. The absence of out-of-sample validation limited the external validity of the findings. While an attempt was made to validate the results by dividing the sample evenly into two subsets, this approach yielded inconsistent and sporadic outcomes.

3. The localisation of regions of interest (ROIs), particularly the smaller regions defined by 4 mm spheres, may have suffered from poor correspondence across subjects. This issue likely contributed to the suboptimal performance of multivariate methods in fitting the models.

4. Some significant edges, particularly the dPAG-PoI1 connection, displayed very low mean correlations. This raises concerns that the significant regression coefficients could be driven by outliers, despite the application of robust statistical methods to mitigate such effects.

5. The variable 'site' was not included as a confounding variable in the analysis. The Oxford site primarily comprised hospitalised patients, who were more severely affected during the acute stage of COVID-19 and predominantly male. In contrast, the Cardiff site consisted entirely of non-hospitalised patients, who were predominantly female. As gender and acute COVID-19 severity were variables of interest for the hypotheses tested in this chapter, 'site' was excluded as a confounding variable of no interest. However, this decision may have introduced site-related noise into the data.

5.6 Conclusion

This chapter has proposed a dual-component neural model to explain the development and persistence of maladaptive breathlessness in post-COVID patients. The model encompasses the following components:

1. A predisposed neurophysiological vulnerability, exacerbated by ventilation or brainstem injury, is independent of severity but becomes more pronounced in the most severe cases requiring ventilation. It is characterised by hypoactivity in safety signal learning due

to impaired integration of visceral inputs, irrespective of anxiety scores. This vulnerability manifests as the decoupling of the dPAG and PoI1.

2. Acute COVID-19-induced neurological alterations, linked to the severity of the infection and varying with general anxiety scores post-COVID. These changes may intensify anticipatory inferencing, thereby enhancing the perception of breathlessness through catastrophic interpretations. This is evident in the coupling of BLA and dACC.

Both the dACC (also referred to as the anterior midcingulate cortex, aMCC)[80, 236] and the dPAG [386](in animal) have been utilised as targets for neuromodulation or pharmacological interventions. Future advancements in the management of post-COVID conditions should consider distinguishing between predisposing factors and COVID-induced subtypes in patients suffering from breathlessness. This differentiation could enable the development of more precise and personalised treatment strategies.

Chapter 6

Large brain networks underlying post-COVID symptom clusters

6.1 Abstract

This study explores potential neurophysiological phenotypes in post-COVID patients using a multivariate approach to link imaging and non-imaging data from 53 patients 334 ± 213 days days after the infection. Brain connectome measures (BM) were derived from ultra-high-resolution 7-Tesla resting-state functional magnetic resonance imaging (rs-fMRI), consisting of 19 features obtained through voxel-based group ICA and PCA dimensionality reduction. Non-imaging symptom and behavioural measures (SM) included 11 features reduced from 137 questionnaire items and 13 cognitive test results, as detailed in Chapter 4, covering breathlessness, fatigue, negative mood, lack of motivation, anxiety, stress, pain, poor function, poor sleep, objective cognitive impairment, and subjective cognitive impairment.

I identified the top three modes with the highest canonical correlations, despite the overfitting inherent in the model. These modes were: a "Stress and Anxiety" phenotype characterised by sensorimotor integration and associative network decoupling, a "Pain and Breathlessness" phenotype with thalamus/brainstem-vision coupling, and an "Anxiety and Breathlessness Mood" phenotype marked by DNM de-integration.

This study highlights the potential of multivariate analysis to identify distinct post-COVID neurophysiological phenotypes, reflecting the complex and multidimensional nature of post-COVID experiences. Furthermore, it emphasises the critical need for large sample sizes per feature to ensure robust and stable results.

6.2 Introduction

6.2.1 Multiple intrinsic brain networks underlying breathlessness

In Chapters 2 and 5, I examined predefined regions of interest (ROIs) and their networks associated with the amygdala and allostatic-interoceptive (allo-intero) networks during breathlessness. It is noteworthy that no evidence supports a single intrinsic network exclusively dedicated to the allo-intero processes, as identified through data-driven approaches. Instead, these processes engage multiple networks [199] that underpin various functions, including emotion, memory, attention, and cognition [311, 27, 70], as well.

The findings from Chapters 2 and 5 supports the importance of orchestration among multiple intrinsic brain networks during breathlessness. Specifically, the "rich club" hubs, namely the precuneus and the dorsal anterior cingulate cortex (dACC), were identified as playing critical roles in explaining the burden of breathlessness and respiratory perception during a resistive breathing task through their connections with the basolateral amygdala. These "rich club" hubs are linked to various intrinsic networks, such as the Default Mode Network (DMN), Salience Network (SN), the limbic system, Fronto-Parietal (Cognitive Control) Network, and the Motor and Premotor Networks, facilitating the integration of emotion, cognition, and action [358]. What gives rise to breathlessness, possibly markers associating with coordination between DMN, SN, and limbic networks, through these 'rich club' hubs, may also contribute to the development of other neurophysiological conditions.

The post-COVID cohort presents a unique opportunity to investigate diverse neurophysiological manifestations potentially arising from a common cause: a period of deviation from normal physiological processes during the acute phase of infection. Long COVID patients exhibit heterogeneous symptom clusters, as highlighted in the literature [81] [76] [288] [282] [383] [104] [196] [243]. In Chapter 4, K-means clustering identified three sub-groups based solely on behavioural data: a "mild symptoms and tired" cluster, consisting primarily of hospitalised patients; a "no symptoms but poor function" cluster, comprising mostly healthy controls and a small number of patients; and a "high symptom burden yet functioning well" cluster, predominantly made up of non-hospitalised patients. This variability points to the possible existence of distinct neurophysiological phenotypes among post-COVID patients, with differing symptom profiles and functional capacities potentially shaped by specific alterations in intrinsic brain networks. For instance, the chronic need to engage in effortful breathing and confront fear-related emotions associated with tonic breathlessness may represent a metabolically taxing state(due to constant non-reflexive breathing), further contributing to perceptions of fatigue, depression, and cognitive disruptions [27].

6.2.2 Functional brain evidence post-COVID

Despite a growing body of evidence implicating the central nervous system (CNS) in the pathophysiology of COVID-19 and its long-term sequelae, research has predominantly focused on structural changes [253, 89, 205, 388, 223]. Understanding of functional brain alterations remains limited. A recent review by Nasir and colleagues [254] summarised all resting-state functional magnetic resonance imaging (rs-fMRI) studies conducted on acute COVID and post-COVID to date. Most studies involve hospitalised patients, with a primary focus on the acute phase (particularly olfactory-related functions) or follow-up periods of up to six months post-infection, with few exceptions [56, 364, 347]. The long-term impact on individuals who experienced either mild or severe symptoms during the acute phase of infection, yet developed significant symptom burdens even 1–2 years later, as documented in long COVID clinics across the UK, remains poorly understood.

Overall, intrinsic brain networks function as interconnected systems that integrate sensory, cognitive, and emotional information. This interconnectedness underscores the complexity of long COVID's impact on the brain, emphasising the need for comprehensive, network-level investigations to understand and address its multisystemic effects. To date, no study has comprehensively utilised functional brain imaging alongside multidimensional behavioural data to investigate neurophysiological phenotypes in long COVID.

6.2.3 Research approach and objectives

This chapter focuses on developing methods to explore whether individual differences in long COVID, as reflected in variations in symptom severity or types, are linked to distinct connectivity patterns in large scale brain networks. To achieve this, canonical-correlation analysis (CCA) was chosen as the analytical framework for integrating imaging and non-imaging data. CCA is a powerful multivariate technique that identifies and quantifies relationships between two sets of variables, making it well-suited for linking brain-derived functional connectivity measures (BMs) and subject symptom and behavioural measures(SMs).

The 11 SMs of breathlessness, fatigue, negative mood, lack of motivation, stress, anxiety, pain, poor function, poor sleep, objective cognitive impairment, and subjective cognitive impairment were derived through domain-based dimension reduction (DDR [220]), which were outlined in details in Chapter 4. BMs are the connectome data obtained from whole brain voxel-based analyses detailed in Chapter 3, which captured large-scale networks in a data-driven manner without reliance on predefined ROIs.

CCA analysis between them enables the identification of shared patterns or latent dimensions that reflect interactions between neuroimaging and clinical/behavioural variables,

facilitating the characterisation of neurophysiological subtypes (phenotypes). This approach enhances our understanding of long COVID and informs the development of targeted therapeutic strategies.

6.3 Methods

6.3.1 Participants

Participant recruitment adhered to the protocols outlined in Chapter 4. Ethical approval was granted by the North West - Preston Research Ethics Committee. All participants provided informed consent for either the CMORE substudy, titled *CMORE-NEURO* (REC reference: 20/NW/0235, IRAS project ID: 282608), or the *Brain and Brainstem Basis of Persistent Symptoms in COVID-19* (BBB-COV) study (REC reference: 21/NW/0090, IRAS project ID: 297314).

As detailed in Chapter 5 as well, the study involved 53 post-COVID-19 patients (32 females, 60%; mean age: 50 ± 14 years; BMI: 28 ± 5). This cohort included 20 hospitalised and 33 non-hospitalised individuals. All participants underwent 7T MRI scans at one of the two sites: (1) the Wellcome Centre for Integrative Neuroimaging (WIN, Oxford, UK), which scanned 28 patients (20 hospitalised, 8 non-hospitalised), and (2) Cardiff University Brain Research Imaging Centre (CUBRIC, Cardiff, UK), which scanned 25 non-hospitalised patients.

Eligibility for 7T MRI was determined via telephone screening to ensure participants met safety and suitability criteria. MRI scans were conducted 334 ± 213 days days post-acute COVID-19. Within five days of scanning, participants completed online questionnaires and cognitive tasks after providing informed consent. Details of the questionnaires, tasks, and the demographic and clinical profiles of the full cohort (N=118) were provided in Chapter 4. Specific clinical and demographic information for the subset of patients (N=53) who underwent imaging is detailed in Chapter 5.

6.3.2 Analysis

The MRI scanning sequence, preprocessing steps, and the group ICA parcellation are detailed in Chapter 3.

Image processing utilised routines from the FMRIB Software Library (FSL) v6.0.7.6, Python 3.11.6, Advanced Normalization Tools (ANTs) v2.2.0, and the Statistical Parametric Mapping library (SPM12) v7219.

Participant measures of post-COVID-19 outcomes, derived from questionnaires and cognitive tasks, are referred to as 'SM', while brain-derived rs-fMRI connectivity measures are termed 'BMs'. Acknowledging the limitations posed by the small sample size for multivariate analysis and the exploratory nature of the method development in this chapter, I employed aggressive dimension reduction for both SM and BM (i.e. variance kept around 50%). The dimension reduction processes and the integrated multivariate analysis using CCA to jointly analyse the SMs and BMs sets are summarised in the following sections.

SMs - 11 behavioural features

As described in Chapter 4, DDR [220] was applied to post-COVID behavioural outcomes using Principal Component Analysis (PCA) within each predefined SM domain.

DDR is an optimised pipeline designed for linking high-dimensional behavioural and brain-based data (e.g. CCA as used by Smith and colleagues [325]), which not only enhances the interpretability of results but also mitigates overfitting in the context of a low observation-to-feature ratio (i.e., small sample sizes). The decision-making process regarding the 11 domains involved both raw data and subscale explorations, detailed comprehensively in Chapter 4.

The resulting 11 domains in SMs are: breathlessness, fatigue, negative mood/depression, lack of motivation, stress, anxiety, pain, poor function, poor sleep, objective cognitive impairment measured by cognitive tasks and subjective cognitive impairment measured by self-report (acronyms: breathlessness, fatigue, negative_mood, lack_of_motivation, stress, anxiety, pain, poor_function, poor_sleep, cogimp_obj, cogimp_subj). This resulted in a SM matrix of 53 x 11 to enter CCA, representing 53 patients and their 11 SMs.

BMs - 19 functional connectome features

As detailed in Chapter 3, data preprocessing, the group ICA parcellation and the subject-specific node time series (dual regression stage 1) were obtained. After Group ICA of the dimensionality of 15, 25, 50, 100 were run, separately, I got the resulting 15-100 nodes' time series of 400 time points for each of the 53 subject. I arbitrarily chose the 100 dimensionality of the Group ICA result (53 patients x 100 nodes' time series) for the subsequent analysis, following analysis plan of Smith and colleagues[325].

Network matrices for individual subjects and group averages Prior to further analysis, 38 out of 100 nodes from the Group ICA parcellation were identified as "bad nodes", representing group-level noise components after single-subject ICA and physiological data

denoising. This left us with 62 "good nodes" for analysis. Using the time series of these 62 nodes, network matrices (also referred to as netmats or parcellated Connectomes) were constructed. They represents connectivity estimates for each subject (53 patients $\times$ 62 nodes $\times$ 62 nodes).

Network modelling was performed using the FSLNets toolbox (http://fsl.fmrib.ox.ac.uk/fsl/fslwiki/FSLNets). The connectivities were based on computation of partial temporal correlations between nodes' time series for each subject. Partial correlation, as opposed to full correlation, better captures connection strengths [230]. As the network matrices are symmetric, only values from one side of the diagonal were retained, resulting in 1891 unique edges ($62 \times 61/2$). One edge refers to the functional connectivity (FC) between a node (the 'map' obtained from Group ICA representing one brain region) pair. Netmat values were transformed from Pearson correlation coefficients (r-values) into z-statistics using Fisher's transformation. Group-average partial and full correlation matrices were computed by averaging z-statistic Netmats across all subjects.

For visualisation of the results of group ICA with 100 dimensions (62 good nodes), I presented a group-average full correlation matrix for the 62 nodes, using hierarchical clustering for illustration.

To prepare the data for further analysis, the 53 $\times$ 53 $\times$ 62 subject-level network matrices were flattened into a matrix of dimensions 53 subjects $\times$ 1891 edges. (The initial size was 53 $\times$ 2809, but replicated edges were irrelevant for PCA.) PCA was then applied to this matrix, retaining 19 principal components (PCs) that cumulatively explained 50% of the variance across all edges.

Together, these steps resulted in a BM matrix of 53 x 19 to enter CCA, representing 53 patients and their 19 BMs.

Canonical Correlation Analysis (CCA)

To link imaging (BM/netmat/edges matrix/Connectomes) and non-imaging(SM/COVID outcomes/
11 dimensions) data within a single multivariate framework, I employed CCA [180, 325]. CCA is a statistical technique that identifies pairs of canonical variates, which are linear combinations of variables from two datasets, and maximises the correlation between them. This analysis reveals the primary modes of co-variation between the datasets, highlighting the strongest associations.

As described by [220], "For column vectors X and Y, CCA finds two sets of linear combinations P = XA and Q = YB that are maximally correlated. P and Q are the canonical

variables, and A and B are the canonical weights for X and Y, respectively. The correlation between P and Q is termed the canonical correlation, R."

These modes represent patterns of abnormality in post-COVID patients, linking SM to BM features, and could be understood as neurophysiological subtypes.

Confounding variables prior to enter into CCA, potential confounding variables that could influence the brain–behaviour relationship were regressed out from both SMs and BMs, separately. These included gender, age, BMI, motion metrics (mean framewise displacement, relative and absolute), and intracranial volume (cube root of total brain volume, including ventricles). Decisions regarding these confounding variables were based on Smith and colleagues [325]'s study on a large cohort using CCA and the characteristics of the current cohort, as detailed in Chapter 4.

6.4 Results

6.4.1 Summary of SMs before CCA

Pearson correlations between the 11 SMs entered into the CCA model are shown in Figure 6.1, following hierarchical clustering. Although all measures were flipped so that higher scores represent worse outcomes (e.g. poorer function or increased anxiety), not all measures are positively correlated. Function, stress, and metabolically related symptoms, such as fatigue and sleep, tend to cluster together, while bodily symptoms (breathlessness, pain) and psychological aspects form a separate cluster. Cognitive impairment, as measured by self-report questionnaires, clusters with other psychophysiological measures, while the cognitive task results show weaker correlations.

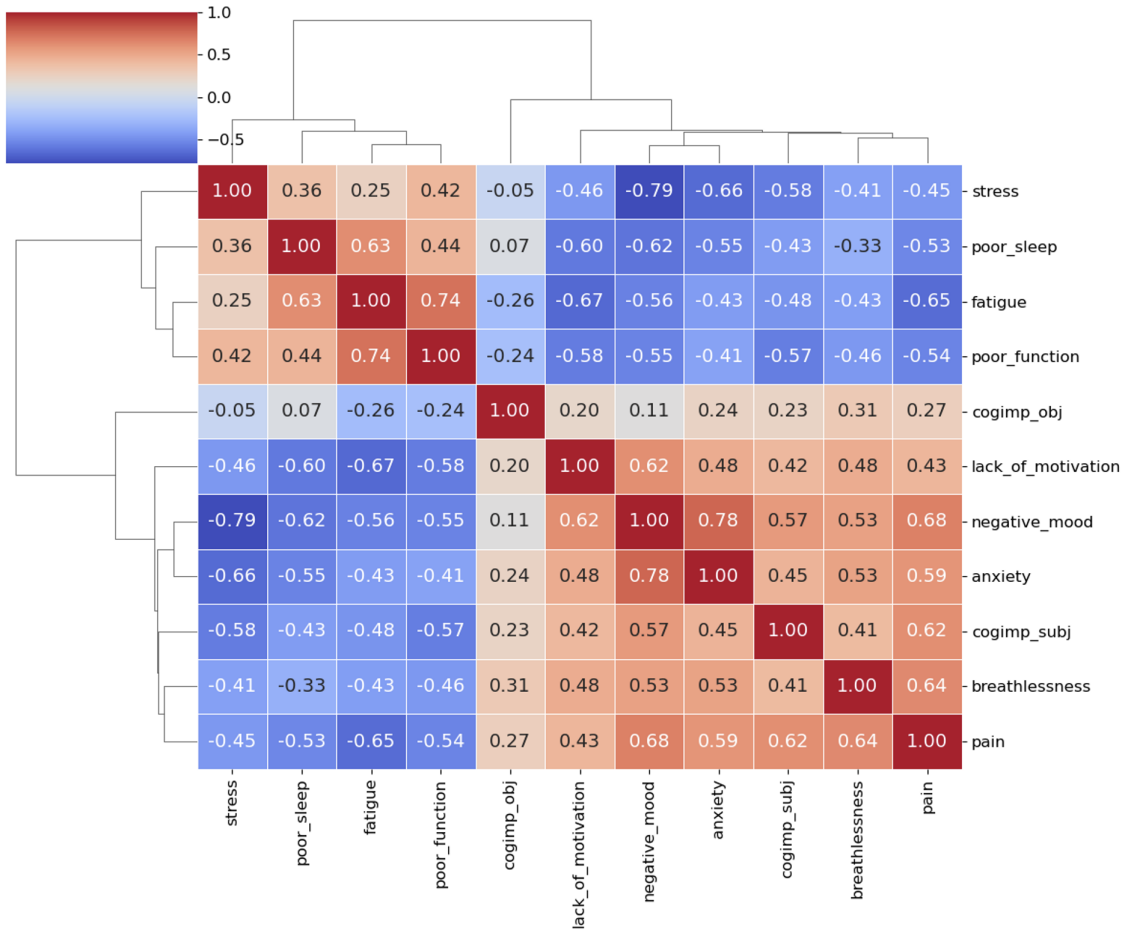


Fig. 6.1 Clustered heatmap of 11 SMs

6.4.2 Summary of BMs before CCA

For illustrative purposes, the group-average Connectomes for the 62 "good nodes" containing signals from the Group ICA with 100 components are presented in Figure 6.2, and similarly in Figure 6.3.

Three major networks are clearly identifiable in the top plane of Figure 6.2:

1. the DMN;
2. the vision and thalamus network.
3. the SN and ventral attention network (VAN), collectively referred to as the "task-positive" network;

These networks can be viewed at a lower hierarchy in the clustermap, as shown in the bottom plane of Figure 6.2. The DMN is divided into three sub-networks with different

focuses: the frontal pole and lateral regions, the medial frontal cortex and posterior cingulate cortex, and the brainstem and cerebellum (indicated by yellow labels 1, 2, and 3). The vision and thalamus network remains segregated from the rest of the brain and stands alone (yellow label 4) at this level. The 'task-positive' network is separated into the sensorimotor network (yellow label 5) and the attentional network (yellow label 6).

Together, this demonstrates that Group ICA performs effectively, even with a smaller sample size, moderate temporal resolution (N=400 time points), and ultra-high resolution functional data at 1.5 mm. Notably, it might have captured additional nuances beyond the two large networks (DMN and task-positive) in findings of Smith and colleagues [325].

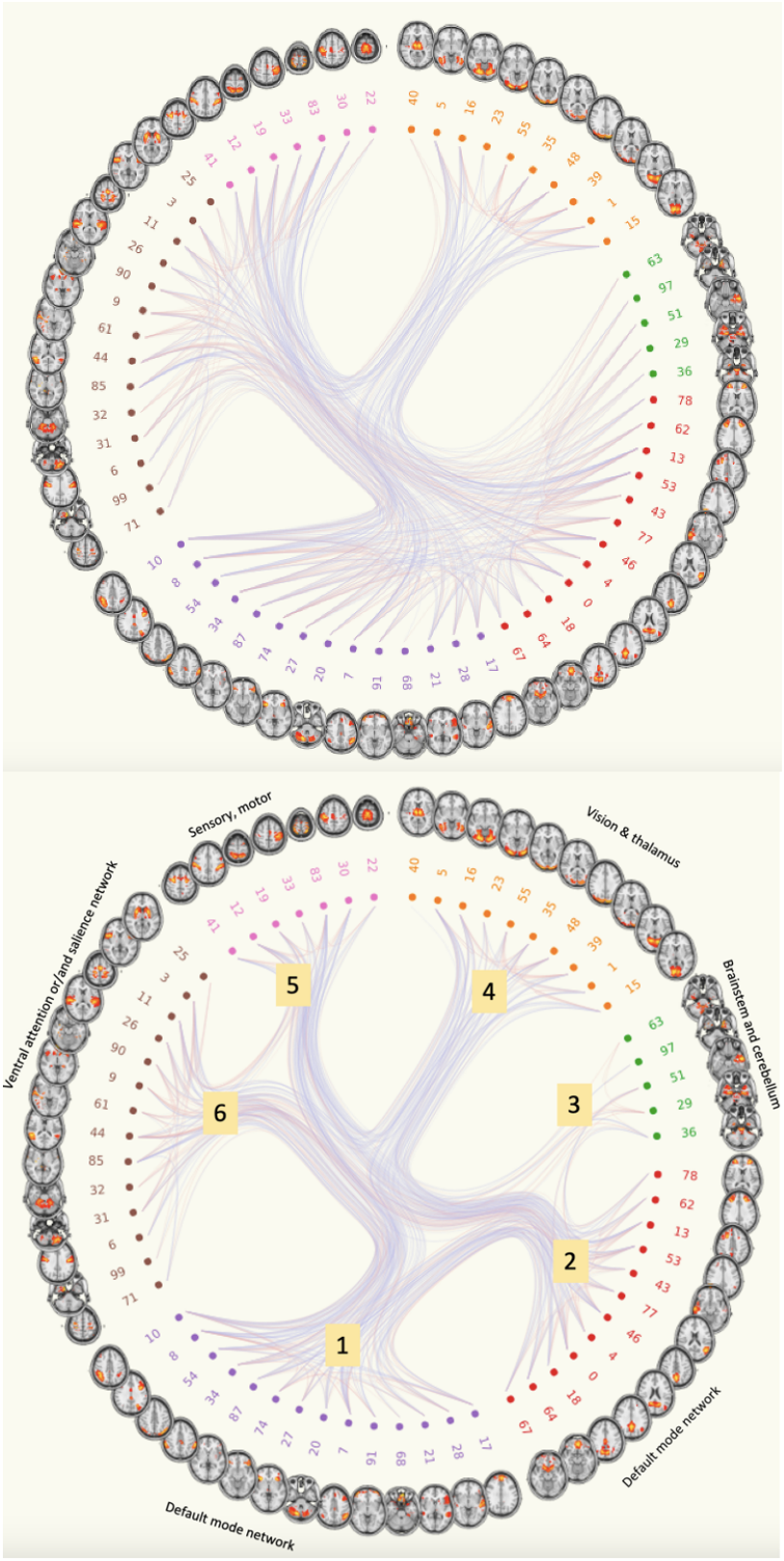


Fig. 6.2 Connectomes of Group ICA100 nodes on group average. This figure illustrates the clustering of 62 'good nodes' at arbitrary 3-cluster and 6-cluster levels, based on data from all 53 patients. The colour of connection links have red representing positive value (coupling), blue representing negative value (de-coupling). The top figure displays a clear segregation between the DMN, the 'task-positive' network, and the vision-thalamus network. The bottom figure shows a further subdivision of these clusters. This step serves as a sanity check for the pre-processing and Group ICA results.

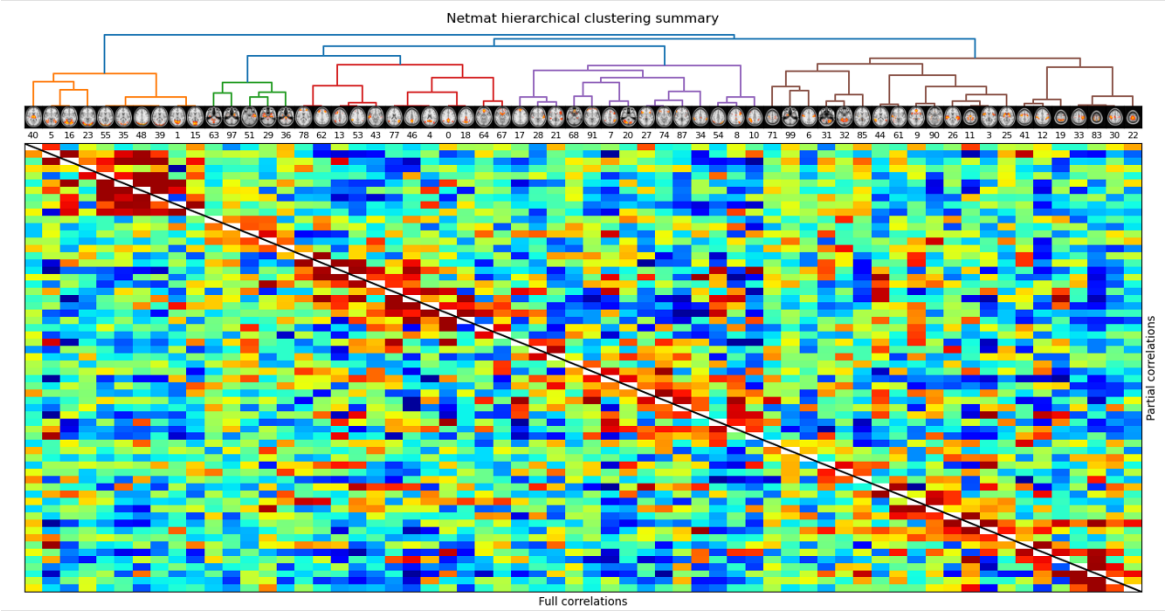


Fig. 6.3 Clustergram of Group ICA100 nodes. Group average connectivity and node clustering. It displays full-correlation connectivity (below the diagonal) and partial-correlation connectivity (above the diagonal). The nodes are ordered based on hierarchical clustering, which is driven by the full correlation, grouping nodes with the most similar resting-state time series.

6.4.3 CCA results

A single integrated multivariate analysis using CCA with 100,000 permutations was conducted to examine the relationships between SMs and BMs. The analysis controlled for confounding variables, including gender, age, BMI, motion (mean framewise displacement, relative and absolute), cube root of total intracranial brain volume, and cube root of total brain volume including ventricles, as described in Chapter 5. Eleven canonical modes were identified, with their corresponding canonical correlations and p-values summarised in Table 6.1.

Mode	Canonical Corr	P-value	Var Explained (SM, %)	Var Explained (BM, %)
1	0.9135	0.0626	4.72	3.87
2	0.8688	0.0299*	4.86	4.58
3	0.8428	0.0026*	3.99	5.17
4	0.7611	0.0404*	2.28	5.24
5	0.7308	0.0067*	2.41	5.30
6	0.6986	0.0006*	9.08	5.11
7	0.5390	0.3121	5.22	5.69
8	0.4152	0.8189	6.69	4.18
9	0.3661	0.6553	4.74	4.70
10	0.3329	0.2840	48.09	5.03
11	0.2415	0.3323	7.92	5.71

Table 6.1 Canonical Correlation Analysis (CCA) results. Canonical correlations, corresponding p-values, and variance explained by each mode are shown for the symptom (SM) and brain (BM) datasets. Significant p-values ($p < 0.05$) are marked with *. Despite a few significant modes, the first mode is not significant, reflecting a poor overall fit. Variance explained for SM and BM does not follow the expected pattern where the first mode captures the largest variance.

The results indicate that the canonical correlations 2, 3, 4, 5, 6 were statistically significant at $\alpha = 0.05$, with p-values ranging from 0.0006 to 0.0404. The first canonical correlation approached significance ($p = 0.0626$), while the remaining correlations (7 through 11) were not statistically significant ($p > 0.05$). Despite that, each mode explained very low variance in the original SM and BM features (below 5%).

Despite aggressive dimension reduction for both the SM and BM datasets, namely, retaining 50% of the variance, the CCA model remains prone to overfitting due to the small sample size (n = 53). This overfitting manifests as high variability across runs, with outcomes ranging from no significant modes to as many as six significant modes, albeit with very low variance explained. Moreover, the canonical modes often display sporadic weightings across the original SM and BM features.

For methodological demonstration purposes, this section reports the top three modes from this single CCA run, irrespective of their statistical significance. The interpretation provided is intended to illustrate the CCA methodology only, rather than to draw definitive conclusions about the relationships between behavioural and brain connectivity features.

Mode 1: An "Stress and anxiety" Phenotype with sensorimotor integration and associative network decoupling

The loadings and correlations between the top three canonical modes and the SM features are displayed in Figure 6.4. In interpreting the meaning of each mode, I focus on the correlation values rather than the weights. While the weights reflect the contributions when constructing the canonical variate, the correlations provide a more direct interpretation of what the mode represents. This distinction arises from the fact that, for ease of interpreting symptom dimensions, I have 'forced' the inclusion of 11 symptom/experience domains, allowing for certain levels of correlation between them, as shown in Figure 6.1. While this may lead to some dilution of loadings (e.g., between negative mood and lack of motivation), this does not affect the CCA model's ability to identify meaningful modes. However, at the reporting stage, the correlations provide a clearer interpretation of the symptom structure in relation to the modes.

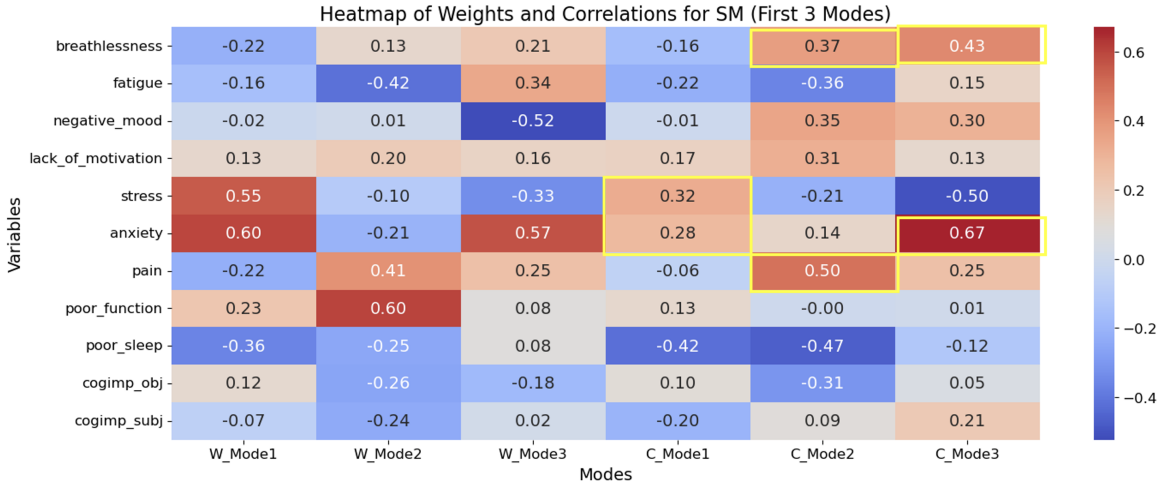


Fig. 6.4 Heatmap of top 3 modes' weights and correlations to SM features. The three columns on the left, labeled 'W_Mode1', 'W_Mode2', 'W_Mode3' in the x-axis, represent the weights. The three columns on the right, labeled 'C_Mode1', 'C_Mode2', 'C_Mode3' in the x-axis, represent the correlations. The top two positively correlated SM features to the mode are highlighted in yellow boxes. The heatmap is colour-coded using a "coolwarm" palette: warmer colours (reds) indicate positive weights or correlations and cooler colours (blues) denote negative weights or correlations.

Mode 1 (canonical correlation = 0.913, $p = 0.062$) primarily reflects a behavioural phenotype characterized by high stress and anxiety, as indicated by their positive correlations. Interestingly, this mode shows a less pronounced yet positive association with mood disorders and is even linked to better physiological outcomes such as reduced pain, fatigue, and

breathlessness. The negative correlation with poor sleep (-0.42) suggests better sleep quality, which is a surprising finding, as depicted in Figure 6.1.

On the brain side, I identified the top 30 edges contributing most to Mode 1 and assigned a minimal value (0.00001) to the remaining edges to exclude them from the final visualization. This minimal value effectively down-weighted irrelevant edges in the final matrix while retaining a complete 62×62 node structure.

The weight of each edge was determined by back-projecting from the Mode 1-weighted 19 PCs to the original edges (62×61 / 2 FC pairs) forming each PC. Specifically, edges were ranked based on their recalculated CCA connectome-modulation weights. These weights were obtained by multiplying the edge's weight within the PC by the PC's loading onto Mode 1, with signs adjusted according to the group-average sign of each edge. A new node-by-node matrix representing the CCA connectome-modulation weights for the top 30 edges (amounting to 22 nodes after removing duplicates) was constructed for visualization using the fsl.nets tool. The same procedure was applied for Modes 2 and 3.

As shown in Figure 6.5, Mode 1 highlights a brain network characterized by increased coupling within the sensorimotor network (nodes 30, 33, and 22), potentially reflecting greater integration between the two hemispheres. Additionally, it reveals decoupling between the primary sensory and motor regions (node 30) and the supplementary motor area (SMA; node 12), inferior parietal lobe (IPL; nodes 12 and 34), posterior cingulate cortex (PCC), and supramarginal gyrus (SMG; node 34). These patterns are illustrated in Figure 6.5.

However, it is important to note that, as with the SM data, this result is derived from an overfitted CCA model, and the findings may not accurately reflect real-world patterns. The interpretation of this mode should be considered cautiously, as the model's statistical significance remains questionable.

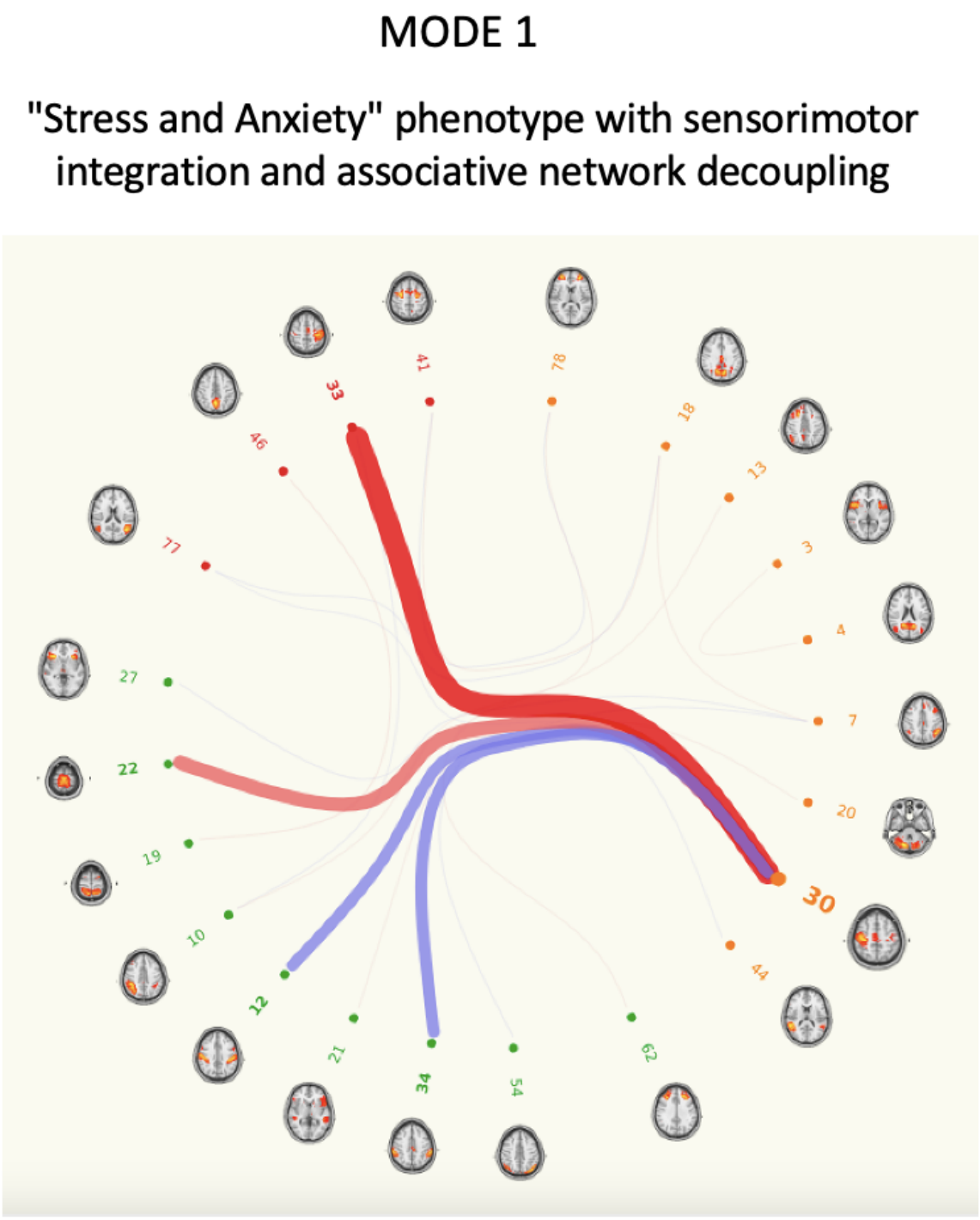


Fig. 6.5 Mode 1 Connectomes illustration. Red connections represent positive coupling, while blue connections represent negative decoupling. The connecting lines for node 30 are highlighted, showing the potential sensorimotor-related characteristics of the "stress-type" phenotype in Mode 1.

Finally, the subject-specific canonical covariates for both SM and BM are displayed in a scatter plot in Figure 6.6. The stress feature, which was the most positively associated SM feature, was colour-coded for each subject. However, the colour coding does not show a clear clustering, with high stress not corresponding to higher SM and BM values at the top right corner of the plot. This lack of clustering further indicates a poor fit, reinforcing that no firm conclusions can be drawn about the dominant role of stress in this mode.

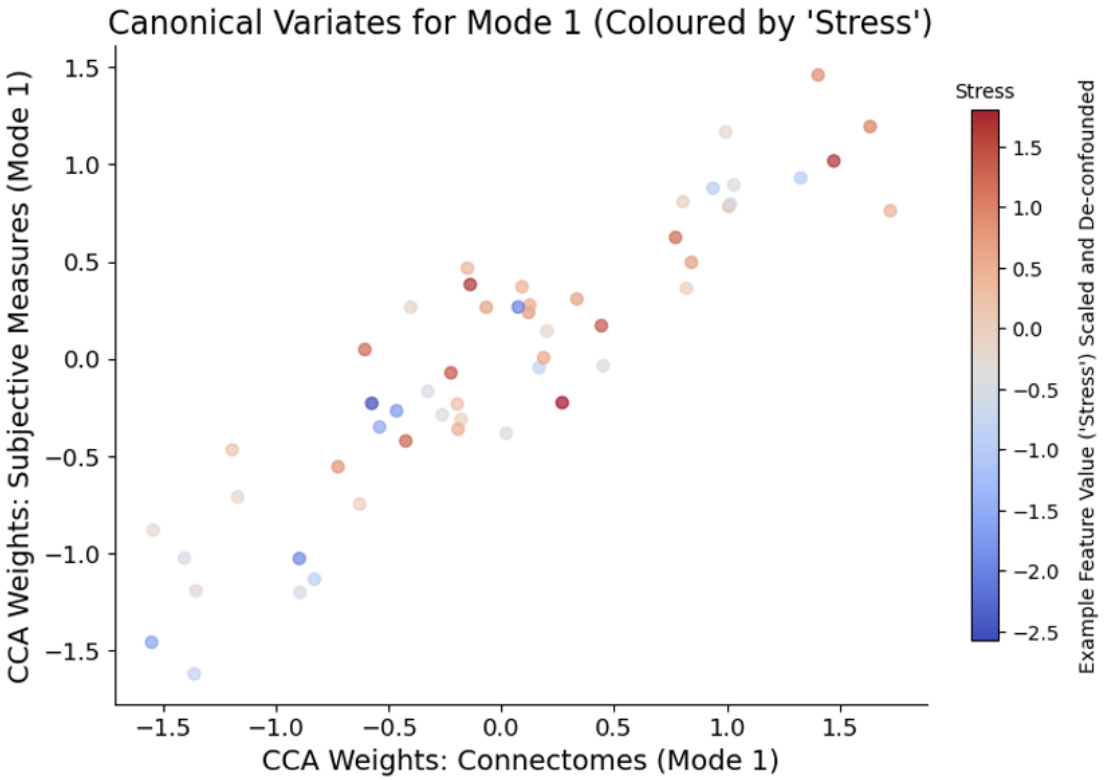


Fig. 6.6 Scatter plot of BM and SM weights for Mode 1, with each point representing an individual participant. The scatter plot is colour-coded using a "coolwarm" palette: warmer colours (reds) indicate higher stress levels, cooler colours (blues) denote lower stress levels, and the midpoint (0) represents group mean.

Mode 2: A "Pain and Breathlessness" with thalamus/brainstem-vision coupling

Mode 2 (canonical correlation = 0.869, $p = 0.029$) represents a behavioural profile characterised by pain and breathlessness, alongside weaker but still positive associations with negative mood and lack of motivation. Notably, this mode exhibits a counter-intuitive relationship with better sleep outcomes and enhanced cognitive task performance. The specific correlations of each SM feature with Mode 2 are detailed above in Figure 6.4. Compared

to Mode 1, where stress and anxiety dominate, Mode 2 is defined primarily by pain and breathlessness.

On the brain connectivity side, 19 nodes were present for the top 30 edges, as illustrated in Figure 6.7. This mode uniquely highlights the involvement of the thalamus and brainstem (node 40), which show a positive connection with higher-order visual processing regions (e.g., node 5, primarily corresponding to area V5). Furthermore, Mode 2 is notably enriched with visual-related nodes, including the primary visual area (V1), the lingual gyrus, and the temporal occipital fusiform cortex (nodes 15, 16, and 23).

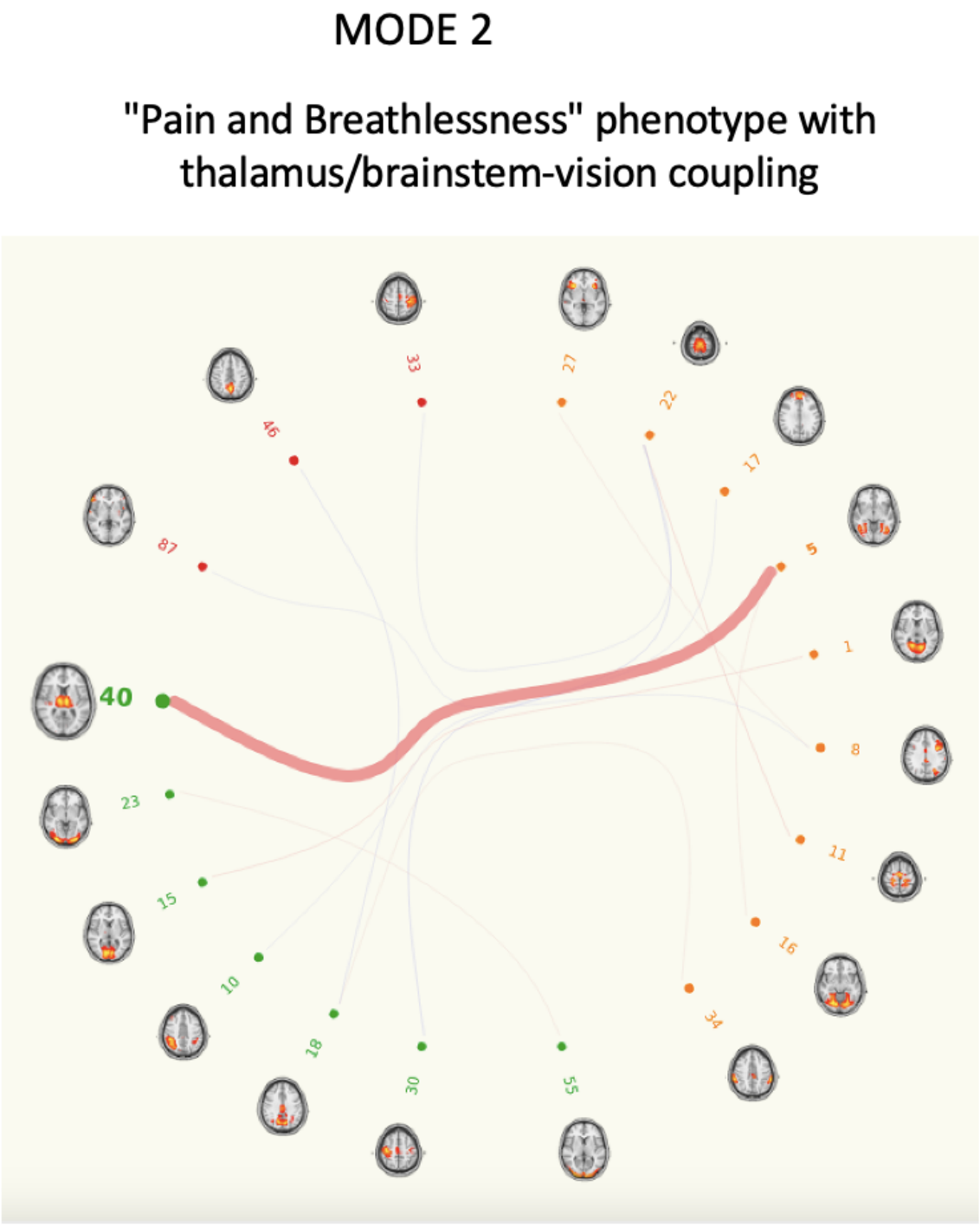


Fig. 6.7 Mode 2 Connectomes illustration. Red connections represent positive coupling, while blue connections represent negative decoupling. The connecting lines for node 30 are highlighted, showing the potential sensorimotor-related characteristics of the 'stress-type' phenotype in Mode 2.

The scatter plot in Figure 6.8 illustrated the relationship between the SM canonical variate and the BM canonical variate for Mode 2. The trend appears to be influenced by a few extreme cases in the upper right corner. These individuals may represent outliers who exhibit both heightened pain symptoms and engagement in higher-order visual processing during rest. This observation underscores the sporadic nature of the results, likely would be resolved with large sample.

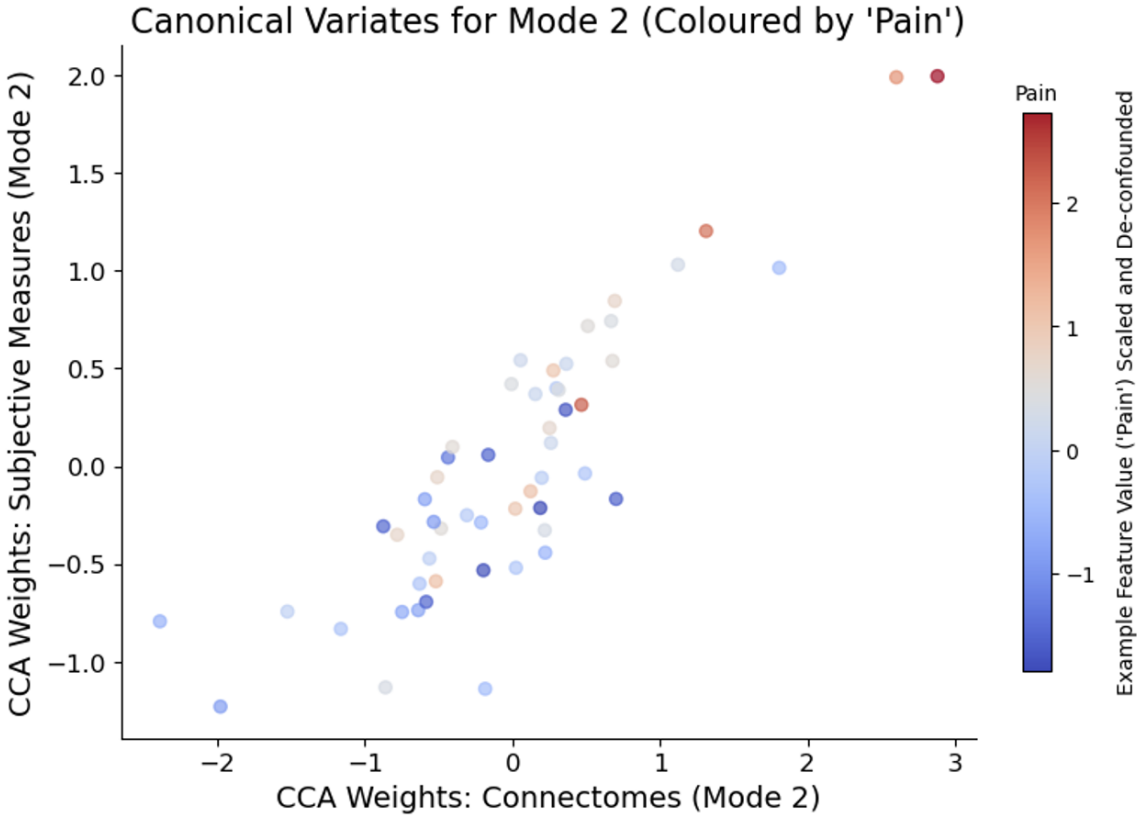


Fig. 6.8 Scatter plot of BM and SM weights for Mode 2, with each point representing an individual participant. The scatter plot is colour-coded using a "coolwarm" palette: warmer colours (reds) indicate higher pain levels, cooler colours (blues) denote lower pain levels, and the midpoint (0) represents group mean.

Mode 3 (canonical correlation = 0.843, $p = 0.003$) captures a behavioural profile characterised by anxiety, breathlessness, and positively correlated to almost all physiological aspects of pain, fatigue, psychological aspect of negative mood, and subjective cognitive impairment. Of note, stress exhibits a negative correlation in this mode, suggesting that higher anxiety levels are associated with lower stress. This finding is unexpected and may

reflect an artefactual relationship. Unlike Modes 1 and 2, poor sleep does not emerge as a notable contributor to this mode.

On the brain connectivity side, 17 nodes were retained from the top 30 edges based on CCA connectome-modulation weights, as shown in Figure 6.9. Notably, the visual cortex (V1, node 15) demonstrates increased FC with the insula regions (nodes 27 and 6). Despite the involvement of the visual cortex, no connectivity with the thalamus is observed—a key distinction from Mode 2.

In addition, this mode reveals decreased FC within the DMN, specifically between the medial prefrontal cortex (mPFC, node 64) and the posterior cingulate cortex (PCC) and precuneus (node 18). This pattern suggests potential de-integration within the DMN.

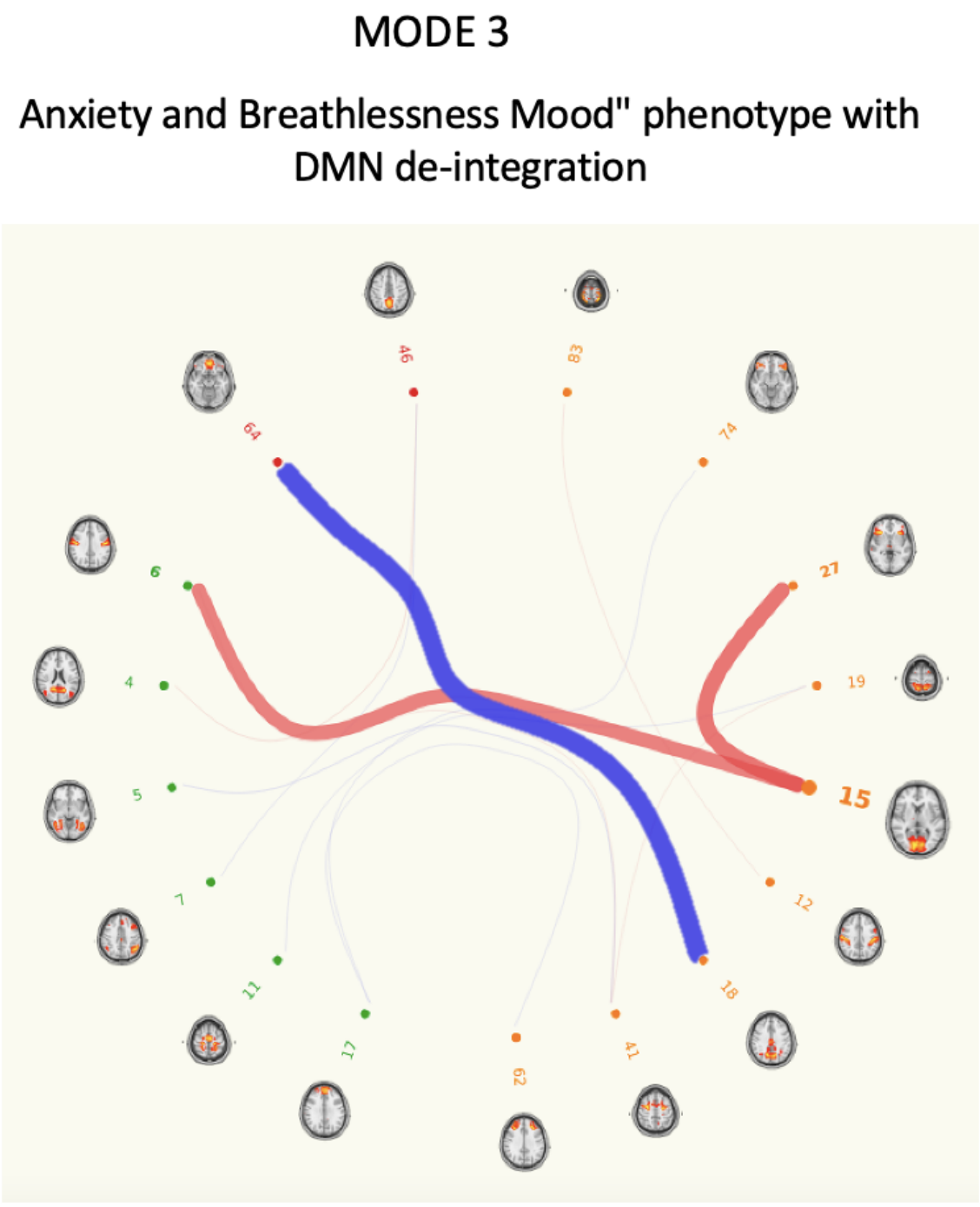


Fig. 6.9 Mode 3 Connectomes illustration. Red lines represent positive functional coupling, while blue lines indicate negative functional decoupling. Highlighted connections include increased coupling between V1 (node 15) and the insula (nodes 27 and 6) and decreased coupling within the DMN, particularly between the mPFC (node 64) and the PCC/precuneus (node 18), reflecting intra-DMN disintegration.

Figure 6.10 presents the scatter plot of the brain (BM) and symptom (SM) canonical covariates for Mode 3. Although the SM and BM weights exhibit a positive relationship, the variability in the scatter suggests substantial individual differences. The example feature, 'Anxiety,' is strongly associated with the SM-BM covariates for this mode, and points are colour-coded to reflect varying anxiety levels. Warm colours correspond to higher anxiety scores, while cool colours represent lower anxiety scores.

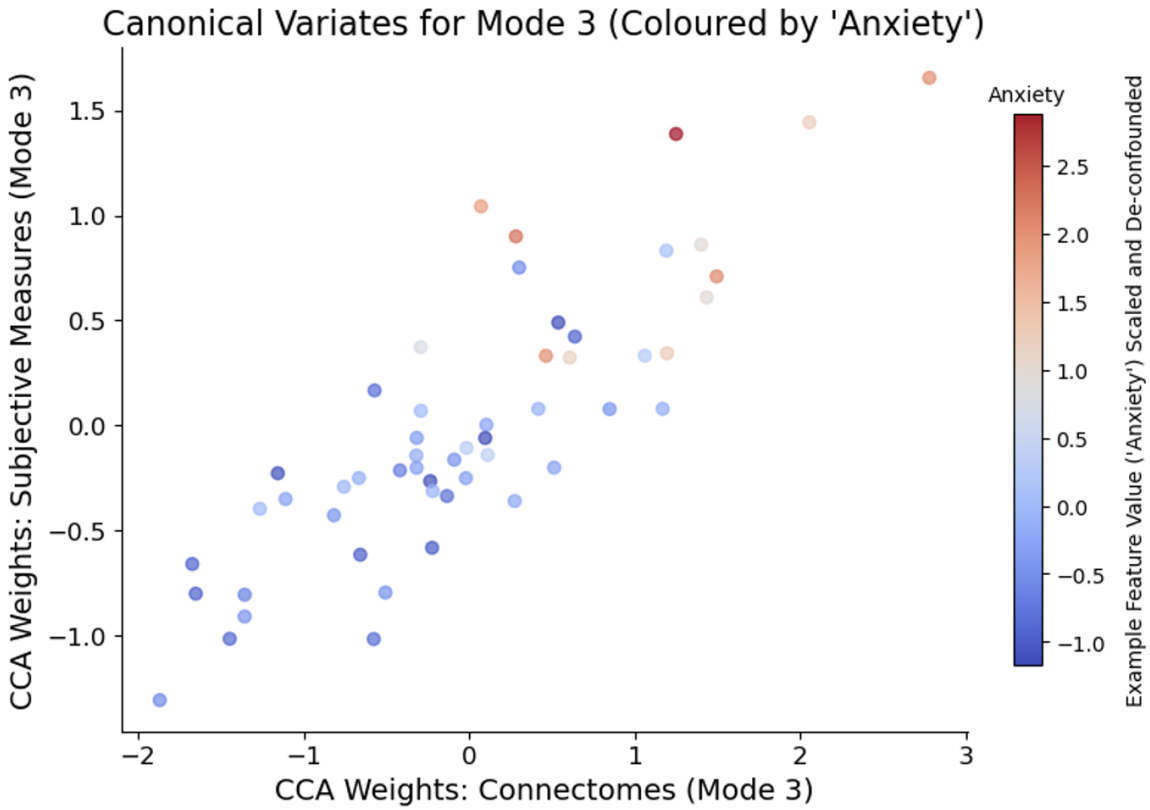


Fig. 6.10 Scatter plot of BM and SM weights for Mode 3. Each point represents an individual participant. The scatter plot is colour-coded using a "coolwarm" palette: warmer colours (reds) indicate higher anxiety levels, cooler colours (blues) denote lower anxiety levels, and the midpoint (0) represents group mean.

Breathlessness in all three modes

Ad hoc, I generated scatter plots for all three modes, colouring the data points based on the SM feature "breathlessness" to visualise its relationship with the three modes (Figure 6.11).

Although breathlessness was the second most heavily loaded feature for both Mode 2 and Mode 3, its distribution along the SM and BM weights appeared scattered. This pattern does not suggest a dominant role in determining any of the three modes.

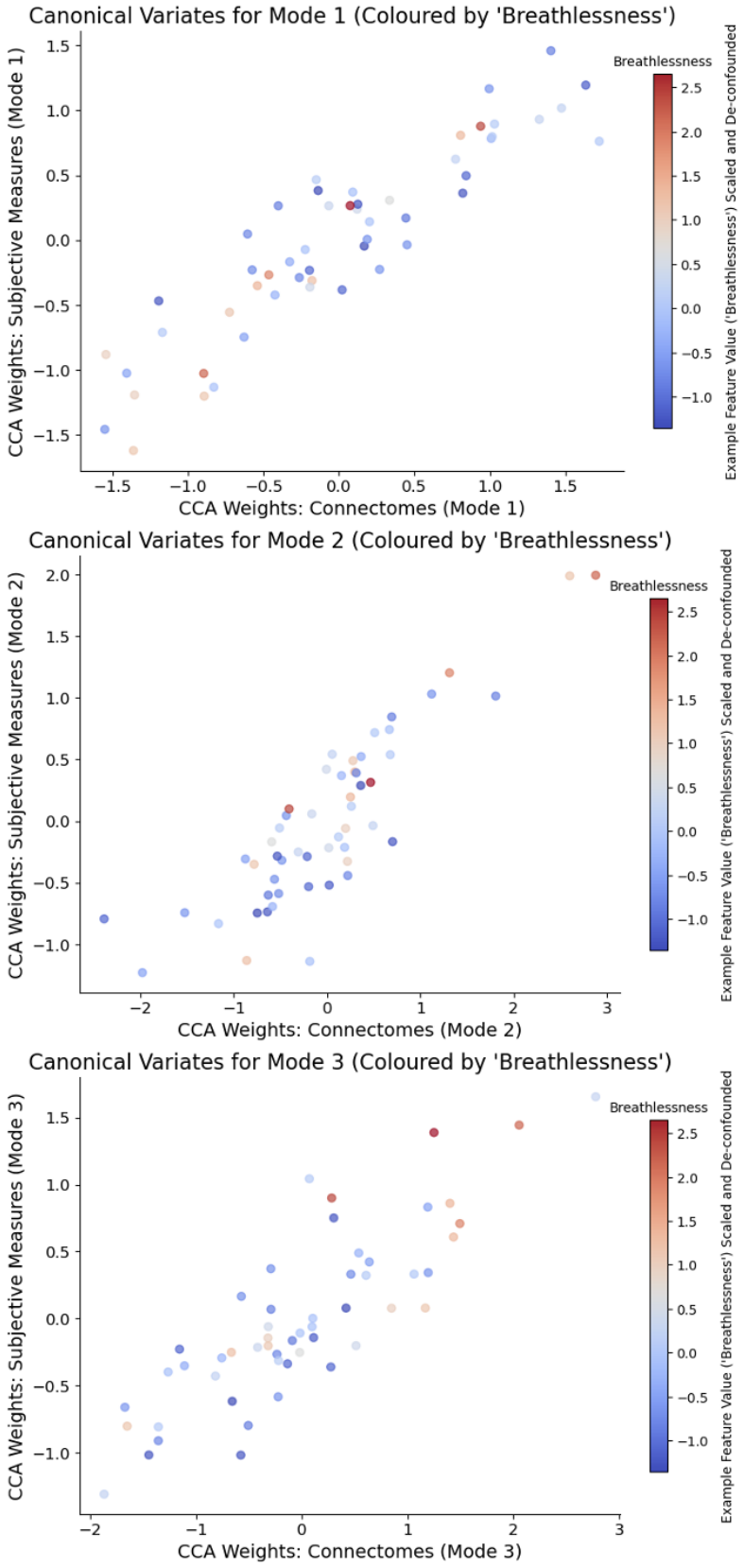


Fig. 6.11 Scatter plot of BM and SM weights for Mode 1, 2, and 3. Each point represents an individual participant, with colours corresponding to the z-scored SM feature 'Breathlessness'. All three scatter plots are colour-coded using a "coolwarm" palette: warmer colours (reds) indicate higher breathlessness levels, cooler colours (blues) denote lower breathlessness levels, and the midpoint (0) represents group mean.

CCA Result Summary

By applying a single multivariate analysis using CCA, I co-analysed a full set of functional networks along with a large subset of the post-COVID symptom and behavioural outcomes, in a cohort of 53 post-COVID patients, comprising both hospitalised and non-hospitalised individuals.

I reported the top three modes, selected based on their highest canonical correlations irrespective of statistical significance or validity, acknowledging the overfitting risk inherent in this analysis. These modes may correspond to distinct post-COVID neurophysiological phenotypes. Specifically, they are:

- **Mode 1:** A "Stress and Anxiety" phenotype characterised by sensorimotor integration and associative network decoupling.
- **Mode 2:** A "Pain and Breathlessness" phenotype with thalamus/brainstem-vision coupling.
- **Mode 3:** An "Anxiety and Breathlessness Mood" phenotype marked by DMN de-integration.

The top three canonical modes highlight distinct behavioural and brain functional network profiles, while also containing counter-intuitive associations, particularly with respect to sleep quality and stress. These results' validity were limited by the small sample size and overfitting concerns. However, they illustrate the potential of CCA to identify meaningful neurophysiological phenotypes, which may become more robust with larger datasets in future research.

6.5 Discussion

This chapter introduced a holistic multivariate approach that integrates a wide range of clinically reported symptoms and behavioural variables with whole-brain network data derived from rs-fMRI to identify neurophysiological post-COVID phenotypes. While the primary focus was on methodological development, this work represents the first 7T resting-state fMRI study exploring associations between multidimensional post-COVID symptoms and behavioural outcomes beyond 18 months post-infection. Using a moderate sample size of 53 patients, which included both hospitalised and non-hospitalised individuals, this study offers a comprehensive perspective on the long-term neurophysiological effects of COVID-19.

Through this analysis, I identified three example neurophysiological phenotypes: a "Stress and Anxiety" phenotype characterised by sensorimotor integration and associative network decoupling, a "Pain and Breathlessness" phenotype involving thalamus/brainstem-vision coupling, and an "Anxiety and Breathlessness Mood" phenotype marked by DMN de-integration. However, due to overfitting and the sporadic nature of the current CCA results, detailed contextualisation of these phenotypes within the existing literature is not meaningful. This chapter emphasises the methodological advancements demonstrated and the potential of multivariate approaches, such as CCA and partial least squares (PLS), for identifying meaningful neurophysiological phenotypes by linking complex behavioural profiles with brain connectivity data.

These findings would help enhancing our understanding of diverse patient profiles by addressing clinically reported symptoms and under-explored dimensions, such as sleep quality, pain, breathlessness, and functional outcomes. Existing studies have largely focused on specific symptoms, leaving gaps in understanding the multidimensional nature of long COVID, where various symptom combinations may co-occur. As reviewed in Chapter 1, prior research has primarily concentrated on three domains: (1) cognitive impairment [86, 265, 351, 364, 347]; (2) mood disorders and post-traumatic stress disorder (PTSD) [30, 132, 347]; and (3) olfactory dysfunction [98, 251, 369, 382]. These approaches, while valuable, often fail to capture the complex and varied experiences of long COVID patients.

The integration of diverse symptoms and behavioural measures with data-driven brain network models provides critical insights into shared and distinct neurophysiological mechanisms underlying diverse symptom expression. This approach highlights how multiple symptoms can arise from common brain vulnerabilities or how a single symptom may stem from diverse neurophysiological alterations. For instance, the comparison of Modes 2 and 3 illustrates this complexity: in Mode 2, breathlessness co-occurs with pain, potentially linked to thalamus and brainstem abnormalities, while in Mode 3, breathlessness is associated with anxiety, potentially reflecting disruptions in emotional and cognitive associative processing. Disambiguating these mechanisms could enable better patient stratification. For example, these two modes could potentially represent a "physiological (functional) type" and an "affective type" of post-COVID breathlessness, which aligns well with the dual pathways identified in the ROI-based allostatic-interoceptive network analysis in Chapter 5. In this last chapter, I have shown that tonic breathlessness may underlying the decoupling of interoceptive areas or/and the coupling of visceromotor regions, which were differentiated by associations with general anxiety and acute infection levels. The current analysis may further contextualise our understanding of why some breathlessness is associated with physiological manifestations, such as pain, while others are particularly burdened by affective disorders, using large brain

networks. These two phenotypes may provide a foundation for the development of distinct treatment focuses.

Moreoever, most published rs-fMRI studies in long COVID have relied on predefined nodes of interest rather than voxel-wise, data-driven approaches, with a few exceptions [132, 254]. The choice of ROIs significantly influences outcomes, especially given the noisy nature of rs-fMRI data. Additionally, all prior studies have used 3-tesla MRI, which offers limited spatial resolution. The largest and most well-powered study to date, conducted by Douaud et al. [89], found no significant FC markers using predefined imaging-derived phenotypes (IDPs), such as dimensionally reduced FC networks [96]. In contrast, my voxel-wise, data-driven approach identified distinct FC characteristics in a cohort of only 53 patients, highlighting its potential to uncover findings with higher external validity.

The increasing interest in linking brain and behavioural measures, particularly in large brain networks [325, 343, 32, 289], underscores the importance of sample size in multivariate analyses such as CCA and PLS. Empirical evidence suggests that only datasets with large sample sizes, often numbering in the thousands, can yield stable and reliable mappings between imaging features and behavioural measures [171]. Insufficient sample sizes can lead to instability, overfitting, inflated association strengths, poor generalisability, and high variability in identified patterns. Indeed, my analysis revealed sporadic findings, including modes where poor psychological and physical outcomes were associated with favourable sleep and function, with visual regions dominating in two of these modes. Moreover, I tested whether repeated runs of the same analysis produced inconsistent results, which was confirmed. This further indicates the low interpretability and validity. Together, I emphasise the necessity of larger datasets, such as the UK Biobank (UKB), to facilitate robust exploration of post-COVID neurophysiological phenotypes.

The number of features is another critical determinant of stability in CCA and PLS. In this study, I reduced the dataset to 11 SM and 19 BM features to demonstrate these methods. This step reduced the variance to approximately 50%, which contrasts with approaches in larger samples, such as the UKB, where 98.5% [224] or 80.37% [325] of the total variance in non-imaging behavioural data is retained, and 81.38% [224] or 41% [325] for connectome population variance. This relatively aggressive dimensionality reduction for both SM and BM was chosen to address the limitations imposed by the small sample size, while retaining sufficient information to avoid excessively diminishing the canonical correlations. It represents the best approach I can take within the constraints of intrinsic high data dimensionality and a small sample size.

Nevertheless, I do not advocate for using a fixed number of features as a universal approach. Researchers must consider the trade-off between dimensionality reduction, which

lowers sample size requirements, and the potential for reduced canonical correlation, which may demand larger samples for stability. Various methods for determining the optimal number of components exist [171], and domain-specific knowledge can aid in selecting relevant features to enhance stability and interpretability, as was done for the SMs of the current analysis.

Finally, robust validation remains essential to ensure reliable findings. Cross-validation was employed in this study to assess model performance and mitigate overfitting. However, out-of-sample replication using independent datasets would have provided a stronger test of generalisability. Future research should prioritise such validation methods to improve the credibility and reproducibility of findings in small-sample multivariate studies.

6.6 Conclusion

This study represents a pioneering effort to integrate multidimensional behavioural and clinical data with high-resolution whole-brain network measures from 7T resting-state fMRI to explore neurophysiological phenotypes of post-COVID conditions. Through a data-driven multivariate framework, I identified potential neurophysiological patterns associated with diverse symptom profiles, underscoring the complex interplay between brain connectivity and behavioural outcomes. However, the sporadic nature of findings and inherent limitations of sample size highlight the need for caution in interpreting these results. Future research leveraging larger datasets, robust validation techniques, and advanced dimensionality reduction strategies will be essential to refine these associations and translate findings into clinically actionable insights. This work lays a foundation for further exploration into the long-term neurophysiological impacts of COVID-19, fostering advancements in personalised medicine and targeted therapeutic interventions.

Chapter 7

Discussion

7.1 Summary of results

This thesis investigated the neural mechanisms underlying the perception of breathlessness and its maladaption, with a particular emphasis on individuals recovering from COVID-19. Building on task-based fMRI research in healthy populations, the work extended to a newly recruited post-COVID cohort. Across all studies, ultra-high-field (7 Tesla) functional magnetic resonance imaging (fMRI) was used to characterise the activity and functional connectivity (FC) patterns of brain regions implicated in interoception, allostatic regulation, and emotion processing. The findings offer novel insights into the central neural substrates of respiratory perception and highlight mechanisms through which these processes may become dysregulated in clinical contexts.

Chapter 1 presented the complex phenomenon of breathlessness, offering a comprehensive overview of the empirical evidence and theoretical frameworks that elucidate its neural mechanisms. Central to this chapter is the introduction of a theoretical framework based on Active Inference [125, 311, 27, 269], alongside its mechanistic hypotheses in the form of the Embodied Predictive Interoception Coding (EPIC) model [199], applied to the domain of the allostatic-interoceptive (allo-intero) process. Building on this, I re-conceptualised reflexive breathing, adaptive phasic breathlessness, and maladaptive tonic breathlessness, incorporating the cortical hierarchy of inferencing within the respiratory system as a theoretical foundation.

Chapter 2 explored the neural correlates of breathlessness in healthy individuals, focusing on activity and FC within amygdala nuclei. This study revealed that during the anticipation and perception of inspiratory resistance, the basolateral amygdala (BLA) exhibited significant deactivation. Furthermore, BLA connectivity with the mediodorsal thalamus (MD) increased during resistance, scaling subthresholdly with anxiety. At rest, the intensity of breathlessness

perception was associated with increased BLA-temporal pole connectivity and decreased BLA-precuneus connectivity. These results highlight the role of BLA-centred functional connectivity in modulating breathlessness perception and suggest potential mechanisms that may underlie misinterpretations of respiratory signals in clinical populations.

Chapter 5 extended these findings to post-COVID patients, many of whom reported persistent breathlessness despite limited evidence of pulmonary dysfunction. Resting-state fMRI data revealed altered functional connectivity patterns associated with maladaptive respiratory perception. Specifically, the study identified functional decoupling between the dorsal periaqueductal gray (dPAG) and posterior insula (PoI1), as well as coupling between the basolateral amygdala (BLA) and dorsal anterior cingulate cortex (dACC), as predictors of heightened breathlessness catastrophizing. Notably, dPAG–PoI1 connectivity and the use of a ventilator showed a significant interaction effect. dPAG–PoI1 connectivity exhibited significant explanatory power in patients who were not ventilated during the acute infection, with even stronger predictive ability observed in those who had been ventilated. This finding may reflect functional disruption in lower-level brain regions responsible for integrating bottom-up visceral signals, particularly in individuals most severely affected during acute COVID-19. Furthermore, dPAG–PoI1 connectivity, but not BLA–dACC connectivity, remained significantly associated with breathlessness even after controlling for general anxiety scores and acute infection severity. These findings suggest that maladaptive breathlessness in post-COVID patients may arise from impaired visceral signal integration and/or an exaggerated anticipatory bias toward adverse respiratory experiences, potentially linked to traumatic acute infection phases.

Chapter 3 presented the MRI pre-processing procedures, the identification of regions of interest, and the reduction of brain-derived data dimensions. Both Chapter 6 and Chapter 4 were based on this.

Chapter 4 provided critical context for the Chapter 6 and Chapter 4 by addressing the heterogeneity within the post-COVID cohort and behavioural data dimension reduction. It highlighted significant variability in symptom presentation and underscored the importance of controlling for confounding factors such as group differences. While direct comparisons with the control group were limited by selection bias, the chapter identified 11 domain-based features that balanced insights from exploratory data analysis with existing literature, enabling robust dimensionality reduction and subsequent analyses for Chapter 6.

Chapter 6 centred on the development of a methodology that employed a multivariate approach to identify neurophysiological phenotypes in post-COVID patients, integrating both high-dimensional imaging and non-imaging data. Despite the overfitting of the analysis, I presented the identification of three distinct phenotypes: (1) a "Stress and Anxiety" pheno-

type, characterised by decoupling within sensorimotor integration and associative networks; (2) a "Pain and Breathlessness" phenotype, involving thalamus/brainstem-vision coupling; and (3) an "Anxiety and Breathlessness Mood" phenotype, characterised by de-integration of the default mode network (DMN). These findings underscore the potential of using a single multivariate model to capture the complexity and multidimensionality of post-COVID experiences, providing a foundation for personalised treatment strategies.

Together, these findings elucidate the neural underpinnings of breathlessness perception and its maladaptive variants, namely, the phasic and tonic breathlessness, particularly in the context of post-COVID conditions. By integrating high-resolution neuroimaging with behavioural and symptom-based measures, this thesis advances our understanding of the brain's role in respiratory perception and regulation, and provides a framework for future research and therapeutic interventions.

7.2 Breathlessness as an affective disorder?

Chapters 2, 4, and 5 examined the relationship between breathlessness and affective constructs. It contained self-reported anxiety levels about respiratory threats during tasks or general anxiety scores in post-COVID populations, from various perspectives. Consistent with the long-standing findings and hypotheses made in breathlessness research [178, 72, 52, 319, 21, 327, 165, 188, 240, 85, 35], affective processes, such as anxiety, significantly influence the perception of breathlessness.

In Chapter 5, Functional connectivity (FC) between the basolateral amygdala (BLA) and dorsal anterior cingulate cortex (dACC) emerged as a key predictor of breathlessness, with the strength of this connection being modulated by the individual's general anxiety levels. Nobly, dependency to general anxiety was not evident for other significant FCs, such as those between the lower-level interoceptive structures, such as the mid-brain and the posterior insula. It is possible that the increase BLA-dACC FC, reflects a disordered affective state, as its disruptions are widely implicated in patients in post-traumatic stress disorder (PTSD), social anxiety disorder, and specific phobia[100, 99, 101]. Behaviourally, relationships between self-reported general anxiety and breathlessness is well acknowledge, and also supported by the behavioural data of the larger cohort described in Chapter 4, from which the neuroimaging sub-sample were derived. Subscales of breathlessness ratings showed a strong correlation with anxiety scores and clustered closely with each other, among other domains of post-COVID neurophysiological outcomes.

From the perspective of interoceptive inference (or active inference in the interoceptive domain) and our conceptualisation of 'tonic breathlessness', the high FC between the BLA

and dACC may reflect a particular affective phenomenon. Possibly, it promotes strong, albeit unnecessary, priors regarding the inability to resolve gas-exchange prediction errors within the lower-level reflex arc. In this scenario, top-down anticipation (along with its copy of volitional motor command) overrides and bypasses the reflex arcs, directly switching to volitional breathing. In this cohort of post-COVID patients who experience breathlessness despite limited evidence of pulmonary dysfunction, their reflex arcs are most likely capable of regulating respiration effortlessly, evident in their little complaints of breathlessness during sleep. It is possible that fluctuations in attention to one's physiological state or anxious state evoked by other sources during the awake hours trigger this 'affective breathlessness' response.

The underlying reasons for the enhanced FC between the BLA and dACC remain unclear. Based on the current mechanistic understanding of interoceptive inference, this connection may be modulated by processes that increase its precision, such as dopaminergic projections from the ventral tegmental area (VTA) and substantia nigra (SN). This scenario is depicted in Figure 7.1, for illustrative reasons.

It remains uncertain whether this represents a pre-existing neurological vulnerability or is induced by a psychologically traumatic experience during acute COVID infection and subsequent hospitalisation[198], given the absence of pre-COVID data or well-matched controls. However, evidence suggesting that the relationship between dACC-BLA FC and breathlessness symptoms is influenced by the severity of the acute infection implies a potential link to the acute COVID experience.

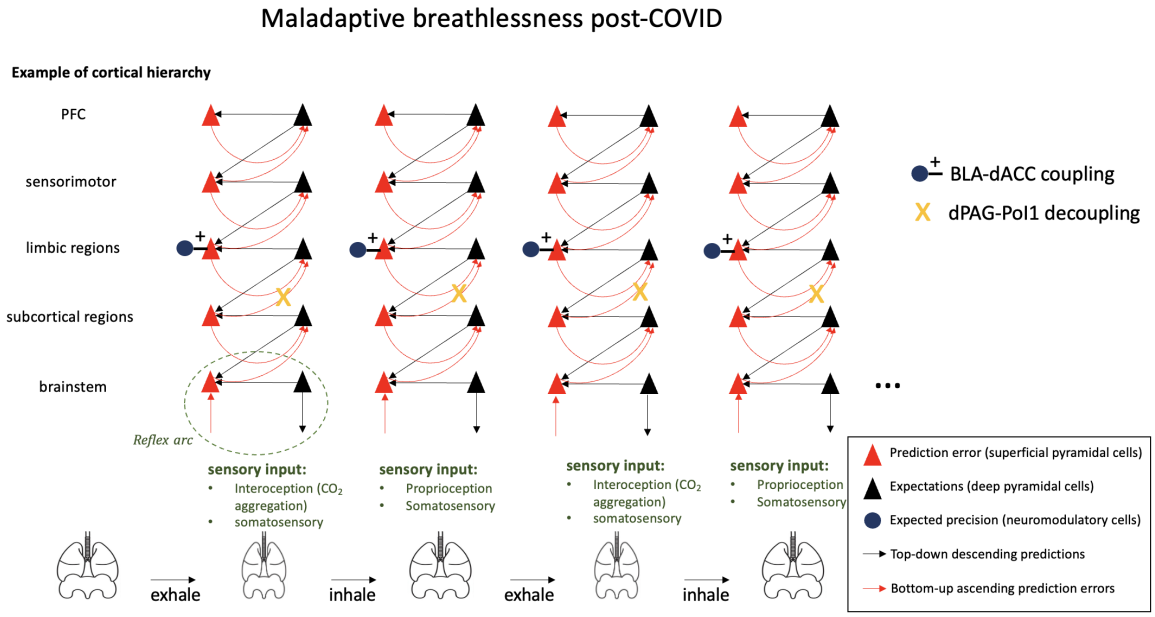


Fig. 7.1 Schematic illustration of possibly neural disruptions in post-COVID tonic breathlessness. This schematic illustrates the alternating dynamics of inspiration and expiration, each occurring within a simplified cortical hierarchy, characterised by ascending prediction errors and descending predictions. The minimisation of prediction error relies on recurrent neuronal interactions across various levels of the cortical hierarchy. In post-COVID maladaptive, tonic breathlessness, the prediction errors cannot be resolved at the reflex arc located in the brainstem. It further presents two possibly neural disruptions: exacerbating of prediction errors at the limbic region centrally around the amygdala (dark blue dot with a plus sign), and the disruptions of afferent sensory signals at the lower-level regions (yellow cross). It is hypothesised that superficial pyramidal cells (red triangles) compare expectations at each hierarchical level with top-down predictions from deep pyramidal cells (black triangles) at higher levels, as reviewed in [28]. Neuromodulatory gating or gain control (represented in dark blue), potentially involving projections from the ventral tegmental area (VTA) and substantia nigra (STN), indicates the weight assigned to prediction error based on expected precision. This figure is adapted from Seth and Friston [311]. Related figures are presented in Section 1.4.3 of Chapter 1.

In contrast to the significant role of general anxiety and BLA-centred affective regulatory pathways in maladaptive tonic breathlessness following COVID, the relationship between anxiety and respiratory perception was less prominent in phasic breathlessness, as shown in Chapter 2.

In Chapter 2, the experimentally induced inspiratory resistive loading mimics a true obstruction during inspiration, indicative of an adaptive phasic breathlessness state. The ratings of anxiety were not significantly correlated with any metrics derived from the activity and functional connectivity features, either during the task or at rest. This finding is consistent

with Section 1.4.3 of Chapter 1, where I hypothesised that affective processes, such as fear of suffocation and anxiety, are not necessary during model updating (i.e., prediction error minimisation, action/belief update, or learning/habituation), especially in phasic breathlessness. This was exemplified by the case of a skilled swimmer adjusting respiratory regulation to respond to CO_2 accumulation without panicking.

One subthreshold finding revealed that increased FC between the BLA and the contralateral mediodorsal thalamus (MD) during resistive breathing was positively associated with anxiety. The BLA is known to function as a sensory gateway [214], and its connectivity with the MD may reflect an ongoing focus on the sensory consequences of executed actions, facilitating model updates (i.e., belief updates and action adaptations, or 'perceptual inference' and 'active inference', as introduced in Section 1.4 of Chapter 1). I hypothesise that this process may underpin the cognitive appraisal of one's affective state, such as anxiety, and could become significantly correlated with anxiety if the resistive load is perceived as more unexpected and threatening. Furthermore, as this process is considered adaptive during phasic breathlessness, I further postulate that the BLA-MD FC observed during resistive breathing would diminish once the model update is complete, allowing the individual to manage respiration through reflexive breathing. This reduction in FC would signify the process of habituation or learning, which could be empirically tested in a longitudinal study.

Taken together, these findings provided evidence of the intricate relationship between affective processes and the perception and regulation of respiration, in both phasic and tonic contexts. I propose that this perspective supports the conceptualisation of tonic breathlessness as an 'affective disorder'. In this condition, therapeutic and pharmacological strategies commonly employed for conditions such as general anxiety, PTSD, and phobia may be effective in its management. This perspective aligns with much of the previously established breathlessness research, which demonstrates that patients with "difficult-to-treat" asthma and chronic obstructive pulmonary disease (COPD), who show limited responsiveness to conventional pharmacological interventions targeting the lungs, experience improvements in symptom severity and quality of life through alternative approaches such as 'breathing retaining' or ' pulmonary rehabilitation' [159, 48, 237, 363]. These improvements are thought to be mediated by a reduction in negative emotions [363]. Neurological markers, such as FC between the BLA and dACC, may help identify patients experiencing tonic breathlessness as distinct from those with adaptive phasic breathlessness - possibly due to other undetected pulmonary or neurological dysfunctions. These BLA-dACC FC markers could possibly serve not only to identify 'affective breathlessness' patients but also to help evaluate treatment responsiveness.

7.3 Breathlessness as a functional neurological disorder?

In Chapter 5, FC between the dorsal periaqueductal gray (dPAG) and posterior insula (PoI1) was found to be negatively correlated with breathlessness symptom burden in post-COVID patients. From the perspective of interoceptive inference and our conceptualisation of 'tonic breathlessness', this low or negative FC within the interoceptive structures [199] may indicate a dysfunction in the bottom-up respiratory signal integration.

As illustrated in Figure 7.1, disrupted FC may occur at lower levels of the cortical hierarchy. The yellow cross in the schematic signifies this disruption between the subcortical region (dPAG) and the upstream components of the salience network (PoI1) [1]. This disruption suggests a failure in bottom-up signal integration, which impedes the updating of the generative model of gas-exchange. In the context of recovery from COVID, it impedes safety learning. This dysfunction may occur in isolation or, in more unlucky cases, co-occur with an over-reliance on anticipatory threat, via increased amygdala-centred top-down gain. Together, these neural dysfunction could result in an inability to update the model (i.e., prediction error minimisation, action/belief update, or learning/habituation), preventing a return to reflexive breathing.

Unlike BLA-dACC FC, this neurological feature is not dependent by anxiety levels or the severity of the acute infection in predicting tonic breathlessness post-COVID. Moreover, the association between dPAG-PoI1 decoupling and breathlessness is even stronger in patients who required ventilation. This suggests that the alteration in dPAG-PoI1 FC is most likely not related to affective processes and, to some extent, cannot be considered 'psychological'. Instead, it could represent a pre-existing neurological vulnerability or be the result of undetected neurological damage in the brainstem or associated subcortical regions in those most severely affected by COVID [295].

It is important to distinguish this functional subtype of tonic breathlessness not only from phasic breathlessness but also from affective (tonic) breathlessness. I propose that the disruption in respiratory (interoceptive, proprioceptive, and exteroceptive) signal integration cannot be treated using the therapeutic approaches suggested for affective tonic breathlessness[159, 48, 237, 363], where cognitive reappraisal, psychological acceptance, or mindfulness may be beneficial. I further hypothesise that, in individuals with poor visceral signal integration—who are unable to relearn reflexive breathing (i.e., safety learning)—their affective response, if present, is adaptive. Forcing them to be less anxious would likely be counterproductive.

[1] Note that the label "limbic regions" is intended solely to indicate the direction of upstream and downstream processes within the reciprocal cortical hierarchy. The insula is part of the cerebral cortex, not the limbic system.

Upon closer examination of the amygdala alone, as shown in Chapter 2, I did not find any breathlessness-related FC characteristics relating to lower-level brainstem regions. Unlike the 'sensory gateway' BLA, the evolutionarily older centromedial amygdala (CMA), specifically the central nucleus (CenA), has the most robust evidence for its role in mediating the autonomic regulation of respiration [385, 389, 18, 163, 380, 259] in a nasal-breathing-dependent manner [122, 380, 259]. Although only weakly supported by the ROI-based approach in Chapter 2, the observation that the CenA deactivates during resistive breathing (phasic) remains promising and warrants further investigation. Disruptions centred on the CenA may represent another pathway contributing to breathlessness as a functional disorder.

Together, this represents a novel perspective on maladaptive breathlessness as a functional neurological disorder, where disruptions in lower-level visceral signal integration prevent the organism from returning to reflexive breathing. This understanding has implications not only for post-COVID breathlessness but also for conditions previously considered "medically unexplained" [159, 277] or "intractable or refractory" [37] breathlessness. It challenges the enigmatizing notion that somatic symptoms without an 'organic' (bodily) cause is 'psychological'.

7.4 Distinguishing tonic and phasic breathlessness

This is the first instance when distinction between tonic and phasic breathlessness has been made. Research on the brain networks underlying breathlessness has commonly utilised resistive inspiratory challenges in combination with brain imaging techniques. These tasks, including those described in Chapter 2 of this thesis, typically involve inducing inspiratory resistance through breath-holding, resistive loads applied via a restrictive breathing mouthpiece, or breathing through a mixture of CO_2 and air [339, 340, 272, 103, 34, 362]. While such studies provide valuable insights, particularly in healthy populations, the extent to which these results can translate to the understanding of neurobiological basis of maladaptive breathlessness in patients is in question.

In pain research, tonic pain (acute, adaptive) and phasic pain (chronic, maladaptive) are considered fundamentally distinct. For instance, the activity of mesolimbic neurons has been found to exhibit temporally distinct modes, designated as phasic and tonic activity [373, 306]. These two modes are inversely related [121, 142], with phasic activity associated with high-amplitude dopamine release in response to environmental stimuli (e.g., rewards), while tonic activity is linked to steady extrasynaptic dopamine. For example, fibromyalgia patients have been found to fail to release striatal dopamine in response to an experimental pain stimulus (intramuscular hypertonic saline injection), in comparison to healthy controls[374]. This

indicates inhibition of phasic dopamine activity due to the chronic experience of ongoing (tonic) pain.

The implication that 'chronic pain patients may have a reduced acute pain response' has profound consequences for linking tonic pain research to phasic pain, as well as for understanding and treating chronic pain. For instance, a treatment that reduces chronic pain patients' response to acute pain stimuli would be counterproductive.

Reflection this to breathlessness research, it is not yet known whether tonic breathlessness patients would exhibit similar patterns to those observed in tonic pain patients, such as inhibition of a phasic adaptive breathlessness response. In this context, treatments aimed at increasing tolerance to respiratory load—essentially a phasic process—would likely not be effective and counteractive.

7.5 Reflecting on negative results

Across the chapters, following expected results have proven to be insignificant or underpowered to be detected.

In Chapter 2, no activity was identified within the CMA during either the anticipation or resistance phases of phasic breathlessness, using the whole-amygdala voxel-wise approach. This result was unexpected, particularly given the substantial evidence supporting the role of the central nucleus of the amygdala in regulation of respiration [385, 389, 18, 163, 380, 259]. Its essential role in autonomic regulation, mediated through projections to lower-level brainstem regions [214, 216], suggests that it is a promising candidate as a node within the visceromotor network, alongside the proposed and studied cingulate regions and the medial part of the ventral anterior insula, as shown in Chapter 5.

Moreover, in the fear conditioning literature, it has been hypothesised that the expression of fear is gated by the BLA, and the extent of its downstream pathway to the central nucleus acts as a deciding factor in whether defensive responses would be present in association with the conditioned stimulus [12]. Identifying fMRI signals within the central nucleus could provide valuable insights into how intra-amygdala functional connectivity contributes to the transition from a state of mild breathlessness to one of panic or fear.

To further investigate, a supplementary analysis was conducted, testing group mean contrasts of activity across nine subnuclei and regions [302] derived from the segmentation of each subject's amygdala in their native anatomical space. This analysis provided some support for our hypothesis regarding the CMA. Despite concerns about the validity of this approach due to the small mask size and 'forced' segmentation, I observed deactivation in the central and anterior nuclei of the amygdala during the resistance phase of breathlessness.

The central nucleus of the amygdala's medial-ventral position, proximity to the sphenoid and ethmoid sinuses, and susceptibility to magnetic field (B0) inhomogeneities significantly contribute to its poor signal-to-noise ratio (SNR), high signal dropout and and geometric distortions in fMRI. Combined with its small size and the physiological noise from adjacent structures, these factors may explain the lack of significant results from the voxel-wise approach on an averaged brain. Nevertheless, the role of the CMA, particularly the central nucleus, remains a highly plausible candidate for further investigation into respiratory perception and regulation.

Second, I did not find any amygdala-related functional or connectivity characteristics during resistive load or its anticipation in relation to exercise. This is consistent with the whole-brain voxel-wise analysis based on the same dataset, published by Faull and colleagues [110]. This may suggest that phasic breathlessness, in most individuals, does not elicit a true 'alarm' response, and therefore does not trigger feelings of fear or changes in self-report anxiety or intensity. In this whole-brain analysis, the athlete group demonstrated extensive task-evoked activity in several regions beyond the amygdala. These included the bilateral ventral posterolateral thalamus, middle insula, primary motor and sensory cortices, and the left anterior insula. Compared to the sedentary control group, this activity was positively correlated with the predicted intensity of breathlessness during anticipation. These regions overlap with the allo-interoceptive network discussed in Chapter 5.

Athletes' brains have been suggested to exhibit superior interoceptive sensitivity to respiratory signals, as demonstrated by a closer alignment between the perception of breathlessness and changes in ventilation compared to sedentary individuals [110]. It is possible that the distinction between athletes and sedentary controls lies not in the affective aspects, but in the sensory signal integration involved in the perception and regulation of respiration. This distinction may resemble the intra-visceromotor regions' coupling, exemplified by the BLA-dACC coupling, and the intra-interoceptive regions' decoupling, exemplied by the dPAG-PoI1 decoupling in post-COVID maladaptive breathlessness. Future research investigating the allo-intero network as a whole in athletes, compared to sedentary controls, during the anticipation and perception of phasic breathlessness would be highly valuable.

Third, one of the most robust findings in COVID research was the neural alterations observed in the olfactory-related cortex, which have been suggested to involve grey matter loss in regions to which the olfactory bulb projects, including the piriform cortex (primary olfactory cortex), the amygdala, orbitofrontal cortex (OFC), and entorhinal cortices [89]. However, I was unable to replicate[98, 251, 369, 382] any resting-state functional connectivity characteristics associated with the olfactory pathway in our post-COVID sample. Further, I was unable to test the hypothesis that disruption of the olfactory network contributes

to breathlessness, representing a deviation from the generative model of gas exchange, where nasal input plays a role[122, 380, 259]. However, this remains a highly intriguing avenue for future research, particularly in the context of COVID-19, where preliminary evidence has indicated impairment of the olfactory network and its association with cognitive functions[369, 251]. This could provide a unique model for understanding how neurophysiological symptoms manifest across psychological, physiological, and cognitive domains, offering further mechanistic support for the unitary brain hypothesis[125, 91].

7.6 Methodological considerations

Chapters 3 to 6 were based on the same post-COVID cohort, which has certain limitations. The research protocol evolved in response to the pandemic, leading to variations in the collection of clinical data, demographic information, and neuroimaging data from multiple sources over different timelines. As a result, there were significant amounts of missing data in some key domains, such as inflammatory markers, blood pressure, and pulmonary function. Patients were recruited either directly from the hospital, where some measures were taken prior to discharge, or from Long COVID clinics, where most participants were months post-acute infection. This discrepancy in timing means that some of the measures may not have been assessing the same constructs across all groups.

Furthermore, the absence of a control group for the imaging studies in Chapters 5 and 6 is a notable limitation. Our initial aim was to recruit well-matched controls, ensuring matching in age, gender, BMI, and medical history with each patient. However, compounded by the high exclusion rate for scanning safety reasons in 7-Tesla MRI, this approach proved inefficient and led to the exclusion of many potential controls during the first half of the recruitment process. Later in the study, we relaxed these requirements and sought uninfected individuals within a specific BMI range. However, by that stage, the majority of people in the UK had already been infected. We would recommend that future studies, particularly those conducted during dynamic situations like the COVID-19 pandemic, place greater emphasis on recruiting controls with less stringent criteria.

In Chapter 5, 18 ROIs were predefined, resulting in 153 features to be statistically tested. The selection of these regions presented a dilemma. The allo-intero network is not confined to a limited set of regions; rather, it encompasses multiple large networks, including the default mode network (DMN), salience network, and sensorimotor network. To capture a more comprehensive picture of the regions involved in respiratory regulation and perception, I ideally would have included additional areas, such as the thalamus, central amygdala, and secondary/associative sensory cortices. However, incorporating a larger number of

nodes would have inevitably increased the number of features (i.e., nodes x nodes) used to explain the outcome measure (breathlessness). This would have required more stringent multiple comparison corrections for univariate tests and would also have necessitated a larger sample size for running a multivariate analysis, which would have been the ideal approach. Interpretation of the current results should be approached with caution, as changes in the definition of masks (with some being as small as $4mm^3$) could significantly affect the results. This is a common issue in ROI-based fMRI studies. Future research employing a more sophisticated whole-brain voxel-wise approach and statistical testing may be able to further explore this issue.

It is important to note that the work presented in Chapter 2 was based on a secondary analysis of a study designed to address a different research question. Secondary analyses are inherently subject to several limitations. One such limitation is the choice of a healthy population for the original study. Our aim, however, was to explore neural dysfunction in the context of maladaptive tonic breathlessness. Investigating conditioned responses within a patient group could provide more relevant and translatable findings.

Another key issue arises from the timing of the imaging data collected in the original study, which pertains to the 'expression' of fear conditioning (referred to as the 'Aversive Delay-Conditioning Paradigm'). In examining the neural correlates of fear-conditioned responses, three phases are of particular interest: acquisition, expression, and extinction. Rather than focusing on the expression phase, I propose that the extinction phase is the most crucial, as it reflects neural activity and functional connectivity when an individual experiences breathlessness in the absence of a resistive load. This mirrors the clinical scenario in which breathlessness occurs despite well-functioning lungs. Understanding how a healthy brain unlearns the breathlessness response or executes safety learning is of paramount importance. The limitation of using data that only captures the expression of conditioned breathlessness restricts our ability to explore how the brain responds to a genuine respiratory threat in an adaptive manner.

Finally, although the task follows a consistent script and timing for stimuli (including both visual conditioned cues and resistive loads), the time taken between blocks, during which participants rate the 'anxiety' and 'intensity' of the resistive load, varies across subjects. This variability results in slight differences in the time series of the fMRI data for each subject. A uniform task stream would provide a more powered foundation for conducting data-driven analyses based on each voxel's time series, rather than relying on its contrasts of parameter estimates (COPE). For instance, time series-based clustering may enable better differentiation of subtle differences between amygdala subnuclei during the difference phases of the resistive breathing and its anticipation. Using decomposition

methods such as Independent Component Analysis (ICA) within an amygdala mask, the distinct role of the central nucleus could potentially emerge more clearly from the broader activation of the basolateral amygdala (BLA). This is particularly relevant given the large task-evoked cluster of BLA activation, extending into its superficial regions, observed using COPEs in Chapter 2. Future research designs should more carefully consider the necessity of introducing time-series variances within the task in the scanner, such as those arising from the act of providing ratings between blocks. This is particularly feasible in contexts where block-to-block changes in subjective ratings are not of interest, as in the study discussed in Chapter 2.

7.7 Final conclusion

Breathlessness can be distinguished between an adaptive phasic state and a maladaptive tonic state. I initially proposed a theoretical framework that conceptualises reflexive breathing, phasic and tonic breathlessness, and clarifies their relationship to affective components. Using task-based fMRI, I demonstrated that the BLA is involved in both the anticipation and perception of phasic breathlessness induced by breathing against an inspiratory load, with its functional connectivity to the mediodorsal thalamus during resistance potentially contributing to heightened anxiety in reporting. Through resting-state fMRI, I identified two pathways contributing to post-COVID tonic breathlessness. One pathway involves increased coupling between the BLA and dACC, potentially leading to the overactivation of affective processes. The other entailing a decoupling between the dPAG and PoI1, possibly reflects a diminished ability to integrate visceral respiratory signals. Both pathways represent maladaptations of gas-exchange regulation, preventing the resolution of respiratory regulation within the reflex arcs. Finally, I presented a methodological development chapter that demonstrated the potential for identifying meaningful post-COVID neurophysiological phenotypes by linking complex behavioural profiles with brain connectome data in a single multivariate model. By understanding the role of the amygdala and the broader allostatic and interoceptive networks in phasic and tonic breathlessness, I have re-conceptualised maladaptive breathlessness as either an 'affective disorder', 'a functional neurological disorder', or a combination of both. The distinction between these conditions, using the neural markers developed in this thesis, may facilitate a better stratification of breathlessness patients and offer opportunities for personalised treatment.

References

[1] (2021). Clinical characteristics and day-90 outcomes of 4244 critically ill adults with covid-19: a prospective cohort study. *Intensive care medicine*, 47:60–73.

[2] Abdallah, S. J., Faull, O. K., Wanigasekera, V., Finnegan, S. L., Jensen, D., and Pattinson, K. T. (2019). Opioids for breathlessness: psychological and neural factors influencing response variability. *European Respiratory Journal*, 54(3).

[3] Abidov, A., Rozanski, A., Hachamovitch, R., Hayes, S. W., Aboul-Enein, F., Cohen, I., Friedman, J. D., Germano, G., and Berman, D. S. (2005). Prognostic significance of dyspnea in patients referred for cardiac stress testing. *New England Journal of Medicine*, 353(18):1889–1898.

[4] Acheson, D. T., Forsyth, J. P., Prenoveau, J. M., and Bouton, M. E. (2007). Interoceptive fear conditioning as a learning model of panic disorder: An experimental evaluation using 20% co2-enriched air in a non-clinical sample. *Behaviour research and therapy*, 45(10):2280–2294.

[5] Adler, D., Herbelin, B., Similowski, T., and Blanke, O. (2014). Reprint of "breathing and sense of self: Visuo-respiratory conflicts alter body self-consciousness". *Respiratory physiology & neurobiology*, 204:131–137.

[6] Adolphs, R., Tranel, D., Damasio, H., and Damasio, A. (1994). Impaired recognition of emotion in facial expressions following bilateral damage to the human amygdala. *Nature*, 372(6507):669–672.

[7] Adrian, E. D. and Buytendijk, F. J. (1931). Potential changes in the isolated brain stem of the goldfish. *The Journal of physiology*, 71(2):121.

[8] Aghajani, M., Veer, I. M., Van Tol, M.-J., Aleman, A., Van Buchem, M. A., Veltman, D. J., Rombouts, S. A., and Van Der Wee, N. J. (2014). Neuroticism and extraversion are associated with amygdala resting-state functional connectivity. *Cognitive, Affective, & Behavioral Neuroscience*, 14:836–848.

[9] Aktaa, S., Wu, J., Nadarajah, R., Rashid, M., de Belder, M., Deanfield, J., Mamas, M. A., and Gale, C. P. (2021). Incidence and mortality due to thromboembolic events during the covid-19 pandemic: Multi-sourced population-based health records cohort study. *Thrombosis research*, 202:17–23.

[10] Aleksandrov, V., Ivanova, T., and Aleksandrova, N. (2007). Prefrontal control of respiration. *Journal of Physiology and Pharmacology*, 58(5):17–23.

[11] Allen, M., Levy, A., Parr, T., and Friston, K. J. (2022). In the body's eye: the computational anatomy of interoceptive inference. *PLoS Computational Biology*, 18(9):e1010490.

[12] Amano, T., Duvarci, S., Popa, D., and Paré, D. (2011). The fear circuit revisited: contributions of the basal amygdala nuclei to conditioned fear. *Journal of Neuroscience*, 31(43):15481–15489.

[13] Amunts, K., Mohlberg, H., Bludau, S., and Zilles, K. (2020). Julich-brain: A 3d probabilistic atlas of the human brain's cytoarchitecture. *Science*, 369(6506):988–992.

[14] Anand, A., Li, Y., Wang, Y., Wu, J., Gao, S., Bukhari, L., Mathews, V. P., Kalnin, A., and Lowe, M. J. (2005). Activity and connectivity of brain mood regulating circuit in depression: a functional magnetic resonance study. *Biological psychiatry*, 57(10):1079–1088.

[15] Anand, B. and Dua, S. (1956). Circulatory and respiratory changes induced by electrical stimulation of limbic system (visceral brain). *Journal of neurophysiology*, 19(5):393–400.

[16] Andersson, J. L., Jenkinson, M., Smith, S., et al. (2007). Non-linear registration, aka spatial normalisation fmrib technical report tr07ja2. *FMRIB Analysis Group of the University of Oxford*, 2(1).

[17] Ang, Y.-S., Lockwood, P., Apps, M. A., Muhammed, K., and Husain, M. (2017). Distinct subtypes of apathy revealed by the apathy motivation index. *PloS one*, 12(1):e0169938.

[18] Applegate, C. D., Kapp, B. S., Underwood, M. D., and McNall, C. L. (1983). Autonomic and somatomotor effects of amygdala central n. stimulation in awake rabbits. *Physiology & Behavior*, 31(3):353–360.

[19] Ashhad, S., Kam, K., Del Negro, C. A., and Feldman, J. L. (2022). Breathing rhythm and pattern and their influence on emotion. *Annual review of neuroscience*, 45(1):223–247.

[20] Attwell, D. and Laughlin, S. B. (2001). An energy budget for signaling in the grey matter of the brain. *Journal of Cerebral Blood Flow & Metabolism*, 21(10):1133–1145.

[21] Bailey, P. H. (2004). The dyspnea-anxiety-dyspnea cycle—copd patients' stories of breathlessness:"it's scary/when you can't breathe". *Qualitative health research*, 14(6):760–778.

[22] Banzett, R. B., Sheridan, A. R., Baker, K. M., Lansing, R. W., and Stevens, J. P. (2020). 'scared to death'dyspnoea from the hospitalised patient's perspective. *BMJ Open Respiratory Research*, 7(1):e000493.

[23] Barbas, H. (2015). General cortical and special prefrontal connections: principles from structure to function. *Annual review of neuroscience*, 38(1):269–289.

[24] Barger, N., Stefanacci, L., and Semendeferi, K. (2007). A comparative volumetric analysis of the amygdaloid complex and basolateral division in the human and ape brain. *American Journal of Physical Anthropology*, 134(3):392–403.

[25] Barnes, P. J., Szefler, S. J., Reddel, H. K., and Chipps, B. E. (2019). Symptoms and perception of airway obstruction in asthmatic patients: clinical implications for use of reliever medications. *Journal of Allergy and Clinical Immunology*, 144(5):1180–1186.

[26] Barrett, L. F. (2017). The theory of constructed emotion: an active inference account of interoception and categorization. *Social cognitive and affective neuroscience*, 12(1):1–23.

[27] Barrett, L. F. and Simmons, W. K. (2015). Interoceptive predictions in the brain. *Nature reviews neuroscience*, 16(7):419–429.

[28] Bastos, A. M., Usrey, W. M., Adams, R. A., Mangun, G. R., Fries, P., and Friston, K. J. (2012). Canonical microcircuits for predictive coding. *Neuron*, 76(4):695–711.

[29] Benedetti, F., Lanotte, M., Lopiano, L., and Colloca, L. (2007). When words are painful: unraveling the mechanisms of the nocebo effect. *Neuroscience*, 147(2):260–271.

[30] Benedetti, F., Palladini, M., Paolini, M., Melloni, E., Vai, B., De Lorenzo, R., Furlan, R., Rovere-Querini, P., Falini, A., and Mazza, M. G. (2021). Brain correlates of depression, post-traumatic distress, and inflammatory biomarkers in covid-19 survivors: a multimodal magnetic resonance imaging study. *Brain, behavior, & immunity-health*, 18:100387.

[31] Benke, C., Alius, M. G., Hamm, A. O., and Pané-Farré, C. A. (2018). Cue and context conditioning to respiratory threat: effects of suffocation fear and implications for the etiology of panic disorder. *International journal of psychophysiology*, 124:33–42.

[32] Bijsterbosch, J. D., Ansari, T. L., Smith, S., Gauld, O., Zika, O., Boessenkool, S., Browning, M., Reinecke, A., and Bishop, S. J. (2018). Stratification of mdd and gad patients by resting state brain connectivity predicts cognitive bias. *NeuroImage: Clinical*, 19:425–433.

[33] Billot, B., Bocchetta, M., Todd, E., Dalca, A. V., Rohrer, J. D., and Iglesias, J. E. (2020). Automated segmentation of the hypothalamus and associated subunits in brain mri. *Neuroimage*, 223:117287.

[34] Binks, A. P., Evans, K. C., Reed, J. D., Moosavi, S. H., and Banzett, R. B. (2014). The time-course of cortico-limbic neural responses to air hunger. *Respiratory physiology & neurobiology*, 204:78–85.

[35] Bogaerts, K., Notebaert, K., Van Diest, I., De Peuter, S., Devriese, S., and Van den Bergh, O. (2006). Accuracy of respiratory symptom perception in different affective contexts. *Biological Psychology*, 72(2):237–238.

[36] Boorman, L., Kennerley, A. J., Johnston, D., Jones, M., Zheng, Y., Redgrave, P., and Berwick, J. (2010). Negative blood oxygen level dependence in the rat: a model for investigating the role of suppression in neurovascular coupling. *Journal of Neuroscience*, 30(12):4285–4294.

[37] Booth, S., Moosavi, S. H., and Higginson, I. J. (2008). The etiology and management of intractable breathlessness in patients with advanced cancer: a systematic review of pharmacological therapy. *Nature Clinical Practice Oncology*, 5(2):90–100.

[38] Boubela, R. N., Kalcher, K., Huf, W., Seidel, E.-M., Derntl, B., Pezawas, L., Našel, C., and Moser, E. (2015). fmri measurements of amygdala activation are confounded by stimulus correlated signal fluctuation in nearby veins draining distant brain regions. *Scientific reports*, 5(1):10499.

[39] Brabec, J., Rulseh, A., Hoyt, B., Vizek, M., Horinek, D., Hort, J., and Petrovicky, P. (2010). Volumetry of the human amygdala—an anatomical study. *Psychiatry Research: Neuroimaging*, 182(1):67–72.

[40] Brenes, G. A. (2003). Anxiety and chronic obstructive pulmonary disease: prevalence, impact, and treatment. *Psychosomatic medicine*, 65(6):963–970.

[41] Broadbent, D. E., Cooper, P. F., FitzGerald, P., and Parkes, K. R. (1982). The cognitive failures questionnaire (cfq) and its correlates. *British journal of clinical psychology*, 21(1):1–16.

[42] Brooks, J. C., Beckmann, C. F., Miller, K. L., Wise, R. G., Porro, C. A., Tracey, I., and Jenkinson, M. (2008). Physiological noise modelling for spinal functional magnetic resonance imaging studies. *Neuroimage*, 39(2):680–692.

[43] Burgel, P.-R., Escamilla, R., Perez, T., Carré, P., Caillaud, D., Chanez, P., Pinet, C., Jebrak, G., Brinchault, G., Court-Fortune, I., et al. (2013). Impact of comorbidities on copd-specific health-related quality of life. *Respiratory medicine*, 107(2):233–241.

[44] Butowt, R. and von Bartheld, C. S. (2021). Anosmia in covid-19: underlying mechanisms and assessment of an olfactory route to brain infection. *The Neuroscientist*, 27(6):582–603.

[45] Buxton, R. B., Uludağ, K., Dubowitz, D. J., and Liu, T. T. (2004). Modeling the hemodynamic response to brain activation. *Neuroimage*, 23:S220–S233.

[46] Buzsáki, G. (2002). Theta oscillations in the hippocampus. *Neuron*, 33(3):325–340.

[47] Carfì, A., Bernabei, R., Landi, F., et al. (2020). Persistent symptoms in patients after acute covid-19. *Jama*, 324(6):603–605.

[48] Carrieri-Kohlman, V., Donesky-Cuenco, D., Park, S. K., Mackin, L., Nguyen, H. Q., and Paul, S. M. (2010). Additional evidence for the affective dimension of dyspnea in patients with copd. *Research in nursing & health*, 33(1):4–19.

[49] Cavicchioli, M., Ferrucci, R., Guidetti, M., Canevini, M. P., Pravettoni, G., and Galli, F. (2021). What will be the impact of the covid-19 quarantine on psychological distress? considerations based on a systematic review of pandemic outbreaks. In *Healthcare*, volume 9, page 101. MDPI.

[50] Cénat, J. M., Blais-Rochette, C., Kokou-Kpolou, C. K., Noorishad, P.-G., Mukunzi, J. N., McIntee, S.-E., Dalexis, R. D., Goulet, M.-A., and Labelle, P. R. (2021). Prevalence of symptoms of depression, anxiety, insomnia, posttraumatic stress disorder, and psychological distress among populations affected by the covid-19 pandemic: A systematic review and meta-analysis. *Psychiatry research*, 295:113599.

[51] Chang, C. and Glover, G. H. (2009). Relationship between respiration, end-tidal co2, and bold signals in resting-state fmri. *Neuroimage*, 47(4):1381–1393.

[52] Chavannes, N. H., Huibers, M., Schermer, T., Hendriks, A., Van Weel, C., Wouters, E., and Van Schayck, C. (2005). Associations of depressive symptoms with gender, body mass index and dyspnea in primary care copd patients. *Family Practice*, 22(6):604–607.

[53] Chi, V. N., Müller, C., Wolfenstetter, T., Yanovsky, Y., Draguhn, A., Tort, A. B., and Brankačk, J. (2016). Hippocampal respiration-driven rhythm distinct from theta oscillations in awake mice. *Journal of Neuroscience*, 36(1):162–177.

[54] Choi, Y. and Lee, M. K. (2020). Neuroimaging findings of brain mri and ct in patients with covid-19: A systematic review and meta-analysis. *European journal of radiology*, 133:109393.

[55] Chopra, V., Flanders, S. A., O'Malley, M., Malani, A. N., and Prescott, H. C. (2021). Sixty-day outcomes among patients hospitalized with covid-19. *Annals of internal medicine*, 174(4):576–578.

[56] Churchill, N. W., Roudaia, E., Chen, J. J., Gilboa, A., Sekuler, A., Ji, X., Gao, F., Lin, Z., Jegatheesan, A., Masellis, M., et al. (2023). Effects of post-acute covid-19 syndrome on the functional brain networks of non-hospitalized individuals. *Frontiers in Neurology*, 14:1136408.

[57] Ciumas, C., Rheims, S., and Ryvlin, P. (2022). fmri studies evaluating central respiratory control in humans. *Frontiers in Neural Circuits*, 16:982963.

[58] Clark, L. A. and Watson, D. (1991). Tripartite model of anxiety and depression: psychometric evidence and taxonomic implications. *Journal of abnormal psychology*, 100(3):316.

[59] Clarke, W. T., Mougin, O., Driver, I. D., Rua, C., Morgan, A. T., Asghar, M., Clare, S., Francis, S., Wise, R. G., Rodgers, C. T., et al. (2020). Multi-site harmonization of 7 tesla mri neuroimaging protocols. *Neuroimage*, 206:116335.

[60] Cohen, S., Kamarck, T., and Mermelstein, R. (1983). A global measure of perceived stress. *Journal of health and social behavior*, pages 385–396.

[61] Colebatch, J., Adams, L., Murphy, K., Martin, A., Lammertsma, A., Tochon-Danguy, H., Clark, J., Friston, K., and Guz, A. (1991). Regional cerebral blood flow during volitional breathing in man. *The Journal of physiology*, 443(1):91–103.

[62] Colgin, L. L. (2013). Mechanisms and functions of theta rhythms. *Annual review of neuroscience*, 36(1):295–312.

[63] Colombo, M., Elkin, L., and Hartmann, S. (2021). Being realist about bayes, and the predictive processing theory of mind. *The British Journal for the Philosophy of Science*.

[64] Colombo, M. and Seriès, P. (2012). Bayes in the brain—on bayesian modelling in neuroscience. *The British journal for the philosophy of science*.

[65] Conant, R. C. and Ross Ashby, W. (1970). Every good regulator of a system must be a model of that system. *International journal of systems science*, 1(2):89–97.

[66] Corfield, D., Fink, G., Ramsay, S., Murphy, K., Harty, H., Watson, J., Adams, L., Frackowiak, R., and Guz, A. (1995). Evidence for limbic system activation during co2-stimulated breathing in man. *The Journal of physiology*, 488(1):77–84.

[67] Craig, A. D. (2002). How do you feel? interoception: the sense of the physiological condition of the body. *Nature reviews neuroscience*, 3(8):655–666.

[68] Craig, A. D. (2003). Interoception: the sense of the physiological condition of the body. *Current opinion in neurobiology*, 13(4):500–505.

[69] Craig, A. D. (2014). How do you feel?: an interoceptive moment with your neurobiological self. In *How Do You Feel?* Princeton University Press.

[70] Critchley, H. D. and Garfinkel, S. N. (2017). Interoception and emotion. *Current opinion in psychology*, 17:7–14.

[71] Culver, B. H., Graham, B. L., Coates, A. L., Wanger, J., Berry, C. E., Clarke, P. K., Hallstrand, T. S., Hankinson, J. L., Kaminsky, D. A., MacIntyre, N. R., et al. (2017). Recommendations for a standardized pulmonary function report. an official american thoracic society technical statement. *American journal of respiratory and critical care medicine*, 196(11):1463–1472.

[72] Currow, D. C., Chang, S., Reddel, H. K., Kochovska, S., Ferreira, D., Kinchin, I., Johnson, M., and Ekström, M. (2020). Breathlessness, anxiety, depression, and function–the bad-f study: a cross-sectional and population prevalence study in adults. *Journal of pain and symptom management*, 59(2):197–205.

[73] Dagli, M. S., Ingeholm, J. E., and Haxby, J. V. (1999). Localization of cardiac-induced signal change in fmri. *Neuroimage*, 9(4):407–415.

[74] Davenport, P., Davenport, M., Feinstein, J., Khalsa, S., and Von Leupoldt, A. (2019). Perception of intensity and unpleasantness for 10-breath inspiratory resistive loads: effect of sex, smoking and insula/amygdala lesion.

[75] Davenport, P. W. and Vovk, A. (2009). Cortical and subcortical central neural pathways in respiratory sensations. *Respiratory physiology & neurobiology*, 167(1):72–86.

[76] Davis, H. E., Assaf, G. S., McCorkell, L., Wei, H., Low, R. J., Re'em, Y., Redfield, S., Austin, J. P., and Akrami, A. (2021). Characterizing long covid in an international cohort: 7 months of symptoms and their impact. *EClinicalMedicine*, 38.

[77] De Cort, K., Griez, E., Büchler, M., and Schruers, K. (2012). The role of "interoceptive" fear conditioning in the development of panic disorder. *Behavior Therapy*, 43(1):203–215.

[78] De Peuter, S., Janssens, T., Van Diest, I., Stans, L., Troosters, T., Decramer, M., Van den Bergh, O., and Vlaeyen, J. W. (2011). Dyspnea-related anxiety: the dutch version of the breathlessness beliefs questionnaire. *Chronic respiratory disease*, 8(1):11–19.

[79] De Peuter, S., Victoir, A., Lemaigre, V., Van Diest, I., Verleden, G., Demedts, M., and Van den Bergh, O. (2006). Catastrophic thinking and symptom perception in asthma: validation of a questionnaire. *The Internet Journal of Asthma, Allergy and Immunology*, 5.

[80] De Ridder, D., Vanneste, S., Kovacs, S., Sunaert, S., and Dom, G. (2011). Transient alcohol craving suppression by rtms of dorsal anterior cingulate: an fmri and loreta eeg study. *Neuroscience letters*, 496(1):5–10.

[81] Deer, R. R., Rock, M. A., Vasilevsky, N., Carmody, L., Rando, H., Anzalone, A. J., Basson, M. D., Bennett, T. D., Bergquist, T., Boudreau, E. A., et al. (2021). Characterizing long covid: deep phenotype of a complex condition. *EBioMedicine*, 74.

[82] Devi, R., Lepsien, J., Lorenz, K., Schlumm, T., Mildner, T., and Möller, H. E. (2022). Multi-echo investigations of positive and negative cbf and concomitant bold changes. *NeuroImage*, 263:119661.

[83] Devonshire, I. M., Papadakis, N. G., Port, M., Berwick, J., Kennerley, A. J., Mayhew, J. E., and Overton, P. G. (2012). Neurovascular coupling is brain region-dependent. *Neuroimage*, 59(3):1997–2006.

[84] Devriese, S., Winters, W., Stegen, K., Van Diest, I., Veulemans, H., Nemery, B., Eelen, P., Van de Woestijne, K., and Van den Bergh, O. (2000). Generalization of acquired somatic symptoms in response to odors: a pavlovian perspective on multiple chemical sensitivity. *Psychosomatic Medicine*, 62(6):751–759.

[85] Di Marco, F., Verga, M., Reggente, M., Casanova, F. M., Santus, P., Blasi, F., Allegra, L., and Centanni, S. (2006). Anxiety and depression in copd patients: the roles of gender and disease severity. *Respiratory medicine*, 100(10):1767–1774.

[86] Díez-Cirarda, M., Yus, M., Gómez-Ruiz, N., Polidura, C., Gil-Martínez, L., Delgado-Alonso, C., Jorquera, M., Gómez-Pinedo, U., Matias-Guiu, J., Arrazola, J., et al. (2023). Multimodal neuroimaging in post-covid syndrome and correlation with cognition. *Brain*, 146(5):2142–2152.

[87] Djärv, T., Metcalfe, C., Avery, K. N., Lagergren, P., and Blazeby, J. M. (2010). Prognostic value of changes in health-related quality of life scores during curative treatment for esophagogastric cancer. *Journal of Clinical Oncology*, 28(10):1666–1670.

[88] Dlouhy, B. J., Gehlbach, B. K., Kreple, C. J., Kawasaki, H., Oya, H., Buzza, C., Granner, M. A., Welsh, M. J., Howard, M. A., Wemmie, J. A., et al. (2015). Breathing inhibited when seizures spread to the amygdala and upon amygdala stimulation. *Journal of Neuroscience*, 35(28):10281–10289.

[89] Douaud, G., Lee, S., Alfaro-Almagro, F., Arthofer, C., Wang, C., McCarthy, P., Lange, F., Andersson, J. L., Griffanti, L., Duff, E., et al. (2022). Sars-cov-2 is associated with changes in brain structure in uk biobank. *Nature*, 604(7907):697–707.

[90] Doya, K. (2007). *Bayesian brain: Probabilistic approaches to neural coding*. MIT press.

[91] Eccles, J. C. (1990). A unitary hypothesis of mind-brain interaction in the cerebral cortex. *Proceedings of the Royal Society of London. B. Biological Sciences*, 240(1299):433–451.

[92] Egbert, A. R., Cankurtaran, S., and Karpiak, S. (2020). Brain abnormalities in covid-19 acute/subacute phase: a rapid systematic review. *Brain, behavior, and immunity*, 89:543–554.

[93] Eisner, M. D., Blanc, P. D., Yelin, E. H., Katz, P. P., Sanchez, G., Iribarren, C., and Omachi, T. A. (2010). Influence of anxiety on health outcomes in copd. *Thorax*, 65(3):229–234.

[94] Ekstrom, A. (2010). How and when the fmri bold signal relates to underlying neural activity: the danger in dissociation. *Brain research reviews*, 62(2):233–244.

[95] Ekström, M. P., Abernethy, A. P., and Currow, D. C. (2015). The management of chronic breathlessness in patients with advanced and terminal illness. *bmj*, 349.

[96] Elliott, L. T., Sharp, K., Alfaro-Almagro, F., Shi, S., Miller, K. L., Douaud, G., Marchini, J., and Smith, S. M. (2018a). Genome-wide association studies of brain imaging phenotypes in uk biobank. *Nature*, 562(7726):210–216.

[97] Elliott, M. L., Romer, A., Knodt, A. R., and Hariri, A. R. (2018b). A connectome-wide functional signature of transdiagnostic risk for mental illness. *Biological psychiatry*, 84(6):452–459.

[98] Esposito, F., Cirillo, M., De Micco, R., Caiazzo, G., Siciliano, M., Russo, A. G., Monari, C., Coppola, N., Tedeschi, G., and Tessitore, A. (2022). Olfactory loss and brain connectivity after covid-19. *Human Brain Mapping*, 43(5):1548–1560.

[99] Etkin, A., Prater, K. E., Hoeft, F., Menon, V., and Schatzberg, A. F. (2010). Failure of anterior cingulate activation and connectivity with the amygdala during implicit regulation of emotional processing in generalized anxiety disorder. *American Journal of Psychiatry*, 167(5):545–554.

[100] Etkin, A., Prater, K. E., Schatzberg, A. F., Menon, V., and Greicius, M. D. (2009). Disrupted amygdalar subregion functional connectivity and evidence of a compensatory network in generalized anxiety disorder. *Archives of general psychiatry*, 66(12):1361–1372.

[101] Etkin, A. and Wager, T. D. (2007). Functional neuroimaging of anxiety: a meta-analysis of emotional processing in ptsd, social anxiety disorder, and specific phobia. *American journal of Psychiatry*, 164(10):1476–1488.

[102] Evans, K. C. (2010). Cortico-limbic circuitry and the airways: insights from functional neuroimaging of respiratory afferents and efferents. *Biological psychology*, 84(1):13–25.

[103] Evans, K. C., Banzett, R. B., Adams, L., Mckay, L., Frackowiak, R. S., and Corfield, D. R. (2002). Bold fmri identifies limbic, paralimbic, and cerebellar activation during air hunger. *Journal of neurophysiology*, 88(3):1500–1511.

[104] Evans, R. A., Leavy, O. C., Richardson, M., Elneima, O., McAuley, H. J., Shikotra, A., Singapuri, A., Sereno, M., Saunders, R. M., Harris, V. C., et al. (2022). Clinical characteristics with inflammation profiling of long covid and association with 1-year recovery following hospitalisation in the uk: a prospective observational study. *The Lancet Respiratory Medicine*, 10(8):761–775.

[105] Fan, F. C., Zhang, S. Y., and Cheng, Y. (2021). Incidence of psychological illness after coronavirus outbreak: a meta-analysis study. *J Epidemiol Community Health*, 75(9):836–842.

[106] Fanselow, M. S. (1998). Pavlovian conditioning, negative feedback, and blocking: mechanisms that regulate association formation. *Neuron*, 20(4):625–627.

[107] Fanselow, M. S. and Gale, G. D. (2003). The amygdala, fear, and memory. *Annals of the New York Academy of Sciences*, 985(1):125–134.

[108] Fanselow, M. S. and LeDoux, J. E. (1999). Why we think plasticity underlying pavlovian fear conditioning occurs in the basolateral amygdala. *Neuron*, 23(2):229–232.

[109] Faull, O. (2015). *The Role of the Periaqueductal Gray in Respiratory Control and Breathlessness*. Phd thesis, University of Oxford.

[110] Faull, O. K., Cox, P. J., and Pattinson, K. T. (2016a). Psychophysical differences in ventilatory awareness and breathlessness between athletes and sedentary individuals. *Frontiers in Physiology*, 7:231.

[111] Faull, O. K., Cox, P. J., and Pattinson, K. T. (2018). Cortical processing of breathing perceptions in the athletic brain. *Neuroimage*, 179:92–101.

[112] Faull, O. K., Hayen, A., and Pattinson, K. T. (2017). Breathlessness and the body: neuroimaging clues for the inferential leap. *Cortex*, 95:211–221.

[113] Faull, O. K., Jenkinson, M., Ezra, M., and Pattinson, K. T. (2016b). Conditioned respiratory threat in the subdivisions of the human periaqueductal gray. *Elife*, 5:e12047.

[114] Faull, O. K. and Pattinson, K. T. (2017). The cortical connectivity of the periaqueductal gray and the conditioned response to the threat of breathlessness. *Elife*, 6:e21749.

[115] Feinstein, J. S., Gould, D., and Khalsa, S. S. (2022). Amygdala-driven apnea and the chemoreceptive origin of anxiety. *Biological psychology*, 170:108305.

[116] Fernández-de Las-Peñas, C., Notarte, K. I., Peligro, P. J., Velasco, J. V., Ocampo, M. J., Henry, B. M., Arendt-Nielsen, L., Torres-Macho, J., and Plaza-Manzano, G. (2022). Long-covid symptoms in individuals infected with different sars-cov-2 variants of concern: a systematic review of the literature. *Viruses*, 14(12):2629.

[117] Ferri, J., Schmidt, J., Hajcak, G., and Canli, T. (2016). Emotion regulation and amygdala-precuneus connectivity: Focusing on attentional deployment. *Cognitive, Affective, & Behavioral Neuroscience*, 16:991–1002.

[118] Figarska, S. M., Boezen, H. M., and Vonk, J. M. (2012). Dyspnea severity, changes in dyspnea status and mortality in the general population: the vlagtwedde/vlaardingen study. *European journal of epidemiology*, 27:867–876.

[119] Finger, S. (2000). *Minds behind the brain: A history of the pioneers and their discoveries*. Oxford University Press.

[120] Fink, G., Adams, L., Watson, J., Innes, J., Wuyam, B., Kobayashi, I., Corfield, D., Murphy, K., Jones, T., and Frackowiak, R. (1995). Hyperpnoea during and immediately after exercise in man: evidence of motor cortical involvement. *The Journal of physiology*, 489(3):663–675.

[121] Floresco, S. B., West, A. R., Ash, B., Moore, H., and Grace, A. A. (2003). Afferent modulation of dopamine neuron firing differentially regulates tonic and phasic dopamine transmission. *Nature neuroscience*, 6(9):968–973.

[122] Fontanini, A., Spano, P., and Bower, J. M. (2003). Ketamine-xylazine-induced slow (< 1.5 hz) oscillations in the rat piriform (olfactory) cortex are functionally correlated with respiration. *Journal of Neuroscience*, 23(22):7993–8001.

[123] Fox, M. D. and Greicius, M. (2010). Clinical applications of resting state functional connectivity. *Frontiers in systems neuroscience*, 4:1443.

[Fraser et al.] Fraser, E., Ng, K., Saunders, L., Grist, J., Collier, G., Strickland, S., Gustafsson, L., Smith, L., Evans, R., Vuddamalay, N., et al. Hyperpolarised xenon magnetic resonance pulmonary imaging in patients with long-covid (explain): Lung diffusion findings.

[125] Friston, K. (2010). The free-energy principle: a unified brain theory? *Nature reviews neuroscience*, 11(2):127–138.

[126] Friston, K. J. (2013). The fantastic organ. *Brain*, 136(4):1328–1332.

[127] Friston, K. J., Buechel, C., Fink, G. R., Morris, J., Rolls, E., and Dolan, R. J. (1997). Psychophysiological and modulatory interactions in neuroimaging. *Neuroimage*, 6(3):218–229.

[128] Friston, K. J., Penny, W., Phillips, C., Kiebel, S., Hinton, G., and Ashburner, J. (2002). Classical and bayesian inference in neuroimaging: theory. *NeuroImage*, 16(2):465–483.

[129] Frostad, A., Søyseth, V., Andersen, A., and Gulsvik, A. (2006). Respiratory symptoms as predictors of all-cause mortality in an urban community: a 30-year follow-up. *Journal of internal medicine*, 259(5):520–529.

[130] Frysinger, R. C. and Harper, R. M. (1989). Cardiac and respiratory correlations with unit discharge in human amygdala and hippocampus. *Electroencephalography and clinical neurophysiology*, 72(6):463–470.

[131] Frysinger, R. C., Zhang, J., and Harper, R. M. (1988). Cardiovascular and respiratory relationships with neuronal discharge in the central nucleus of the amygdala during sleep-waking states. *Sleep*, 11(4):317–332.

[132] Fu, Z., Tu, Y., Calhoun, V. D., Zhang, Y., Zhao, Q., Chen, J., Meng, Q., Lu, Z., and Hu, L. (2021). Dynamic functional network connectivity associated with post-traumatic stress symptoms in covid-19 survivors. *Neurobiology of stress*, 15:100377.

[133] Fumoto, M., Sato-Suzuki, I., Seki, Y., Mohri, Y., and Arita, H. (2004). Appearance of high-frequency alpha band with disappearance of low-frequency alpha band in eeg is produced during voluntary abdominal breathing in an eyes-closed condition. *Neuroscience research*, 50(3):307–317.

[134] Gamberini, L., Mazzoli, C. A., Sintonen, H., Colombo, D., Scaramuzzo, G., Allegri, D., Tonetti, T., Zani, G., Capozzi, C., Giampalma, E., et al. (2021). Quality of life of covid-19 critically ill survivors after icu discharge: 90 days follow-up. *Quality of Life Research*, 30:2805–2817.

[135] Gandevia, S. and Rothwell, J. (1987). Activation of the human diaphragm from the motor cortex. *The Journal of physiology*, 384(1):109–118.

[136] Garrigues, E., Janvier, P., Kherabi, Y., Le Bot, A., Hamon, A., Gouze, H., Doucet, L., Berkani, S., Oliosi, E., Mallart, E., et al. (2020). Post-discharge persistent symptoms and health-related quality of life after hospitalization for covid-19. *Journal of Infection*, 81(6):e4–e6.

[137] Ge, T., Holmes, A. J., Buckner, R. L., Smoller, J. W., and Sabuncu, M. R. (2017). Heritability analysis with repeat measurements and its application to resting-state functional connectivity. *Proceedings of the National Academy of Sciences*, 114(21):5521–5526.

[138] Glasser, M. F., Coalson, T. S., Robinson, E. C., Hacker, C. D., Harwell, J., Yacoub, E., Ugurbil, K., Andersson, J., Beckmann, C. F., Jenkinson, M., et al. (2016). A multi-modal parcellation of human cerebral cortex. *Nature*, 536(7615):171–178.

[139] Glover, G. H., Li, T.-Q., and Ress, D. (2000). Image-based method for retrospective correction of physiological motion effects in fmri: Retroicor. *Magnetic Resonance in Medicine: An Official Journal of the International Society for Magnetic Resonance in Medicine*, 44(1):162–167.

[140] Goense, J., Merkle, H., and Logothetis, N. K. (2012). High-resolution fmri reveals laminar differences in neurovascular coupling between positive and negative bold responses. *Neuron*, 76(3):629–639.

[141] Goldberger, J., Hinton, G. E., Roweis, S., and Salakhutdinov, R. R. (2004). Neighbourhood components analysis. *Advances in neural information processing systems*, 17.

[142] Grace, A. A. (1991). Phasic versus tonic dopamine release and the modulation of dopamine system responsivity: a hypothesis for the etiology of schizophrenia. *Neuroscience*, 41(1):1–24.

[143] Greening, S. G. and Mitchell, D. G. (2015). A network of amygdala connections predict individual differences in trait anxiety. *Human brain mapping*, 36(12):4819–4830.

[144] Greicius, M. (2008). Resting-state functional connectivity in neuropsychiatric disorders. *Current opinion in neurology*, 21(4):424–430.

[145] Greve, D. N. and Fischl, B. (2009). Accurate and robust brain image alignment using boundary-based registration. *Neuroimage*, 48(1):63–72.

[146] Griffanti, L., Salimi-Khorshidi, G., Beckmann, C. F., Auerbach, E. J., Douaud, G., Sexton, C. E., Zsoldos, E., Ebmeier, K. P., Filippini, N., Mackay, C. E., et al. (2014). Ica-based artefact removal and accelerated fmri acquisition for improved resting state network imaging. *Neuroimage*, 95:232–247.

[147] Grist, J. T., Chen, M., Collier, G. J., Raman, B., Abueid, G., McIntyre, A., Matthews, V., Fraser, E., Ho, L.-P., Wild, J. M., et al. (2021). Hyperpolarized 129xe mri abnormalities in dyspneic patients 3 months after covid-19 pneumonia: preliminary results. *Radiology*, 301(1):E353–E360.

[148] Grist, J. T., Collier, G. J., Walters, H., Kim, M., Chen, M., Abu Eid, G., Laws, A., Matthews, V., Jacob, K., Cross, S., et al. (2022). Lung abnormalities detected with hyperpolarized 129xe mri in patients with long covid. *Radiology*, 305(3):709–717.

[149] Grønseth, R., Vollmer, W. M., Hardie, J. A., Ólafsdóttir, I. S., Lamprecht, B., Buist, A. S., Gnatiuc, L., Gulsvik, A., Johannessen, A., and Enright, P. (2014). Predictors of dyspnoea prevalence: results from the bold study. *European Respiratory Journal*, 43(6):1610–1620.

[150] Grosbois, J.-M., Gephine, S., Kyheng, M., Henguelle, J., Le Rouzic, O., Saey, D., Maltais, F., and Chenivesse, C. (2022). Physical and affective components of dyspnoea are improved by pulmonary rehabilitation in copd. *BMJ open respiratory research*, 9(1):e001160.

[151] Gu, X., Hof, P. R., Friston, K. J., and Fan, J. (2013). Anterior insular cortex and emotional awareness. *Journal of Comparative Neurology*, 521(15):3371–3388.

[152] Guillery, R. and Sherman, S. (2002). The thalamus as a monitor of motor outputs. *Philosophical Transactions of the Royal Society of London. Series B: Biological Sciences*, 357(1428):1809–1821.

[153] Gysels, M. and Higginson, I. J. (2008). Access to services for patients with chronic obstructive pulmonary disease: the invisibility of breathlessness. *Journal of pain and symptom management*, 36(5):451–460.

[154] Haberly, L. B. and Price, J. L. (1978). Association and commissural fiber systems of the olfactory cortex of the rat. i. systems originating in the piriform cortex and adjacent areas. *Journal of Comparative Neurology*, 178(4):711–740.

[155] Halpin, S., O'Connor, R., and Sivan, M. (2021a). Long covid and chronic covid syndromes. *Journal of medical virology*, 93(3):1242.

[156] Halpin, S. J., McIvor, C., Whyatt, G., Adams, A., Harvey, O., McLean, L., Walshaw, C., Kemp, S., Corrado, J., Singh, R., et al. (2021b). Postdischarge symptoms and rehabilitation needs in survivors of covid-19 infection: A cross-sectional evaluation. *Journal of medical virology*, 93(2):1013–1022.

[157] Hampshire, A., Azor, A., Atchison, C., Trender, W., Hellyer, P. J., Giunchiglia, V., Husain, M., Cooke, G. S., Cooper, E., Lound, A., et al. (2024). Cognition and memory after covid-19 in a large community sample. *New England Journal of Medicine*, 390(9):806–818.

[158] Hampshire, A., Trender, W., Chamberlain, S. R., Jolly, A. E., Grant, J. E., Patrick, F., Mazibuko, N., Williams, S. C., Barnby, J. M., Hellyer, P., et al. (2021). Cognitive deficits in people who have recovered from covid-19. *EClinicalMedicine*, 39.

[159] Han, J.-n., Zhu, Y.-j., Li, S.-w., Luo, D.-m., Hu, Z., Van Diest, I., De Peuter, S., Van de Woestijne, K., and Van den Bergh, O. (2004). Medically unexplained dyspnea: psychophysiological characteristics and role of breathing therapy. *Chinese medical journal*, 117(01):6–13.

[160] Han, J.-n., Zhu, Y.-j., Luo, D.-m., Li, S.-w., Van Diest, I., Van den Bergh, O., and Van de Woestijne, K. P. (2008). Fearful imagery induces hyperventilation and dyspnea in medically unexplained dyspnea. *Chinese medical journal*, 121(1):56–62.

[161] Handwerker, D. A., Ollinger, J. M., and D'Esposito, M. (2004). Variation of bold hemodynamic responses across subjects and brain regions and their effects on statistical analyses. *Neuroimage*, 21(4):1639–1651.

[162] Harel, N., Lee, S.-P., Nagaoka, T., Kim, D.-S., and Kim, S.-G. (2002). Origin of negative blood oxygenation level—dependent fmri signals. *Journal of cerebral blood flow & metabolism*, 22(8):908–917.

[163] Harper, R., Frysinger, R., Trelease, R., and Marks, J. (1984). State-dependent alteration of respiratory cycle timing by stimulation of the central nucleus of the amygdala. *Brain research*, 306(1-2):1–8.

[164] Harper, R. M., Poe, G. R., Rector, D. M., and Kristensen, M. P. (1998). Relationships between hippocampal activity and breathing patterns. *Neuroscience & Biobehavioral Reviews*, 22(2):233–236.

[165] Harris, S. (2007). Copd and coping with breathlessness at home: a review of the literature. *British Journal of Community Nursing*, 12(9):411–415.

[166] Harrison, O. K., Köchli, L., Marino, S., Luechinger, R., Hennel, F., Brand, K., Hess, A. J., Frässle, S., Iglesias, S., Vinckier, F., et al. (2021). Interoception of breathing and its relationship with anxiety. *Neuron*, 109(24):4080–4093.

[167] Harvey, A. K., Pattinson, K. T., Brooks, J. C., Mayhew, S. D., Jenkinson, M., and Wise, R. G. (2008). Brainstem functional magnetic resonance imaging: disentangling signal from physiological noise. *Journal of Magnetic Resonance Imaging: An Official Journal of the International Society for Magnetic Resonance in Medicine*, 28(6):1337–1344.

[168] Havlicek, M., Ivanov, D., Roebroeck, A., and Uludağ, K. (2017). Determining excitatory and inhibitory neuronal activity from multimodal fmri data using a generative hemodynamic model. *Frontiers in neuroscience*, 11:616.

[169] Hayen, A., Herigstad, M., and Pattinson, K. T. (2013). Understanding dyspnea as a complex individual experience. *Maturitas*, 76(1):45–50.

[170] Hayen, A., Wanigasekera, V., Faull, O. K., Campbell, S. F., Garry, P. S., Raby, S. J., Robertson, J., Webster, R., Wise, R. G., Herigstad, M., et al. (2017). Opioid suppression of conditioned anticipatory brain responses to breathlessness. *Neuroimage*, 150:383–394.

[171] Helmer, M., Warrington, S., Mohammadi-Nejad, A.-R., Ji, J. L., Howell, A., Rosand, B., Anticevic, A., Sotiropoulos, S. N., and Murray, J. D. (2024). On the stability of canonical correlation analysis and partial least squares with application to brain-behavior associations. *Communications Biology*, 7(1):217.

[172] Helmholtz, H. v. (1948). Concerning the perceptions in general, 1867.

[173] Henderson, L. A., Macey, K. E., Macey, P. M., Woo, M. A., Yan-Go, F. L., and Harper, R. M. (2006). Regional brain response patterns to cheyne–stokes breathing. *Respiratory physiology & neurobiology*, 150(1):87–93.

[174] Herigstad, M., Faull, O. K., Hayen, A., Evans, E., Hardinge, F. M., Wiech, K., and Pattinson, K. T. (2017). Treating breathlessness via the brain: changes in brain activity over a course of pulmonary rehabilitation. *European Respiratory Journal*, 50(3).

[175] Herigstad, M., Hayen, A., Wiech, K., and Pattinson, K. T. (2011). Dyspnoea and the brain. *Respiratory medicine*, 105(6):809–817.

[176] Hintiryan, H., Bowman, I., Johnson, D. L., Korobkova, L., Zhu, M., Khanjani, N., Gou, L., Gao, L., Yamashita, S., Bienkowski, M. S., et al. (2021). Connectivity characterization of the mouse basolateral amygdalar complex. *Nature communications*, 12(1):2859.

[177] Hitchcock, J. M. and Davis, M. (1987). Fear-potentiated startle using an auditory conditioned stimulus: effect of lesions of the amygdala. *Physiology & behavior*, 39(3):403–408.

[178] Ho, S. F., O'Mahony, M. S., Steward, J. A., Breay, P., Buchalter, M., and Burr, M. L. (2001). Dyspnoea and quality of life in older people at home. *Age and ageing*, 30(2):155–159.

[179] Homma, I. and Masaoka, Y. (2008). Breathing rhythms and emotions. *Experimental physiology*, 93(9):1011–1021.

[180] Hotelling, H. (1936). The relationship between two of variables.

[181] Hull, J. H. (2022). Challenges in the approach to the management of complex or unexplained breathlessness. *Complex Breathlessness (ERS Monograph). Sheffield, European Respiratory Society*, pages 206–214.

[182] Hull, J. H. and Haines, J. (2022). *Complex breathlessness*. European Respiratory Society.

[183] Hutchinson, A., Barclay-Klingle, N., Galvin, K., and Johnson, M. J. (2018). Living with breathlessness: a systematic literature review and qualitative synthesis. *European Respiratory Journal*, 51(2).

[184] Iacovella, V. and Hasson, U. (2011). The relationship between bold signal and autonomic nervous system functions: implications for processing of "physiological noise". *Magnetic resonance imaging*, 29(10):1338–1345.

[185] Ironside, M., Browning, M., Ansari, T. L., Harvey, C. J., Sekyi-Djan, M. N., Bishop, S. J., Harmer, C. J., and O'Shea, J. (2019). Effect of prefrontal cortex stimulation on regulation of amygdala response to threat in individuals with trait anxiety: a randomized clinical trial. *JAMA psychiatry*, 76(1):71–78.

[186] Ismail, I. I. and Gad, K. A. (2021). Absent blood oxygen level–dependent functional magnetic resonance imaging activation of the orbitofrontal cortex in a patient with persistent cacosmia and cacogeusia after covid-19 infection. *JAMA neurology*, 78(5):609–610.

[187] Janak, P. H. and Tye, K. M. (2015). From circuits to behaviour in the amygdala. *Nature*, 517(7534):284–292.

[188] Janssens, T., De Peuter, S., Stans, L., Verleden, G., Troosters, T., Decramer, M., and Van den Bergh, O. (2011). Dyspnea perception in copd: association between anxiety, dyspnea-related fear, and dyspnea in a pulmonary rehabilitation program. *Chest*, 140(3):618–625.

[189] Janssens, T., Dupont, L., Goossens, S., Sterckx, Y., and Van den Bergh, O. (2020). Acquisition and generalization of cough trigger beliefs in allergic rhinitis. *Journal of Behavioral Medicine*, 43:286–296.

[190] Jenkinson, M., Bannister, P., Brady, M., and Smith, S. (2002). Improved optimization for the robust and accurate linear registration and motion correction of brain images. *Neuroimage*, 17(2):825–841.

[191] Johnston, J. (1924). Further contributions to the study of the evolution of the forebrain v. survey of forebrain morphology. *Contributions from the Department of Anatomy*, 8:483.

[192] Jones, M. W. and Wilson, M. A. (2005). Theta rhythms coordinate hippocampal–prefrontal interactions in a spatial memory task. *PLoS biology*, 3(12):e402.

[193] Kaada, B. R. and Jasper, H. (1952). Respiratory responses to stimulation of temporal pole, insula, and hippocampal and limbic gyri in man. *AMA Archives of Neurology & Psychiatry*, 68(5):609–619.

[194] Kaubisch, L. T., Reck, C., von Tettenborn, A., and Woll, C. F. J. (2022). The covid-19 pandemic as a traumatic event and the associated psychological impact on families–a systematic review. *Journal of Affective Disorders*, 319:27–39.

[195] Kennerley, A. J., Mayhew, J. E., Boorman, L., Zheng, Y., and Berwick, J. (2012). Is optical imaging spectroscopy a viable measurement technique for the investigation of the negative bold phenomenon? a concurrent optical imaging spectroscopy and fmri study at high field (7 t). *Neuroimage*, 61(1):10–20.

[196] Kenny, G., McCann, K., O'Brien, C., Savinelli, S., Tinago, W., Yousif, O., Lambert, J. S., O'Broin, C., Feeney, E. R., De Barra, E., et al. (2022). Identification of distinct long covid clinical phenotypes through cluster analysis of self-reported symptoms. In *Open forum infectious diseases*, volume 9, page ofac060. Oxford University Press US.

[197] Kim, M. J., Gee, D. G., Loucks, R. A., Davis, F. C., and Whalen, P. J. (2011). Anxiety dissociates dorsal and ventral medial prefrontal cortex functional connectivity with the amygdala at rest. *Cerebral cortex*, 21(7):1667–1673.

[198] Kira, I. A., Shuwiekh, H. A., Ashby, J. S., Elwakeel, S. A., Alhuwailah, A., Sous, M. S. F., Baali, S. B. A., Azdaou, C., Oliemat, E. M., and Jamil, H. J. (2021). The impact of covid-19 traumatic stressors on mental health: Is covid-19 a new trauma type. *International Journal of Mental Health and Addiction*, pages 1–20.

[199] Kleckner, I. R., Zhang, J., Touroutoglou, A., Chanes, L., Xia, C., Simmons, W. K., Quigley, K. S., Dickerson, B. C., and Feldman Barrett, L. (2017). Evidence for a large-scale brain system supporting allostasis and interoception in humans. *Nature human behaviour*, 1(5):0069.

[200] Klein-Flügge, M. C., Jensen, D. E., Takagi, Y., Priestley, L., Verhagen, L., Smith, S. M., and Rushworth, M. F. (2022). Relationship between nuclei-specific amygdala connectivity and mental health dimensions in humans. *Nature human behaviour*, 6(12):1705–1722.

[201] Klüver, H. and Bucy, P. C. (1937). " psychic blindness" and other symptoms following bilateral temporal lobectomy in rhesus monkeys. *American Journal of Physiology*.

[202] Koos, B. J., Chau, A., Matsuura, M., Punla, O., and Kruger, L. (1998). Thalamic locus mediates hypoxic inhibition of breathing in fetal sheep. *Journal of neurophysiology*, 79(5):2383–2393.

[203] Koos, B. J., Chau, A., Matsuura, M., Punla, O., and Kruger, L. (2000). Thalamic lesions dissociate breathing inhibition by hypoxia and adenosine in fetal sheep. *American Journal of Physiology-Regulatory, Integrative and Comparative Physiology*, 278(4):R831–R837.

[204] Koos, B. J., Kawasaki, Y., Hari, A., Bohorquez, F., Jan, C., Roostaeian, J., Wilson, C. L., and Kruger, L. (2004). Electrical stimulation of the posteromedial thalamus modulates breathing in unanesthetized fetal sheep. *Journal of Applied Physiology*, 96(1):115–123.

[205] Koralnik, I. J. and Tyler, K. L. (2020). Covid-19: a global threat to the nervous system. *Annals of neurology*, 88(1):1–11.

[206] Kroenke, K., Spitzer, R. L., and Williams, J. B. (2001). The phq-9: validity of a brief depression severity measure. *Journal of general internal medicine*, 16(9):606–613.

[207] Kroenke, K., Spitzer, R. L., and Williams, J. B. (2002). The phq-15: validity of a new measure for evaluating the severity of somatic symptoms. *Psychosomatic medicine*, 64(2):258–266.

[208] Kroenke, K., Spitzer, R. L., Williams, J. B., and Löwe, B. (2010). The patient health questionnaire somatic, anxiety, and depressive symptom scales: a systematic review. *General hospital psychiatry*, 32(4):345–359.

[209] Krupp, L. B., LaRocca, N. G., Muir-Nash, J., and Steinberg, A. D. (1989). The fatigue severity scale: application to patients with multiple sclerosis and systemic lupus erythematosus. *Archives of neurology*, 46(10):1121–1123.

[210] Lacuey, N., Zonjy, B., Londono, L., and Lhatoo, S. D. (2017). Amygdala and hippocampus are symptomatogenic zones for central apneic seizures. *Neurology*, 88(7):701–705.

[211] Laird, A. R., Eickhoff, S. B., Rottschy, C., Bzdok, D., Ray, K. L., and Fox, P. T. (2013). Networks of task co-activations. *Neuroimage*, 80:505–514.

[212] Laviolette, L. and Laveneziana, P. (2014). Dyspnoea: a multidimensional and multidisciplinary approach. *European Respiratory Journal*, 43(6):1750–1762.

[213] Lechien, J. R., Chiesa-Estomba, C. M., De Siati, D. R., Horoi, M., Le Bon, S. D., Rodriguez, A., Dequanter, D., Blecic, S., El Afia, F., Distinguin, L., et al. (2020). Olfactory and gustatory dysfunctions as a clinical presentation of mild-to-moderate forms of the coronavirus disease (covid-19): a multicenter european study. *European Archives of Oto-rhino-laryngology*, 277(8):2251–2261.

[214] LeDoux, J. (2007). The amygdala. *Current biology*, 17(20):R868–R874.

[215] LeDoux, J. E. (2000). Emotion circuits in the brain. *Annual review of neuroscience*, 23(1):155–184.

[216] LeDoux, J. E., Iwata, J., Cicchetti, P., and Reis, D. (1988). Different projections of the central amygdaloid nucleus mediate autonomic and behavioral correlates of conditioned fear. *Journal of Neuroscience*, 8(7):2517–2529.

[217] LeDoux, J. E. and Pine, D. S. (2016). Using neuroscience to help understand fear and anxiety: a two-system framework. *American journal of psychiatry*, 173(11):1083–1093.

[218] Li, W., Cui, H., Zhu, Z., Kong, L., Guo, Q., Zhu, Y., Hu, Q., Zhang, L., Li, H., Li, Q., et al. (2016). Aberrant functional connectivity between the amygdala and the temporal pole in drug-free generalized anxiety disorder. *Frontiers in Human Neuroscience*, 10:549.

[219] Lieberman, M. D. and Eisenberger, N. I. (2015). The dorsal anterior cingulate cortex is selective for pain: Results from large-scale reverse inference. *Proceedings of the National Academy of Sciences*, 112(49):15250–15255.

[220] Liu, Z., Whitaker, K. J., Smith, S. M., and Nichols, T. E. (2022). Improved interpretability of brain-behavior cca with domain-driven dimension reduction. *Frontiers in Neuroscience*, 16:851827.

[221] Logothetis, N. K. (2003). The underpinnings of the bold functional magnetic resonance imaging signal. *Journal of Neuroscience*, 23(10):3963–3971.

[222] Logothetis, N. K., Pauls, J., Augath, M., Trinath, T., and Oeltermann, A. (2001). Neurophysiological investigation of the basis of the fmri signal. *nature*, 412(6843):150–157.

[223] Lu, Y., Li, X., Geng, D., Mei, N., Wu, P.-Y., Huang, C.-C., Jia, T., Zhao, Y., Wang, D., Xiao, A., et al. (2020). Cerebral micro-structural changes in covid-19 patients–an mri-based 3-month follow-up study. *EClinicalMedicine*, 25.

[224] Luettich, A., Sievers, C., Alfaro Almagro, F., Allen, M., Jbabdi, S., Smith, S. M., and Pattinson, K. T. (2023). Functional connectivity between interoceptive brain regions is associated with distinct health-related domains: A population-based neuroimaging study. *Human Brain Mapping*, 44(8):3210–3221.

[225] Ma, W. J., Beck, J. M., Latham, P. E., and Pouget, A. (2006). Bayesian inference with probabilistic population codes. *Nature neuroscience*, 9(11):1432–1438.

[226] MacQueen, J. et al. (1967). Some methods for classification and analysis of multivariate observations. In *Proceedings of the fifth Berkeley symposium on mathematical statistics and probability*, volume 1, pages 281–297. Oakland, CA, USA.

[227] Mandal, S., Barnett, J., Brill, S. E., Brown, J. S., Denneny, E. K., Hare, S. S., Heightman, M., Hillman, T. E., Jacob, J., Jarvis, H. C., et al. (2021). 'long-covid': a cross-sectional study of persisting symptoms, biomarker and imaging abnormalities following hospitalisation for covid-19. *Thorax*, 76(4):396–398.

[228] Mao, L., Jin, H., Wang, M., Hu, Y., Chen, S., He, Q., Chang, J., Hong, C., Zhou, Y., Wang, D., et al. (2020). Neurologic manifestations of hospitalized patients with coronavirus disease 2019 in wuhan, china. *JAMA neurology*, 77(6):683–690.

[229] Marlow, L. L., Faull, O. K., Finnegan, S. L., and Pattinson, K. T. (2019). Breathlessness and the brain: the role of expectation. *Current opinion in supportive and palliative care*, 13(3):200–210.

[230] Marrelec, G., Krainik, A., Duffau, H., Pélégrini-Issac, M., Lehéricy, S., Doyon, J., and Benali, H. (2006). Partial correlation for functional brain interactivity investigation in functional mri. *Neuroimage*, 32(1):228–237.

[231] Marshall, J. C., Murthy, S., Diaz, J., Adhikari, N., Angus, D. C., Arabi, Y. M., Baillie, K., Bauer, M., Berry, S., Blackwood, B., et al. (2020). A minimal common outcome measure set for covid-19 clinical research. *The Lancet Infectious Diseases*, 20(8):e192–e197.

[232] Marshall, M. (2021). The four most urgent questions about long covid. *Nature*, 594(7862):168–170.

[233] Masaoka, Y., Hirasawa, K., Yamane, F., Hori, T., and Homma, I. (2003). Effects of left amygdala lesions on respiration, skin conductance, heart rate, anxiety, and activity of the right amygdala during anticipation of negative stimulus. *Behavior modification*, 27(5):607–619.

[234] Masaoka, Y., Koiwa, N., and Homma, I. (2005). Inspiratory phase-locked alpha oscillation in human olfaction: source generators estimated by a dipole tracing method. *The Journal of physiology*, 566(3):979–997.

[235] Matheson, A. M., McIntosh, M. J., Kooner, H. K., Lee, J., Desaigoudar, V., Bier, E., Driehuys, B., Svenningsen, S., Santyr, G. E., Kirby, M., et al. (2022). Persistent 129xe mri pulmonary and ct vascular abnormalities in symptomatic individuals with post-acute covid-19 syndrome. *Radiology*, 305(2):466–476.

[236] Mattavelli, G., Lo Presti, S., Tornaghi, D., and Canessa, N. (2022). High-definition transcranial direct current stimulation of the dorsal anterior cingulate cortex modulates decision-making and executive control. *Brain Structure and Function*, 227(5):1565–1576.

[237] McCarthy, B., Casey, D., Devane, D., Murphy, K., Murphy, E., and Lacasse, Y. (2015). Pulmonary rehabilitation for chronic obstructive pulmonary disease. *Cochrane database of systematic reviews*, (2).

[238] McNally, G. P., Pigg, M., and Weidemann, G. (2004). Blocking, unblocking, and overexpectation of fear: a role for opioid receptors in the regulation of pavlovian association formation. *Behavioral neuroscience*, 118(1):111.

[239] McNally, R. J. (1989). Is anxiety sensitivity distinguishable from trait anxiety? reply to lilienfeld, jacob, and turner (1989).

[240] McNally, R. J. and Eke, M. (1996). Anxiety sensitivity, suffocation fear, and breath-holding duration as predictors of response to carbon dioxide challenge. *Journal of abnormal psychology*, 105(1):146.

[241] Mesulam, M.-M. and Mufson, E. J. (1982). Insula of the old world monkey. architectonics in the insulo-orbito-temporal component of the paralimbic brain. *Journal of Comparative Neurology*, 212(1):1–22.

[242] Meulders, A., Fannes, S., Van Diest, I., De Peuter, S., Vansteenwegen, D., and Van den Bergh, O. (2010). Resistance to extinction in an odor–20% co2 inhalation paradigm: Further evidence for a symptom learning account of multiple chemical sensitivity. *Journal of Psychosomatic Research*, 68(1):47–56.

[243] Michelen, M., Manoharan, L., Elkheir, N., Cheng, V., Dagens, A., Hastie, C., O'Hara, M., Suett, J., Dahmash, D., Bugaeva, P., et al. (2021). Characterising long covid: a living systematic review. *BMJ global health*, 6(9):e005427.

[244] Miro, O., Llorens, P., Jimenez, S., Pinera, P., Burillo-Putze, G., Martin, A., Martin-Sanchez, F. J., Del Castillo, J. G., Salmeron, P. P., Chaib, F. B., et al. (2021). Frequency of five cardiovascular/hemostatic entities as primary manifestations of sars-cov-2 infection: Results of the umc-19-s2. *International Journal of Cardiology*, 330:268–272.

[245] Mo, X., Jian, W., Su, Z., Chen, M., Peng, H., Peng, P., Lei, C., Chen, R., Zhong, N., and Li, S. (2020). Abnormal pulmonary function in covid-19 patients at time of hospital discharge. *European Respiratory Journal*, 55(6).

[246] Modi, S., Kumar, M., Kumar, P., and Khushu, S. (2015). Aberrant functional connectivity of resting state networks associated with trait anxiety. *Psychiatry Research: Neuroimaging*, 234(1):25–34.

[247] Moon, H. S., Jiang, H., Vo, T. T., Jung, W. B., Vazquez, A. L., and Kim, S.-G. (2021). Contribution of excitatory and inhibitory neuronal activity to bold fmri. *Cerebral cortex*, 31(9):4053–4067.

[248] Moonis, G., Filippi, C. G., Kirsch, C. F., Mohan, S., Stein, E. G., Hirsch, J. A., and Mahajan, A. (2021). The spectrum of neuroimaging findings on ct and mri in adults with covid-19. *American Journal of Roentgenology*, 217(4):959–974.

[249] Morecraft, R. J. and Van Hoesen, G. W. (1998). Convergence of limbic input to the cingulate motor cortex in the rhesus monkey. *Brain research bulletin*, 45(2):209–232.

[250] Mörschel, M. and Dutschmann, M. (2009). Pontine respiratory activity involved in inspiratory/expiratory phase transition. *Philosophical Transactions of the Royal Society B: Biological Sciences*, 364(1529):2517–2526.

[251] Muccioli, L., Sighinolfi, G., Mitolo, M., Ferri, L., Rochat, M. J., Pensato, U., Taruffi, L., Testa, C., Masullo, M., Cortelli, P., et al. (2023). Cognitive and functional connectivity impairment in post-covid-19 olfactory dysfunction. *NeuroImage: Clinical*, 38:103410.

[252] Mufson, E., Mesulam, M.-M., and Pandya, D. (1981). Insular interconnections with the amygdala in the rhesus monkey. *Neuroscience*, 6(7):1231–1248.

[253] Najt, P., Richards, H. L., and Fortune, D. G. (2021). Brain imaging in patients with covid-19: A systematic review. *Brain, behavior, & immunity-health*, 16:100290.

[254] Nasir, S. M., Yahya, N., and Manan, H. A. (2024). Functional brain alterations in covid-19 patients using resting-state fmri: a systematic review. *Brain Imaging and Behavior*, pages 1–20.

[255] Nasreddine, Z. S., Phillips, N. A., Bédirian, V., Charbonneau, S., Whitehead, V., Collin, I., Cummings, J. L., and Chertkow, H. (2003). Montreal cognitive assessment. *The American Journal of Geriatric Psychiatry*.

[256] Nelson, W. and Mayhew, S. D. (2025). Investigating the consistency of negative bold responses to combinations of visual, auditory, and somatosensory stimuli and their modulation by the level of task demand. *Human Brain Mapping*, 46(4):e70177.

[257] Neuman, Å., Gunnbjörnsdottir, M., Tunsäter, A., Nyström, L., Franklin, K. A., Norrman, E., and Janson, C. (2006). Dyspnea in relation to symptoms of anxiety and depression: a prospective population study. *Respiratory medicine*, 100(10):1843–1849.

[258] Nishimura, K., Izumi, T., Tsukino, M., Oga, T., et al. (2002). Dyspnea is a better predictor of 5-year survival than airway obstruction in patients with copd. *Chest*, 121(5):1434–1440.

[259] Nobis, W. P., Schuele, S., Templer, J. W., Zhou, G., Lane, G., Rosenow, J. M., and Zelano, C. (2018). Amygdala-stimulation-induced apnea is attention and nasal-breathing dependent. *Annals of neurology*, 83(3):460–471.

[260] Notarte, K. I., de Oliveira, M. H. S., Peligro, P. J., Velasco, J. V., Macaranas, I., Ver, A. T., Pangilinan, F. C., Pastrana, A., Goldrich, N., Kavteladze, D., et al. (2022). Age, sex and previous comorbidities as risk factors not associated with sars-cov-2 infection for long covid-19: a systematic review and meta-analysis. *Journal of clinical medicine*, 11(24):7314.

[261] Ogawa, S., Lee, T.-M., Kay, A. R., and Tank, D. W. (1990). Brain magnetic resonance imaging with contrast dependent on blood oxygenation. *proceedings of the National Academy of Sciences*, 87(24):9868–9872.

[262] Olson, I. R., Plotzker, A., and Ezzyat, Y. (2007). The enigmatic temporal pole: a review of findings on social and emotional processing. *Brain*, 130(7):1718–1731.

[263] Öngür, D., Ferry, A. T., and Price, J. L. (2003). Architectonic subdivision of the human orbital and medial prefrontal cortex. *Journal of Comparative Neurology*, 460(3):425–449.

[264] O'Reilly, J. X., Woolrich, M. W., Behrens, T. E., Smith, S. M., and Johansen-Berg, H. (2012). Tools of the trade: psychophysiological interactions and functional connectivity. *Social cognitive and affective neuroscience*, 7(5):604–609.

[265] Paolini, M., Palladini, M., Mazza, M. G., Colombo, F., Vai, B., Rovere-Querini, P., Falini, A., Poletti, S., and Benedetti, F. (2023). Brain correlates of subjective cognitive complaints in covid-19 survivors: A multimodal magnetic resonance imaging study. *European Neuropsychopharmacology*, 68:1–10.

[266] Pappens, M., Schroijen, M., Sütterlin, S., Smets, E., Van den Bergh, O., Thayer, J. F., and Van Diest, I. (2014). Resting heart rate variability predicts safety learning and fear extinction in an interoceptive fear conditioning paradigm. *PloS one*, 9(9):e105054.

[267] Pappens, M., Smets, E., Vansteenwegen, D., Van den Bergh, O., and Van Diest, I. (2012). Learning to fear suffocation: a new paradigm for interoceptive fear conditioning. *Psychophysiology*, 49(6):821–828.

[268] Pappens, M., Vandenbossche, E., Van den Bergh, O., and Van Diest, I. (2015). Interoceptive fear learning to mild breathlessness as a laboratory model for unexpected panic attacks. *Frontiers in psychology*, 6:1150.

[269] Parr, T., Pezzulo, G., and Friston, K. J. (2022). *Active inference: the free energy principle in mind, brain, and behavior*. MIT Press.

[270] Pasley, B. N., Inglis, B. A., and Freeman, R. D. (2007). Analysis of oxygen metabolism implies a neural origin for the negative bold response in human visual cortex. *Neuroimage*, 36(2):269–276.

[271] Pattinson, K. T., Governo, R. J., MacIntosh, B. J., Russell, E. C., Corfield, D. R., Tracey, I., and Wise, R. G. (2009a). Opioids depress cortical centers responsible for the volitional control of respiration. *Journal of Neuroscience*, 29(25):8177–8186.

[272] Pattinson, K. T. and Johnson, M. J. (2014). Neuroimaging of central breathlessness mechanisms. *Current opinion in supportive and palliative care*, 8(3):225–233.

[273] Pattinson, K. T., Mitsis, G. D., Harvey, A. K., Jbabdi, S., Dirckx, S., Mayhew, S. D., Rogers, R., Tracey, I., and Wise, R. G. (2009b). Determination of the human brainstem respiratory control network and its cortical connections in vivo using functional and structural imaging. *Neuroimage*, 44(2):295–305.

[274] Pergola, G., Danet, L., Pitel, A.-L., Carlesimo, G. A., Segobin, S., Pariente, J., Suchan, B., Mitchell, A. S., and Barbeau, E. J. (2018). The regulatory role of the human mediodorsal thalamus. *Trends in cognitive sciences*, 22(11):1011–1025.

[275] Perica, M. I., Ravindranath, O., Calabro, F. J., Foran, W., and Luna, B. (2021). Hippocampal-prefrontal connectivity prior to the covid-19 pandemic predicts stress reactivity. *Biological Psychiatry Global Open Science*, 1(4):283–290.

[276] Peuter, S. D., Put, C., Lemaigre, V., Demedts, M., Verleden, G., and Bergh, O. V. D. (2007). Context-evoked overperception in asthma. *Psychology and Health*, 22(6):737–748.

[277] Peveler, R., Kilkenny, L., and Kinmonth, A.-L. (1997). Medically unexplained physical symptoms in primary care: a comparison of selfreport screening questionnaires and clinical opinion. *Journal of psychosomatic research*, 42(3):245–252.

[278] Phillips, R. and LeDoux, J. (1992). Differential contribution of amygdala and hippocampus to cued and contextual fear conditioning. *Behavioral neuroscience*, 106(2):274.

[279] Piroth, L., Cottenet, J., Mariet, A.-S., Bonniaud, P., Blot, M., Tubert-Bitter, P., and Quantin, C. (2021). Comparison of the characteristics, morbidity, and mortality of covid-19 and seasonal influenza: a nationwide, population-based retrospective cohort study. *The Lancet Respiratory Medicine*, 9(3):251–259.

[280] Pivovarov, A. S., Calahorro, F., and Walker, R. J. (2019). Na+/k+-pump and neurotransmitter membrane receptors. *Invertebrate Neuroscience*, 19(1):1.

[281] Power, J. D., Barnes, K. A., Snyder, A. Z., Schlaggar, B. L., and Petersen, S. E. (2012). Spurious but systematic correlations in functional connectivity mri networks arise from subject motion. *Neuroimage*, 59(3):2142–2154.

[282] Prabhakaran, D., Day, G. S., Munipalli, B., Rush, B. K., Pudalov, L., Niazi, S. K., Brennan, E., Powers, H. R., Durvasula, R., Athreya, A., et al. (2023). Neurophenotypes of covid-19: risk factors and recovery outcomes. *Brain, Behavior, & Immunity-Health*, 30:100648.

[283] Prager, E. M., Bergstrom, H. C., Wynn, G. H., and Braga, M. F. (2016). The basolateral amygdala γ-aminobutyric acidergic system in health and disease. *Journal of neuroscience research*, 94(6):548–567.

[284] Price, J. and Powell, T. (1971). Certain observations on the olfactory pathway. *Journal of anatomy*, 110(Pt 1):105.

[285] Quirk, G. J. and Gehlert, D. R. (2003). Inhibition of the amygdala: key to pathological states? *Annals of the New York Academy of Sciences*, 985(1):263–272.

[286] Rahman, J., Muralidharan, A., Quazi, S. J., Saleem, H., and Khan, S. (2020). Neurological and psychological effects of coronavirus (covid-19): an overview of the current era pandemic. *Cureus*, 12(6).

[287] Rapee, R. M. and Medoro, L. (1994). Fear of physical sensations and trait anxiety as mediators of the response to hyperventilation in nonclinical subjects. *Journal of Abnormal Psychology*, 103(4):693.

[288] Reese, J. T., Blau, H., Casiraghi, E., Bergquist, T., Loomba, J. J., Callahan, T. J., Laraway, B., Antonescu, C., Coleman, B., Gargano, M., et al. (2023). Generalisable long covid subtypes: findings from the nih n3c and recover programmes. *EBioMedicine*, 87.

[289] Reggente, N., Moody, T. D., Morfini, F., Sheen, C., Rissman, J., O'Neill, J., and Feusner, J. D. (2018). Multivariate resting-state functional connectivity predicts response to cognitive behavioral therapy in obsessive–compulsive disorder. *Proceedings of the National Academy of Sciences*, 115(9):2222–2227.

[290] Reiss, S., Peterson, R. A., Gursky, D. M., and McNally, R. J. (1986). Anxiety sensitivity, anxiety frequency and the prediction of fearfulness. *Behaviour research and therapy*, 24(1):1–8.

[291] Rhone, A. E., Kovach, C. K., Harmata, G. I., Sullivan, A. W., Tranel, D., Ciliberto, M. A., Howard, M. A., Richerson, G. B., Steinschneider, M., Wemmie, J. A., et al. (2020). A human amygdala site that inhibits respiration and elicits apnea in pediatric epilepsy. *JCI insight*, 5(6).

[292] Rikhye, R. V., Wimmer, R. D., and Halassa, M. M. (2018). Toward an integrative theory of thalamic function. *Annual review of neuroscience*, 41(1):163–183.

[293] Rizvi, T. A., Ennis, M., Behbehani, M. M., and Shipley, M. T. (1991). Connections between the central nucleus of the amygdala and the midbrain periaqueductal gray: topography and reciprocity. *Journal of Comparative Neurology*, 303(1):121–131.

[294] Rosvold, H. E., Mirsky, A. F., and Pribram, K. H. (1954). Influence of amygdalectomy on social behavior in monkeys. *Journal of comparative and physiological psychology*, 47(3):173.

[295] Rua, C., Raman, B., Rodgers, C. T., Newcombe, V. F., Manktelow, A., Chatfield, D. A., Sawcer, S. J., Outtrim, J. G., Lupson, V. C., Stamatakis, E. A., et al. (2024). Quantitative susceptibility mapping at 7 t in covid-19: brainstem effects and outcome associations. *Brain*, 147(12):4121–4130.

[296] Rubin, R. (2020). As their numbers grow, covid-19 "long haulers" stump experts. *Jama*, 324(14):1381–1383.

[297] Rybak, I. A., Shevtsova, N. A., Paton, J., Dick, T. E., John, W. S., Mörschel, M., and Dutschmann, M. (2004). Modeling the ponto-medullary respiratory network. *Respiratory physiology & neurobiology*, 143(2-3):307–319.

[298] Sah, P., Faber, E. L., Lopez de Armentia, M., and Power, J. (2003). The amygdaloid complex: anatomy and physiology. *Physiological reviews*, 83(3):803–834.

[299] Sanders, B. J., Wirtz-Nole, C., DeFord, S. M., and Erling, B. F. (1994). Central amygdaloid lesions attenuate cardiovascular responses to acute stress in rats with borderline hypertension. *Physiology & behavior*, 56(4):709–713.

[300] Sandkühler, J. and Lee, J. (2013). How to erase memory traces of pain and fear. *Trends in neurosciences*, 36(6):343–352.

[301] Sarvandani, M. N., Koohsar, J. S., Rafaiee, R., Saeedi, M., Tamijani, S. M. S., Ghazvini, H., and Sheibani, H. (2023). Covid-19 and the brain: A psychological and restingstate functional magnetic resonance imagin (fmri) study of the whole-brain functional connectivity. *Basic & Clinical Neuroscience*, 14(6).

[302] Saygin, Z. M., Kliemann, D., Iglesias, J. E., van der Kouwe, A. J., Boyd, E., Reuter, M., Stevens, A., Van Leemput, K., McKee, A., Frosch, M. P., et al. (2017). High-resolution magnetic resonance imaging reveals nuclei of the human amygdala: manual segmentation to automatic atlas. *Neuroimage*, 155:370–382.

[303] Scaramuzzo, G., Ronzoni, L., Campo, G., Priani, P., Arena, C., La Rosa, R., Turrini, C., Volta, C. A., Papi, A., Spadaro, S., et al. (2022). Long-term dyspnea, regional ventilation distribution and peripheral lung function in covid-19 survivors: a 1 year follow up study. *BMC Pulmonary Medicine*, 22(1):408.

[304] Schachter, S. and Singer, J. (1962). Cognitive, social, and physiological determinants of emotional state. *Psychological review*, 69(5):379.

[305] Schridde, U., Khubchandani, M., Motelow, J. E., Sanganahalli, B. G., Hyder, F., and Blumenfeld, H. (2008). Negative bold with large increases in neuronal activity. *Cerebral cortex*, 18(8):1814–1827.

[306] Schultz, W. (2007). Multiple dopamine functions at different time courses. *Annu. Rev. Neurosci.*, 30(1):259–288.

[307] Schumann, C. M., Bauman, M. D., and Amaral, D. G. (2011). Abnormal structure or function of the amygdala is a common component of neurodevelopmental disorders. *Neuropsychologia*, 49(4):745–759.

[308] Seeßle, J., Waterboer, T., Hippchen, T., et al. (2021). Persistent symptoms in adult patients one year after covid-19: a prospective cohort study [manuscript published online ahead of print 5 july 2021]. *Clin Infect Dis*, 10.

[309] Seth, A. (2015). The cybernetic bayesian brain: From interoceptive inference to sensorimotor contingencies [w:] open mind. *Frankfurt A. M: MIND Group*.

[310] Seth, A. K. and Friston, K. J. (2016). Active interoceptive inference and the emotional brain. *Philosophical Transactions of the Royal Society B: Biological Sciences*, 371(1708):20160007.

[311] Seth, A. K., Suzuki, K., and Critchley, H. D. (2012). An interoceptive predictive coding model of conscious presence. *Frontiers in psychology*, 2:395.

[312] Shallice, T. (1982). Specific impairments of planning. *Philosophical Transactions of the Royal Society of London. B, Biological Sciences*, 298(1089):199–209.

[313] Shao, X., Guo, F., Kim, J., Ress, D., Zhao, C., Shou, Q., Jann, K., and Wang, D. J. (2024). Laminar multi-contrast fmri at 7t allows differentiation of neuronal excitation and inhibition underlying positive and negative bold responses. *Imaging Neuroscience*, 2:1–19.

[314] Shehzad, Z., Kelly, A. C., Reiss, P. T., Gee, D. G., Gotimer, K., Uddin, L. Q., Lee, S. H., Margulies, D. S., Roy, A. K., Biswal, B. B., et al. (2009). The resting brain: unconstrained yet reliable. *Cerebral cortex*, 19(10):2209–2229.

[315] Shih, Y.-Y. I., Chen, C.-C. V., Shyu, B.-C., Lin, Z.-J., Chiang, Y.-C., Jaw, F.-S., Chen, Y.-Y., and Chang, C. (2009). A new scenario for negative functional magnetic resonance imaging signals: endogenous neurotransmission. *Journal of Neuroscience*, 29(10):3036–3044.

[316] Shmuel, A., Augath, M., Oeltermann, A., and Logothetis, N. K. (2006). Negative functional mri response correlates with decreases in neuronal activity in monkey visual area v1. *Nature neuroscience*, 9(4):569–577.

[317] Shmuel, A., Yacoub, E., Pfeuffer, J., Van de Moortele, P.-F., Adriany, G., Hu, X., and Ugurbil, K. (2002). Sustained negative bold, blood flow and oxygen consumption response and its coupling to the positive response in the human brain. *Neuron*, 36(6):1195–1210.

[318] Silverman, I., Choi, J., Mackewn, A., Fisher, M., Moro, J., and Olshansky, E. (2000). Evolved mechanisms underlying wayfinding: Further studies on the hunter-gatherer theory of spatial sex differences. *Evolution and Human Behavior*, 21(3):201–213.

[319] Simon, N. M., Weiss, A. M., Kradin, R., Evans, K. C., Reese, H. E., Otto, M. W., Oppenheimer, J. E., Smoller, J. W., Zalta, A., Worthington III, J. J., et al. (2006). The relationship of anxiety disorders, anxiety sensitivity and pulmonary dysfunction with dyspnea-related distress and avoidance. *The Journal of nervous and mental disease*, 194(12):951–957.

[320] Simsic, A. A., Yorke, J., Regueiro, E. G., Di Lorenzo, V. P., and Baddini-Martinez, J. (2018). Validation of the dyspnoea-12 scale into p ortuguese speaking copd patients. *The Clinical Respiratory Journal*, 12(5):1942–1948.

[321] Sladky, R., Baldinger, P., Kranz, G. S., Tröstl, J., Höflich, A., Lanzenberger, R., Moser, E., and Windischberger, C. (2013). High-resolution functional mri of the human amygdala at 7 t. *European journal of radiology*, 82(5):728–733.

[322] Smith, J. C., Ellenberger, H. H., Ballanyi, K., Richter, D. W., and Feldman, J. L. (1991). Pre-bötzinger complex: a brainstem region that may generate respiratory rhythm in mammals. *Science*, 254(5032):726–729.

[323] Smith, S. M., Fox, P. T., Miller, K. L., Glahn, D. C., Fox, P. M., Mackay, C. E., Filippini, N., Watkins, K. E., Toro, R., Laird, A. R., et al. (2009). Correspondence of the brain's functional architecture during activation and rest. *Proceedings of the national academy of sciences*, 106(31):13040–13045.

[324] Smith, S. M. and Nichols, T. E. (2009). Threshold-free cluster enhancement: addressing problems of smoothing, threshold dependence and localisation in cluster inference. *Neuroimage*, 44(1):83–98.

[325] Smith, S. M., Nichols, T. E., Vidaurre, D., Winkler, A. M., Behrens, T. E., Glasser, M. F., Ugurbil, K., Barch, D. M., Van Essen, D. C., and Miller, K. L. (2015). A positive-negative mode of population covariation links brain connectivity, demographics and behavior. *Nature neuroscience*, 18(11):1565–1567.

[326] Smith, S. M., Vidaurre, D., Beckmann, C. F., Glasser, M. F., Jenkinson, M., Miller, K. L., Nichols, T. E., Robinson, E. C., Salimi-Khorshidi, G., Woolrich, M. W., et al. (2013). Functional connectomics from resting-state fmri. *Trends in cognitive sciences*, 17(12):666–682.

[327] Smoller, J. W., Pollack, M. H., Otto, M. W., Rosenbaum, J. F., and Kradin, R. L. (1996). Panic anxiety, dyspnea, and respiratory disease. theoretical and clinical considerations. *American journal of respiratory and critical care medicine*, 154(1):6–17.

[328] Solomon, B. K., Wilson, K. G., Henderson, P. R., Poulin, P. A., Kowal, J., and McKim, D. A. (2015). A breathlessness catastrophizing scale for chronic obstructive pulmonary disease. *Journal of Psychosomatic Research*, 79(1):62–68.

[329] Spampanato, J., Polepalli, J., and Sah, P. (2011). Interneurons in the basolateral amygdala. *Neuropharmacology*, 60(5):765–773.

[330] Spathis, A., Booth, S., Moffat, C., Hurst, R., Ryan, R., Chin, C., and Burkin, J. (2017). The breathing, thinking, functioning clinical model: a proposal to facilitate evidence-based breathlessness management in chronic respiratory disease. *NPJ primary care respiratory medicine*, 27(1):27.

[331] Spitzer, R. L., Kroenke, K., Williams, J. B., and Löwe, B. (2006). A brief measure for assessing generalized anxiety disorder: the gad-7. *Archives of internal medicine*, 166(10):1092–1097.

[332] Stefanovic, B., Warnking, J. M., and Pike, G. B. (2004). Hemodynamic and metabolic responses to neuronal inhibition. *Neuroimage*, 22(2):771–778.

[333] Steffen, P. R., Austin, T., DeBarros, A., and Brown, T. (2017). The impact of resonance frequency breathing on measures of heart rate variability, blood pressure, and mood. *Frontiers in public health*, 5:222.

[334] Stegen, K., De Bruyne, K., Rasschaert, W., Van de Woestijne, K. P., and Van den Bergh, O. (1999). Fear-relevant images as conditioned stimuli for somatic complaints, respiratory behavior, and reduced end-tidal pco_2. *Journal of Abnormal Psychology*, 108(1):143.

[335] Stephan, H., Frahm, H., and Baron, G. (1987). Comparison of brain structure volumes in insectivora and primates. vii. amygdaloid components. *Journal fur Hirnforschung*, 28(5):571–584.

[336] Stephan, K. E., Manjaly, Z. M., Mathys, C. D., Weber, L. A., Paliwal, S., Gard, T., Tittgemeyer, M., Fleming, S. M., Haker, H., Seth, A. K., et al. (2016). Allostatic self-efficacy: A metacognitive theory of dyshomeostasis-induced fatigue and depression. *Frontiers in human neuroscience*, 10:550.

[337] Steriade, M. and Llinás, R. R. (1988). The functional states of the thalamus and the associated neuronal interplay. *Physiological reviews*, 68(3):649–742.

[338] Stewart, I., Jacob, J., George, P., Porter, J., Allen, R., Aslani, S., Baillie, J., Baratt, S., Bianchi, S., Blaikley, J., et al. (2023). Residual lung abnormalities following covid-19 hospitalisation: interim analysis of the ukild post-covid study. *American Journal of Respiratory and Critical Care Medicine*, 207(6):693–703.

[339] Stoeckel, M. C., Esser, R. W., Gamer, M., Büchel, C., and von Leupoldt, A. (2016). Brain responses during the anticipation of dyspnea. *Neural plasticity*, 2016(1):6434987.

[340] Stoeckel, M. C., Esser, R. W., Gamer, M., Büchel, C., and von Leupoldt, A. (2018). Dyspnea catastrophizing and neural activations during the anticipation and perception of dyspnea. *Psychophysiology*, 55(4):e13004.

[341] Strang, S., Ekberg-Jansson, A., and Henoch, I. (2014). Experience of anxiety among patients with severe copd: A qualitative, in-depth interview study. *Palliative & supportive care*, 12(6):465–472.

[342] Sullivan, M. J., Bishop, S. R., and Pivik, J. (1995). The pain catastrophizing scale: development and validation. *Psychological assessment*, 7(4):524.

[343] Takagi, Y., Sakai, Y., Lisi, G., Yahata, N., Abe, Y., Nishida, S., Nakamae, T., Morimoto, J., Kawato, M., Narumoto, J., et al. (2017). A neural marker of obsessive-compulsive disorder from whole-brain functional connectivity. *Scientific reports*, 7(1):7538.

[344] Taruffi, L., Muccioli, L., Mitolo, M., Ferri, L., Descovich, C., Mazzoni, S., Michelucci, R., Lodi, R., Liguori, R., Cortelli, P., et al. (2023). Neurological manifestations of long covid: a single-center one-year experience. *Neuropsychiatric Disease and Treatment*, pages 311–319.

[345] Teeter, J. G. and Bleecker, E. R. (1998). Relationship between airway obstruction and respiratory symptoms in adult asthmatics. *Chest*, 113(2):272–277.

[346] Telch, M. J., Harrington, P. J., Smits, J. A., and Powers, M. B. (2011). Unexpected arousal, anxiety sensitivity, and their interaction on co2-induced panic: Further evidence for the context-sensitivity vulnerability model. *Journal of anxiety disorders*, 25(5):645–653.

[347] Thomasson, M., Voruz, P., Cionca, A., Jacot de Alcântara, I., Nuber-Champier, A., Allali, G., Benzakour, L., Lalive, P. H., Lövblad, K.-O., Braillard, O., et al. (2023). Markers of limbic system damage following sars-cov-2 infection. *Brain Communications*, 5(4):fcad177.

[348] Tikhonov, A. N. (1963). On the solution of ill-posed problems and the method of regularization. In *Doklady akademii nauk*, volume 151, pages 501–504. Russian Academy of Sciences.

[349] Tong, Y., Hocke, L. M., and Frederick, B. B. (2019). Low frequency systemic hemodynamic "noise" in resting state bold fmri: characteristics, causes, implications, mitigation strategies, and applications. *Frontiers in neuroscience*, 13:787.

[350] Touroutoglou, A., Andreano, J., Dickerson, B. C., and Barrett, L. F. (2020). The tenacious brain: How the anterior mid-cingulate contributes to achieving goals. *Cortex*, 123:12–29.

[351] Tsvetanov, K. A., Spindler, L. R., Stamatakis, E. A., Newcombe, V. F., Lupson, V. C., Chatfield, D. A., Manktelow, A. E., Outtrim, J. G., Elmer, A., Kingston, N., et al. (2022). Hospitalisation for covid-19 predicts long lasting cerebrovascular impairment: A prospective observational cohort study. *NeuroImage: Clinical*, 36:103253.

[352] Van den Bergh, O., Brown, R. J., Petersen, S., and Witthöft, M. (2017a). Idiopathic environmental intolerance: a comprehensive model. *Clinical Psychological Science*, 5(3):551–567.

[353] Van den Bergh, O., Devriese, S., Winters, W., Veulemans, H., Nemery, B., Eelen, P., and Van de Woestijne, K. P. (2001). Acquiring symptoms in response to odors: a learning perspective on multiple chemical sensitivity. *Annals of the New York Academy of Sciences*, 933(1):278–290.

[354] Van Den Bergh, O., Kempynck, P. J., Van De Woestijne, K. P., Baeyens, F., and Eelen, P. (1995). Respiratory learning and somatic complaints: a conditioning approach using co2-enriched air inhalation. *Behaviour Research and Therapy*, 33(5):517–527.

[355] Van den Bergh, O., Stegen, K., and Van de Woestijne, K. P. (1997). Learning to have psychosomatic complaints: conditioning of respiratory behavior and somatic complaints in psychosomatic patients. *Biopsychosocial Science and Medicine*, 59(1):13–23.

[356] Van den Bergh, O., Stegen, K., Van Diest, I., Raes, C., Stulens, P., Eelen, P., Veulemans, H., Van de Woestijne, K. P., and Nemery, B. (1999). Acquisition and extinction of somatic symptoms in response to odours: a pavlovian paradigm relevant to multiple chemical sensitivity. *Occupational and Environmental Medicine*, 56(5):295–301.

[357] Van den Bergh, O., Witthöft, M., Petersen, S., and Brown, R. J. (2017b). Symptoms and the body: taking the inferential leap. *Neuroscience & Biobehavioral Reviews*, 74:185–203.

[358] Van Den Heuvel, M. P. and Sporns, O. (2011). Rich-club organization of the human connectome. *Journal of Neuroscience*, 31(44):15775–15786.

[359] Vazdarjanova, A. and McGaugh, J. L. (1999). Basolateral amygdala is involved in modulating consolidation of memory for classical fear conditioning. *Journal of Neuroscience*, 19(15):6615–6622.

[360] Vialatte, F. B., Bakardjian, H., Prasad, R., and Cichocki, A. (2009). Eeg paroxysmal gamma waves during bhramari pranayama: a yoga breathing technique. *Consciousness and cognition*, 18(4):977–988.

[361] Vogt, B. A. (2016). Midcingulate cortex: structure, connections, homologies, functions and diseases. *Journal of chemical neuroanatomy*, 74:28–46.

[362] von Leupoldt, A., Sommer, T., Kegat, S., Baumann, H. J., Klose, H., Dahme, B., and Büchel, C. (2008). The unpleasantness of perceived dyspnea is processed in the anterior insula and amygdala. *American Journal of Respiratory and Critical Care Medicine*, 177(9):1026–1032.

[363] von Leupoldt, A., Taube, K., Lehmann, K., Fritzsche, A., and Magnussen, H. (2011). The impact of anxiety and depression on outcomes of pulmonary rehabilitation in patients with copd. *Chest*, 140(3):730–736.

[364] Voruz, P., Cionca, A., Jacot de Alcântara, I., Nuber-Champier, A., Allali, G., Benzakour, L., Lalive, P. H., Lövblad, K. O., Braillard, O., Nehme, M., et al. (2023). Brain functional connectivity alterations associated with neuropsychological performance 6–9 months following sars-cov-2 infection. *Human Brain Mapping*, 44(4):1629–1646.

[365] Ware Jr, J. E. and Sherbourne, C. D. (1992). The mos 36-ltem short-form health survey (sf-36): I. conceptual framework and item selection. *Medical care*, 30(6):473–483.

[366] Weir-McCall, J. R., Galea, G., Mak, S. M., Joshi, K., Agrawal, B., Screaton, N., Toshner, M., Ruggiero, A., Benedetti, G., Brozik, J., et al. (2022). Vascular thrombosis in severe covid-19 requiring extracorporeal membrane oxygenation: a multicenter study. *Critical Care Medicine*, 50(4):624–632.

[367] Williams, M. T., John, D., and Frith, P. (2017). Comparison of the dyspnoea-12 and multidimensional dyspnoea profile in people with copd. *European Respiratory Journal*, 49(3).

[368] Williams, T. and Carel, H. (2018). Breathlessness: From bodily symptom to existential experience. *Existential medicine*.

[369] Wingrove, J., Makaronidis, J., Prados, F., Kanber, B., Yiannakas, M. C., Magee, C., Castellazzi, G., Grandjean, L., Golay, X., Tur, C., et al. (2023). Aberrant olfactory network functional connectivity in people with olfactory dysfunction following covid-19 infection: an exploratory, observational study. *EClinicalMedicine*, 58.

[370] Winkler, A. M., Ridgway, G. R., Webster, M. A., Smith, S. M., and Nichols, T. E. (2014). Permutation inference for the general linear model. *Neuroimage*, 92:381–397.

[371] Winters, W., Devriese, S., Van Diest, I., Nemery, B., Veulemans, H., Eelen, P., Van de Woestijne, K., and Van den Bergh, O. (2003). Media warnings about environmental pollution facilitate the acquisition of symptoms in response to chemical substances. *Biopsychosocial Science and Medicine*, 65(3):332–338.

[372] Wolff, M., Alcaraz, F., Marchand, A. R., and Coutureau, E. (2015). Functional heterogeneity of the limbic thalamus: from hippocampal to cortical functions. *Neuroscience & Biobehavioral Reviews*, 54:120–130.

[373] Wood, P. B. (2006). Mesolimbic dopaminergic mechanisms and pain control. *Pain*, 120(3):230–234.

[374] Wood, P. B., Schweinhardt, P., Jaeger, E., Dagher, A., Hakyemez, H., Rabiner, E. A., Bushnell, M. C., and Chizh, B. A. (2007). Fibromyalgia patients show an abnormal dopamine response to pain. *European Journal of Neuroscience*, 25(12):3576–3582.

[375] Woolrich, M. W., Behrens, T. E., and Smith, S. M. (2004). Constrained linear basis sets for hrf modelling using variational bayes. *NeuroImage*, 21(4):1748–1761.

[376] Woolrich, M. W., Ripley, B. D., Brady, M., and Smith, S. M. (2001). Temporal autocorrelation in univariate linear modeling of fmri data. *Neuroimage*, 14(6):1370–1386.

[377] Woolsey, T. A., Rovainen, C. M., Cox, S. B., Henegar, M. H., Liang, G. E., Liu, D., Moskalenko, Y. E., Sui, J., and Wei, L. (1996). Neuronal units linked to microvascular modules in cerebral cortex: response elements for imaging the brain. *Cerebral cortex*, 6(5):647–660.

[378] Yildirim, D., Kandemirli, S. G., Sanli, D. E. T., Akinci, O., and Altundag, A. (2022). A comparative olfactory mri, dti and fmri study of covid-19 related anosmia and post viral olfactory dysfunction. *Academic radiology*, 29(1):31–41.

[379] Yorke, J., Moosavi, S. H., Shuldham, C., and Jones, P. W. (2010). Quantification of dyspnoea using descriptors: development and initial testing of the dyspnoea-12. *Thorax*, 65(1):21–26.

[380] Zelano, C., Jiang, H., Zhou, G., Arora, N., Schuele, S., Rosenow, J., and Gottfried, J. A. (2016). Nasal respiration entrains human limbic oscillations and modulates cognitive function. *Journal of Neuroscience*, 36(49):12448–12467.

[381] Zeng, L.-L., Shen, H., Liu, L., Wang, L., Li, B., Fang, P., Zhou, Z., Li, Y., and Hu, D. (2012). Identifying major depression using whole-brain functional connectivity: a multivariate pattern analysis. *Brain*, 135(5):1498–1507.

[382] Zhang, H., Chung, T. W.-H., Wong, F. K.-C., Hung, I. F.-N., and Mak, H. K.-F. (2022a). Changes in the intranetwork and internetwork connectivity of the default mode network and olfactory network in patients with covid-19 and olfactory dysfunction. *Brain sciences*, 12(4):511.

[383] Zhang, H., Zang, C., Xu, Z., Zhang, Y., Xu, J., Bian, J., Morozyuk, D., Khullar, D., Zhang, Y., Nordvig, A. S., et al. (2023a). Data-driven identification of post-acute sars-cov-2 infection subphenotypes. *Nature Medicine*, 29(1):226–235.

[384] Zhang, J., Chen, D., Srirangarajan, T., Theriault, J., Kragel, P. A., Hartley, L., Lee, K. M., McVeigh, K., Wager, T. D., Wald, L. L., et al. (2023b). Cortical and subcortical mapping of the allostatic-interoceptive system in the human brain: replication and extension with 7 tesla fmri. *bioRxiv*.

[385] Zhang, J.-X., Harper, R. M., and Frysinger, R. C. (1986). Respiratory modulation of neuronal discharge in the central nucleus of the amygdala during sleep and waking states. *Experimental Neurology*, 91(1):193–207.

[386] Zhang, T., Wang, Z., Liang, H., Wu, Z., Li, J., Ou-Yang, J., Yang, X., Peng, Y. B., and Zhu, B. (2022b). Transcranial focused ultrasound stimulation of periaqueductal gray for analgesia. *IEEE Transactions on Biomedical Engineering*, 69(10):3155–3162.

[387] Zhao, S., Shibata, K., Hellyer, P. J., Trender, W., Manohar, S., Hampshire, A., and Husain, M. (2022). Rapid vigilance and episodic memory decrements in covid-19 survivors. *Brain communications*, 4(1):fcab295.

[388] Zheng, B., Daines, L., Han, Q., Hurst, J. R., Pfeffer, P., Shankar-Hari, M., Elneima, O., Walker, S., Brown, J. S., Siddiqui, S., et al. (2022). Prevalence, risk factors and treatments for post-covid-19 breathlessness: a systematic review and meta-analysis. *European Respiratory Review*, 31(166).

[389] Zhou, G., Tsai, H.-W., and Davenport, P. (2014). Respiratory activation of neurons in the central nucleus of the amygdala (cea) and effect of cea neuron stimulation on respiration (1178.5). *The FASEB Journal*, 28:1178–5.

Appendix A

Cognitron task

Cognitive task descriptions

Object Memory Task

Twenty greyscale images of common items were presented in a random sequence, each displayed for 2000 ms with a 500 ms interstimulus gap. Immediately after viewing, participants were tested on their recall using a 3x3 grid containing eight images, with the central position left empty. One image in the grid was an exact match to one of the 20 previously displayed items. The grid also included a mirrored version of the correct image, another image from the same category (and its mirrored version), and four images from different categories. Errors were classified into three types: (1) Spatial Error, (2) Item Error, or (3) Category Error (a guess). The sum of Correct responses, Spatial Errors, Item Errors, and Category Errors for each trial equalled 1. Following the completion of other cognitive tasks, participants were unexpectedly retested on the same objects. Performance was assessed based on the percentage of correct identifications.

Word Memory Task

Participants were shown 12 English words, each presented for 1000 ms with a 200 ms interstimulus gap. The words were selected from three semantic categories: animals, clothing, and vegetables. After the initial presentation, participants were shown 24 words and asked to identify which words had appeared previously. Half of these words were from the original set, while the other half were new, with an equal portion of the new words being semantically similar to the original words. After completing all other tasks, participants were retested on their recall of these words without prior notice, using a delay similar to the Object Memory

Task. Performance metrics included the total number of correct identifications, as well as the ability to correctly reject non-original words and those with semantic similarities.

Spatial Span

Participants were instructed to remember a sequence of numbers displayed on the screen. After viewing each sequence, they reproduced it using a numeric keypad. The length of the sequence increased by one digit with each correct attempt. The task terminated after three consecutive incorrect attempts at a particular sequence length. The maximum sequence length successfully recalled, ranging from 1 to 20 digits, was used as the measure of memory performance.

Simple Reaction

This task assessed basic cognitive processes involving perception and response execution. Participants were instructed to click on a red circle as soon as it appeared at the centre of the screen. A total of 60 stimuli were presented, with the interstimulus interval (ISI) randomly jittered between 0.5 and 2 seconds, following a uniform distribution. The outcome measure was the mean response time.

Motor Control

This task was similar to the Simple Reaction task, with the distinction that the location of the red circle varied with each presentation. Participants were required to move their cursor to the target and respond as quickly as possible. A total of 30 stimuli were presented, with the next stimulus appearing immediately (0 ms delay) after the previous response. The outcome measure was the mean response time.

Choice Reaction

Participants responded to a black arrow pointing either left or right. They were instructed to click on the corresponding side of the screen as quickly as possible. A total of 60 stimuli were presented, each with a 50% probability of pointing left. The interstimulus interval (ISI) was randomly jittered between 0.5 s and 2 s, following a uniform distribution. The mean reaction time for button presses on both sides was the outcome measure.

Target Detection

This visuospatial attention task required participants to identify and click on a target shape amidst distractor shapes. The target shape was displayed on the left side of the screen, while a probe area appeared on the right. After 3 s, shapes began to populate the probe area. Participants identified and clicked on the target shape while ignoring distractors. Shapes were added every 1 s, and a subset of the shapes was removed at the same interval. Each trial included 120 addition/removal cycles. The target shape appeared pseudo-randomly 12 times in every 20 cycles. The outcome measure was the total number of target shapes clicked.

Tower of London

This task assessed spatial planning and was adapted from the original Tower of London task[312]. Participants were presented with two sets of three pegs holding coloured beads: one represented the initial state, and the other the target state. Participants determined the minimum number of moves required to transition from the initial state to the target state and entered this number using an on-screen numeric keypad. The task included 10 trials of varying difficulty, defined by the number of moves required that did not place a bead in its final target position. Unlike the original task[312], the pegs were of equal height, and participants completed the task mentally, as the beads could not be physically moved. The outcome measure was the total number of correct trials.

Verbal Analogies

This task evaluated semantic reasoning. Participants were presented with pairs of written relationships and determined whether they shared the same association (e.g., *"Lion is to feline as cabbage is to vegetable"*). Responses were made by selecting either the *True* or *False* buttons displayed below the analogies. The analogies varied in semantic distance to adjust difficulty, and the types of associations alternated throughout the trials. Participants had 3 minutes to solve as many problems as possible. Scores increased by one point for each correct response, while incorrect answers deducted one point. The outcome measure was the total score.

2D Mental Rotations

This task assessed spatial manipulation skills using 6×6 grids with coloured cell arrangements[318]. Participants identified which of four additional grids matched the target grid but was rotated by 90°, 180°, or 270°. Incorrect grids contained five cells with incorrect colours. Participants

completed as many trials as possible within 3 minutes, earning one point per correct response. The outcome measure was the total points earned.

3D Mental Rotation

In this task, participants identified a rotated version of a target object from four options. The stimuli consisted of 3D scenes of buildings arranged on a green surface. The correct option matched the target object from a different viewpoint (rotated by 90°, 180°, or 270°), while incorrect options had misplaced buildings. Each participant completed 12 trials, with one point awarded per correct response. The outcome measure was the total points earned.

Appendix B

Breathlessness task

The following supplementary information was adapted from previously published studies based on the same dataset used in Chapter 2 [114, 113].

B.1 Aversive Delay-conditioning breathlessness task

Participants completed one training session followed by an MRI scan 12–24 hours later. The training involved an aversive delay-conditioning task where participants learned to associate shapes with an inspiratory resistance stimulus. Two conditions were used: A shape of 'star' always predicted resistance (100% contingency), and a shape of a 'square' always predicted no resistance (0% contingency).

The "resistance" shape (star) was shown for 30 seconds (including a 5–15 second anticipation period), and the "no resistance" shape (square) for 20 seconds. Each appeared 14 times in a semi-random order. A finger-tapping task was also included, prompted by a "TAP" cue for 15 seconds, repeated 10 times. Conditioning was verified post-training and pre-scan.

Participants rated breathing difficulty ('Not at all difficult' to 'Extremely difficult') after each symbol and at the beginning and end of the task using a visual analogue scale (0–100%). They also rated symbol-induced anxiety immediately after scanning ('Not at all anxious to 'Extremely anxious'). Additionally, they reported weekly physical activity, including type, duration, and intensity.

B.2 Breathing system

A breathing system was used to remotely deliver inspiratory resistance based on conditioned cues. During rest periods, compressed medical air was supplied at a rate sufficient to

maintain free breathing, ensuring the reservoir bag remained inflated. During resistance periods, airflow was halted; once the bag collapsed, participants inhaled atmospheric air through a resistive arm of the circuit.

To minimise BOLD signal fluctuations due to changes in arterial O_2 and CO_2, two strategies were employed: (1) medical oxygen flow was manually adjusted to stabilise end-tidal O_2 ($PETO_2$) at approximately 18 kPa, and (2) short hypercapnic challenges (10% CO_2, 21% O_2, balance N_2) were administered at 20 L/min for 5–10 seconds during rest, to match $PETCO_2$ levels observed during resistance. Participants breathed exclusively through the mouth with their nose occluded using foam earplugs.

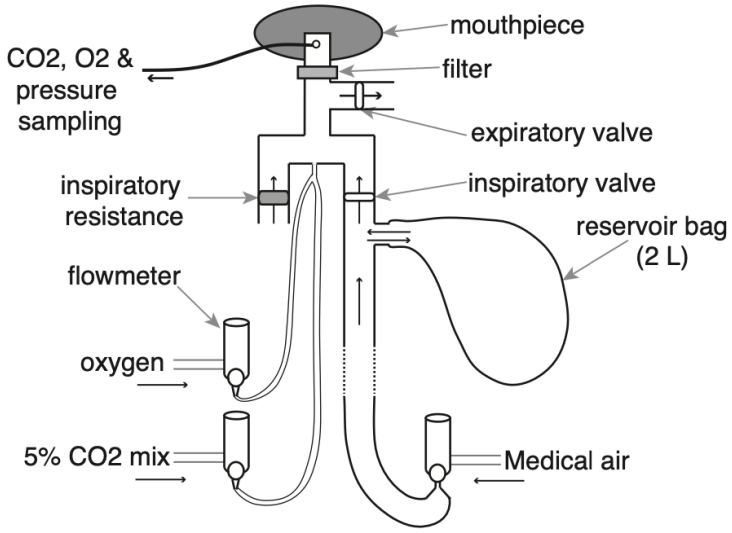


Fig. B.1 Schematic diagram of the breathing system used for remote administration of inspiratory resistance, adapted with permission from Faull et al.[113, 114]. The design is based on the system described in these studies, which provided the dataset for the current secondary analysis. Medical air is delivered through a flow meter to a 2L reservoir, with excess flow and exhalation vented via a one-way expiratory valve near the mouth to minimise re-breathing (valves: Hans Rudolf, USA). Resistance is introduced by halting airflow; once the reservoir deflates, the subject inhales through a porous glass disc. Normal airflow resumes with the reintroduction of medical air. The system includes a diving mouthpiece (Scubapro, UK) connected to a bacterial/viral filter (GVS, UK). Respiratory gases and pressure are sampled via polyethylene tubing (Vygon, France): one line to a pressure transducer (Validyne Corp., USA) with an amplifier (PK Morgan Ltd, UK), and another to a gas analyser (ADInstruments, UK) for O_2 and CO_2 levels. A hyperoxic state was maintained via continuous O_2 at 0.5 L/min. Periodic CO_2 challenges (10% CO_2 at 20 L/min mixed with medical air) were used to match $PETCO_2$ levels during resistance.